On the Mechanism of Cytoprotection by Ferrostatin-1 and Liproxstatin-1 and the Role of Lipid Peroxidation in Ferroptotic Cell Death

&

Targeting Tetrahydronaphthyridinols to the Mitochondria

By

Omkar Zilka

A thesis submitted to the Department of Chemistry and Biomolecular Sciences
in conformity with the requirements for the degree of
Master of Science in Chemistry

University of Ottawa
Ottawa, Ontario, Canada
March 2018

Abstract

Lipid peroxidation is well established to contribute to the etiology of many deteriorative conditions including neurodegeneration, cardiovascular disease, cancer, aging, and recently in ferroptosis—a regulated, necrotic modality of cell death that results from the accumulation of lipid hydroperoxides. Recent high-throughput screening efforts have uncovered ferrostatin-1 (Fer-1) and liproxstatin-1 (Lip-1) as two premiere inhibitors of ferroptosis. We propose that these compounds function as radical trapping antioxidants. We employ a systematic methodology of evaluating inherent radical trapping antioxidant (RTA) activity of Lip-1, Fer-1, and various aryl amine and aryl nitroxide analogues to put forward a biologically relevant mechanism of action based on our previous work in the field. Joining these observations with the efficacy of tetrahydronaphthyridinols (THNs), the results support a clear role of autoxidation in the execution of ferroptosis.

Next, we expand the THN repertoire by targeting the payload towards the engine of our cells, the mitochondria. Decades of research have implicated mitochondrial dysfunction brought about by the peroxidation of mitochondrial membranes and the leaking of downstream oxidants, in the death of their symbiotic host cells. Isolated successes in the field have been demonstrated academically, though viable drugs remain to be developed, partially due to the lack of effective diagnostic tools. We endeavor to address some of these issues by investigating mitochondrially-targeted THNs (MitoTHNs) as a targeted chain-breaking antioxidant of unparalleled potency. Furthermore, we advance development of the THNs towards therapeutic applications by demonstrating their biodistribution in mice.

Acknowledgements

First of all, I would like to thank my supervisor, Dr. Derek A. Pratt, for the teachable moments and afforded opportunities. I am grateful for your dedication and patience that has supported me throughout my graduate education. Thanks to my lab partners and friends Evan, Ron, Zosia, JP, Bo, Markus, Luke, Kareem, Pierre, Jia-Fei, Anthony, Emily, Katie, Nadia, Manuel and to all other past and present members of our group, for the support, laughter, and food and drink. Thank you to James, Jeff, Sheema and Amanda for your friendship and encouragements over the years.

This work is dedicated to my parents and sisters that have supported me in numerous ways throughout my education.

Statement of Originality

I hereby certify that all of the work described within this thesis is the original work of the author, with exceptions noted that are carried out by collaborators listed in the preface of each chapter. Any published (or unpublished) ideas and/or techniques from the work of others are fully acknowledged in accordance with the references.

Omkar Zilka

Table of Contents

Abstract ..... **ii**
Acknowledgements ..... **iii**
Statement of Originality ..... **iv**
Table of Contents ..... **v**
List of Schemes ..... **ix**
List of Figures ..... **xi**
List of Tables ..... **xix**
List of Charts ..... **xx**
List of Abbreviations ..... **xxi**
Chapter 1: Background and Significance **1**
1.1 Reactive Oxygen Species and Lipid Peroxidation 2
1.1.1 Endogenous Sources of ROS 2
1.1.2 Preventative antioxidants 7
1.1.3 Lipid peroxidation 10
1.1.4 Mechanism of lipid autoxidation 11
1.2 Inhibition of Lipid Autoxidation by Phenolic and Aminic Radical Trapping Antioxidants 15
1.2.1 Methods of evaluating RTA efficacy 15
1.2.2 Radical-trapping antioxidants 19
1.2.3 The 'superoxide dismutase-mimetic' activity of nitroxides 22
1.3 Ferroptosis 24
1.3.1 Discovery 24
1.3.2 Experimental models of ferroptosis and ferroptosis-inducing compounds 25
1.3.3 Inhibitors of ferroptosis and proposed modes of action 28
1.4 Research Objectives 29
1.4.1 Proposed mechanism of Lip-1 and Fer-1 29
1.4.2 Preparation of mitochondrially-targeted THNs 31
1.5 References 33

Preface to Chapter 2 39

Chapter 2: On the Mechanism of Cytoprotection by Ferrostatin-1 & Liproxstatin-1 and the Role of Lipid Peroxidation in Ferroptotic Cell Death 40

2.1 Introduction 40

2.2 Results 42

2.2.1 Fer-1 and Lip-1 Are Inherently Good, But Not Great, Radical-Trapping Antioxidants. 42

2.2.3 Fer-1 and Lip-1 Are Excellent Radical-Trapping Antioxidants in Phospholipid Bilayers. 46

2.2.4 Fer-1 and Lip-1 Are Poor Inhibitors of 15-Lipoxygenase at Best, as is a-TOH. 48

2.2.5 Lipophilic THNs are Potent Ferroptosis Inhibitors. 50

2.3 Discussion 52

2.4 Experimental Methods 60

2.5 Supporting Information 66

2.5.1 Coautoxidations of cumene in chlorobenzene and coautoxidations of THF in DMSO and chlorobenzene. 66

2.5.2 Experimental procedures 67

2.5.3 Synthesis of Lip-1. 69

2.5.4 Generation of nitroxides. 70

2.6 References 72

2.7 Supplementary Results and Discussion 77

2.7.1 Synthesis and rationale for spiroquinoxalinamine derivatives 77

2.7.2 RTA activity of spiroquinoxalinamine derivatives 83

2.7.3 Inhibition of RSL3-induced ferroptosis by spiroquinoxalinamine derivatives 96

2.8 Conclusions 97

2.9 Future Work 98

2.10 Supplementary Experimental 99

2.10.1 General 99

2.10.2 Synthesis of spiroquinoxalinamine derivatives. 99

2.10.3 PMHC-BODIPY and Dimethyl-BODIPY liposome autoxidations 109

2.10.4 Inhibition of RSL3-induced ferroptosis. 109

2.11 Supplementary References 110
Preface to Chapter 3 112
Chapter 3: Targeting Tetrahydronaphthyridinols to the Mitochondria 113
3.1 Introduction 113
3.1.1 Mitochondrial dysfunction and lipid peroxidation 113
3.1.2 Modelling mitochondrial oxidative stress 116
3.1.3 Mitochondria targeting strategies 117
3.1.4 Methods used to evaluate mitochondrial uptake of small molecules 120
3.1.5 Probes for sensing mitochondrial lipid peroxidation 123
3.1.6 Mitochondrially-targeted antioxidants 124
3.1.7 Mitochondrial dysfunction in ferroptosis 125
3.2 Results and Discussion 128
3.2.1 Synthesis of mitochondrially targeted tetrahydronaphthyridinols (Mito-THNs) 128
3.2.2 Synthesis of a mitochondrially-targeted peroxidation probe 130
3.2.3 MitoTHNs are equivalently potent to THNs in both homogeneous and heterogeneous media 131
3.2.4 Cytotoxicity of MitoTHNs 132
3.2.5 Towards rescue of mitochondrial oxidative stress-induced apoptosis 133
3.2.6 Towards monitoring mitochondrial lipid peroxidation using MitoSTY-BODIPY 134
3.2.7 Medium-chain length MTHNs are mediocre ferroptosis inhibitors 142
3.2.8 MitoTHNs significantly inhibit DEM-induced lipid peroxidation 147
3.2.9 Long chain MTHNs bind to human α-tocopherol transport protein 148
3.2.10 THNs and MitoTHNs are broadly bioavailable among tissues 150
3.3 Future work 154
3.4 Experimental 157
3.4.1 General 157
3.4.2 MitoTHN syntheses 157
3.4.3 MitoSTY-BODIPY synthesis 163
3.4.4 Inhibition of mitochondrial lipid peroxidation in live cells using MSB.. 169
3.4.5 Inhibition of mitochondrial oxidative stress-induced apoptosis by MTHNs. 169
3.4.6 Confocal microscopy 169

3.4.7 Bioavailability of THNs and MitoTHNs 170
3.5 References 172
Appendix 1: NMR Spectra for Chapter 2 181
Appendix 2: NMR Spectra for Chapter 3 193

List of Schemes

Scheme 1.1 Examples of reactive oxygen species that can arise from one electron reduction of molecular oxygen. 1

Scheme 1.2 Termination mechanism of peroxyl radicals resulting in formation of carbonyl electrophiles. *b*, barrierless. Inset: transition state of tetraoxide decomposition, facilitated by C_α H-bonds (2.37Å and 2.29Å). 13

Scheme 1.3 Mechanism of lipid hydroperoxide formation by LOX enzymes. Inset: Active site iron(III)-OH in rabbit 15-LO. 14

Scheme 1.4 The RTA mechanism of phenols and tocopherols. 19

Scheme 1.5 The effect of hydrogen bond accepting (**A**), basic (**B**) and acidic (**C**) solvents on the mechanism of phenolic RTAs. 20

Scheme 1.6 Electron rich phenolic RTAs produce hydroperoxyl radicals by undesired reactions with oxygen or hydroperoxides. 21

Scheme 1.7 The initial radical trapping rate (k_7) correlates with PhO-H BDE.' The heteroatom ED ability is maximized when the lone pair (shown as a 2p orbital) has optimal overlap ($\theta \approx 0°$) with the aromatic plane.' 21

Scheme 1.8 The RTA activity (k_7) of phenols is maximized by lowering PhO-H BDE without decreasing IP to the point of direct reaction with oxygen. 22

Scheme 1.9 Possible mechanisms proposed in the literature for 'superoxide dismutase-mimetic' activity of hindered aliphatic nitroxides. 23

Scheme 1.10 Mechanistic proposals for the catalytic radical trapping activity of TEMPO and diarylamines under high-temperature autoxidation conditions. 29

Scheme 2.1 Phenols, such as PMHC (shown) and α-TOH are better H-bond donors than arylamines, such as Fer-1 and Lip-1, leading to lower observed reactivity to peroxyl radicals in the presence of good H-bond accepting solvents (or other solutes) ***S***. 48

Scheme 2.2 Increased Radical-Trapping Capacity of Lip-1 (shown) and Fer-1 (not shown) Relative to Phenolic Antioxidants Such as α-TOH and PMHC Arises

Due to their Ability to Form Products that Remain Highly Reactive to Peroxyl Radicals..... 56

Scheme 2.3 Mechanism and synthesis of spiroquinoxalinamine derivatives. (**A**) Mechanism of the multicomponent reaction between a diamine, ketone, isocyanide, and lewis acid (TMSCl) to afford spiroquinoxalinamines. Synthesis of Lip-1 (**B**), L1 (**C**) and L2 (**D**). 78

Scheme 2.4 Synthesis of aryl substituted spiroquinoxalinamines: *p*-*t*-Bu-L1 and *m*-*t*-Bu-L1 (**A**), L2-OH (**B**) and attempted synthesis of spiroquinoxalinamine-phenol (**C**). 79

Scheme 2.5 Mechanism and synthesis of dihydroquinolines. Mechanism of dihydroquinoline synthesis by condensation of an aniline with two ketones (**A**). Synthesis of L3 (**B**), L4 and derived nitroxide L4-NO (**C**), and aryl amine L5 and derived nitroxide L5-NO (**D**). 81

Scheme 3.1 Synthesis of mitochondrially-targeted THNs (MitoTHNs, **4**). 128

Scheme 3.2 Retrosynthesis (**A**) and synthesis (**B**) of MitoSTY-BODIPY (MSB, **7**). 130

List of Figures

Figure 1.1 The physiological outcome of various sources of ROS based on relative concentrations *in vivo*. Adapted from reference 4. 2

Figure 1.2 Major sources of ROS *in vivo* from the flavoenzymes NADPH oxidase (A) and xanthine oxidoreductase (B) from which the reduced form of $FADH_2$ can react with oxygen to produce superoxide and other oxidants (C). Heme-based myeloperoxidase (MPO) (D) and elemental iron and also produce potent oxidants via Fenton chemistry (E). 3

Figure 1.3 (**A**) The electron transport chain is embedded in the inner mitochondrial membrane. Blue arrows: electron transfer. Adapted from reference . (**B**) Subunits of the ETC are transcribed both in the mitochondria and from nuclear DNA. (**C**) The cycles of the ubiquinone/ubiquinol pool that can produce superoxide. 5

Figure 1.4 The fates of superoxide in the mitochondria. Adapted from reference 7

Figure 1.5 Annual (non-cumulative) SciFinder entries for "Oxidative stress" and "Lipid peroxidation" since 1969, when SOD was discovered. 8

Figure 1.6 Mechanism of superoxide dismutation by CuZnSOD. 8

Figure 1.7 Hydroperoxides are detoxified to the corresponding alcohols by CAT and GPX (A). Mechanism of hydroperoxide reaction with selenoenzymes and glutathione cofactors (B). Catalytic tetrad in the active site of GPX enzymes (B). 9

Figure 1.8 Common classes of glycerophospholipids (left) composed of triesterified glycerol (black) with various fatty acid side chains (green, right) and various polar head groups (purple), which assemble as bilayers, micelles and liposomes..... 10

Figure 1.9 Highly autoxidizable lipophilic biomolecules (A). The primary products of linoleate autoxidation (B). Adapted from reference 12

Figure 1.10 The general inhibited autoxidation scheme with common autoxidizable substrates and azo-initiators. 16

Figure 1.11 Representative autoxidation plot monitored by oxygen consumption uninhibited by an RTA (A). Representative antioxidants of excellent (B), average (C) and modest (D) reactivities inhibit the reaction relative to the untreated control. $\tau \equiv t_{inh}$. Reproduced from reference 52. 17

Figure 1.12 Biochemical pathways involved in the induction of ferroptosis. Ferroptosis inducing pathways *i-v* prevent GPX4 activity, leading to accumulation of lipid hydroperoxides that are generated by two mechanisms: the autoxidation-mediated path (box **A**), or, a lipoxygenase-mediated path (box **B**). Adapted from reference 87..... 27

Figure 2.1 PBD-BODIPY serves as the signal carrier in styrene autoxidations (**A**), enabling determination of rate constants and reaction stoichiometries for reactions of inhibitors with chain-carrying peroxyl radicals (**B**). Co-autoxidations of styrene (4.3 M) and PBDBODIPY (10 μM) initiated by AIBN (6 mM) in chlorobenzene at 37°C (black trace) and inhibited by 2 μM (red trace), 3 μM (green trace) and 4 μM (blue trace) of Fer-1 (**C**), Lip-1 (**D**), C15-THN (**E**) α-TOH (**F**) and PMHC (**G**). Average inhibition rate constants and stoichiometry summarized in (**H**). Reaction progress was monitored by absorbance at 591 nm (ε = 139,000 $M^{-1}cm^{-1}$). [a] From ref. 29; the inhibition rate constant is greater than that which can be determined from the data in panel (**E**)..... 44

Figure 2.2 Computed (CBS-QB3) minimum energy structures of Fer-1 (left)[41] and Lip-1 (right) and the corresponding N-H bond dissociation enthalpies of the labile aminic H-atoms. 45

Figure 2.3 STY-BODIPY serves as the signal carrier in liposome oxidations (**A**), enabling determinations of rate constants and reaction stoichiometries for reactions of inhibitors with chain-carrying peroxyl radicals (**B**). Average inhibition rate constants and stoichiometry summarized in (**C**). Co-autoxidations of egg phosphatidylcholine lipids (1 mM) and STY-BODIPY (8 μM) suspended in phosphate-buffered saline (10 mM) at pH 7.4 initiated by MeOAMVN (0.2 mM) at 37°C (black trace) and inhibited by 2 μM (red trace), 3 μM (green trace) and 4 μM (blue trace) of Lip-1 (**D**), Fer-1 (**E**), α-

TOH (**F**), C15-THN (**G**) and PMHC (**H**). Reaction progress was monitored by absorbance at 565 nm (ε = 139,000 $M^{-1}cm^{-1}$). [a] Could not be determined and is assumed to be 2.0. 47

Figure 2.4 Expression, functional characterization and inhibition of 15-LO overexpressed in HEK-293 cells. Western blots showing the overexpression of 15-LO in transfected cells compared to wild-type (**A**). Structures of 5-, 12- and 15-HETEs monitored by UPLC/MS/MS and their characteristic MS/MS transitions (**B**). Representative chromatograms of H(P)ETEs formed by wild-type and 15-LO over-expressing cells (**C**). Effect of Fer-1, Lip-1, C_{15}-THN, α-TOH, PMHC and PD146176 on 15-H(P)ETE formation (**D**). 49

Figure 2.5 (**A**) Anti-ferroptotic activity of the THNs in mouse embryonic fibroblasts. Ferroptosis was initiated by tamoxifen-induced Cre-mediated deletion of the *gpx4* gene and cell survival was determined 6 hours post-induction by AquaBluer assay. Corresponding data obtained for Fer-1, Lip-1 and α-TOH are also shown. (**B**) The THNs prevent glutamate-induced cell death in mouse HT-22 hippocampal cells. Cells were treated with 5 mM glutamate and 100 nM of test compound for 10 hours, after which cell viability was assessed by AquaBluer assay. Corresponding data obtained for Fer-1, Lip-1, α-TOH and β-mercaptoethanol (β-Me) are also shown. HT-22 cell viability was associated with inhibition of lipid peroxidation, as revealed by suppression of BODIPY-$C11^{581/591}$ oxidation. 52

Figure 2.6 Co-autooxidations of egg phosphatidylcholine lipids (1 mM) and STY-BODIPY (8 μM) suspended in phosphate-buffered saline (10 mM) at pH 7.4 initiated by MeOAMVN (0.2 mM) at 37°C (black trace) and inhibited by 2 μM (red trace), 3 μM (green trace) and 4 μM (blue trace) of 1 (dotted line) and Lip-1 (solid line) (**A**), EPR spectrum of the nitroxide derived from 1 (**B**), and corresponding co-autoxidations inhibited by 1 (dotted line) and the nitroxide derived therefrom (dashed line) (**C**). Reaction progress in the co-autoxidations was monitored by absorbance at 565 nm (ε = 139,000 $M^{-1}cm^{-1}$). 57

Figure 2.7 Coautoxidations of STY-BODIPY and cumene in chlorobenzene. STY-BODIPY serves as the signal carrier in cumene autoxidations (**A**), enabling

determination of rate constants and reaction stoichiometries for reactions of inhibitors with chain-carrying peroxyl radicals (**B**). Coautoxidations of cumene (3.6 M) and STY-BODIPY (10 μM) initiated by AIBN (6 mM) in chlorobenzene at 37 °C (black trace) and inhibited by 2 μM (red trace), 3 μM (green trace), and 4 μM (blue trace) of Fer-1 (**C**) and Lip-1 (**D**). Average inhibition rate constants and stoichiometry summarized in (**E**). Reaction progress was monitored by absorbance at 571 nm (ε = 128,000 M^{-1} cm^{-1}). .. 66

Figure 2.8 Coautoxidations of PBD-BODIPY and THF in DMSO and chlorobenzene. PBDBODIPY serves as the signal carrier in THF autoxidations (**A**), enabling determination of rate constants and reaction stoichiometries for reactions of inhibitors with chain-carrying peroxyl radicals (**B**). Coautoxidations of THF (3.1 M) and PBD-BODIPY (10 μM) initiated by AIBN (6 mM) in DMSO (25 vol%) and chlorobenzene at 37°C (black trace) and inhibited by 2 μM (red trace), 3 μM (green trace), and 4 μM (blue trace) of Fer-1 (**C**), Lip-1 (**D**), C15-THN (**E**), α-TOH (**F**), and PMHC (**G**). Average inhibition rate constants and stoichiometry summarized in (H). Reaction progress was monitored by absorbance at 588 nm (ε = 128,000 M^{-1} cm^{-1}).[a] The stoichiometry could not be determined from the data in panel D and stoichiometry was assumed to be 2 for calculation of k_{inh}. 67

Figure 2.9 EPR spectrum of Lip-1 oxidation products. 71

Figure 2.10 Spiroquinoxalinamines synthesized and evaluated in structure-activity relationship study herein. 77

Figure 2.11 Co-autooxidations of styrene (4.3 M) and PBD-BODIPY (10 μM) initiated by AIBN (6 mM) in chlorobenzene at 37°C (black trace) and inhibited by 2 μM (red trace), 3 μM (green trace) and 4 μM (blue trace) of Lip-1 (**A**), L1 (**B**), *p*-*t*BuL1 (**C**), *m*-*t*BuL1 (**D**) and L2 (**E**). Average inhibition rate constants and stoichiometry summarized in (**F**). Reaction progress was monitored by absorbance at 591 nm (ε = 139,000 $M^{-1}cm^{-1}$). [a] Stoichiometry could not be determined from the data and n=1 was assumed for k_{inh} calculations. 83

Figure 2.12 When Y = N-H, an intramolecular H-bond from the aniline/amidine N-H (***a, b***) could prevent radical trapping steps analogous to a kinetic solvent effect in

H-bond accepting media. This may also allow opportunity to react with O_2 (***b***). Steric bulk around the amidine may prevent approach of a second peroxyl (***c***) reducing stoichiometry or becoming rate limiting. The nitroxides (***d***) could be responsible for the observed catalytic activity. 84

Figure 2.13 Co-autoxidations of cumene (3.6 M) and STY-BODIPY (10 μM) initiated by AIBN (6 mM) in chlorobenzene at 37°C (black trace) and inhibited by 2 μM (red trace), 3 μM (green trace) and 4 μM (blue trace) of Lip-1 (**A**), L1 (**B**), L2 (**C**), *p*-*t*BuL1 (**D**), *m*-*t*BuL1 (**E**), L3 (**F**), and L4 (**G**). Average inhibition rate constants and stoichiometry summarized in (**H**). Reaction progress was monitored by absorbance at 571 nm (ε = 128,000 $M^{-1}cm^{-1}$). [a] k_{inh} greater than can be measured from the data. 85

Figure 2.14 Co-autoxidations of egg PC liposomes (1 mM) and STY-BODIPY (8 μM) initiated by MeO-AMVN (200 μM) in pH 7.4 PBS (10 mM) at 37°C (black trace) and inhibited by 2 μM (red trace), 3 μM (green trace) and 4 μM (blue trace) of Lip-1 (**A**), L1 (**B**), *p*-*t*BuL1 (**C**), *m*-*t*BuL1 (**D**), L2 (**E**), L2-OH (**F**) and L4 (**G**). Average inhibition rate constants and stoichiometry summarized in (H). Reaction progress was monitored by absorbance at 565 nm (ε = 123676 $M^{-1}cm^{-1}$) 87

Figure 2.15 Co-autoxidations of egg PC liposomes (1 mM) and STY-BODIPY (8 μM) initiated by MeO-AMVN (200 μM) in pH 7.4 PBS (10 mM) at 37°C (black trace) and inhibited by 2 μM (red trace), 3 μM (green trace) and 4 μM (blue trace) of TEMPO (**A**), L4-NO (**B**), L5-NO (**C**), LONG-TEMPO (**D**). Average inhibition rate constants and stoichiometry summarized in (**E**). Reaction progress was monitored by absorbance at 565 nm (ε = 123676 $M^{-1}cm^{-1}$). 89

Figure 2.16 Autoxidations of egg PC liposomes (1 mM initiated by 0.68 mM MeOAMVN in 10 mM pH 7.4 PBS at 37°C) inhibited by 0.15 μM H_2B-PMHC (**A**) and RTAs Lip-1 (**B**), Fer-1 (**C**), L1 (**D**) and L2 (**E**). Analogous results obtained for AAPH initiated autoxidations (data not shown). 90

Figure 2.17 Autoxidations of egg PC liposomes (1 mM initiated by 0.68 mM MeOAMVN in 10 mM pH 7.4 PBS at 37°C) with 0.15 μM Dimethyl-BODIPY (**A**) and inhibited by RTAs Fer-1 (**B**), Lip-1 (**C**), PMHC (**D**), L5-

NO (**E**) and L4-NO (**F**). Dotted traces lack MeOAMVN initiator. Analogous results obtained for AAPH initiated autoxidations (data not shown). 91

Figure 2.18 Autoxidations of egg PC liposomes (1 mM initiated by 0.68 mM MeOAMVN in 10 mM pH 7.4 PBS at 37°C) inhibited by 0.15 μM PMHC-BODIPY (**A**) and RTAs diaryl-nitroxide (**B**), L5-NO (**C**), PMHC (**D**), TEMPO (**E**) and Long-TEMPO (**F**). Analogous results obtained for AAPH initiated autoxidations (data not shown). 93

Figure 2.19 Autoxidations of egg PC liposomes (1 mM initiated by 0.68 mM MeOAMVN in 10 mM PBS at pH 5.8 (**A**-**C**) and pH 10.8 (**D**-**F**) at 37°C) inhibited by 0.15 μM PMHC-BODIPY and RTAs TEMPO (**A**,**D**), Lip-1 (**B**,**E**), and Fer-1 (**C**-**F**). Analogous results obtained for AAPH initiated autoxidations (data not shown). 94

Figure 2.20 Ferroptosis is induced by covalent modification of the enzyme Gpx4 by the small molecule (1*S*,3*R*)-RSL3, leading to accumulation of lipid hydroperoxides (PUFA-OOH) arising from autoxidation (**A**). Spiroquinoxalinamines and the related derivatives rescue Pfa1 cells from ferroptotic death in a dose dependent manner (**B**). Efficacy summarized in (**C**). 96

Figure 2.21 Possible dihydroquinoline- and tetrahydroquinoline-derived tocopherol analogues 98

Figure 3.1 (**A**) Structure of cardiolipin and common acyl chains in mammals. (**B**) Various roles of cardiolipin in mitochondrial function.' 114

Figure 3.2 One electron redox cycle of ParaQuat (PQ) and MitoParaQuat (MPQ) (**A**) and doxorubicin (DOX) (**B**) that can lead to superoxide generation and lipid autoxidation. ETC inhibitors Antimycin A and Rotenone inhibit Complex III and I, respectively (**C**). 116

Figure 3.3 Common strategies to target pharmacophores to mitochondria. Adapted from reference 41. 118

Figure 3.4 Apparatus (**A** and **C**) used to verify and evaluate electrophoretic accumulation of ions (**B**) across charged subcellular organelles. Images reproduced from references 55 and 56. 121

Figure 3.5 Lipid peroxidation probes targeted to the mitochondria. 123
Figure 3.6 Prominent mitochondrially-targeted TPP-based antioxidants. 124
Figure 3.7 The inherent RTA activity of the THNs translates to MitoTHNs in organic solution autoxidations (Panels **A-C**, 4.3 M styrene in acetonitrile, initiated by 6 mM AIBN at 37°C) and in heterogeneous egg phosphatidylcholine lipid bilayer autoxidations (Panels **D-F**, 1 mM liposomes in 10 mM pH 7.4 PBS, initiated by 0.2 mM MeOAMVN at 37°C). 131
Figure 3.8 MTHNs and RTAs do not rescue MEF cells treated with mitochondrial oxidative stress initiators MitoParaquat (MPQ, Top) and doxorubicin (DOX, bottom) from cell death. 133
Figure 3.9 MSB localizes in the mitochondria. Pfa-1 cells were stained with the mitochondrial dye MitoView 633 and either MSB (top row) or C11-BODIPY (bottom row). The overlay represents areas of colocalization in purple. 134
Figure 3.10 Mitochondrial initiators cause lipid peroxidation measured by MSB (FL2; untreated □, treated with initiator ■) and C11-BODIPY (FL1; untreated □, treated with initiator ■). Pfa-1 cells were treated with PQ (**A**, 1 mM, 22 h), ANT (**B**, 100 μM, 22 h), MPQ (**C** and **E**, 250 μM, 5 h), or DOX (**D** and **F**, 10 μM, 4 h), followed by MSB (250 nM, 30 min) or C11-BODIPY (1 μM, 30 min). 135
Figure 3.11 Medium-chain length MTHNs partially rescue cells from ferroptosis induced by RSL3 (100 nM) in Pfa-1 MEFs. 142
Figure 3.12 C_{10}- and C_{14}-MitoTHN are similar in physical size to $MitoQ_{10}$ and $MitoQ_{15}$, respectively (**A**). In isolated mitochondria, chain length affects the extent of incorporation. Approximately 50% (2.6 of 5 μM) of $MitoQ_{10}$ and 84% (4.2 of 5 μM) of $MitoQ_{15}$ incorporate in non-energized mitochondria, increasing to 72% and 96% respectively, upon establishment of a membrane potential with succinate (**B**). Image reproduced from Asin-Cayuela *et al.* 2014. 145
Figure 3.13 MTHNs are highly effective inhibitors of lipid peroxidation initiated by 2 hours of 9 mM DEM treatment in HEK293 cells measured by C11-BODIPY. 147
Figure 3.14 The fluorescent α-TOH analogue NBD-Toc (**A**) binds to the active side of hTTP (crystal structure with native ligand α-TOH shown) (**B**) and is titrated

with test molecules to produce titration curves (**C**) allowing determination of the effective dissociation constant, $K_{d,eff}$ (**D**), for binding to hTTP (1 μM NBD-Toc and 0.5 μM hTTP in SET buffer). [a] Non-competitive with NBD-Toc. [b] Values from reference 100. 149

Figure 3.15 Biodistribution of C_{15}-THN in BALB/c and ApoE$^{-/-}$ mice after 2, 4 and 24 h of a single 2 mg dose by gavage. 152

Figure 3.16 Biodistribution of C_{14}-MitoTHN in BALB/c mice after 2, 4 and 24 h of a single 2 mg dose by gavage. 152

List of Tables

Table 2.1 Anti-ferroptotic activity of THNs in mouse embryonic fibroblasts. Ferroptosis was induced with (1*S*,3*R*)-RSL3 (100 nM) and cell survival was determined 6 hours post-induction by AquaBluer[18] assay. Data for α-TOH, Fer-1 and Lip-1 are also shown. 51

Table 3.1 Advantages and disadvantages of current mitochondrial targeting strategies. 119

Table 3.2 Cytotoxicity of MitoTHNs in HEK293 cells. Compounds were incubated for 22 h and viability determined using the AquaBluer assay. 132

Table 3.3 Comparison of tissue bioavailability of α-TOH (in rats) and THNs (in mice). 150

List of Charts

Chart 2.1 The tetrahydronaphthyridinols (THNs) studied here. 42

List of Abbreviations

α-TOH	α-tocopherol
AAPH	2,2'-azobis-(2-amidinopropane) monohydrochloride
AIBN	azobisisobutyronitrile
ApoE	apolipoprotein E
ATP	adenosine triphosphate
BDE	bond dissociation enthalpy
BODIPY	boron-dipyrromethene, 4,4-difluoro-4-bora-3a,4a-diaza-s-indacene
CAT	catalase
CoQ	coenzyme Q10, ubiquinone
DCM	dichloromethane
DMSO	dimethylsulfoxide
DMEM	Dulbecco's Modified Eagle Medium
DNA	deoxyribonucleic acid
EDG	electron donating group
EggPC	L-α-phosphatidyl choline from egg
EWG	electron withdrawing group
EPR	electron paramagnetic resonance
ESI	electrospray ionization
ETC	electron transport chain
GPX	glutathione peroxidase
GSH	glutathione
GSSG	glutathione disulfide
HAT	hydrogen-atom transfer
HOMO	highest occupied molecular orbital
HPLC	high-pressure liquid chromatography
IMM	inner mitochondrial membrane
IP	ionization potential
KIE	kinetic isotope effect
KSE	kinetic solvent effect

LOOH	lipid hydroperoxides
LOX	lipoxygenase
LUMO	lowest unoccupied molecular orbital
MeOAMVN	2,2'-azobis(4-methoxy-2,4-dimethylvaleronitrile)
MPT	mitochondrial permeability transition
NADPH	nicotinamide adenine dinucleotide phosphate
NHE	normal hydrogen electrode
OMM	outer mitochondrial membrane
PBS	phosphate buffered saline
PCET	proton coupled electron transfer
PQ	N,N′-dimethyl-4,4′-bipyridinium dichloride, ParaQuat
PUFA	polyunsaturated fatty acid
PMHC	2,2,5,7,8-pentamethyl-6-chromanol
ROO•	alkyl peroxyl
ROOH	alkyl hydroperoxide
ROS	reactive oxygen species
RTA	radical trapping antioxidant
SOD	superoxide dismutase
SOMO	singly occupied molecular orbital
TEMPO	(2,2,6,6-tetramethylpiperidin-1-yl)oxyl
THN	tetrahydronaphthyridinol
THF	tetrahydrofuran
TPP	triphenylphosphonium
TTP	tocopherol transport protein

Chapter 1: Background and Significance

The oxidation of hydrocarbons is ubiquitous in Nature and notably results in the degradation and/or dysfunction of essential biomolecules such as lipids, proteins, DNA,[1] and petroleum-derived synthetic products such as oils, lubricants and polymers.[2] A battery of reactive oxygen species (ROS, **Scheme 1.1**) can originate from (triplet) molecular oxygen through single electron transfer and reactions with other radicals to form highly oxidizing species that can react in a variety of ways. For example, the extremely reactive hydroxyl radical can arise from single electron transfer from hypochlorous and peroxynitrous acid, or directly from hydrogen peroxide. *In vivo*, some ROS contribute to normal defense and signaling pathways intrinsic to cellular redox balance.[3] However, the accumulation of ROS beyond "normal" levels contributes to oxidative stress (**Figure 1.1**) and is at the core of the 'free-radical theories' of many detrimental biological conditions including aging,[4] ischemia reperfusion injury (IRI),[5] neurodegeneration,[6,7] and cancer.[8,9]

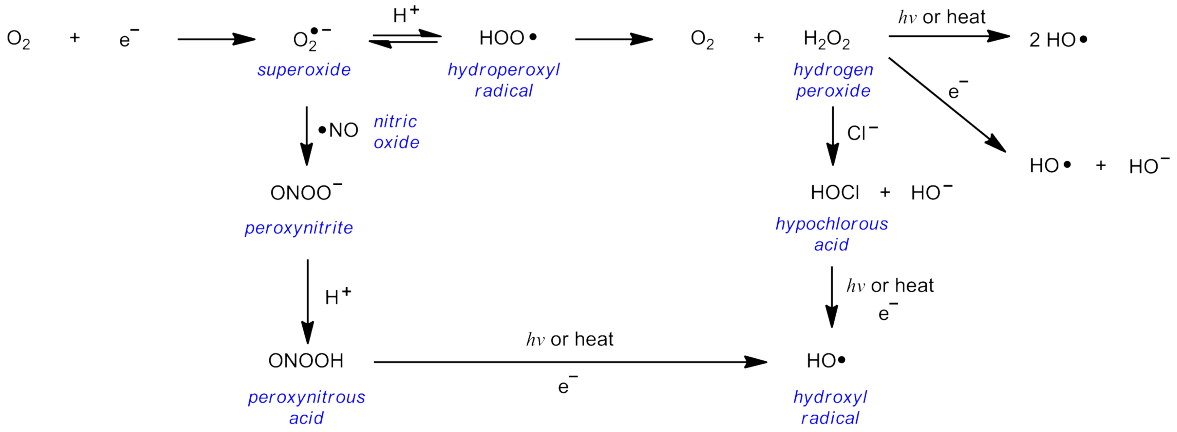

Scheme 1.1 Examples of reactive oxygen species that can arise from one electron reduction of molecular oxygen.[10]

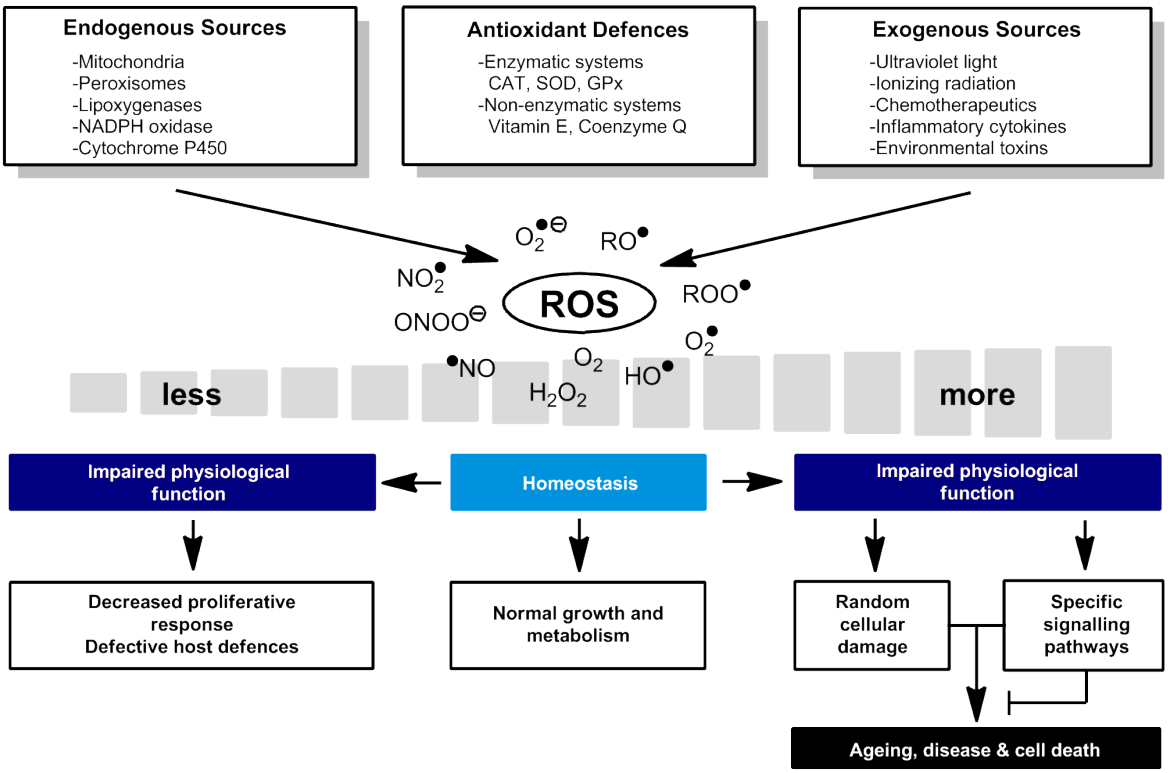

Figure 1.1 The physiological outcome of various sources of ROS based on relative concentrations *in vivo*. Adapted from reference 4.

1.1 Reactive Oxygen Species and Lipid Peroxidation

1.1.1 Endogenous Sources of ROS

ROS are formed spontaneously from normal metabolism, but are also deliberately generated (**Figure 1.2**) for pathogen defense and signaling. The best-studied systems include myeloperoxidase (MPO), and the flavoenzymes nicotinamide adenine dinucleotide phosphate (NADPH) oxidase and xanthine oxidoreductase (XOR).[11]

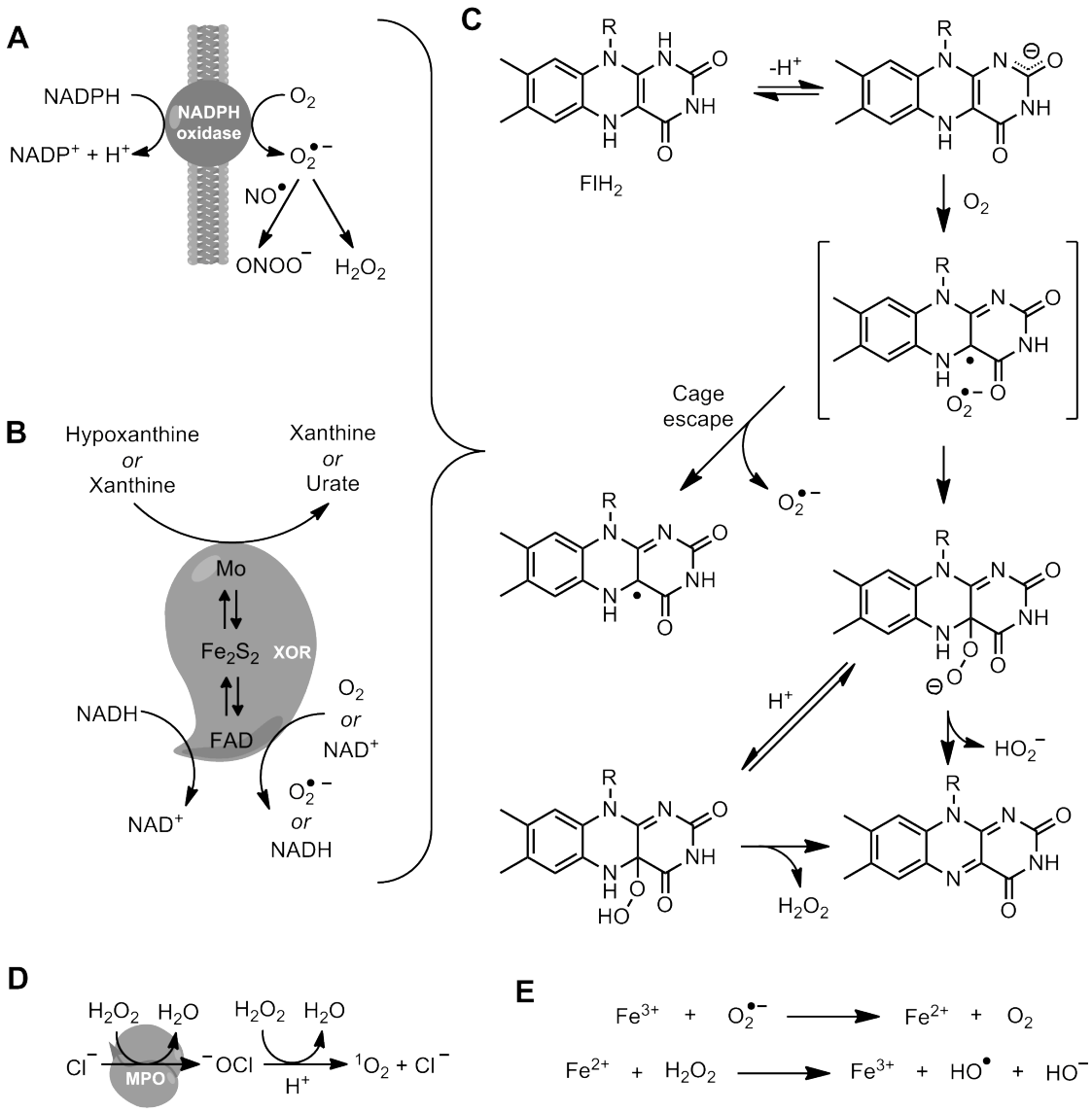

Figure 1.2 Major sources of ROS *in vivo* from the flavoenzymes NADPH oxidase (**A**) and xanthine oxidoreductase (**B**) from which the reduced form of $FADH_2$ can react with oxygen to produce superoxide and other oxidants (**C**). Heme-based myeloperoxidase (MPO) (**D**) and elemental iron and also produce potent oxidants via Fenton chemistry (**E**).

Our immune system employs activated leukocytes that express NADPH oxidase to generate a burst of superoxide from one electron reduction of O_2 by NADPH in response to invaders (**Figure 1.2A**). Similarly, XOR present in milk and sera can produce superoxide (**Figure 1.2B**),[12] possibly for bacterial defense,[13] and neutrophil granulocytes express MPO that oxidizes chloride to hypochlorite (**Figure 1.2D**).[14] The production of superoxide from

NADPH oxidase and XOR arises from the reaction of reduced flavin of $FADH_2$ (FlH_2) with molecular oxygen, which after cage escape yields superoxide, or after a spin flip yields flavin hydroperoxide (**Figure 1.2C**).[12,15] MPO, and other heme-based proteins such as cytochromes P450, generate ROS through Fenton chemistry via the redox cycling iron II/III couple. The highly reactive HO• is also produced natively through Fenton chemistry from reaction of low valent transition metals such as iron and copper with hydrogen peroxide (or alkyl hydroperoxides) (**Figure 1.2E**).[16]

Mitochondria are often regarded as the largest source of cellular ROS. Mitochondria are small organelles featuring double membrane morphology with the inner membrane folded into itself forming cristae. The respiratory machinery of mitochondria is embedded in the inner membrane, and is composed of the four core complexes I-IV, numbered consecutively in the order with which they pass electrons originating from electron carriers NADPH and succinate (**Figure 1.3A**). An electrochemical gradient is maintained by the complexes I, III, and IV by pumping protons into the intermembrane space bound by the inner and outer membranes, and thus the central matrix is negatively charged. This electrochemical gradient generates a protonmotive force (Δp) and allows ATP synthase to produce the majority of ATP that cells use. The nominal electron flow through these pathways constitutes the electron transport chain (ETC). Some subunits of the ETC proteins are synthesized solely in the mitochondria, whereas other are translocated to the mitochondria following nuclear transcription (**Figure 1.3B**).[17]

The ETC contains a variety of redox active components between +0.39 V (cytochrome a_3, complex IV) and −0.32 V (NADPH) *vs* SHE. This reducing environment contains many species capable of transferring electrons to oxygen, which has standard

reduction potential to superoxide of −0.16 V *vs* SHE. These species include ubisemiquinone (**Figure 1.3C**), iron-sulfur clusters and flavoproteins.[18] Complexes I and III have been implicated in isolated mitochondria as the sites of major ROS generation under normal and abnormal conditions.[19]

Complex I has been shown to generate the greatest levels of superoxide under conditions when electron transport is prevented and subsequent ATP production is low. This occurs in two particular situations: *i*) with high $CoQH_2$:CoQ ratio and high Δp, and *ii*)

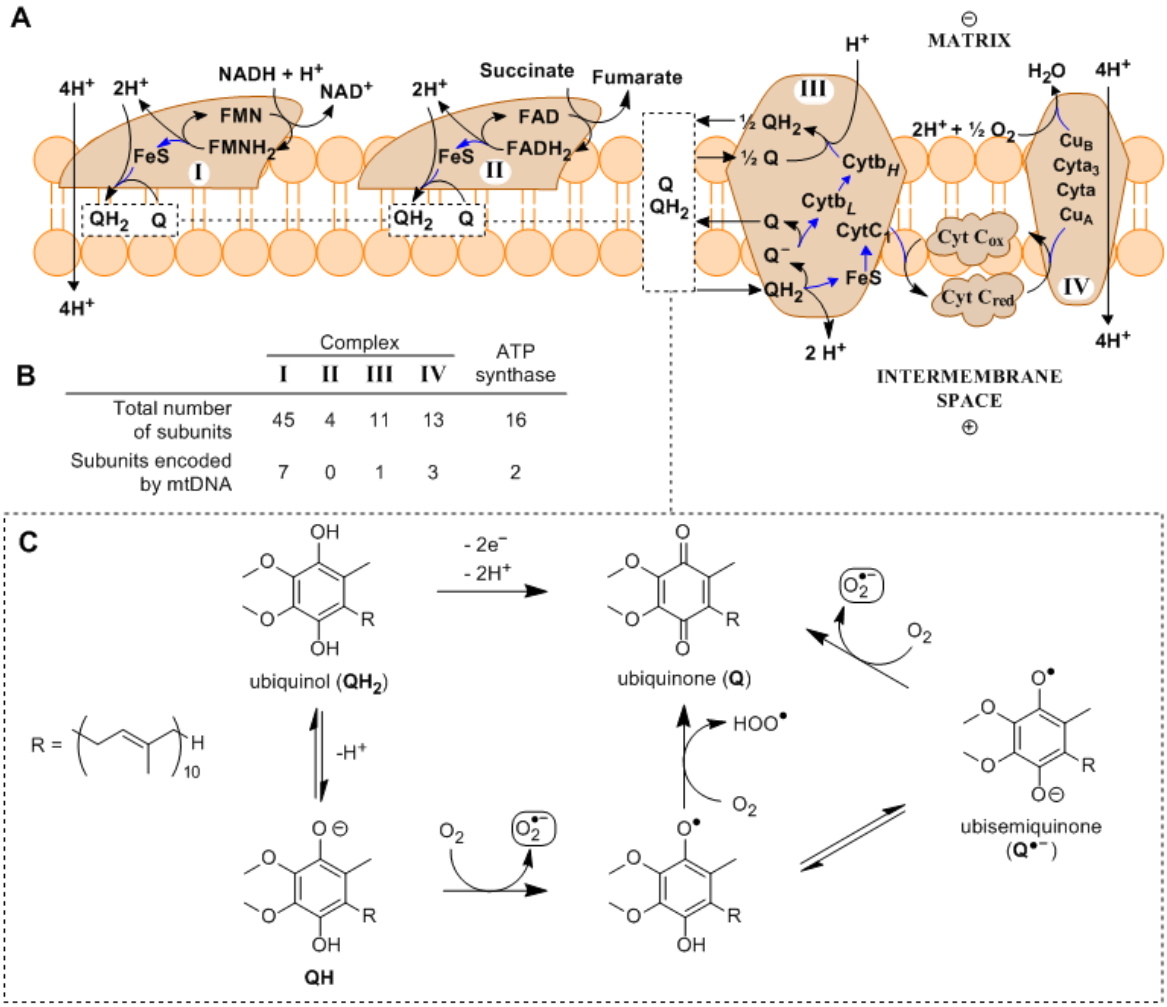

Figure 1.3 (**A**) The electron transport chain is embedded in the inner mitochondrial membrane. Blue arrows: electron transfer. Adapted from reference 20. (**B**) Subunits of the ETC are transcribed both in the mitochondria and from nuclear DNA.[17] (**C**) The cycles of the ubiquinone/ubiquinol pool that can produce superoxide.

with an elevated NADH/NAD^+ ratio. Under the former condition, excess electrons carried by QH_2 undergo reverse electron transport (RET) and are forced back to Complex I, which reduces flavin mononucleotide (FMN) that in turn reduces NAD^+ to NADH (**Figure 1.2C**). A Complex I inhibitor, rotenone, can bind to the CoQ-binding site and abolish superoxide production under these conditions. The exact site of superoxide production under RET conditions is not known, however it could be related to the latter condition, wherein an elevated NADH/NAD^+ ratio fully reduces FMN, and FMN directly reacts with O_2 to produce superoxide (**Figure 1.2C**).[21] Under these conditions, rotenone *increases* superoxide generation. There is likely an interplay between the two conditions, which is borne out experimentally when trying to accurately measure ROS production both in isolated mitochondria and in cells. The methods used are generally regarded as unreliable due to the high dependence on NADH/NAD+ ratio, membrane Δp, $CoQH_2$:CoQ ratio, and local oxygen concentration—not to mention redox sensitive messaging, activation of the pro-apoptotic machinery and superoxide dismutase (SOD) activity.[19]

The fates of superoxide are numerous; it can be rapidly dismutated to hydrogen peroxide and water by SOD (2×10^9 $M^{-1}s^{-1}$), or react with nitric oxide (6.7×10^9 $M^{-1}s^{-1}$) to produce peroxynitrite (**Figure 1.4**).[22] SOD1 (CuZnSOD) is the isoform present in the intermembrane space and cytoplasm, while SOD2 (MnSOD) is synthesized in and unique to the mitochondrial matrix. As a result of these antioxidant defenses, the steady state concentration of hydrogen peroxide and superoxide in the mitochondrion has been estimated to be $1\sim5\times10^{-10}$ M.[23]

Respiratory chain inhibition resulting from mutations, ischemia, cytochrome c loss and ETC uncouplers can result in oxidative stress. Various small molecule inhibitors have

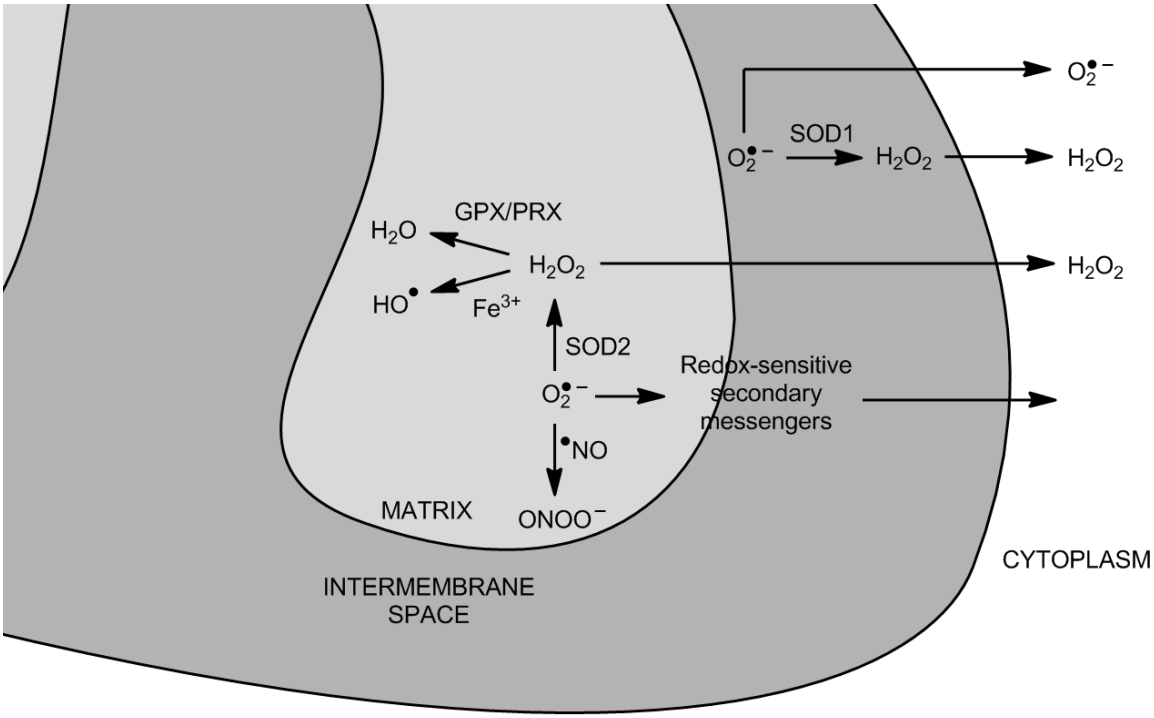

Figure 1.4 The fates of superoxide in the mitochondria. Adapted from reference 24.

been discovered and developed to model oxidative stress, and are discussed further in Chapter 3.

1.1.2 Preventative antioxidants

Aerobic organisms have evolved to strike a balance between the production of ROS from respiration or defense/signaling and protection from their inherent detrimental effects through elaborate antioxidant defense strategies. This has been especially realized since the discovery of superoxide dismutase (SOD) in 1969,[58] and accordingly research in oxidative stress has increased exponentially in the past decades (**Figure 1.5**).

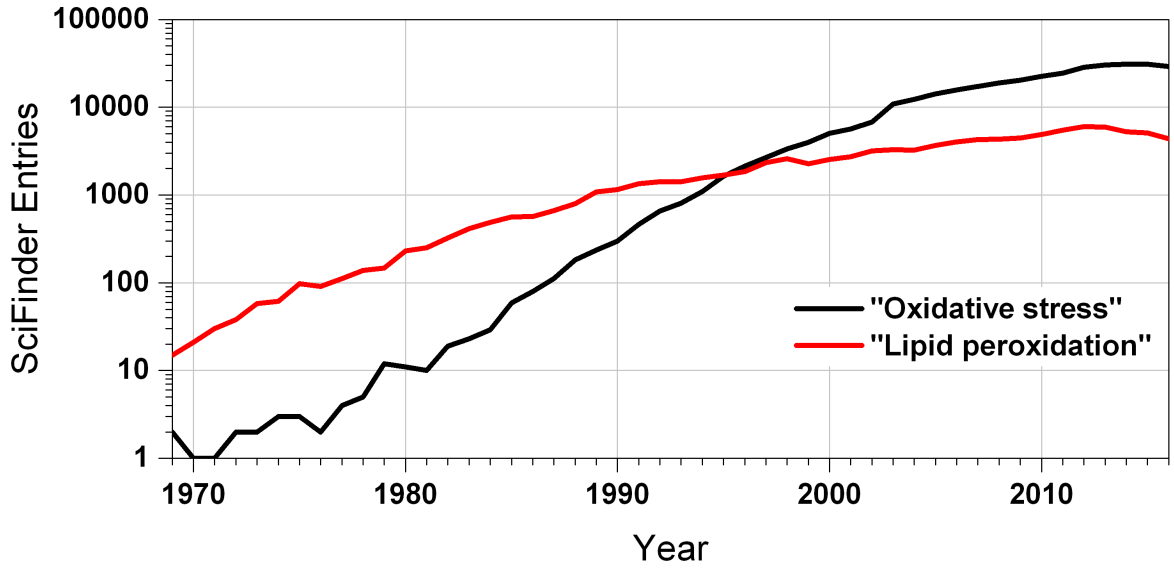

Figure 1.5 Annual (non-cumulative) SciFinder[25] entries for "Oxidative stress" and "Lipid peroxidation" since 1969, when SOD was discovered.

SODs are metalloenzymes that are a critical part of the cell's antioxidant defense as they catalyze the dismutation of superoxide to hydrogen peroxide and oxygen (**Figure 1.6**).

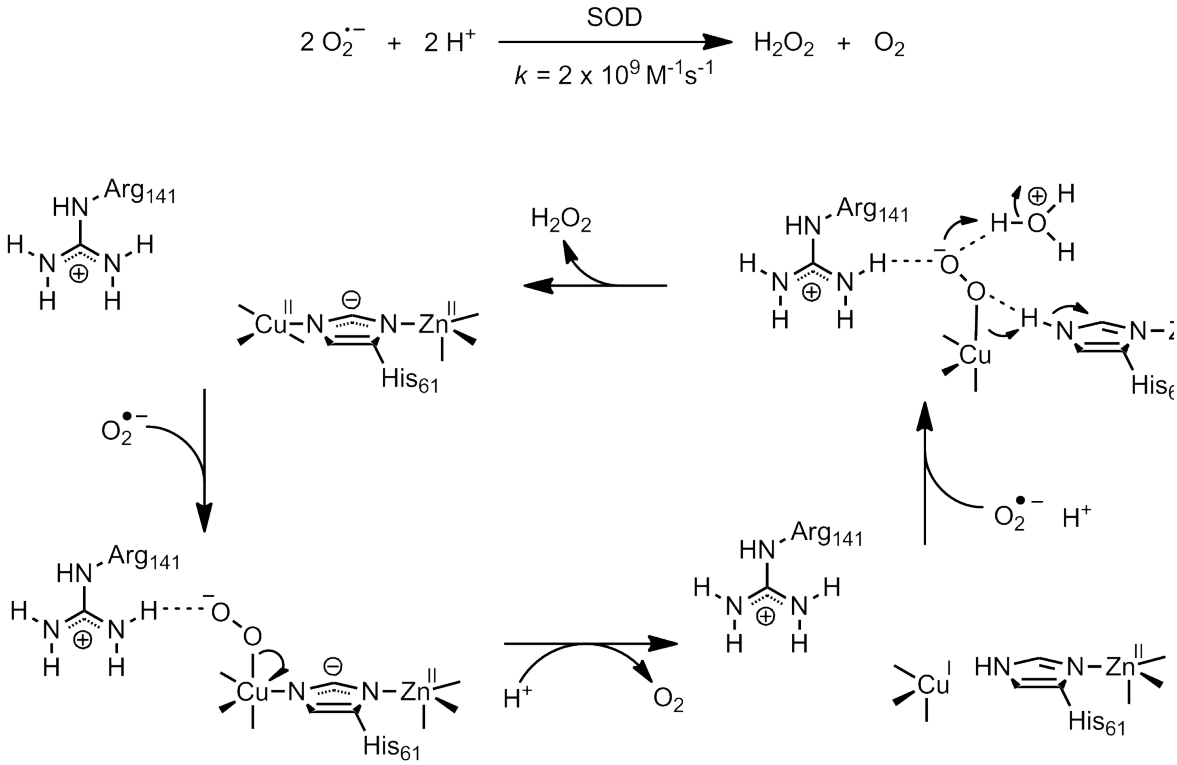

Figure 1.6 Mechanism of superoxide dismutation by CuZnSOD.[26]

SOD reacts at near diffusion-controlled rates with superoxide. The active sites of SODs vary between isoforms and can have metals such as: Cu and Zn (cytosolic isoform), or Mn or Fe (mitochondrial isoform).[26] Hydrogen peroxide levels in cells are then kept in balance by catalase (CAT) and glutathione peroxidases (GPX) (**Figure 1.7A**). GPX's are selenoenzymes that react with hydroperoxides to produce the corresponding alcohols. The selenol is then reduced by glutathione to regenerate the enzyme (**Figure 1.7B**). The exact mechanism has yet to be firmly established, though a catalytic tetrad is conserved between GPX homologs (**Figure 1.7C**).[27]

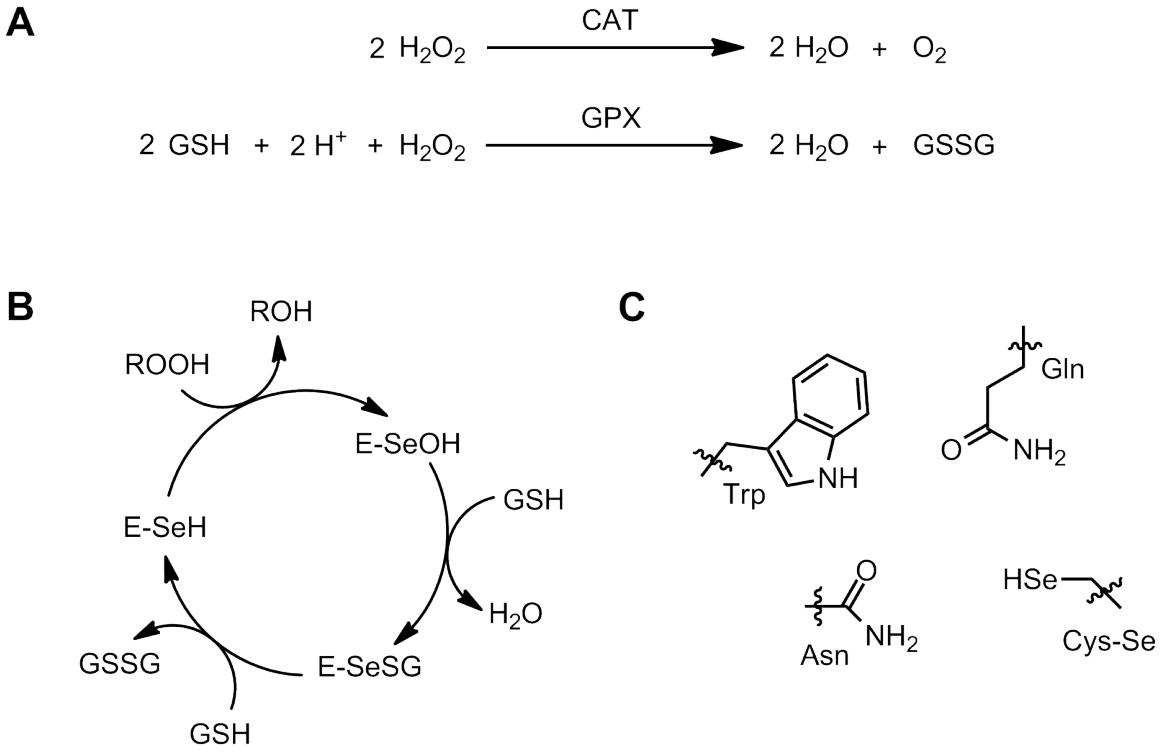

Figure 1.7 Hydroperoxides are detoxified to the corresponding alcohols by CAT and GPX (**A**). Mechanism of hydroperoxide reaction with selenoenzymes and glutathione cofactors (**B**). Catalytic tetrad in the active site of GPX enzymes (**C**).[27]

1.1.3 Lipid peroxidation

Lipids—nature's hydrocarbons—are particularly susceptible to oxidation *in vivo*. Biological membranes and lipoproteins comprise of a variety of lipids, and exploit the amphipathic nature of phospholipids to afford a phase separation between organic and aqueous phases. The interior organic phase is composed of the hydrocarbon tails that are bound to polar phosphate head groups resting at the aqueous interface (**Figure 1.8**). This can physically bar large molecules from diffusion, and small charged species such as superoxide from passage. The diverse lipids serve a myriad of purposes such as: signaling, energy storage, structural integrity, and membrane fluidity.[28]

The unsaturation present in the structure of these various fatty acids and steroids is thought to contribute to maintaining membrane fluidity by introducing 'kinks' in the hydrocarbon tails. However, the critical *reactivity* of these unsaturated C-H bonds, such as in cholesterol (C_7-H BDE = 83 kcal/mol),[29] and bisallylic C-H bonds of polyunsaturated

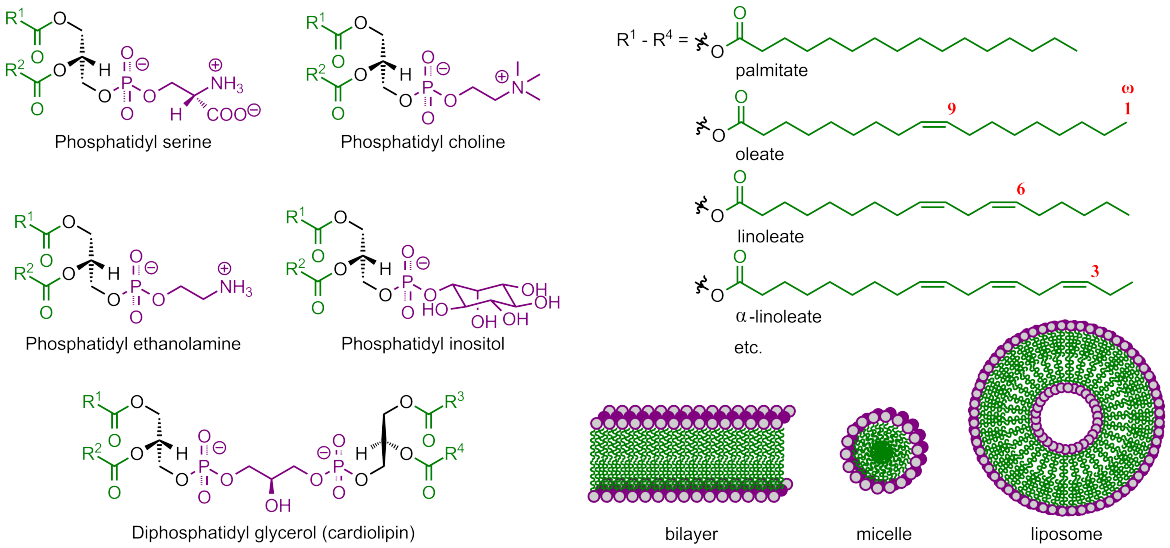

Figure 1.8 Common classes of glycerophospholipids (left) composed of triesterified glycerol (black) with various fatty acid side chains (green, right) and various polar head groups (purple), which assemble as bilayers, micelles and liposomes.

fatty acids (PUFA, BDE = ~76 kcal/mol)[30] leads to formation of stabilized carbon centered radicals that rapidly combine with molecular oxygen ($k \sim 2 \times 10^9$ $M^{-1}s^{-1}$).[31] The fates and disease relevance of the resultant lipid peroxyl radicals form the basis for intensive research into the products, kinetics and mechanism of their reactions. Porter made notable advances in the field in 1970's[32,33] with inhibited hydrocarbon autoxidation work pioneered by Ingold.[34,35]

1.1.4 Mechanism of lipid autoxidation

Lipid autoxidation follows the archetype radical chain reaction of hydrocarbon autoxidation involving initiation, propagation and termination events.

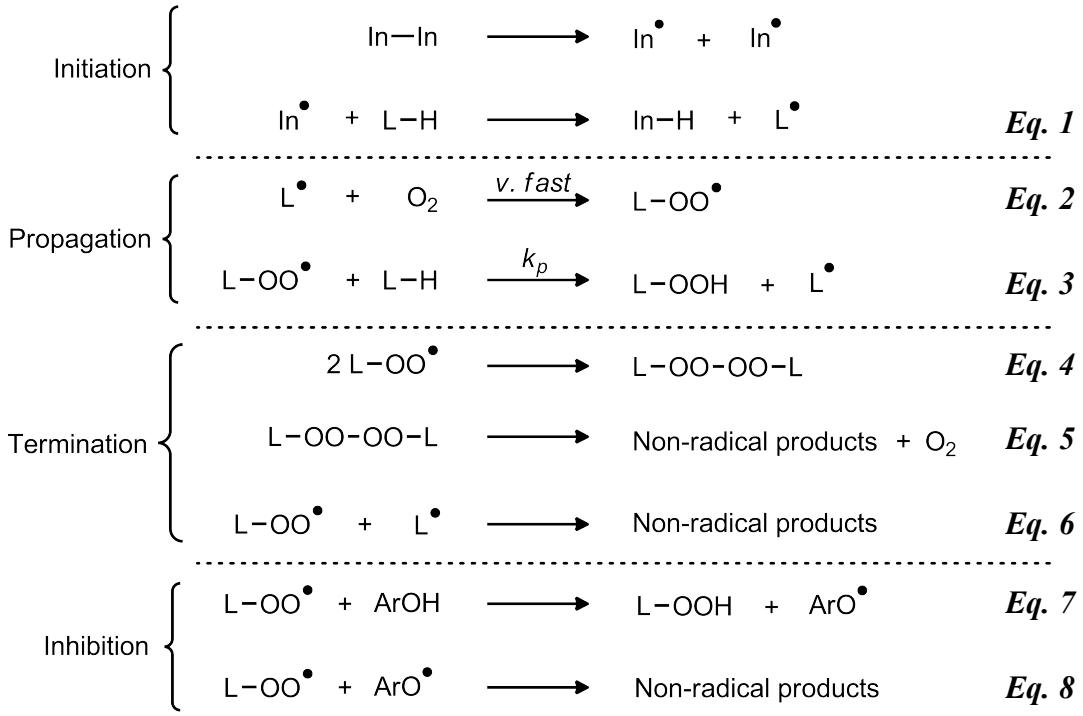

Initiation involves generation of a lipid-based alkyl radical, L• (***Eq. 1***), which can occur via abstraction of a H-atom from one of the activated C-H bonds of mono- and polyunsaturated lipids (**Figure 1.9A**) to form stabilized allylic or bisallylic carbon-centered radicals. In principle, any event that generates a radical can be an initiation event, such as:

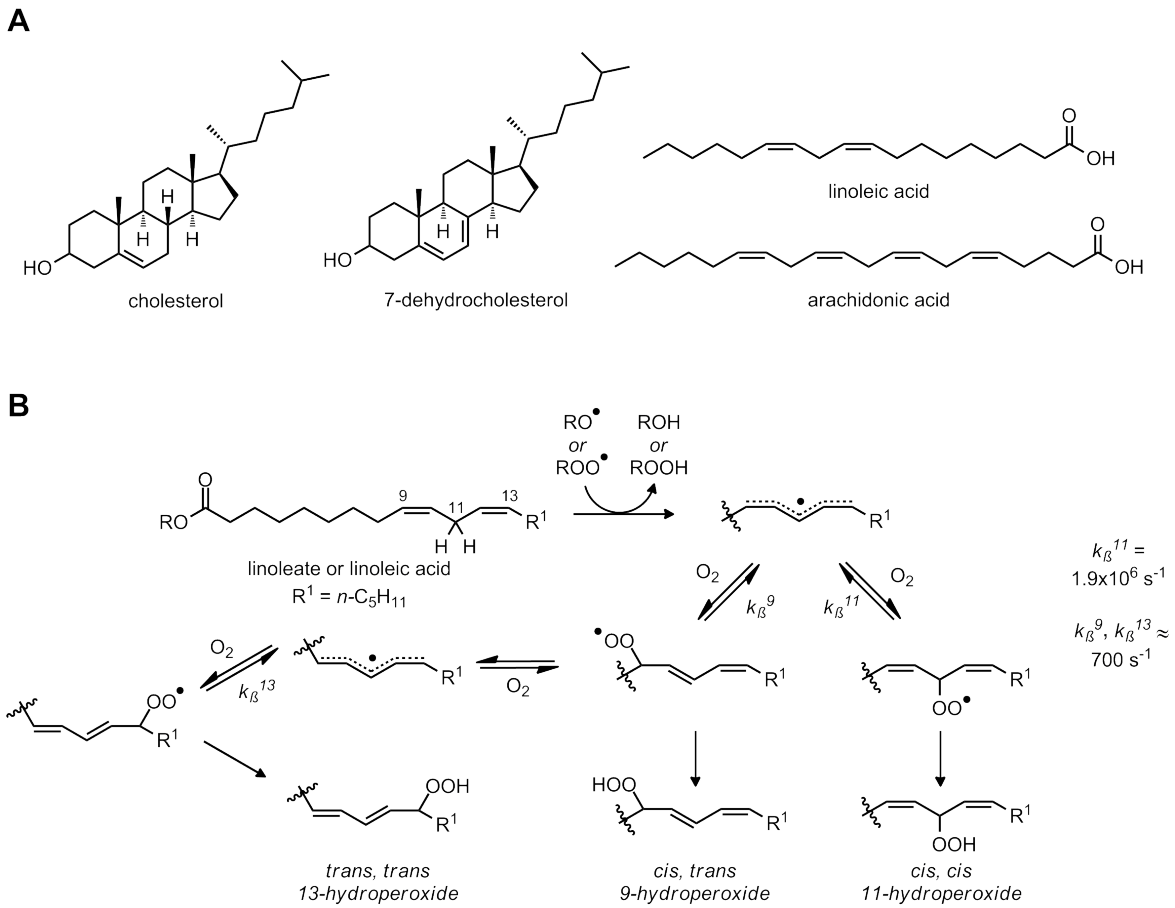

Figure 1.9 Highly autoxidizable lipophilic biomolecules (**A**). The primary products of linoleate autoxidation (**B**). Adapted from reference 36.

decomposition of lipid hydroperoxyls (LO−OH) to highly reactive alkyoxyl (LO•) and hydroxyl (•OH) radicals, decomposition of azo-initiators (R-N=N-R), Fenton-type chemistry with transition metals (**Figure 1.2E**), and irradiative stressors (*e.g.* UV, X-ray or gamma irradiation).

Propagation of the radical chain reaction occurs by very rapid addition of oxygen to a carbon-centered radical[31] to accumulate lipid peroxyl radicals, L-OO• (***Eq. 2***). These peroxyl radicals further propagate by H-atom abstraction to result in more lipid radicals (***Eq. 3***). The key propagation rate constant, k_p, is much slower than oxygen addition, making it the rate-limiting step of autoxidation.

Termination events involving high-energy radicals such as carbon-centered radicals are relatively fast (***Eq. 6***), however these reactions have to compete with their reaction with O_2, which is generally present in the millimolar range, and thus termination events generally comprise only of the peroxyl-peroxyl radical reaction (***Eq. 4***). This reaction is known to lead to accumulation of lipid-derived electrophiles such as aldehydes (***Eq. 5*** & **Scheme 1.2**),[37] which are implicated in the downstream effects of peroxidation such as their reaction with DNA and proteins.[38,39] The overall rate constant of termination is quantified by k_t.

Research by Porter *et al.* has demonstrated that the product distribution of lipid-derived peroxides is quite diverse owing to numerous factors. For example, oxygen can add to the 9-, 11- or 13-position of the delocalized pentadienyl radical derived from

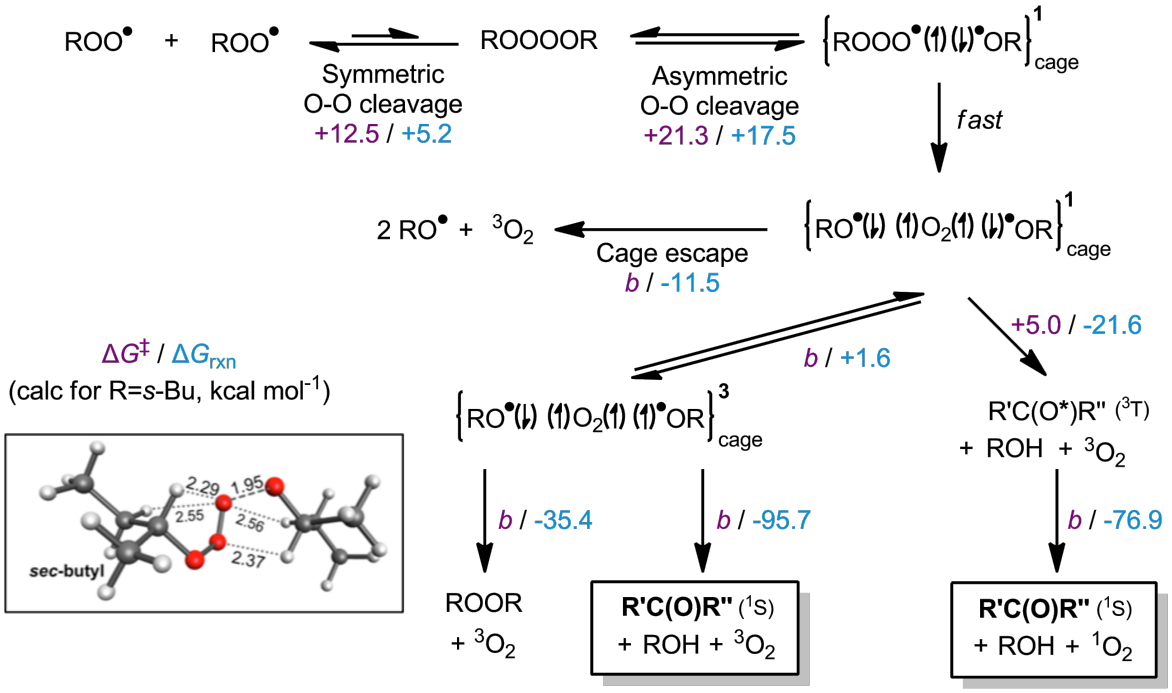

Scheme 1.2 Termination mechanism of peroxyl radicals resulting in formation of carbonyl electrophiles. *b*, barrierless. Inset: transition state of tetraoxide decomposition, facilitated by C_α H-bonds (2.37Å and 2.29Å).[37]

linoleate. Importantly, oxygen addition is *reversible*. The fragmentation is characterized by the β-fragmentation rate constant, k_β, which is three orders of magnitude greater from the 11-peroxyl compared to the 9- and 11-peroxyl; thus, the 11-hydroperoxide is not observed unless a very fast H-atom donor can trap the 11-peroxyl before it fragments since rearrangement to the thermodynamic *trans, trans* and kinetic *cis, trans* conjugated products is favoured.[40] The product distributions arising from arachidonate autoxidation are much more complex, since intramolecular cyclizations of peroxyl radicals can lead to isofurans, endoperoxides (prostaglandins), and aldehydes.

Lipid peroxides also result enzymatically from the activities of lipoxygenase (LOX, **Scheme 1.3**)[41] and cyclooxygenase (COX) enzymes. Different isoforms of these enzymes produce stereospecific lipid hydroperoxides, whereas autoxidation results in mixtures dictated by thermodynamics and kinetics.

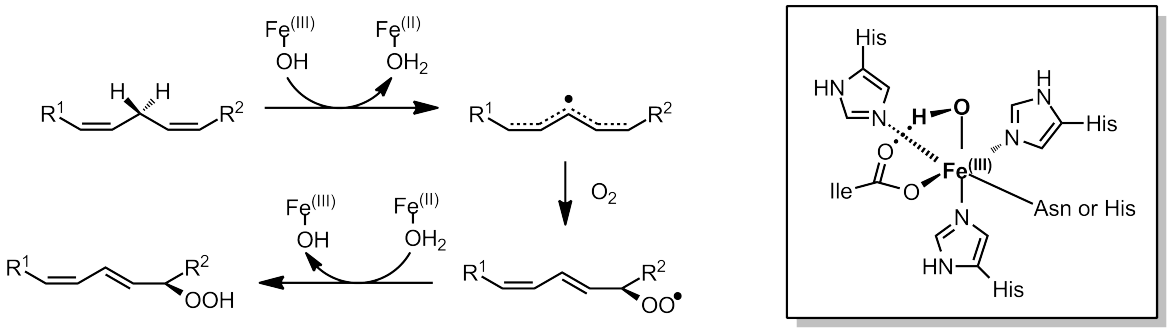

Scheme 1.3 Mechanism of lipid hydroperoxide formation by LOX enzymes. Inset: Active site iron(III)-OH in rabbit 15-LO.[42]

1.2 Inhibition of Lipid Autoxidation by Phenolic and Aminic Radical Trapping Antioxidants

Cells have native antioxidant defenses that aim to reduce the rate of the initiation step of autoxidation. They include enzyme families previously discussed such as GPX, CAT and SOD. With the exception of GPX4, these large proteins are sequestered from the lipid domain. Such defenses are considered *preventative antioxidants* as they lower the rate at which *new* radical chains are produced. Antioxidants that function to inhibit the propagation of the radical chain reaction, *i.e.* quenching LOO• before it can further produce initiating radical species, are termed *chain-breaking antioxidants* or *radical-trapping antioxidants* (RTAs).

The goal of understanding the role of endogenous antioxidants has driven efforts towards discovery of novel—often naturally-derived—antioxidants, and thus methodology to accurately determine a putative RTA's mechanism of action and kinetics remains of utmost importance.

1.2.1 Methods of evaluating RTA efficacy

The kinetics of radical trapping antioxidant activity are best evaluated by the inhibited autoxidation methodology (**Figure 1.10**).[34] The experiments employ an excess of autoxidizable substrate and oxygen, and a small amount of initiator such as dialkyl azo compounds or alkyl hydroperoxides. The azo-initiator decomposes at a constant rate over the course of the reaction to ensure a small, steady state concentration of radicals—and thereby maintains a chain reaction of the substrate as long as oxygen is present. The reactions are reliably monitored via O_2 uptake by differential pressure measurements

between the reaction (RTA untreated) and an inhibited (RTA treated) reaction under investigation.

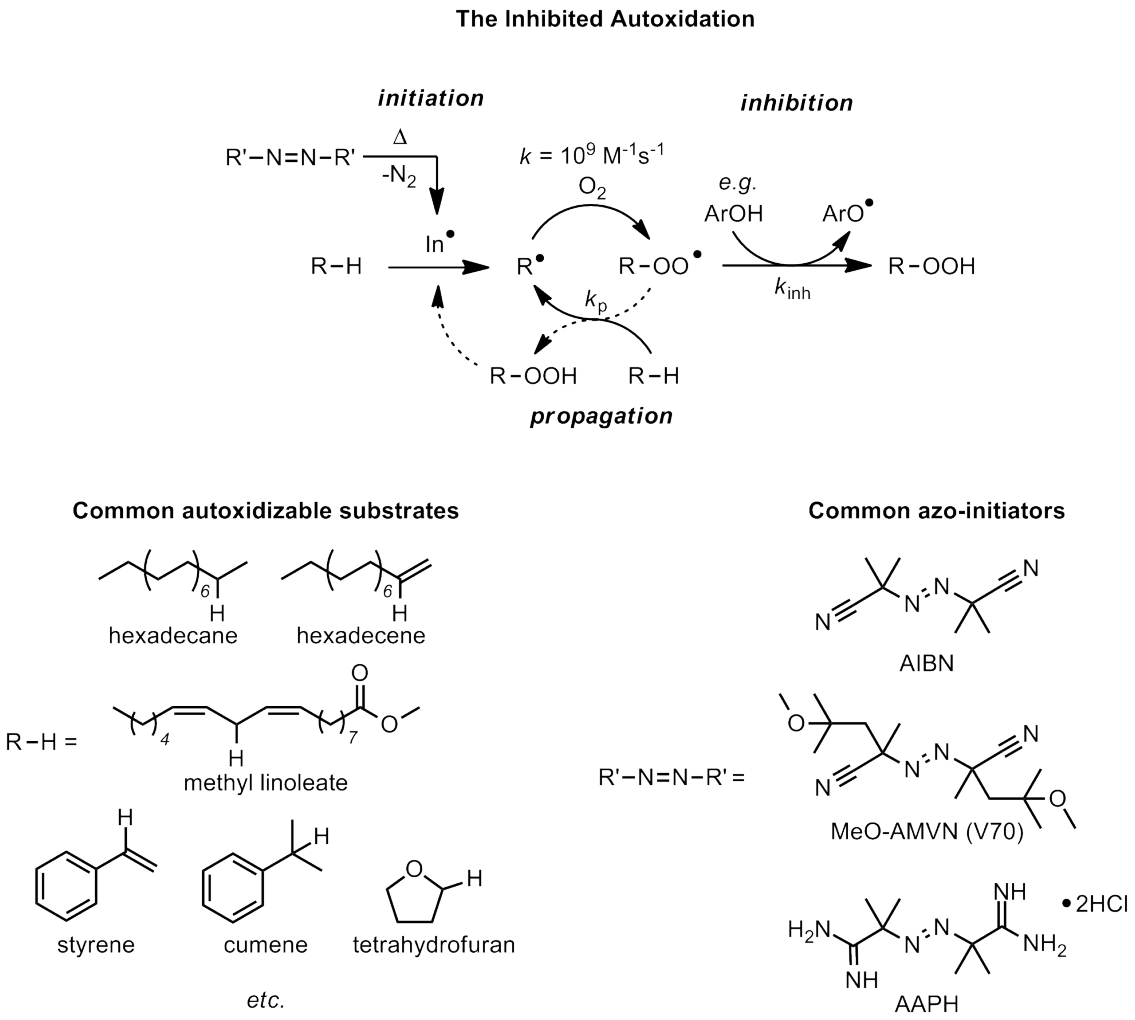

Figure 1.10 The general inhibited autoxidation scheme with common autoxidizable substrates and azo-initiators.

A sample autoxidation plot by oxygen consumption in shown in **Figure 1.11**. The uninhibited rate (A) depends on the propagation and termination rates of the autoxidizable substrate and rate of initiation from the initiator (***Eq. 9***).

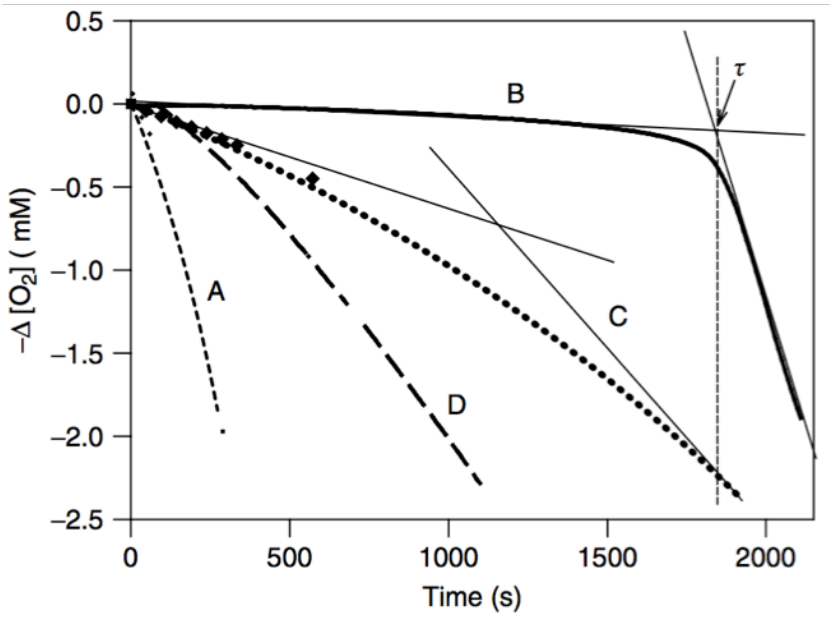

Figure 1.11 Representative autoxidation plot monitored by oxygen consumption uninhibited by an RTA (**A**). Representative antioxidants of excellent (**B**), average (**C**) and modest (**D**) reactivities inhibit the reaction relative to the untreated control. $\tau \equiv t_{inh}$. Reproduced from reference 52.

$$\frac{-\mathrm{d}[O_2]}{\mathrm{d}t} = \frac{-\mathrm{d}[RH]}{\mathrm{d}t} = \frac{\mathrm{d}[ROOH]}{\mathrm{d}t} = \frac{k_p}{\sqrt{2k_t}}\sqrt{R_i}[RH]_0 + R_i \qquad \textit{Eq. 9}$$

The slope of the inhibited region of an RTA treated reaction is used to derive the inhibition rate constant, k_{inh} (also k_7, above), ***Eq. 10***. The intersection of the lines formed from the inhibited region and uninhibited region give the inhibition time, or t_{inh}. By standardizing with an antioxidant of known stoichiometry (often PMHC, n = 2), both R_i and the number of radicals trapped by a RTA can be determined by ***Eq. 11***.

$$\frac{-\mathrm{d}[O_2]}{\mathrm{d}t} = \frac{k_p[RH]R_i}{2k_{inh}[ArOH]} + R_i \qquad \textit{Eq. 10}$$

$$n = \frac{\tau \times R_i}{[ArOH]_0} \qquad \textit{Eq. 11}$$

Reaction progress in inhibited autoxidations can also be monitored 'discontinuously' by analyzing aliquots of the reaction over time by a variety of methods, including: iodometric titration of hydroperoxides; utilizing an ROOH sensitive phosphine probe,[43] or; directly quantifying hydroperoxides (often reduced to their alcohol form) by HPLC.[44] These methods suffer from laborious and lengthy procedures. The latter method is effective with small, predictable product distributions, however, complex mixtures composed of hydroperoxide isomers, polymers, *etc.* can arise from the chain reactions. Other methods used to determine RTA activity include peroxyl radical clocks,[45] electron paramagnetic resonance spectroscopy, laser flash photolysis and pulse radiolysis.[44]

Work in our group has complemented conventional autoxidation approaches by adapting methodology inspired by the lipid oxidation indicator C11-BODIPY$^{581/591}$® that is often used in cell assays.[46] This probe features a phenylbutadiene moiety conjugated to a BODIPY fluorophore that undergoes a fluorescence shift upon oxidation. Haidasz *et al.* demonstrated that both inhibition kinetics and stoichiometry can be accurately determined by co-autoxidation of analogous BODIPY probes with various hydrocarbon substrates.[47] The reaction is continuously monitored by consumption of the BODIPY dye through absorbance spectrophotometry—much more convenient than the conventional methods described above. The inhibition kinetics and stoichiometry can then be derived from the absorbance traces once the rate constants at the appropriate temperature and substrate/solvent are determined: k_t for the exact substrate, and; k_p for the probe in that substrate.

1.2.2 Radical-trapping antioxidants

Nature's best lipophilic RTA is α-tocopherol (α-TOH), a member of the tocopherol family of lipid-soluble phenols. The radical-trapping mechanism has been well studied and follows the mechanism of phenols, where an H-bonded complex between the phenol O-H and peroxyl O• facilitates a proton coupled electron transfer (PCET) reaction. PCET is distinct from H-atom transfer (HAT) in that the electron and proton are transferred between different pairs of orbitals[48]—in this case, the proton moves between nominal lone pairs on the phenolic oxygen atom and the terminal oxygen atom of the peroxyl radical while an electron moves between the approximately orthogonal phenol π-HOMO and the π*-SOMO of the peroxyl radical. This yields the stabilized phenoxyl radical and ROOH (**Scheme 1.4A**). Among the fates of the resultant phenoxyl radical, the fastest reaction traps another peroxyl radical ($k = 10^8$ $M^{-1}s^{-1}$)[49] in the para position to yield a quinone (**Scheme 1.4B**). The overall inhibition reaction reliably yields a net stoichiometry of 2 radicals trapped per molecule of RTA.

The mechanism and rate constant for the initial peroxyl trapping event is dependent on solvent and phenol substitution. The H-bond accepting and anion solvation ability of the solvent is especially relevant in the biological (aqueous) environment since *i*) H-bonding to

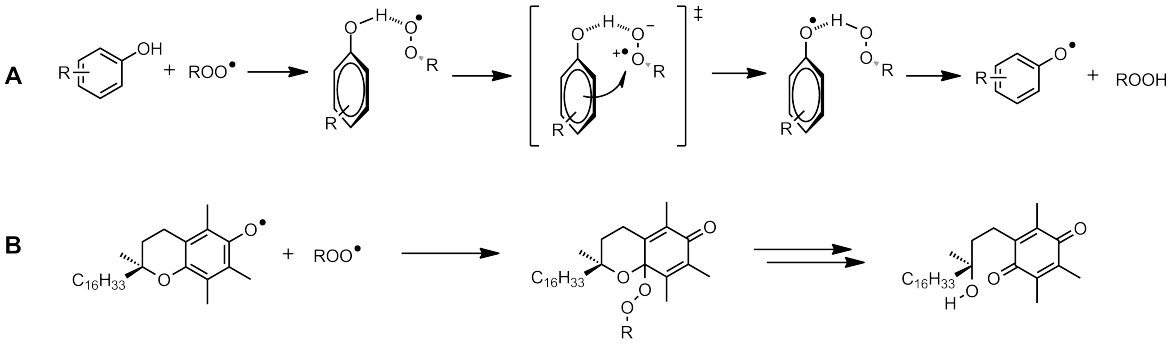

Scheme 1.4 The RTA mechanism of phenols and tocopherols.

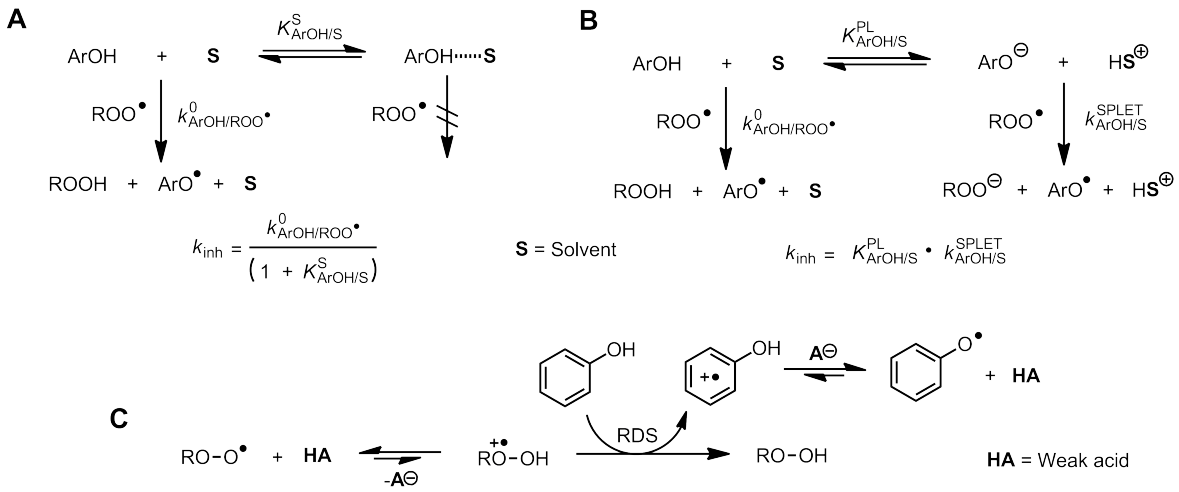

Scheme 1.5 The effect of hydrogen bond accepting (**A**), basic (**B**) and acidic (**C**) solvents on the mechanism of phenolic RTAs.[44]

phenolic O-H bond prevents formation of the pre-reaction complex in the PCET reaction, thus retarding the initial radical-trapping rate (**Scheme 1.5A**), and *ii*) ionizing solvents promote the equilibrium contribution of phenoxide with phenol (**Scheme 1.5B**), which can react with the peroxyl radical directly by electron transfer, in what has been termed the sequential proton loss electron transfer (SPLET) mechanism.[50]

Another important factor in RTA reactivity is that the RTA-derived phenoxyl radical should be unreactive to the substrate to prevent the RTA from behaving as a chain transfer reagent, or producing radicals, and propagating the chain rather than functioning as a chain-breaking reagent (**Scheme 1.6**).[2,51] This undesired reactivity is favoured with electron rich phenols that are prone to one-electron reduction by oxygen or autoxidation-derived hydroperoxides.

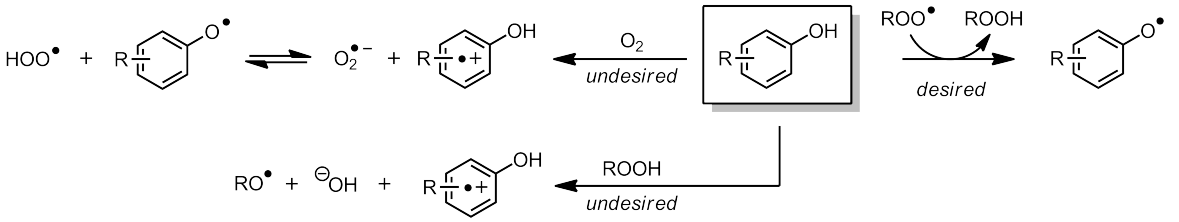

Scheme 1.6 Electron rich phenolic RTAs produce hydroperoxyl radicals by undesired reactions with oxygen or hydroperoxides.

It has been demonstrated that the phenoxyl radical is stabilized to favour the desired reactivity as a function of the extent of orbital overlap by electron donating (ED) heteroatoms with the aromatic π-electron system, and the relative strength of those ED substituents (σ^+).[52] The extent of overlap depends on the angle of the heteroatom lone pair with the aromatic π-system (**Scheme 1.7**).[51] These combined stereoelectronic effects manifest in lowering the BDE of the O-H bond, which has been demonstrated to give an excellent Hammett correlation with the initial radical trapping rate (k_7) of both phenolic[53] ($\rho^+ = -1.58$)[2] and (to a lesser extent) aminic RTAs.[54,55]

While the addition of good ED substituents lowers PhO-H BDE and increases reactivity, very highly ED substituents (*e.g.* NR_2) lowers the ionization potential (IP) to the

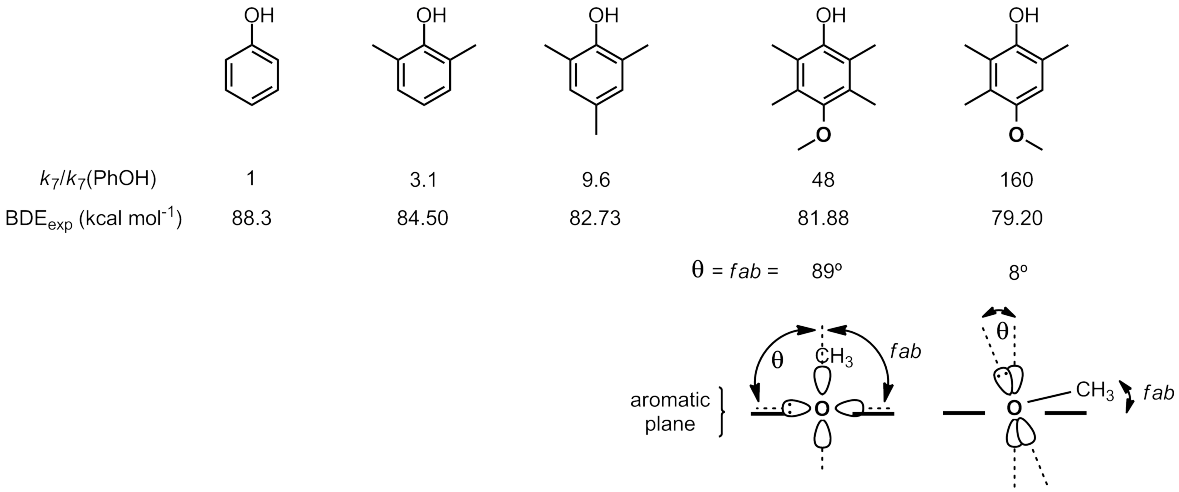

Scheme 1.7 The initial radical trapping rate (k_7) correlates with PhO-H BDE.[2,53] The heteroatom ED ability is maximized when the lone pair (shown as a 2p orbital) has optimal overlap ($\theta \approx 0°$) with the aromatic plane.[2,51]

point of direct reaction with oxygen (**Scheme 1.6**). An ideal RTA balances low BDE without significantly lowering IP, a distinction that was addressed computationally by the observation that nitrogen incorporation into the ring significantly increases ionization potential and only slightly increases BDE (**Scheme 1.7**).[56,57]

This was borne out experimentally when rate enhancements of ~100 fold over α-TOH were measured for the best RTA **2** (**Scheme 1.8**), which results from: ring size of 5 atoms, allowing maximum overlap of the nitrogen lone pair and the aromatic π-system; incorporation of nitrogen in the 5-position, which increases IP enough to prevent direct reaction with oxygen, and; two ED methyl groups. The rational design of these superior, near diffusion-controlled chain-breaking RTAs led to the successful preparation of biomimetic α-TOH analogues: the lipophilic tetrahydronapthyridinols, **1** (THNs), compromising reactivity slightly relative to **2** for greater half-life in solution and ease of preparation.[2,44,57]

1.2.3 The 'superoxide dismutase-mimetic' activity of nitroxides

Since the discovery of superoxide dismutase (SOD) in 1969,[58] considerable interest has been focused on the discovery of novel agents that can catalyze the same reaction as

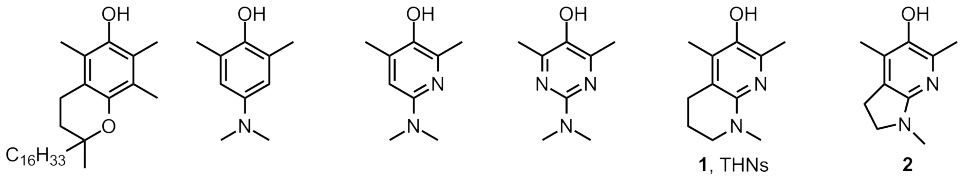

k_7 (10^5 $M^{-1}s^{-1}$)	32	--	160	86	880	2800
BDE_{exp} (kcal mol^{-1})	78.3	(72.3)	77.0	78.2	76.3	75.4
IP_{calc} (kcal mol^{-1})	159.3	152.3	157.7	167.0	154.6	152.3

Scheme 1.8 The RTA activity (k_7) of phenols is maximized by lowering PhO-H BDE without decreasing IP to the point of direct reaction with oxygen.

SOD.[59,60] These agents are collectively known as 'superoxide dismutase *mimetics*' that are thought to function as preventative and/or radical trapping antioxidants. Notably, Samuni *et al.* observed that certain sterically hindered nitroxides possess this SOD mimetic activity against superoxide in a xanthine oxidase *in vitro* assay, and further suggested a mechanism resulting in dismutation of superoxide involving oxidation of a nitroxide with a hydroperoxyl radical (HOO•) followed by reduction of the resultant oxoammonium ion by superoxide ($O_2^{-\bullet}$) (**Scheme 1.9A**).[61,62,63,64,65] An alternative redox cycle of nitroxides can be envisioned to involve reduction by $O_2^{-\bullet}$ first (**Scheme 1.9B**), though a wealth of evidence suggests an oxoammonium ion as a catalytic intermediate.[62,63]

In addition to nitroxides' SOD mimetic activity, several groups have reported inhibition of lipid peroxidation by lipophilic hindered aliphatic nitroxides, such as TEMPO. This has been demonstrated through reduction kinetics by EPR,[66,67,68,69] antioxidant activity by the TBARs assay[67,68,70] inhibition of oxygen consumption,[66] conjugated diene formation,[67,71] malondialdehyde production[72] and, lipid hydroperoxide formation.[66,67] Further, nitroxides have been demonstrated to mitigate disease in animal models of oxidative stress, such as IRI injury,[73] aging,[74] and neurodegenerative disease.[75]

While the precedence for the unique reactivity of nitroxides to ameliorate oxidative stress is clear, several questions exist regarding the mechanistic proposals in the literature.

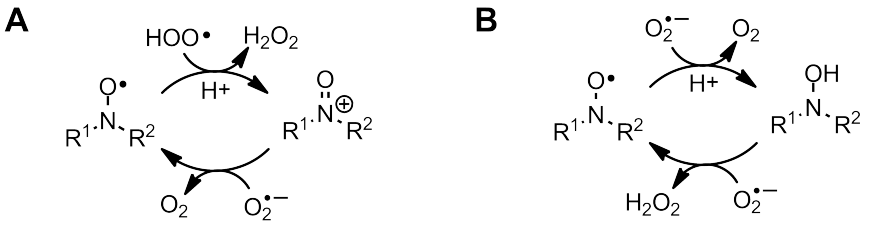

Scheme 1.9 Possible mechanisms proposed in the literature for 'superoxide dismutase-mimetic' activity of hindered aliphatic nitroxides.

Given the high concentration of SOD *in vivo*, it seems unlikely that a relatively low concentration of nitroxide could out-compete SOD for superoxide. Furthermore, the mechanism of nitroxide regeneration in **Scheme 1.9 A** and **B** is not supported in *hydrophobic* environments because $O_2^{-\bullet}$ is well compartmentalized from the propagating species of lipid autoxidation, which precludes nitroxide regeneration by superoxide. Methods used in the literature, such as the TBARs assay, DPPH, *etc.* fail to adequately probe the mechanism of action. Accordingly, the radical-trapping mechanism of action of nitroxides in biphasic systems, and notably in the context of lipid peroxidation, remains unclear.

1.3 Ferroptosis

1.3.1 Discovery

Ferroptosis is a newly-characterized pathway of regulated cell death that is biochemically, morphologically and genetically distinct from the three 'classic' modes of cell death: apoptosis, necrosis and autophagy.[76] Its discovery stems from efforts in the scientific community to identify *non-apoptotic* pathways of cell death expressed selectively in cells in a disease state, such as cancer.[77] One could envision that understanding the biochemical mechanisms of any non-apoptotic pathways could then be exploited as a target[78]—especially in cancer, where apoptosis is notably dysregulated.[79] Thus, there has been considerable recent development of various ferroptosis-inducing (FIN) compounds.[80]

Moreover, implication of ferroptosis in neurodegenerative disease (ND) alongside the concomitant discovery of inhibitors suggests precedence for therapeutic avenues to

inhibit this form of cell death. Notably, the aromatic amines ferrostatin-1 (Fer-1)[76] and liproxstatin-1 (Lip-1)[81] were discovered from high-throughput screening to be highly potent inhibitors, rescuing cells from ferroptosis in the tens of nanomolar range. Moreover, Lip-1 rescues $Gpx4^{-/-}$ mice from renal failure and subsequent death,[81] and Fer-1 analogues have been developed with enhanced ADME properties[82] towards evaluation in similar ND animal models.

Several key features that differentiate ferroptotic cell-death from the other modes of cell death include: lack of apoptosis hallmarks such as caspase activity, BAK and BAX pathway activation; shrinking of mitochondria with concomitant increase in mitochondrial membrane density; dependence on intracellular iron, and; an increase in lipid peroxides.[76,83] The latter feature is critically significant since it represents the first implication of lipid peroxidation in a specific pathway of cell death. Lipid peroxidation was identified to *precede* cell death by monitoring the fluorescence shift of C11-$BODIPY^{581/591}$.

1.3.2 Experimental models of ferroptosis and ferroptosis-inducing compounds

Ferroptosis is experimentally modeled by compromising the activity of the cell's only lipid hydroperoxide-detoxifying enzyme, Gpx4 (**Figure 1.12**), by a handful of related methods:

i) covalent inhibition of Gpx4 using the small molecule inhibitor (1*S*,3*R*)-RSL3;[84]

ii) preventing Gpx4 transcription genetically, by tamoxifen-induced Cre recombinase deletion of Gpx4[76] or RNAi-mediated targetting of the Gpx4 gene with shRNAs or a pool of siRNA.[84]

iii) inhibition of glutamate-cysteine ligase by buthionine sulfoxamine (BSO),[84] which prevents biosynthesis of GSH—the requisite reducing co-substrate of Gpx4;

iv) inhibition of the cysteine/glutamate antiporter (system x_c^-) by small molecules erastin, sulfasalazine[76] or sorafenib,[85] which precludes biosynthesis of GSH by blocking cellular uptake of oxidized cysteine;

v) competitive inhibition of system x_c^- by glutamate,[86,87] which similarly precludes biosynthesis of GSH by preventing cellular uptake of oxidized cysteine.

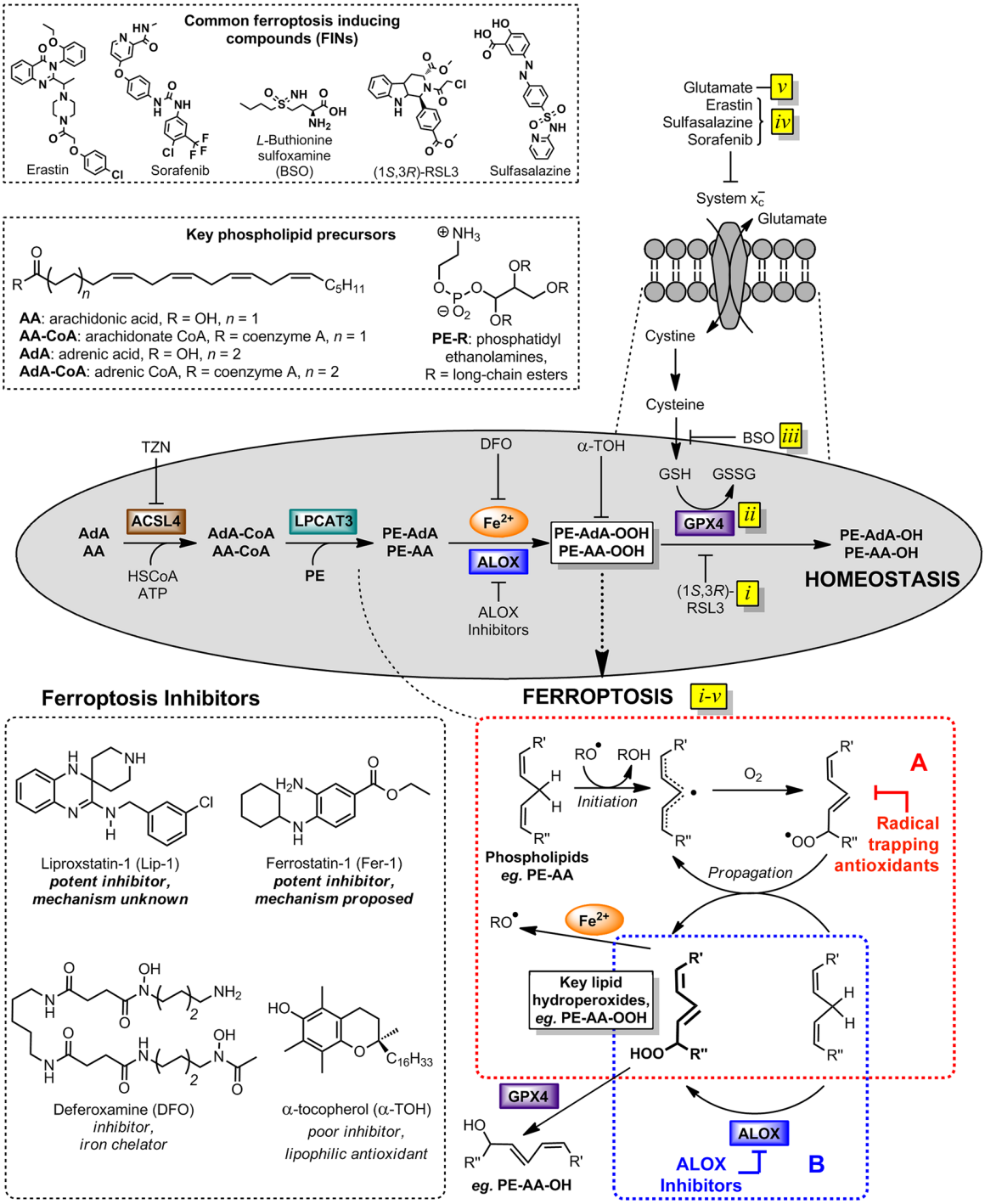

Figure 1.12 Biochemical pathways involved in the induction of ferroptosis. Ferroptosis inducing pathways *i*-*v* prevent GPX4 activity, leading to accumulation of lipid hydroperoxides that are generated by two mechanisms: the autoxidation-mediated path (box **A**), or, a lipoxygenase-mediated path (box **B**). Adapted from reference 87.

1.3.3 Inhibitors of ferroptosis and proposed modes of action

The small molecules Lip-1[78] and Fer-1[76] were discovered through library screening and possess the ability to inhibit ferroptosis to rescue cells in the various assays and in the low nM concentration range—yet the mechanism of action of Lip-1 has not been investigated, and that suggested for Fer-1 remains speculative.[88] At the outset of implicating lipid peroxidation in ferroptotic cells, a number of hypotheses have been put forward for the mechanism of action of Lip-1 and Fer-1. First, they could chelate iron. Non-heme iron is requisite for ferroptotic death, since iron chelators (*i.e.* deferoxamine, ciclopiroxolamine, 2,2'-bipyridyl) prevent the induction of ferroptosis.[76] Second, they could inhibit lipoxygenase catalysis that produces lipid hydroperoxides (**Figure 1.12 box B**). The third possibility is that these small molecules act as chain-breaking antioxidants of lipid autoxidation (**Figure 1.12 box A**). If the latter classification were true, their demonstrated potency in cells would suggest that Lip-1 and Fer-1 possess superior antioxidant action to Nature's best lipophilic antioxidant, α-TOH, which is a comparatively *poor* inhibitor of ferroptosis.

1.4 Research Objectives

1.4.1 Proposed mechanism of Lip-1 and Fer-1

The potency of the foremost ferroptosis inhibitors, Lip-1 and Fer-1, suggest their mechanism of action may be catalytic, and related to structurally similar amine RTAs such as diarylamines, and nitroxides such as TEMPO. On close inspection, the structures of Lip-1 and Fer-1 contain features of both these RTAs—first, an aryl amine with an abstractable H-atom, and second, the potential for reaction of the resultant nitrogen-centered radical to a persistent nitroxide. TEMPO has been known for decades as a potent RTA, and our group has recently proposed a mechanism for the catalytic activity *at high temperature*

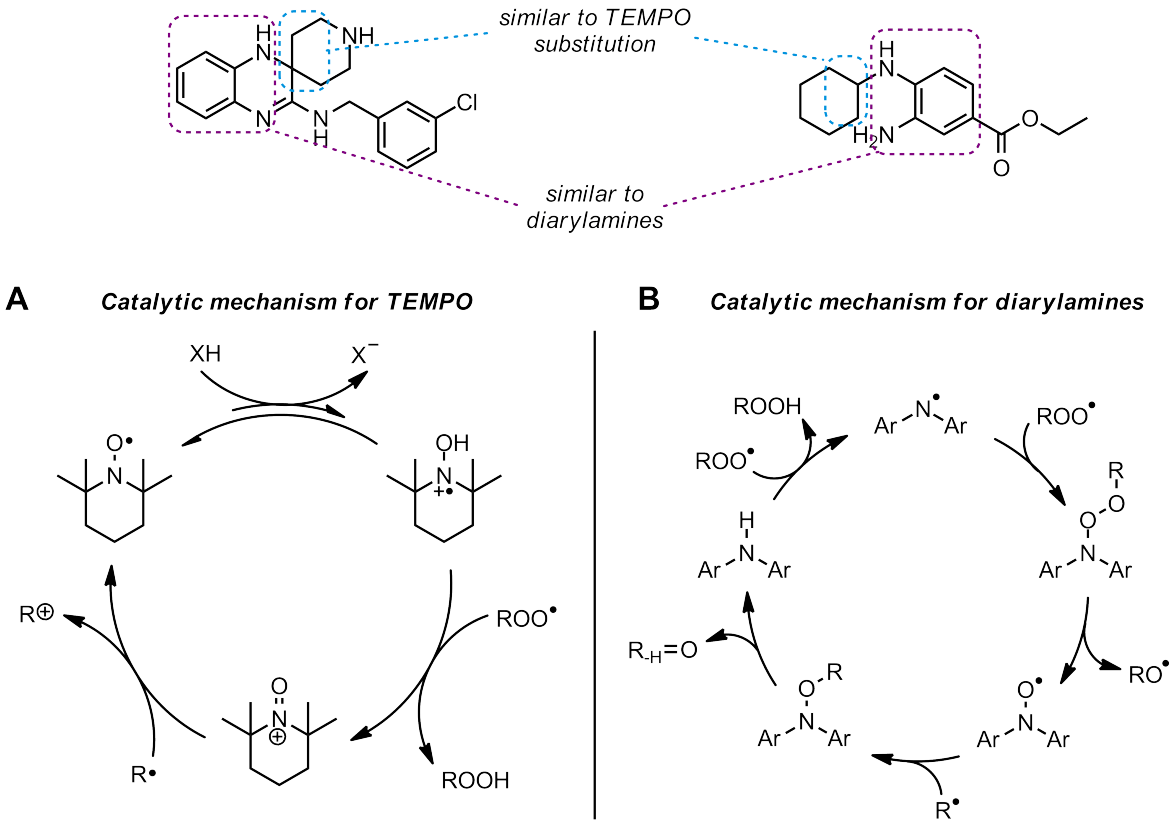

Scheme 1.10 Mechanistic proposals for the catalytic radical trapping activity of TEMPO[89] and diarylamines[91] under high-temperature autoxidation conditions.

(**Scheme 1.10**).[89,90] Therein, the hydroxylamine radical cation, formed with a hydrogen donor from the nitroxide, traps a peroxyl radical to form an oxoammonium ion. The nitroxide is regenerated from the oxoammonium ion by reaction with alkyl radicals. For diarylamines, the N-H BDE is sufficiently low to allow H-atom abstraction by peroxyl radicals. The aminyl radical reacts with peroxyl radicals, and decomposes to yield a nitroxide and an alkoxyl radical. The nitroxide then traps an alkyl radical and decomposed to regenerate the diarylamine.[91]

While these mechanisms appear to contribute to the inhibition of high-temperature autoxidations of hydrocarbons by hindered amine light stabilizers (HALS) and/or the nitroxides derived therefrom, it is unclear if they may play a role *in vivo*.

We hypothesize that the amines are capable of being oxidized *in situ* to persistent nitroxides and result in RTA activity against lipid autoxidation in an analogous manner to the intervention of nitroxides as RTAs at high temperature. Indeed, Thomas and coworkers discovered that diaryl nitroxides arise from inhibited autoxidation of parent diaryl amines.[92] Diaryl nitroxides (but not dialkyl nitroxides) have been demonstrated to react efficiently with peroxyl radicals in styrene autoxidation.[93,94,95] ESR studies by Steir *et al.* in 1980 detected the bioconversion of certain arylamines to nitroxides in rabbit liver microsomes,[96] and nitroxides have been demonstrated to be *persistent* in liposomes stressed by irradiation and autoxidation.[97,98] However, elucidation of nitroxide RTA mechanisms in the biological context of lipid peroxidation remain to be investigated, and could involve nitroxide regeneration proposed in **Scheme 1.10C** for TEMPO.

The evaluation of this hypothesis would not only shine light on the mechanism of action of Lip-1 and Fer-1, but may also implicate lipid autoxidation as the major

contributor to ferroptotic cell death over LOX inhibition (**Figure 1.12A** and **B**). This distinction may then lead the rational design of ferroptosis inhibitors towards those that prevent lipid autoxidation. Such inhibitors would likely serve as important lead candidates for the many diseases implicating lipid peroxidation, ferroptosis, and oxidative stress etiology.

Chapter 2 describes the systematic approach of investigating these hypotheses by: evaluating the RTA activity of Lip-1 and Fer-1 by 'classical' approaches; determining LOX-inhibitory activity, if any, and; disclosing the activity of the tetrahydronaphthyridinols (THNs), rationally-designed chain breaking RTAs of unparalleled reactivity, thereby probing contribution of lipid autoxidation in ferroptotic cell death. Moreover, we extend the study to a small library of aryl amines to explore the structure-activity relationship of the key functional groups these inhibitors feature.

1.4.2 Preparation of mitochondrially-targeted THNs

As previously introduced, the THNs have been rationally designed to be superior to Nature's best lipid-soluble RTA, α-tocopherol. The preparation of a THN targeted to the mitochondria (a MitoTHN) would represent the most potent RTAs to be targeted to the mitochondria to date. The demonstration of inhibition of mitochondrial lipid peroxidation would not only allow the evaluation of MitoTHN RTAs for various mitochondrial dysfunctions, but would also provide one more tool for scientists studying contribution of mitochondrial lipid peroxidation in diseases where mitochondrial dysfunction is implicated, since potent mitochondrial chain-breaking antioxidants have yet to be developed. Moreover, the recent report of a mitochondrially-targeted nitroxide[99] rescuing

ferroptotic cells, among other observations,[81] raises the question of MLP contribution in ferroptosis.

We aim to prepare MitoTHNs and develop assays for evaluation and comparison to previously reported mitochondrial and non-targeted antioxidants in pursuit of understanding these open questions. Chapter 3 describes the synthesis and *in vitro* activity of a group of MitoTHNs, a mitochondrial peroxidation probe and preliminary murine biodistribution data for both MitoTHNs and THNs in anticipation of their evaluation in various animal models of disease.

1.5 References

[1] Halliwell, B.; Gutteridge, J. *Free Radicals in Biology and Medicine*, 4th ed.; Oxford University Press: Oxford, 2007.

[2] Ingold, K. U.; Pratt, D. A. Advances in Radical-Trapping Antioxidant Chemistry in the 21st Century: a Kinetics and Mechanisms Perspective. *Chem. Rev.* **2014**, *114* (18), 9022–9046.

[3] D'Autréaux, B.; Toledano, M. B. ROS as Signalling Molecules: Mechanisms That Generate Specificity in ROS Homeostasis. *Nat. Rev. Mol. Cell Biol.* **2007**, *8*, 813–824.

[4] Finkel, T.; Holbrook, N. J. Oxidants, Oxidative Stress and the Biology of Ageing. *Nature* **2000**, *408*, 239–247.

[5] McCord, J. M. Oxygen-Derived Free Radicals in Postischemic Tissue Injury. *N. Engl. J. Med.* **1985**, *312*, 159–163.

[6] Barnham, K. J.; Masters, C. L.; Bush, A. I. Neurodegenerative Diseases and Oxidative Stress. *Nat. Rev. Drug Discov.* **2004**, *3* (3), 205–214.

[7] McDougall, M.; Choi, J.; Magnusson, K.; Truong, L.; Tanguay, R.; Traber, M. G. Chronic Vitamin E Deficiency Impairs Cognitive Function in Adult Zebrafish via Dysregulation of Brain Lipids and Energy Metabolism. *Free Radic. Biol. Med.* **2017**, *112*, 308–317.

[8] Benz, C. C.; Yau, C. Ageing, Oxidative Stress and Cancer: Paradigms in Parallax. *Nat. Rev. Cancer* **2008**, *8*, 875–879.

[9] Hussain, S. P.; Hofseth, L. J.; Harris, C. C. Radical Causes of Cancer. *Nat. Rev. Cancer* **2003**, *3*, 276–285.

[10] Krumova, K.; Cosa, G. Overview of Reactive Oxygen Species. In *Singlet Oxygen Applications in Biosciences and Nanosciences, Volume 1*; Jori, G., Trotta, M., Eds.; The Royal Society of Chemistry: Oxford, 2016; pp 3–21.

[11] Bayır, H. Reactive Oxygen Species. *Crit. Care Med.* **2005**, *33* (Suppl), S498–S501.

[12] Massey, V. Activation of Molecular Oxygen by Flavins and Flavoproteins. *J. Biol. Chem.* **1994**, *269* (36), 22459–22462.

[13] Harrison, R. Structure and Function of Xanthine Oxidoreductase: Where Are We Now? *Free Radic. Biol. Med.* **2002**, *33* (6), 774–797.

[14] Hampton, M. B.; Kettle, A. J.; Winterbourn, C. C. Inside the Neutrophil Phagosome: Oxidants, Myeloperoxidase, and Bacterial Killing. *Blood* **1998**, *92* (9), 3007–3017.

[15] Bruice, T. C. Oxygen-Flavin Chemistry. *Isr. J. Chem.* **1984**, *24*, 54-61.

[16] Halliwell, B.; Gutteridge, J. M. C. Biologically Relevant Metal Ion-Dependent Hydroxyl Radical Generation an Update. *FEBS Letters* **1992**, *307* (1), 108–112.

[17] Smith, R. A. J.; Hartley, R. C.; Cochemé, H. M.; Murphy, M. P. Mitochondrial Pharmacology. *Trends Pharmacol. Sci.* **2012**, *33* (6), 341–352.

[18] Turrens, J. F. Mitochondrial Formation of Reactive Oxygen Species. *J. Physiol.* **2003**, *552* (2), 335–344.

[19] Murphy, M. P. How Mitochondria Produce Reactive Oxygen Species. *Biochem. J.* **2009**, *417* (1), 1–13.

[20] Sivitz, W. I.; Yorek, M. A. Mitochondrial Dysfunction in Diabetes: From Molecular Mechanisms to Functional Significance and Therapeutic Opportunities. *Antioxid. Redox Signal.* **2010**, *12* (4), 537–577.

[21] Kussmaul, L.; Hirst, J. The Mechanism of Superoxide Production by NADH:Ubiquinone Oxidoreductase (Complex I) From Bovine Heart Mitochondria. *Proc. Natl. Acad. Sci. USA* **2006**, *103* (20), 7607–7612.

[22] Szabó, C.; Ischiropoulos, H.; Radi, R. Peroxynitrite: Biochemistry, Pathophysiology and Development of Therapeutics. *Nat. Rev. Drug Discov* **2007**, *6* (8), 662–680.

[23] Cadenas, E.; Davies, K. Mitochondrial Free Radical Generation, Oxidative Stress, and Aging. *Free Radic. Biol. Med.* **2000**, *29* (3-4), 222–230.

[24] Shadel, G. S.; Horvath, T. L. Mitochondrial ROS Signaling in Organismal Homeostasis. *Cell* **2015**, *163* (3), 560–569.

[25] *SciFinder*; Chemical Abstracts Service: Columbus, OH; https://scifinder.cas.org (accessed December 20, 2016).

[26] Tainer, J. A.; Getzoff, E. D.; Richardson, J. S.; Richardson, D. C. Structure and Mechanism of Copper, Zinc Superoxide Dismutase. *Nature* **1983**, *306* (5940), 284–287.

[27] Toppo, S.; Flohé, L.; Ursini, F.; Vanin, S.; Maiorino, M. Catalytic Mechanisms and Specificities of Glutathione Peroxidases: Variations of a Basic Scheme. *Biochim. Biophys. Acta* **2009**, *1790* (11), 1486–1500.

[28] van Meer, G.; Voelker, D. R.; Feigenson, G. W. Membrane Lipids: Where They Are and How They Behave. *Nat. Rev. Mol. Cell Biol.* **2008**, *9* (2), 112–124.

[29] Zielinski, Z.; Pratt, D. A. Cholesterol Autoxidation Revisited: Debunking the Dogma Associated with the Most Vilified of Lipids. *J. Am. Chem. Soc.* **2016**, *138* (22), 6932–6935.

[30] Pratt, D. A.; Mills, J. H.; Porter, N. A. Theoretical Calculations of Carbon-Oxygen Bond Dissociation Enthalpies of Peroxyl Radicals Formed in the Autoxidation of Lipids. *J. Am. Chem. Soc.* **2003**, *125* (19), 5801–5810.

[31] Maillard, B.; Ingold, K. U.; Scaiano, J. C. Rate Constants for the Reactions of Free-Radicals with Oxygen in Solution. *J. Am. Chem. Soc.* **1983**, *105* (15), 5095–5099.

[32] Porter, N. A. Mechanisms for the Autoxidation of Polyunsaturated Lipids. *Acc. Chem. Res.* **1986**, *19*, 262–268.

[33] Yin, H.; Xu, L.; Porter, N. A. Free Radical Lipid Peroxidation: Mechanisms and Analysis. *Chem. Rev.* **2011**, *111* (10), 5944–5972.

[34] Ingold, K. U. Inhibition of the Autoxidation of Organic Substances in the Liquid Phase. *Chem. Rev.* **1961**, *61* (6), 563–589.

[35] Howard, J. A.; Ingold, K. U. The inhibited autoxidation of styrene: Part I. The deuterium isotope effect for inhibition by 2,6-di-tert-butyl-4-methylphenol. *Can. J. Chem.* **1962**, *40* (9), 1851–1864.

[36] Zielinski, Z. A. M.; Pratt, D. A. Lipid Peroxidation: Kinetics, Mechanisms, and Products. *J. Org. Chem.* **2017**, *82* (6), 2817–2825.

[37] Lee, R.; Gryn'ova, G.; Ingold, K. U.; Coote, M. L. Why Are Sec-Alkylperoxyl Bimolecular Self-Reactions Orders of Magnitude Faster Than the Analogous Reactions of Tert-Alkylperoxyls? The Unanticipated Role of CH Hydrogen Bond Donation. *Phys. Chem. Chem. Phys.* **2016**, *18* (34), 23673–23679.

[38] Esterbauer, H.; Schaur, R. J.; Zollner, H. Chemistry and Biochemistry of 4-Hydroxynonenal, Malonaldehyde and Related Aldehydes. *Free Radic. Biol. Med.* **1991**, *11* (1), 81–128.

[39] Marnett, L. J.; Riggins, J. N.; West, J. D. Endogenous Generation of Reactive Oxidants and Electrophiles and Their Reactions with DNA and Protein. *Journal of Clinical Investigation* **2003**, *111* (5), 583–593.

[40] Tallman, K. A.; Pratt, D. A.; Porter, N. A. Kinetic Products of Linoleate Peroxidation: Rapid Beta-Fragmentation of Nonconjugated Peroxyls. *J. Am. Chem. Soc.* **2001**, *123* (47), 11827–11828.

[41] Glickman, M. H.; Klinman, J. P. Lipoxygenase Reaction Mechanism: Demonstration That Hydrogen Abstraction From Substrate Precedes Dioxygen Binding During Catalytic Turnover. *Biochemistry* **1996**, *35*, 12882-12892.

[42] Solomon, E. I.; Brunold, T. C.; Davis, M. I.; Kemsley, J. N. Geometric and Electronic Structure/Function Correlations in Non-Heme Iron Enzymes. *Chem. Rev.* **2000**, *100* (1), 235–349.

[43] Hanthorn, J. J.; Haidasz, E.; Gebhardt, P.; Pratt, D. A. A Versatile Fluorescence Approach to Kinetic Studies of Hydrocarbon Autoxidations and Their Inhibition by Radical-Trapping Antioxidants. *Chem. Commun. (Camb.)* **2012**, *48* (81), 10141–10143.

[44] Li, B.; Pratt, D. A. Methods for Determining the Efficacy of Radical-Trapping Antioxidants. *Free Radic. Biol. Med.* **2015**, *82*, 187–202.

[45] Griller, D.; Ingold, K. U. Free-Radical Clocks. *Acc. Chem. Res.* **1980**, *13*, 317-323.

[46] Pap, E. H.; Drummen, G. P.; Winter, V. J.; Kooij, T. W.; Rijken, P.; Wirtz, K. W.; Op den Kamp, J. A.; Hage, W. J.; Post, J. A. Ratio-Fluorescence Microscopy of Lipid Oxidation in Living Cells Using C11-BODIPY$^{581/591}$. *FEBS Lett.* **1999**, *453* (3), 278–282.

[47] Haidasz, E. A.; Van Kessel, A. T. M.; Pratt, D. A. A Continuous Visible Light Spectrophotometric Approach to Accurately Determine the Reactivity of Radical-Trapping Antioxidants. *J. Org. Chem.* **2016**, *81* (3), 737–744.

[48] DiLabio, G. A.; Johnson, E. R. Lone Pair-Pi and Pi-Pi Interactions Play an Important Role in Proton-Coupled Electron Transfer Reactions. *J. Am. Chem. Soc.* **2007**, *129* (19), 6199–6203.

[49] Erben-Russ, M.; Bors, W.; Saran, M. Reactions of Linoleic Acid Peroxyl Radicals with Phenolic Antioxidants: a Pulse Radiolysis Study. *Int. J. Radiat. Biol.* **1987**, *52* (3), 393–412.

[50] Litwinienko, G.; Ingold, K. U. Solvent Effects on the Rates and Mechanisms of Reaction of Phenols with Free Radicals. *Acc. Chem. Res.* **2007**, *40* (3), 222–230.

[51] Burton, G. W.; Doba, T.; Gabe, E.; Hughes, L.; Lee, F. L.; Prasad, L.; Ingold, K. U. Autoxidation of Biological Molecules. 4. Maximizing the Antioxidant Activity of Phenols. *J. Am. Chem. Soc.* **1985**, *107* (24), 7053–7065.

[52] Valgimigli, L.; Pratt, D. A. *Antioxidants in Chemistry and Biology*, 2nd ed.; John Wiley & Sons, Ltd: Chichester, UK, 2012; Vol. 95.

[53] Lucarini, M.; Pedrielli, P.; Pedulli, G. F.; Cabiddu, S.; Fattuoni, C. Bond Dissociation Energies of O−H Bonds in Substituted Phenols From Equilibration Studies. *J. Org. Chem.* **1996**, *61* (26), 9259–9263.

[54] Pratt, D. A.; DiLabio, G. A.; Mulder, P.; Ingold, K. U. Bond Strengths of Toluenes, Anilines, and Phenols: to Hammett or Not. *Acc. Chem. Res.* **2004**, *37* (5), 334–340.

[55] Hanthorn, J. J.; Valgimigli, L.; Pratt, D. A. Incorporation of Ring Nitrogens Into Diphenylamine Antioxidants: Striking a Balance Between Reactivity and Stability. *J. Am. Chem. Soc.* **2012**, *134* (20), 8306–8309.

[56] Pratt, D. A.; DiLabio, G. A.; Brigati, G.; Pedulli, G. F.; Valgimigli, L. 5-Pyrimidinols: Novel Chain-Breaking Antioxidants More Effective Than Phenols. *J. Am. Chem. Soc.* **2001**, *123* (19), 4625–4626.

[57] Wijtmans, M.; Pratt, D. A.; Valgimigli, L.; DiLabio, G. A.; Pedulli, G. F.; Porter, N. A. 6-Amino-3-Pyridinols: Towards Diffusion-Controlled Chain-Breaking Antioxidants. *Angew. Chem. Int. Ed.* **2003**, *42* (36), 4370–4373.

[58] McCord, J. M.; Fridovich, I. Superoxide Dismutase. An Enzymic Function for Erythrocuprein (Hemocuprein). *J. Biol. Chem.* **1969**, *244* (22), 6049–6055.

[59] Salvemini, D.; Riley, D. P.; Cuzzocrea, S. SOD Mimetics Are Coming of Age. *Nat. Rev. Drug Discov.* **2002**, *1* (5), 367–374.

[60] Wilcox, C. S.; Pearlman, A. Chemistry and Antihypertensive Effects of Tempol and Other Nitroxides. *Pharmacol. Rev.* **2008**, *60* (4), 418–469.

[61] Samuni, A.; Krishna, C. M.; Riesz, P.; Finkelstein, E. A Novel Metal-Free Low Molecular Weight Superoxide Dismutase Mimic. *J. Biol. Chem.* **1988**, *263*, 17921–17924.

[62] Krishna, M. C.; Grahame, D. A.; Samuni, A.; Mitchell, J. B.; Russo, A. Oxoammonium Cation Intermediate in the Nitroxide-Catalyzed Dismutation of Superoxide. *Proc. Natl. Acad. Sci. USA* **1992**, *89* (12), 5537–5541.

[63] Goldstein, S.; Merenyi, G.; Russo, A.; Samuni, A. The Role of Oxoammonium Cation in the SOD-Mimic Activity of Cyclic Nitroxides. *J. Am. Chem. Soc.* **2003**, *125* (3), 789–795.

[64] Israeli, A.; Patt, M.; Oron, M.; Samuni, A.; Kohen, R.; Goldstein, S. Kinetics and Mechanism of the Comproportionation Reaction Between Oxoammonium Cation and Hydroxylamine Derived From Cyclic Nitroxides. *Free Radic. Biol. Med.* **2005**, *38* (3), 317–324.

[65] Krishna, M. C.; Russo, A.; Mitchell, J. B.; Goldstein, S.; Dafni, H.; Samuni, A. Do Nitroxide Antioxidants Act as Scavengers of $O_2^{-\bullet}$ or as SOD Mimics? *J. Biol. Chem.* **1996**, *271* (42), 26026–26031.

[66] Miura, Y.; Utsumi, H.; Hamada, A. Antioxidant Activity of Nitroxide Radicals in Lipid Peroxidation of Rat Liver Microsomes. *Arch. Biochem. Biophys.* **1993**, *300* (1), 148–156.

[67] Cimato, A. N.; Piehl, L. L.; Facorro, G. B.; Torti, H. B.; Hager, A. A. Antioxidant Effects of Water- and Lipid-Soluble Nitroxide Radicals in Liposomes. *Free Radic. Biol. Med.* **2004**, *37* (12), 2042–2051.

[68] Mobbili, G.; Crucianelli, E.; Barbon, A.; Marcaccio, M.; Pisani, M.; Dalzini, A.; Ussano, E.; Bortolus, M.; Stipa, P.; Astolfi, P. Liponitroxides: EPR Study and Their Efficacy as Antioxidants in Lipid Membranes. *RSC Adv.* **2015**, *5* (120), 98955–98966.

[69] Sasaki, K.; Ito, T.; Fujii, H. G.; Sato, S. Synthesis and Reduction Kinetics of Five Ibuprofen-Nitroxides for Ascorbic Acid and Methyl Radicals. *Chem. Pharm. Bull.* **2016**, *64* (10), 1509–1513.

[70] Yamasaki, T.; Ito, Y.; Mito, F.; Kitagawa, K.; Matsuoka, Y.; Yamato, M.; Yamada, K.-I. Structural Concept of Nitroxide as a Lipid Peroxidation Inhibitor. *J. Org. Chem.* **2011**, *76* (10), 4144–4148.

[71] Nilsson, U. A.; Olsson, L. I.; Carlin, G.; Bylund-Fellenius, A. C. Inhibition of Lipid Peroxidation by Spin Labels. Relationships Between Structure and Function. *J. Biol. Chem.* **1989**, *264* (19), 11131–11135.

[72] Antosiewicz, J.; Popinigis, J.; Wozniak, M.; Damiani, E.; Carloni, P.; Greci, L. Effects of Indolinic and Quinolinic Aminoxyls on Protein and Lipid Peroxidation of Rat Liver Microsomes. *Free Radic. Biol. Med.* **1995**, *18* (5), 913–917.

[73] Udassin, R.; Haskel, Y.; Samuni, A. Nitroxide Radical Attenuates Ischaemia/Reperfusion Injury to the Rat Small Intestine. *Gut* **1998**, *42* (5), 623–627.

[74] Canistro, D.; Boccia, C.; Falconi, R.; Bonamassa, B.; Valgimigli, L.; Vivarelli, F.; Soleti, A.; Genova, M. L.; Lenaz, G.; Sapone, A.; Zaccanti, F.; Abdel-Rahman, S. Z.; Paolini, M. Redox-Based Flagging of the Global Network of Oxidative Stress Greatly Promotes Longevity. *J. Gerontol. A Biol. Sci. Med. Sci.* **2015**, *70* (8), 936–43.

[75] Lipman, T.; Tabakman, R.; Lazarovici, P. Neuroprotective Effects of the Stable Nitroxide Compound Tempol on 1-Methyl-4-Phenylpyridinium Ion-Induced Neurotoxicity in the Nerve Growth Factor-Differentiated Model of Pheochromocytoma PC12 Cells. *Eur. J. Pharmacol.* **2006**, *549* (1-3), 50–57.

[76] Dixon, S. J.; Lemberg, K. M.; Lamprecht, M. R.; Skouta, R.; Zaitsev, E. M.; Gleason, C. E.; Patel, D. N.; Bauer, A. J.; Cantley, A. M.; Yang, W. S.; Morrison, B., III; Stockwell, B. R. Ferroptosis: an Iron-Dependent Form of Nonapoptotic Cell Death. *Cell* **2012**, *149* (5), 1060–1072.

[77] Okada, H.; Mak, T. W. Pathways of Apoptotic and Non-Apoptotic Death in Tumour Cells. *Nat. Rev. Cancer* **2004**, *4* (8), 592–603.

[78] Conrad, M.; Angeli, J. P. F.; Vandenabeele, P.; Stockwell, B. R. Regulated Necrosis: Disease Relevance and Therapeutic Opportunities. *Nat. Rev. Drug Discov.* **2016**, *15* (5), 348–366.

[79] Lowe, S. W.; Lin, A. W. Apoptosis in Cancer. *Carcinogenesis* **2000**, *21* (3), 485–495.

[80] Cao, J. Y.; Dixon, S. J. Mechanisms of Ferroptosis. *Cell. Mol. Life Sci.* **2016**, *73* (11-12), 2195–2209.

[81] Friedmann Angeli, J. P.; Schneider, M.; Proneth, B.; Tyurina, Y. Y.; Tyurin, V. A.; Hammond, V. J.; Herbach, N.; Aichler, M.; Walch, A.; Eggenhofer, E.; Basavarajappa, D.; Rådmark, O.; Kobayashi, S.; Seibt, T.; Beck, H.; Neff, F.; Esposito, I.; Wanke, R.; Förster, H.; Yefremova, O.; Heinrichmeyer, M.; Bornkamm, G. W.; Geissler, E. K.; Thomas, S. B.; Stockwell, B. R.; O'Donnell, V. B.; Kagan, V. E.; Schick, J. A.; Conrad, M. Inactivation of the Ferroptosis Regulator Gpx4 Triggers Acute Renal Failure in Mice. *Nat Cell Biol* **2014**, *16* (12), 1180–1191.

[82] Hofmans, S.; Vanden Berghe, T.; Devisscher, L.; Hassannia, B.; Lyssens, S.; Joossens, J.; Van Der Veken, P.; Vandenabeele, P.; Augustyns, K. Novel Ferroptosis Inhibitors with Improved Potency and ADME Properties. *J. Med. Chem.* **2016**, *59* (5), 2041–2053.

[83] Yang, W.S. and Stockwell, B.R. Synthetic lethal screening identifies compounds activating iron-dependent, nonapoptotic cell death in oncogenic-RAS-harboring cancer cells. *Chem. Biol.* **2008**, *15*, 234–245.

[84] Yang, W. S.; SriRamaratnam, R.; Welsch, M. E.; Shimada, K.; Skouta, R.; Viswanathan, V. S.; Cheah, J. H.; Clemons, P. A.; Shamji, A. F.; Clish, C. B.; Brown, L. M.; Girotti, A. W.; Cornish, V. W.; Schreiber, S. L.; Stockwell, B. R. Regulation of Ferroptotic Cancer Cell Death by GPX4. *Cell* **2014**, *156* (1-2), 317–331.

[85] Lachaier, E.; Louandre, C.; Godin, C.; Saidak, Z.; Baert, M.; Diouf, M.; Chauffert, B.; Galmiche, A. Sorafenib Induces Ferroptosis in Human Cancer Cell Lines Originating From Different Solid Tumors. *Anticancer Res.* **2014**, *34* (11), 6417–6422.

[86] Yang, W. S.; Stockwell, B. R. Ferroptosis: Death by Lipid Peroxidation. *Trends Cell Biol.* **2016**, *26* (3), 165–176.

[87] Angeli, J. P. F.; Shah, R.; Pratt, D. A.; Conrad, M. Ferroptosis Inhibition: Mechanisms and Opportunities. *Trends Pharmacol. Sci.* **2017**, *38* (5), 489–498.

[88] Skouta, R.; Dixon, S. J.; Wang, J.; Dunn, D. E.; Orman, M.; Shimada, K.; Rosenberg, P. A.; Lo, D. C.; Weinberg, J. M.; Linkermann, A.; Stockwell, B. R. Ferrostatins Inhibit Oxidative Lipid Damage and Cell Death in Diverse Disease Models. *J. Am. Chem. Soc.* **2014**, *136* (12), 4551–4556.

[89] Haidasz, E. A.; Meng, D.; Amorati, R.; Baschieri, A.; Ingold, K. U.; Valgimigli, L.; Pratt, D. A. Acid Is Key to the Radical-Trapping Antioxidant Activity of Nitroxides. *J. Am. Chem. Soc.* **2016**, *138* (16), 5290–5298.

[90] Amorati, R.; Pedulli, G. F.; Pratt, D. A.; Valgimigli, L. TEMPO Reacts with Oxygen-Centered Radicals Under Acidic Conditions. *Chem. Commun.* **2010**, *46* (28), 5139–5141.

[91] Haidasz, E. A.; Shah, R.; Pratt, D. A. The Catalytic Mechanism of Diarylamine Radical-Trapping Antioxidants. *J. Am. Chem. Soc.* **2014**, *136* (47), 16643–16650.

[92] Thomas, J. R. The Identification of Radical Products From the Oxidation of Diphenylamine. *J. Am. Chem. Soc.* **1960**, *82*, 5955–5956.

[93] Brownlie, I. T.; Ingold, K. U. The Inhibited Autoxidation of Styrene. Part VII. Inhibition by Nitroxides and Hydroxylamines. *Can. J. Chem.* **1967**, *45*, 2427-2432.

[94] Beckwith, A.; Bowry, V. W.; Ingold, K. U. Kinetics of Nitroxide Radical Trapping. I: Solvent Effects. *J. Am. Chem. Soc.* **1992**, *114* (13), 4983-4992.

[95] Bowry, V. W.; Ingold, K. U. Kinetic of Nitroxide Radical Trapping. II: Structural Effects. *J. Am. Chem. Soc.* **1992**, *114* (13), 4992-4996.

[96] Stier, A.; Clauss, R.; Lücke, A.; Reitz, I. Redox Cycle of Stable Mixed Nitroxides Formed From Carcinogenic Aromatic Amines. *Xenobiotica* **1980**, *10* (7-8), 661–673.

[97] Samuni, A. M.; Barenholz, Y. Stable Nitroxide Radicals Protect Lipid Acyl Chains From Radiation Damage. *Free Radic. Biol. Med.* **1997**, *22* (7), 1165–1174.

[98] Samuni, A. M.; Barenholz, Y. Site-Activity Relationship of Nitroxide Radical's Antioxidative Effect. *Free Radic. Biol. Med.* **2003**, *34* (2), 177–185.

[99] Krainz, T.; Gaschler, M. M.; Lim, C.; Sacher, J. R.; Stockwell, B. R.; Wipf, P. A Mitochondrial-Targeted Nitroxide Is a Potent Inhibitor of Ferroptosis. *ACS Cent. Sci.* **2016**, *2* (4), 653-659.

Preface to Chapter 2

The material in Chapter 2 Sections **2.1**-**2.6** appears as published in Zilka, O.; Shah, R.; Li, B.; Angeli, J. F.; Griesser, M.; Conrad, M.; Pratt, D. A. On the Mechanism of Cytoprotection by Ferrostatin-1 and Liproxstatin-1 and the Role of Lipid Peroxidation in Ferroptotic Cell Death. *ACS Central Science* **2017**, *3*, 232–243, and is followed by supplementary results in Sections **2.7-2.11**.

Coauthor and coworker contributions

Ron Shah completed the expression, functional characterization and inhibition of 15-LO overexpressed in HEK-293 cells. Bo Li completed initial inhibition of DEM-induced lipid peroxidation experiments and synthesis of some of the THNs. José Pedro Friedmann Angeli completed cellular anti-ferroptotic activity and related cell experiments. Markus Griesser completed Lip-1, Fer-1 and dihydroquinoline **1** BDE computations and all EPR experiments. Evan Haidasz synthesized dihydroquinoline **1**. Antonius T. M. Van Kessel developed the method of liposome and buffered water-THF co-autoxidations with STY-BODIPY.

Chapter 2: On the Mechanism of Cytoprotection by Ferrostatin-1 & Liproxstatin-1 and the Role of Lipid Peroxidation in Ferroptotic Cell Death

2.1 Introduction

The accumulation of lipid hydroperoxides (LOOH) has long been implicated in cell death and dysfunction, leading to ageing,[1,2] the onset and progression of degenerative disease[3,4] and cancer.[5,6] However, only recently has the accumulation of LOOH been directly related to a specific cell death pathway—coined ferroptosis.[7,8] Ferroptosis is a recently characterized form of regulated necrosis that is biochemically and morphologically distinct from apoptosis and autophagy, the more well-established cell death mechanisms.[9,10,11] The induction of ferroptosis offers a new strategy for killing cancer cells, and disruption of the regulatory framework that keeps ferroptosis in check may contribute to the pathogenesis of degenerative diseases in which LOOH accumulation has been implicated.[9,12,13]

The accumulation of cellular LOOH occurs by two primary mechanisms: an iron-catalyzed spontaneous peroxyl radical-mediated process called autoxidation[14,15] and enzyme-mediated processes catalyzed by (non-heme) iron-dependent lipoxygenases (LOs).[16,17] Accordingly, compounds that inhibit either or both of these processes have the potential to inhibit ferroptosis and may provide important leads for preventive and/or therapeutic agents to combat degenerative disease.

The Stockwell and Conrad groups recently independently discovered the first potent inhibitors of ferroptosis: ferrostatin-1 (Fer-1)[7] and liproxstatin-1 (Lip-1).[18] Fer-1 and Lip-1 were discovered by high-throughput screening of small molecule libraries using cell assays where ferroptosis was induced by either deletion of the gene encoding the LOOH-

detoxifying enzyme glutathione peroxidase-4 (Gpx4)[18] or pharmacological inhibition of system x_c^-, an antiporter that mediates the exchange of intracellular glutamate for extracellular cystine used for glutathione (GSH) synthesis.[7] Both compounds were found to suppress the accumulation of LOOH,[18,19] but the mechanism(s) by which they do so is (are) unknown.[20]

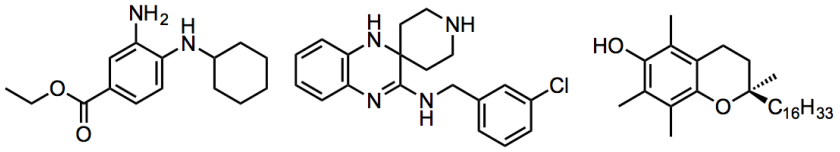

Fer-1 Lip-1 α-TOH

Since lipid autoxidation (peroxidation) is one of the two processes that contribute directly to cellular LOOH production, compounds that trap the peroxyl radicals that propagate the radical chain reaction, i.e. radical-trapping antioxidants (RTAs),[21] should be highly effective inhibitors of ferroptosis. Interestingly, both the Conrad and Stockwell groups found that although α-tocopherol (α-TOH), the most biologically active form of Vitamin E and Nature's premier lipid-soluble RTA,[22] is a relatively poor inhibitor of ferroptosis compared to either Fer- 1 or Lip-1.[18,19] These results suggest that either Fer-1 and Lip-1 are extremely potent RTAs or that the inhibition of autoxidation may not be at the root of their activity. Indeed, Fer-1 and Lip-1 may be effective inhibitors of lipoxygenases, since α-TOH has been shown to be only a modest inhibitor at best.[23,24] Herein we provide an assessment of both the RTA activity of Fer-1 and Lip-1, as well as their potency as inhibitors of human 15-lipoxygenase, the isoform recently implicated in ferroptosis.[25,26,27] Over the years, we have made use of our comprehensive understanding of the structure-reactivity relationships in radical trapping antioxidants to optimize the reactivity of phenolic RTAs.[28,29,30] The tetrahydronaphthyridinols (THNs, Chart 2.1) are

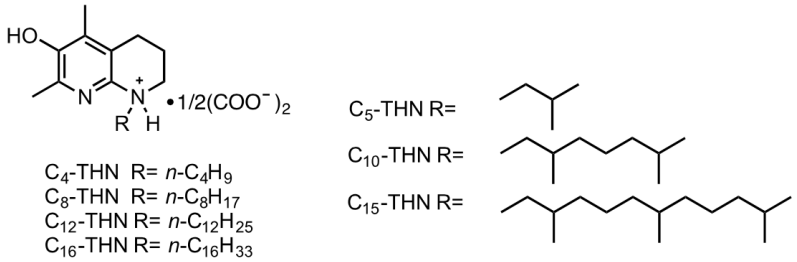

Chart 2.1 The tetrahydronaphthyridinols (THNs) studied here.

ca. 30-fold more reactive than α-TOH in organic solution,[29,30,31] and in lipid bilayer models of cellular membranes (liposomes).[32] Accordingly, if preventing LOOH accumulation by autoxidation is important in subverting ferroptosis, it follows that the THNs should be highly effective inhibitors. However, to date these derivatives have not been studied in cell culture.[33] Herein, we have assayed a small library of substituted THNs of varying lipid solubility and report on their efficacy to inhibit ferroptosis in several established cell models, including 1) pharmacological inhibition of Gpx4 with (1*S*,3*R*)-RSL3,[7,34] 2) deletion of the gene encoding Gpx4,[18] and 3) GSH depletion via inhibition of the cystine/glutamate antiporter.[27]

2.2 Results

2.2.1 Fer-1 and Lip-1 Are Inherently Good, But Not Great, Radical-Trapping Antioxidants.

To provide some insight to the mechanism of Fer-1 and Lip-1 as inhibitors of lipid peroxidation, their inherent RTA activities were determined by the venerable inhibited autoxidation of styrene approach pioneered by Ingold.[35] Our modern twist on these experiments involves addition of an autoxidizable co-substrate (PBD-BODIPY)[36] such that the reaction can be monitored by spectrophotometry in lieu of conventional (but tedious) oxygen consumption measurements. Thus, reaction progress is monitored simply by loss of

the absorbance at 591 nm due to the addition of peroxyl radicals to the 1-phenylbutadiene moiety of PBD-BODIPY (**Figure 2.1A**), which occurs with $k_{PBD\text{-}BODIPY}$ = 2720 $M^{-1}s^{-1}$ in chlorobenzene at 37ºC. Styrene is present in order to maintain a radical chain reaction, ensuring a steady-state concentration of peroxyl radicals and enabling derivation of the rate constant for the reaction of the added RTA with peroxyl radicals (k_{inh}) from the initial rate of the inhibited reaction (**Figure 2.1B**). The stoichiometry (n) of the RTA-peroxyl reaction is determined from the duration of the inhibited period (t_{inh}, also in **Figure 2.1B**).[36]

Representative results are shown for Fer-1 and Lip-1 in **Figure 2.1C** alongside corresponding data for α-TOH, its truncated analog, 2,2,5,7,8-pentamethyl-6-hydroxychroman (PMHC), and a representative THN (C_{15}-THN) for comparison. The traces clearly indicate that Fer-1 and Lip-1 are less reactive to peroxyl radicals than α-TOH (and PMHC). From the initial rates, rate constants for reactions of Fer-1 and Lip-1 with peroxyl radicals were determined to be (3.5±0.1) and (2.4±0.2)×10^5 $M^{-1}s^{-1}$, respectively—an order of magnitude lower than the rate constant determined for α-TOH of k_{inh} = (3.6±0.1)×10^6 $M^{-1}s^{-1}$. It is interesting to note that the rate constants determined for Fer-1 and Lip-1 are similar to those determined for conventional diarylamine antioxidants used as additives to petroleum-derived products,[37] while the representative THN is so reactive that a rate constant for its reaction cannot be determined using this approach (using different methodology, but under similar conditions a rate constant of 8.8×10^7 $M^{-1}s^{-1}$ was obtained).[28,38] The duration of the inhibited periods indicate that while α-TOH, PMHC and the THN each trap two peroxyl radicals, Fer-1 and Lip-1 trap roughly only one (actually 0.9±0.1 and 1.3±0.1, respectively). Interestingly, when the oxidizable substrate was

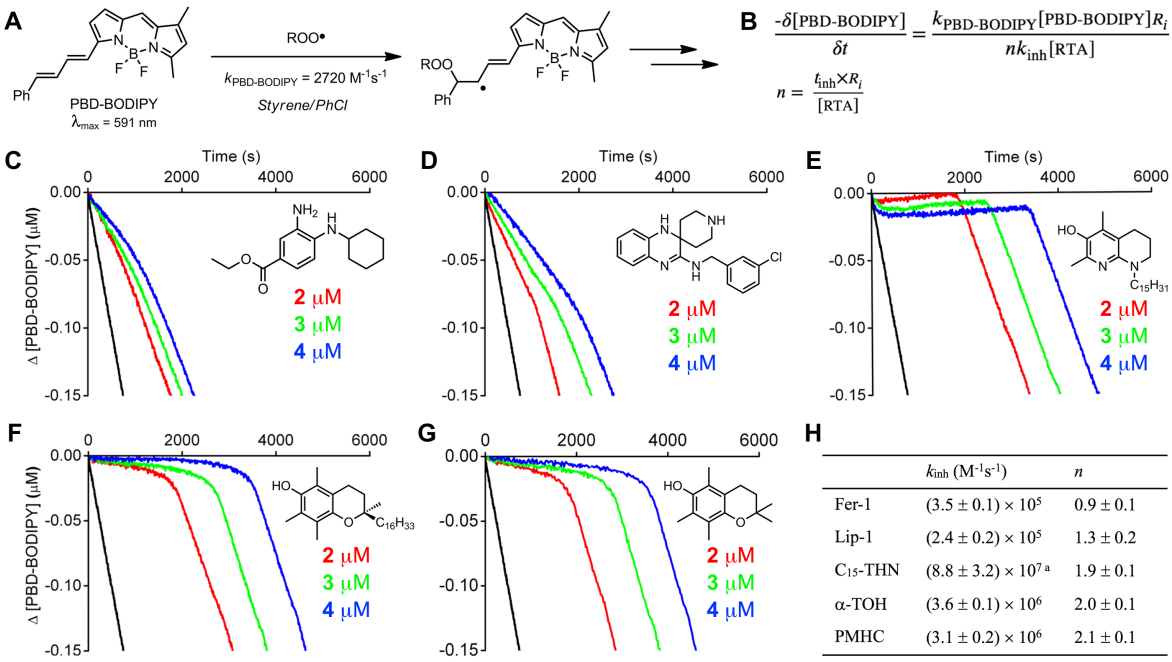

	k_{inh} ($M^{-1}s^{-1}$)	n
Fer-1	$(3.5 \pm 0.1) \times 10^5$	0.9 ± 0.1
Lip-1	$(2.4 \pm 0.2) \times 10^5$	1.3 ± 0.2
C_{15}-THN	$(8.8 \pm 3.2) \times 10^7$ [a]	1.9 ± 0.1
α-TOH	$(3.6 \pm 0.1) \times 10^6$	2.0 ± 0.1
PMHC	$(3.1 \pm 0.2) \times 10^6$	2.1 ± 0.1

Figure 2.1 PBD-BODIPY serves as the signal carrier in styrene autoxidations (**A**), enabling determination of rate constants and reaction stoichiometries for reactions of inhibitors with chain-carrying peroxyl radicals (**B**). Co-autoxidations of styrene (4.3 M) and PBDBODIPY (10 μM) initiated by AIBN (6 mM) in chlorobenzene at 37°C (black trace) and inhibited by 2 μM (red trace), 3 μM (green trace) and 4 μM (blue trace) of Fer-1 (**C**), Lip-1 (**D**), C15-THN (**E**) α-TOH (**F**) and PMHC (**G**). Average inhibition rate constants and stoichiometry summarized in (**H**). Reaction progress was monitored by absorbance at 591 nm (ε = 139,000 $M^{-1}cm^{-1}$). [a] From ref. 29; the inhibition rate constant is greater than that which can be determined from the data in panel (**E**).

changed from styrene to cumene, Fer-1 and Lip-1 trapped two peroxyl radicals, as do α-TOH, PMC and the THN (see **2.5** Supporting Information).

Kinetic isotope effects of $k_{inh,H}/k_{inh,D}$ = 2.2±0.2 and 1.8±0.1 were determined from autoxidations of Fer-1 and Lip-1, respectively, carried out in the presence of 1% of either MeOH or MeOD (see **2.5** Supporting Information). These values provide evidence for transfer of the aminic H-atom of Fer-1 and Lip-1 to chain-carrying peroxyl radicals—analogous to the mechanism of diarylamine radical-trapping antioxidants, as well as phenolic H-atom transfer from α-TOH, PMHC and the THNs.[29,39] Given the implication of H-atom transfer in the reactions of Fer-1 and Lip-1 with peroxyl radicals, we calculated the N-H bond dissociation enthalpies (BDEs) of Fer-1 and Lip-1 using the high accuracy CBS-

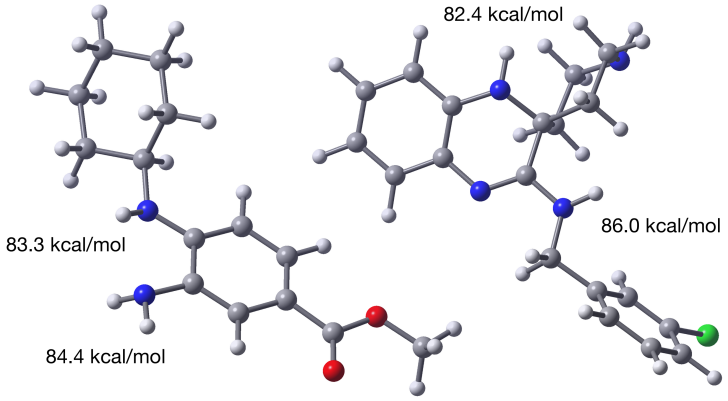

Figure 2.2 Computed (CBS-QB3) minimum energy structures of Fer-1 (left)[41] and Lip-1 (right) and the corresponding N-H bond dissociation enthalpies of the labile aminic H-atoms.

QB3 methodology of Petersson and coworkers.[40] The results are shown alongside the calculated structures of the model compounds in **Figure 2.2**.[41] The weakest N-H bonds in Fer-1 and Lip-1 are predicted to be 83.3 and 82.7 kcal/mol, respectively. These BDEs are significantly higher than in α-TOH and the THNs (77.7 and 75.0 kcal/mol calculated using the same methodology),[42] consistent with the lower reactivity of Fer-1 and Lip-1 to peroxyl radicals. In fact, Fer-1 and Lip-1 have similar N-H BDEs to conventional diarylamine antioxidants (*e.g.* 4,4-dialkyldiphenylamine N-H BDE = 82.2 kcal/mol),[43] in line with their similar inherent reactivity.

2.2.3 Fer-1 and Lip-1 Are Excellent Radical-Trapping Antioxidants in Phospholipid Bilayers.

The reactivity of Fer-1 and Lip-1 to peroxyl radicals was also assayed in the lipid bilayers of unilamellar liposomes prepared from egg phosphatidylcholine (PC). Reaction progress was followed by the competitive oxidation of STY-BODIPY (**Figure 2.3**), the more slowly oxidized analog of PBD-BODIPY wherein the 1-phenylbutadienyl moiety is replaced with a styryl moiety.[36] STY-BODIPY has been determined to react with peroxyl radicals with k_p = 894 $M^{-1}s^{-1}$ in this exact system.[44] Under these conditions, Fer-1 and Lip-1 were both more reactive than α-TOH (k_{inh} = (4.7±0.4)×10^3 $M^{-1}s^{-1}$), with rate constants of k_{inh} = (4.6±0.8)×10^4 and (1.2±0.1)×10^4 $M^{-1}s^{-1}$, respectively. The inhibition rate constants derived for Fer-1 and Lip-1 are similar to that of PMHC (k_{inh} = (3.7±0.2) ×10^4 $M^{-1}s^{-1}$)—which is believed to have greater reactivity than α-TOH in lipid bilayers due to superior dynamics.[45] Again, the THN was the most reactive of the compounds, with k_{inh} = (9.3±0.4)×10^4 $M^{-1}s^{-1}$. Perhaps most interestingly, while the inhibited period corresponding to the trapping of two peroxyl radicals is clear in the autoxidations inhibited by PMHC and the THN, Fer-1 and Lip-1 inhibited the autoxidations for longer. In fact, it would appear that not only are the inhibited periods of longer duration at the same antioxidant concentrations, but also that the rate of the autoxidation of Lip-1 never matches the uninhibited rate after the inhibited period (as it does with PMHC and the THN). This implies that the reactions of Fer-1 and Lip-1 with peroxyl radicals lead to compounds that remain reactive to peroxyl radicals and further retard the autoxidation past the nominal inhibition period corresponding to n~2.

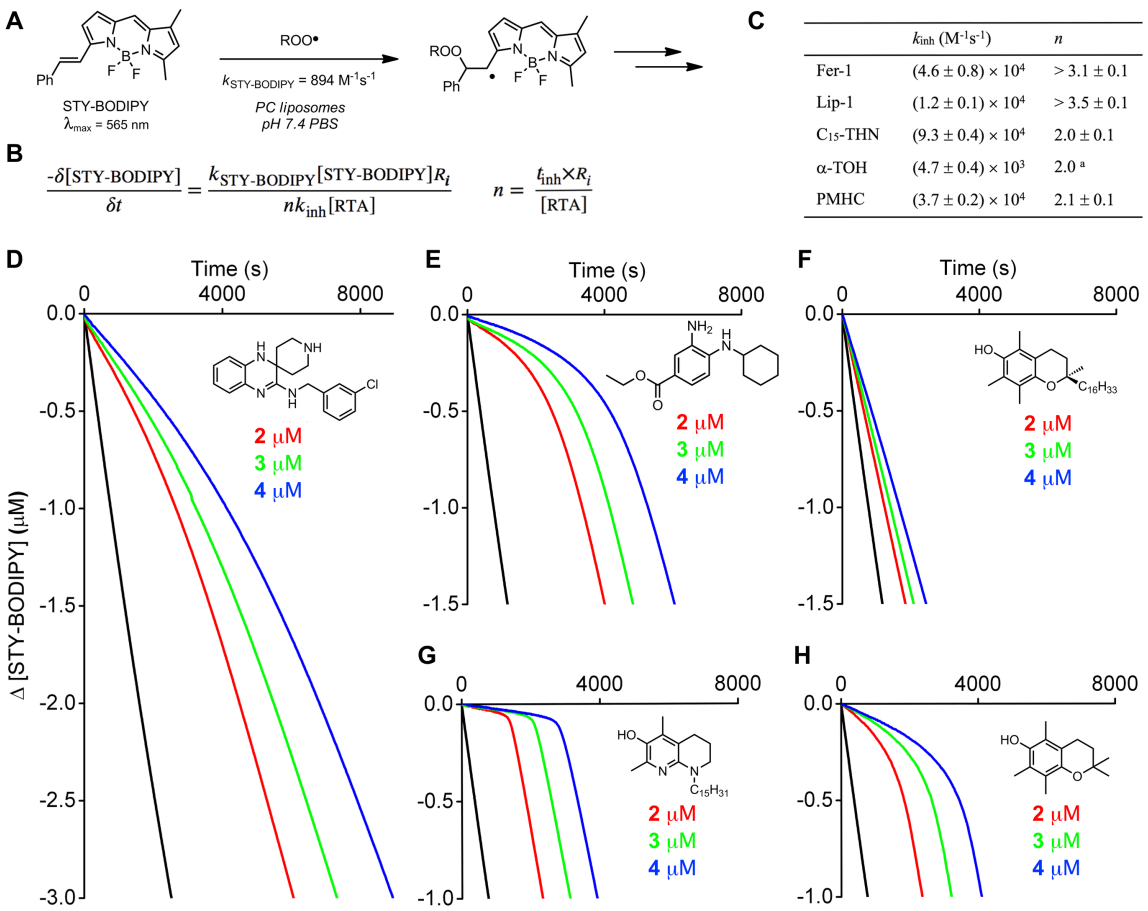

	k_{inh} ($M^{-1}s^{-1}$)	n
Fer-1	$(4.6 \pm 0.8) \times 10^4$	$> 3.1 \pm 0.1$
Lip-1	$(1.2 \pm 0.1) \times 10^4$	$> 3.5 \pm 0.1$
C_{15}-THN	$(9.3 \pm 0.4) \times 10^4$	2.0 ± 0.1
α-TOH	$(4.7 \pm 0.4) \times 10^3$	2.0 [a]
PMHC	$(3.7 \pm 0.2) \times 10^4$	2.1 ± 0.1

Figure 2.3 STY-BODIPY serves as the signal carrier in liposome oxidations (**A**), enabling determinations of rate constants and reaction stoichiometries for reactions of inhibitors with chain-carrying peroxyl radicals (**B**). Average inhibition rate constants and stoichiometry summarized in (**C**). Co-autoxidations of egg phosphatidylcholine lipids (1 mM) and STY-BODIPY (8 μM) suspended in phosphate-buffered saline (10 mM) at pH 7.4 initiated by MeOAMVN (0.2 mM) at 37°C (black trace) and inhibited by 2 μM (red trace), 3 μM (green trace) and 4 μM (blue trace) of Lip-1 (**D**), Fer-1 (**E**), α-TOH (**F**), C15-THN (**G**) and PMHC (**H**). Reaction progress was monitored by absorbance at 565 nm (ε = 139,000 $M^{-1}cm^{-1}$). [a] Could not be determined and is assumed to be 2.0.

Although it seems that improved dynamics are likely to contribute to the greater reactivity of Fer-1 and Lip-1 as RTAs in lipid bilayers compared to α-TOH, there must be more to it since they are similarly reactive to PMHC despite their far lower inherent reactivity to peroxyl radicals (as determined in chlorobenzene, *vide supra*). PMHC is a much poorer RTA in lipid bilayers than in hydrocarbons due to H-bonding interactions between the phenolic O-H and water and/or the phospholipid headgroups at the interface of

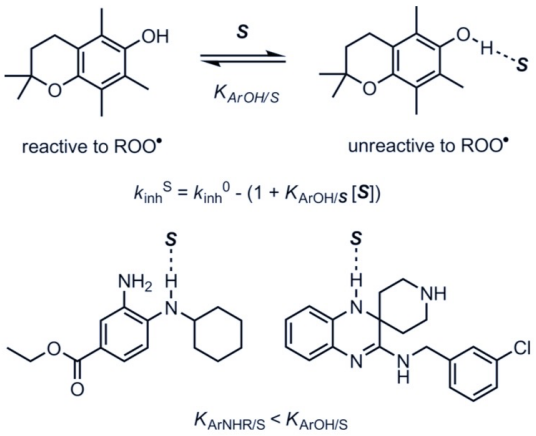

Scheme 2.1 Phenols, such as PMHC (shown) and α-TOH are better H-bond donors than arylamines, such as Fer-1 and Lip-1, leading to lower observed reactivity to peroxyl radicals in the presence of good H-bond accepting solvents (or other solutes) ***S***.

the lipid and aqueous phases.[46] When participating in a H-bond, the phenolic H-atom is no longer accessible to peroxyl radicals (**Scheme 2.1**).[47] For example, upon changing solvent from chlorobenzene to DMSO, k_{inh} for PMHC dropped 30-fold from $(3.1\pm0.2)\times10^{6}$ to $(1.1\pm0.2)\times10^{5}$ $M^{-1}s^{-1}$. Fer-1 and Lip-1, being arylamines, are expected to be poorer H-bond donors than phenols, such as α-TOH or PMHC.

The α_2^H value (which quantifies H-bond donating ability)[48] of a hindered monoarylamine closely related to Fer-1 and Lip-1 was determined to be 0.17 [49]—significantly lower than that of PMHC/α-TOH (0.37).[50] Consistent with this small α_2^H value, the reactivity of Fer-1 and Lip-1 towards peroxyl radicals differed only by factors of 1.7 and 0.6 when measured in DMSO (an excellent H-bond accepting solvent) compared to chlorobenzene (see **2.5** Supporting Information for details).

2.2.4 Fer-1 and Lip-1 Are Poor Inhibitors of 15-Lipoxygenase at Best, as is a-TOH.

The potencies of Fer-1 and Lip-1 as inhibitors of 15-LO were assessed in lysates of HEK-293 cells transfected to overexpress this isoform. Enzyme activity was determined

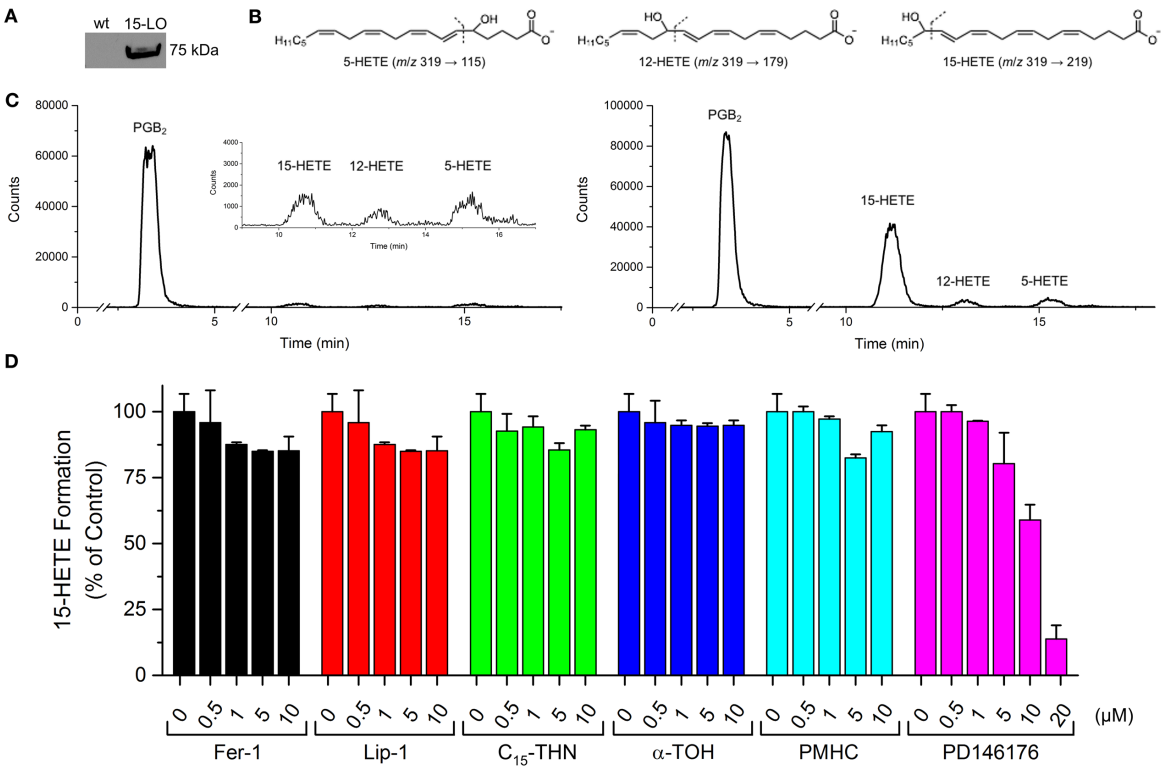

Figure 2.4 Expression, functional characterization and inhibition of 15-LO overexpressed in HEK-293 cells. Western blots showing the overexpression of 15-LO in transfected cells compared to wild-type (**A**). Structures of 5-, 12- and 15-HETEs monitored by UPLC/MS/MS and their characteristic MS/MS transitions (**B**). Representative chromatograms of H(P)ETEs formed by wild-type and 15-LO over-expressing cells (**C**). Effect of Fer-1, Lip-1, C_{15}-THN, α-TOH, PMHC and PD146176 on 15-H(P)ETE formation (**D**).

following incubation of the cell lysate with the test compound by quantifying 15-hydroperoxyeicosatetraenoic acid (15-HPETE), the product of 15-LO-catalyzed oxygenation of arachidonic acid, its natural substrate. In fact, the product was determined as the alcohol (15-HETE) following reduction with TCEP and extraction from the lysate by ESI-UPLC/MS/MS. α-TOH, PMHC and C_{15}-THN were assayed alongside Fer-1 and Lip-1. The data are shown in **Figure 2.4**.

Lysates of wild-type HEK293 cells did not produce significant amounts of H(P)ETE when incubated with free arachidonic acid due to the low expression of LO in these cells (**Figure 2.4A-C**). In contrast, enhanced formation of 15-H(P)ETE was clearly

observed in the transfected cells. Fer-1 and Lip-1, which were each assayed up to 10 μM—almost 1000-fold higher than their EC_{50}s for subverting RSL3-induced ferroptosis in these cells (15 and 27 nM, respectively), did not exhibit significant inhibitory activity (**Figure 2.4D**). The small effect on 15-H(P)ETE levels relative to the (untreated) control is most likely due to inhibition of lipid autoxidation (which can be initiated by 15-LO),[51] since no dose response is observed. α-TOH was also a poor inhibitor—in agreement with previous reports.[18,34] In contrast, the 15-LO inhibitor PD146176 prevented 15-H(P)ETE production in a dose-dependent manner with similar potency as reported.[52]

2.2.5 Lipophilic THNs are Potent Ferroptosis Inhibitors.

Given the comparatively excellent RTA activity of the C_{15}-THN relative to Fer-1 and Lip-1, the anti-ferroptotic activity of a library of THNs of differing lipophilicity[32] was investigated. Ferroptosis was induced in Pfa-1 mouse fibroblasts by Gpx4 inhibition with (1*S*,3*R*)-RSL3,[18] which was co-administered with the test compounds. The data are presented in **Table 2.1**. Although relatively hydrophilic THNs were ineffective inhibitors in these cells, lipophilic THNs were similarly potent to Fer-1 (EC_{50} = 45±5 nM) and Lip-1 (EC_{50} = 38±3 nM), with EC_{50} values of 13±5 and 50±2 nM for the C_{12}- and C_{15}-THNs, respectively. Clearly, there is an ideal sidechain length for the THN, since the potency decreases as the sidechain deviates from twelve carbon atoms (C_{15} has three tertiary sites with methyl branching, see Chart 2.1).

The THNs were also investigated in a genetic model of Gpx4 deficiency. This experiment enables resolution of any drug-drug interactions that may confound the results obtained by the pharmacological inhibition of Gpx4 (*vide supra*). Genetic disruption of Gpx4 was carried out in mouse embryonic fibroblasts carrying two floxed *gpx4* alleles

Table 2.1 Anti-ferroptotic activity of THNs in mouse embryonic fibroblasts. Ferroptosis was induced with (1*S*,3*R*)-RSL3 (100 nM) and cell survival was determined 6 hours post-induction by AquaBluer[18] assay. Data for α-TOH, Fer-1 and Lip-1 are also shown.

	EC_{50} (μM)
C_4-THN	> 10
C_5-THN	> 10
C_8-THN	0.47 ± 0.16
C_{10}-THN	0.37 ± 0.10
C_{12}-THN	0.013 ± 0.005
C_{15}-THN	0.050 ± 0.002
C_{16}-THN	0.48 ± 0.09
α-TOH	1.8 ± 0.3
PMHC	0.059 ± 0.003
Fer-1	0.045 ± 0.005
Lip-1	0.038 ± 0.003

transfected to express the fusion protein MerCreMer, which is Cre recombinase (Cre) flanked by two mutated estrogen receptors (Mer) which maintain it in the cytosol.[18] Upon treatment with 4-hydroxytamoxifen, Cre is released from its cytosolic complex, translocates to the nucleus and mediates *gpx4* gene deletion. The results of these experiments, shown in **Figure 2.5A**, were consistent with the trends observed upon pharmacological inhibition of Gpx4 using RSL3. That is, the lipophilic THNs were similarly potent to Fer-1 and Lip-1—all much more potent than α-TOH—whereas the hydrophobic THNs were ineffective. Interestingly, C_{12}-THN again appeared to be the most potent THN.

The cytoprotective abilities of the THNs were also compared to Fer-1 and Lip-1 in HT22 mouse hippocampal cells, wherein cell death was induced by high extracellular concentrations of glutamate. These conditions inhibit the cystine/glutamate antiporter (system x_c^-), depleting cells of cystine and resulting in the rapid depletion of GSH.[53] Cells treated with β-mercaptoethanol (β-Me) were employed as a positive control. β-Me

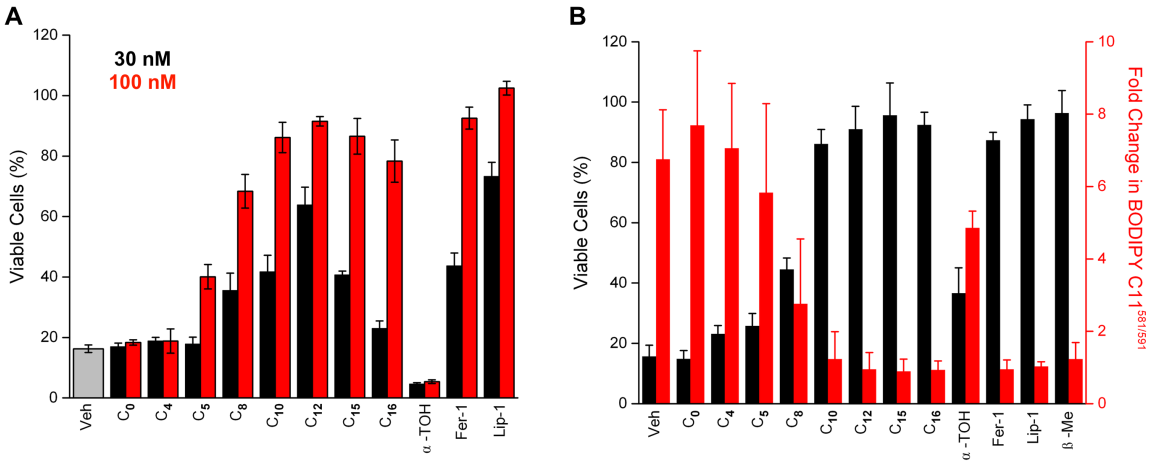

Figure 2.5 (**A**) Anti-ferroptotic activity of the THNs in mouse embryonic fibroblasts. Ferroptosis was initiated by tamoxifen-induced Cre-mediated deletion of the *gpx4* gene and cell survival was determined 6 hours post-induction by AquaBluer assay. Corresponding data obtained for Fer-1, Lip-1 and α-TOH are also shown. (**B**) The THNs prevent glutamate-induced cell death in mouse HT-22 hippocampal cells. Cells were treated with 5 mM glutamate and 100 nM of test compound for 10 hours, after which cell viability was assessed by AquaBluer assay. Corresponding data obtained for Fer-1, Lip-1, α-TOH and β-mercaptoethanol (β-Me) are also shown. HT-22 cell viability was associated with inhibition of lipid peroxidation, as revealed by suppression of BODIPY-C11$^{581/591}$ oxidation.

undergoes disulfide exchange with cystine and the resultant mixed disulfide can be taken up by the cells independently of system x_c^-, thereby supplying cysteine for GSH synthesis.[54] Cell viability was assayed using AquaBluer and the data are presented in **Figure 2.5B**. Consistent with foregoing results, the lipophilic THNs were again similarly effective to Lip-1 and Fer-1. Parallel studies indicated that cell survival coincided with the inhibition of lipid peroxidation (**Figure 2.5B**) and not with sustaining and/or restoring GSH levels (see **2.5** Supporting Information).

2.3 Discussion

The mechanism by which Fer-1 and Lip-1 prevent cell death brought about by Gpx4 inhibition, *gpx4* deletion or GSH depletion has been ascribed to their ability to inhibit lipid peroxidation directly by trapping chain-carrying radicals.[19,55] Both compounds are arylamines, and decades of research have shown that arylamines are good radical-

trapping antioxidants.[21,56] However, arylamines are generally only moderately reactive at ambient temperatures; they require temperatures above 100°C to achieve the catalytic reactivity that make them essential additives to engine lubricants, rubber and many other petroleum-derived products. In fact, industry standard alkylated diphenylamines react *ca.* 20-fold more slowly with peroxyl radicals than does α-TOH at ambient temperatures (k_{inh} = 1.8×10^5 and 3.2×10^6 $M^{-1}s^{-1}$ for the former and latter, respectively, measured in chlorobenzene at 37°C),[30] which is inconsistent with the fact that Fer-1 and Lip-1 are much more effective than α-TOH at preventing ferroptosis. At first glance, this suggests that Fer-1 and Lip-1 possess a different mechanism of action and/or that lipid peroxidation does not contribute significantly to ferroptosis.

The kinetic studies detailed above reveal that Fer-1 and Lip-1 have inherent reactivities to peroxyl radicals that are almost indistinguishable from alkylated diphenylamines, with rate constants of 3.1×10^5 $M^{-1}s^{-1}$ measured in chlorobenzene at 37°C. Although these rate constants are still an order of magnitude lower than that measured for α-TOH under the same conditions, this difference is erased in lipid bilayers. In fact, Fer-1 and Lip-1 are both significantly more reactive than α-TOH in unilamellar phosphatidylcholine liposomes. The origin of the differences in reactivity on going from a non-polar organic solvent (chlorobenzene) to lipid bilayers is revealed by additional experiments carried out using PMHC, an analog of α-TOH in which the $-C_{16}H_{33}$ sidechain is truncated to a methyl group. The reactivity of PMHC in lipid bilayers is roughly 10-fold greater than that of α-TOH – consistent with previous observations[45] and the notion that the lengthy sidechain leads to poorer dynamics in the bilayer. This is compounded by the fact that PMHC (and α-TOH) are significantly less reactive to peroxyl radicals in H-bond

accepting media—such as the lipid/water interface of the lipid bilayers—since the phenolic H-atom can be engaged in a H-bond, precluding its transfer to peroxyl radicals. Fer-1 and Lip-1, being amines, are weaker H-bond donors, making them relatively insensitive to interactions with H-bond accepting entities and consequently more reactive to radicals.

Although weaker H-bonding interactions and better dynamics account for the greater reactivity of Fer-1 and Lip-1 to peroxyl radicals in lipid bilayers compared to α-TOH it also suggests that the potency of α-TOH should be greater if its lipophilic sidechain was truncated. Indeed, PMHC was found to have similar activity to Fer-1 and Lip-1 when ferroptosis was induced by Gpx4 inhibition with RSL3 (EC_{50} = 59±3 nM compared to 45±5 and 38±3 nM for Fer-1 and Lip-1, respectively). While this is a useful mechanistic experiment, PMHC is ineffective *in vivo* because the sidechain of tocopherols are essential for their bioavailability.[57,58]

Interestingly, Lip-1 (and to a lesser extent, Fer-1) is more effective in subverting ferroptosis compared to PMHC despite its lower reactivity toward peroxyl radicals in lipid bilayers (smaller k_{inh}). We wondered if this difference could be ascribed to the fact that Lip-1 (and to a lesser extent, Fer-1) exhibits a greater capacity to trap peroxyl radicals (larger n) in lipid bilayers. Indeed, in contrast to PMHC (and α-TOH), the reaction stoichiometry measured for the reaction of Lip-1 (and Fer-1) with peroxyl radicals was highly variant with medium. That is, while PMHC and α-TOH always displayed n = 2, Lip-1 (and Fer-1) were characterized by $n \sim 1$ in styrene autoxidations, $n \sim 2$ in cumene autoxidations and $n >> 2$ in phosphatidylcholine lipid bilayers. This implies a different fate of the aminyl radical that is formed following initial H-atom transfer under the different autoxidation conditions. The different behaviour of Lip-1 (and Fer-1) in styrene and

cumene autoxidations is reminiscent of the behaviour of catechol and hydroquinone RTAs.[59] In styrene autoxidations, where there is a low steady-state concentration of radicals due to rapid termination of the secondary peroxyl radicals ($k_t = 2.1\times10^7$ $M^{-1}s^{-1}$), the aminyl radicals that are formed following H-atom transfer to styrylperoxyl radicals have time to react with O_2, eroding *n*. In contrast, cumene autoxidations feature much higher steady-state concentration of radicals due to comparatively slow termination ($k_t = 2.3\times10^4$ $M^{-1}s^{-1}$) preventing erosion of *n*.

The observation that $n >> 2$ for Lip-1 (and Fer-1) in phospholipid bilayers implies that their oxidation products are capable of trapping additional radicals. Two possibilities stemming from the key aminyl radical intermediate are illustrated in Scheme 2. In **path a**, H-atom transfer from the aminyl radical to trap a second peroxyl radical yields the highly electrophilic **o**-quinone diimide, which reacts with water to restore the reactive N-H bonds of Lip-1 following tautomerization. The requirement for water to both hydrate the **o**-quinone diimide and drive tautomerization would explain why this is not observed in the hydrocarbon autoxidations that were carried out – only in the phospholipid liposome autoxidations. In **path b,** the intermediate aminyl radical reacts with a second peroxyl radical to produce a nitroxide. Although this is not a radical-trapping step (an alkoxyl radical is produced), the nitroxide that is formed is capable of trapping radicals in a catalytic fashion – first by reaction with a peroxyl radical and then by reaction with an alkyl radical to restore the nitroxide from the oxoammonium ion.[60] The electron transfer processes key to this cycle would be facilitated in the polar interfacial region of the phospholipid liposomes compared to neat hydrocarbons—again consistent with our observations in the different media.

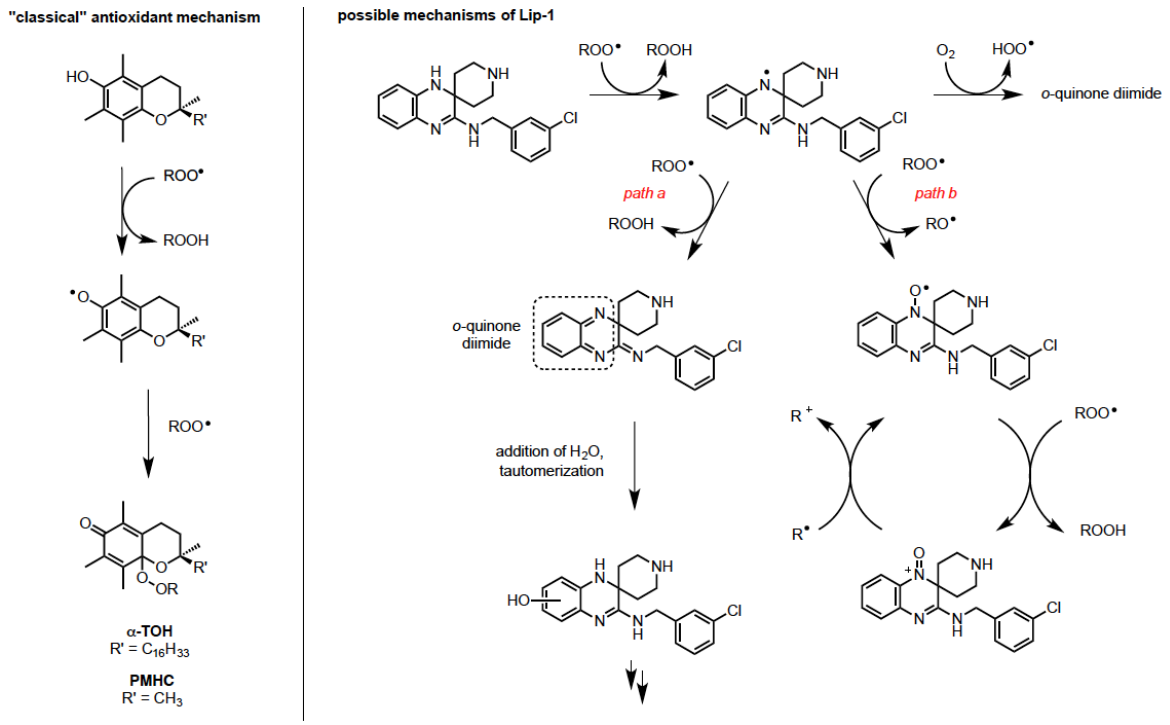

Scheme 2.2 Increased Radical-Trapping Capacity of Lip-1 (shown) and Fer-1 (not shown) Relative to Phenolic Antioxidants Such as α-TOH and PMHC Arises Due to their Ability to Form Products that Remain Highly Reactive to Peroxyl Radicals

In order to provide support for either of these mechanisms, we carried out additional experiments with the dihydroquinoline **1**, which features a similarly hindered aryl N-H to Lip-1.

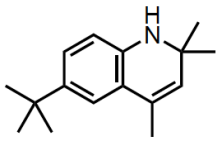

1

Although **1** is predicted to have an essentially identical N-H BDE to Lip-1 (calculated using CBS-QB3 to be 82.8 kcal/mol, compared to 82.7 kcal/mol for Lip-1), and can therefore be expected to transfer its aminic H-atom to a peroxyl radical in a similar fashion, it cannot undergo a second H-atom transfer reaction to form an *o*-quinone diimide intermediate. Nevertheless, autoxidations of phosphatidylcholine liposomes inhibited by **1** were strikingly similar to those inhibited by Lip-1, with only a slightly larger k_{inh} of

$(2.2\pm0.2)\times10^4$ $M^{-1}s^{-1}$, and most importantly, featuring $n >> 2$ (**Figure 2.6A**). These results suggest that **path a** in **Scheme 2.2** is unlikely to be responsible for the increased radical-trapping capacity of Lip-1 compared to conventional RTAs. Moreover, **1** was effective in subverting ferroptosis in mouse fibroblasts treated with RSL3, with a similar potency (EC_{50} = 77 nM) to that determined for Lip-1 (EC_{50} = 38 nM).

Strong evidence in support of the mechanism in **path b** of **Scheme 2.2** would best include the independent preparation of the Lip-1-derived nitroxide and demonstration that it can also inhibit lipid peroxidation. Unfortunately, our attempts to independently prepare the authentic Lip-1-derived nitroxide were unsuccessful, leading to intractable mixtures of products that included at least two nitroxides, as determined by electron paramagnetic resonance (EPR) spectroscopy (see **2.5** Supporting Information for example spectra). However, we were able to prepare the nitroxide derived from the dihydroquinoline **1** (see EPR spectrum in **Figure 2.6B**), and found that it was a very good RTA in this system

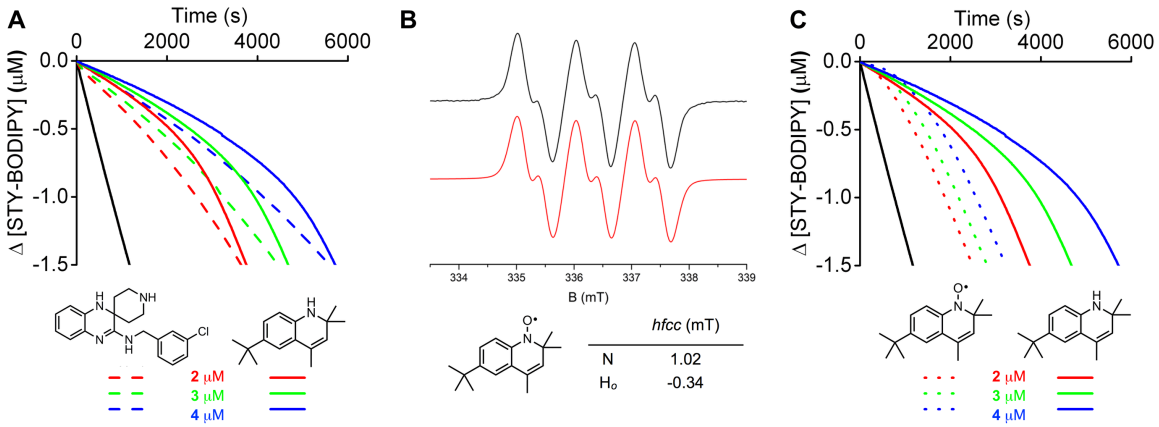

Figure 2.6 Co-autooxidations of egg phosphatidylcholine lipids (1 mM) and STY-BODIPY (8 μM) suspended in phosphate-buffered saline (10 mM) at pH 7.4 initiated by MeOAMVN (0.2 mM) at 37°C (black trace) and inhibited by 2 μM (red trace), 3 μM (green trace) and 4 μM (blue trace) of 1 (dotted line) and Lip-1 (solid line) (**A**), EPR spectrum of the nitroxide derived from 1 (**B**), and corresponding co-autoxidations inhibited by 1 (dotted line) and the nitroxide derived therefrom (dashed line) (**C**). Reaction progress in the co-autoxidations was monitored by absorbance at 565 nm (ε = 139,000 $M^{-1}cm^{-1}$).

(**Figure 2.6C**). The duration of the nominal inhibited period of the nitroxide is less than that of the amine since the amine must trap a radical prior to being converted to the nitroxide. However, the rate of oxidation following the inhibited period is indistinguishable between the amine and the nitroxide—both being less than the uninhibited rate—consistent with the formation of a common intermediate that can still retard the oxidation as suggested in **Scheme 2.2**. The nitroxide was also capable of subverting ferroptosis; we found EC_{50} = 99±5 nM under the same conditions that yielded 77 nM for **1** and 38 nM for Lip-1. Interestingly, Wipf and co-workers recently reported that mitochondrially-targeted nitroxide derivatives are good inhibitors of ferroptotic cell death;[61] their best examples being slightly less effective than Fer-1, similar to the nitroxide derived from dihydroquinoline **1**.

The central role of lipid peroxidation in ferroptosis—and radical-trapping antioxidants in subverting it—is further supported by the lack of significant inhibitory activity of Fer-1 and Lip-1 on lipoxygenase catalysis. Each of Fer-1, Lip-1 and α-TOH were unable to inhibit arachidonic acid oxidation to 15-H(P)ETE in lysates of HEK-293 cells transfected to overexpress 15-LO when treated up to 10 μM – almost three orders of magnitude more than the concentration at which Fer-1 and Lip-1 inhibit ferroptosis in the same cells (EC_{50} = 15 and 27 nM, respectively). The suppression of 15-H(P)ETE formation that is observed at low concentrations of these compounds must be due to the inhibition of arachidonic acid autoxidation that occurs under the assay conditions—indicated by both the lack of a dose-response for Fer-1, Lip-1 and α-TOH that is clearly observed when 15-H(P)ETE formation is suppressed (fully) by the known 15-LO inhibitor PD146176 and also by suppression of other regioisomeric H(P)ETEs that arise from

autoxidation (e.g. 5- and 12-H(P)ETE, see **2.5** Supporting Information). Despite being a better 15-LO inhibitor than Fer-1, Lip-1 and α-TOH, PD146176 is a relatively poor inhibitor of ferroptosis—with no inhibition of RSL-3-induced cell death up to 10 μM in the 15-LO overexpressing cells, and an EC_{50} of 8.5 μM in the wild-type cells. It should be pointed out that Angeli *et al.* showed that 1 μM and PD146176 was effective at subverting ferroptosis brought about by *gpx4* deletion in mouse embryonic fibroblasts[18] and Yang *et al.* showed that 5 μM PD146176 subverted erastin-induced ferroptosis in HT-1080 human fibrosarcoma cells.[25] Consistent with our own observations, Angeli and Yang each found that Fer-1 and/or Lip-1 (and α-TOH) were effective at significantly lower concentrations under the same assay conditions.[62]

Although 15-LO is but one of six isoforms of lipoxygenase that occur in humans, it is the isoform that has been implicated in several recent studies linking lipoxygenase catalysis and ferroptosis.[25,26,53,63] One such study suggested that α-TOH inhibits ferroptosis by LO inhibition.[60] The basis for this assertion was that tocotrienols were demonstrably more effective inhibitors of ferroptosis than tocopherols, and tocotrienols were predicted to bind more strongly to 15-LO than tocopherols owing to the three unsaturations in their lipophilic sidechains. An alternative explanation must exist in order to reconcile our observation that removal of α-TOH's sidechain improves its potency as an inhibitor of ferroptosis. Indeed, it is known that tocotrienols are incorporated into cells more quickly than tocopherols;[64] thus, their increased potency in cell assays may simply reflect a greater concentration in the cell at the time of the assay. We wonder if alternative explanations may account for other observations that have prompted suggestions that LOs drive ferroptosis.

Since the results of our studies on the mechanism by which Fer-1 and Lip-1 subvert ferroptosis pointed strongly at their ability to prevent lipid peroxidation by trapping chain-carrying peroxyl radicals, we surmised that the THNs should be excellent ferroptosis inhibitors. This proved to be the case. Lipophilic THNs were similarly potent to Fer-1 and Lip-1 in three different established cell models of ferroptosis (RSL3-inhibition of Gpx4, Cre-mediated deletion of *gpx4* and glutamate inhibition of cysteine uptake). Consistent with our recent studies on the radical-trapping antioxidant activity of the same set of THNs in lipid bilayers,[32] the more hydrophilic derivatives were significantly less potent, suggesting poor cell incorporation and/or their facile autoxidation in the cytosol or cell culture medium. Similarly to Fer-1, Lip-1 and α-TOH, the THNs were not effective inhibitors of 15-LO. These results reinforce the notion that, in the cell types that we have studied here, non-enzymatic lipid peroxidation drives ferroptosis. However, it must be acknowledged that lipid peroxidation and lipoxygenase catalysis may contribute differently to ferroptosis in other cell types. Clearly, further investigation is necessary, as is the need to understand why phosphoethanolamine-esterified polyunsaturated fatty acids appear to play a particularly important role in ferroptosis. Regardless, we anticipate that the foregoing results, and the insights they afford on the radical-trapping mechanisms of Lip-1 and Fer-1, will enable the development of improved inhibitors of ferroptosis that may be useful as therapeutics in diseases where ferroptosis is likely to contribute.

2.4 Experimental Methods

Materials. The THNs,[32] Fer-1,[19] PBD-BODIPY and STY-BODIPY[36] were synthesized according to literature procedures and Lip-1 was synthesized as described in **2.5** Supporting Information. Egg phosphatidylcholine, AIBN, MeOAMVN, BODIPY-

$C11^{581/591}$, RPMI-1640 media with/without phenol red, (D)MEM with/without phenol red, Dulbecco's phosphate-buffered saline (DPBS), fetal bovine serum (FBS), penicillin-streptomycin, Aquabluer and reagents for synthesis were purchased from commercial sources and used as received. Autoxidations employed HPLC grade solvents.

Inhibited Autoxidation of Styrene. These experiments were carried out in a manner similar to that described in our previous work.[36] In brief, styrene (Sigma-Aldrich) was washed thrice with 1 M aqueous NaOH, dried over $MgSO_4$, filtered, distilled under vacuum and purified by percolating through silica, then basic alumina. To a cuvette of 1.25 mL styrene was added 1.18 mL chlorobenzene and the solution equilibrated for 5 minutes at 37°C. The cuvette was blanked and 12.5 μL of 2 mM PBD-BODIPY in 2,3,5-trichlorobenzene was added followed by 50 μL of 0.3 M AIBN in chlorobenzene and the solution was thoroughly mixed. After 20 minutes, an aliquot of Lip-1, Fer-1, C_{15}-THN, PMHC or α-TOH stock solution (1 mM) in chlorobenzene was added and the loss of absorbance at 591 nm followed. The inhibition rate constant (k_{inh}) and stoichiometry (n) was determined for each experiment according to Eq. (2) and (3), respectively (see **2.5** Supporting Information for complete details). Autoxidations were carried out with three technical replicates at each concentration and kinetics are reported as the mean ± standard deviation.

Inhibited Autoxidation of PC Liposomes. To a cuvette of 2.34 mL of 10 mM PBS at pH 7.4 was added liposomes (125 μL of 20 mM stock in PBS at pH 7.4)[32] and the solution equilibrated for 5 minutes at 37°C. The cuvette was blanked and 10 μL of 2 mM STY-BODIPY in DMSO was added followed by 10 μL of 0.05 M MeOAMVN in acetonitrile and the solution was thoroughly mixed. After 5 minutes, an aliquot of Lip-1,

Fer-1, C_{15}-THN, PMHC or α-TOH stock solution (1 mM) in DMSO was added and the loss of absorbance at 565 nm followed. The inhibition rate constant (k_{inh}) and stoichiometry (n) was determined for each experiment according to Eq. (2) and (3), respectively (see the Supporting Information for complete details). Autoxidations were carried out with three technical replicates at each concentration and kinetics are reported as the mean ± standard deviation. Indistinguishable results were obtained in select control experiments where the antioxidant was added prior to liposome extrusion.

Cell Culture. All cell lines were cultured at 37 °C in a 5% CO_2 atmosphere unless otherwise indicated. HEK-293 cells were cultured in MEM with 10% FBS, 1% 100× non-essential amino acid solution, 1 mM sodium pyruvate and 1% penicillin-streptomycin. Pfa-1 mouse embryonic fibroblasts[27] were cultured in DMEM containing 10% FBS, 10 mM glutamine, 100 IU/ml penicillin and 100 μg/ml streptomycin. HT22 cells were cultured in DMEM containing 10% FBS, 10 mM glutamine, 100 IU/ml penicillin and 100 μg/ml streptomycin in a 10% CO_2 atmosphere. Cells were passaged by dissociation with 0.05% trypsin and 0.2% EDTA every other day.

Overexpression of 15-LO in HEK 293 cells. Cells were plated to 30% confluency and were transfected with a recombinant pcDNA3/15-LO construct[65] using LipoJet reagent according to the manufacturer's recommendations. The cells were passaged to 35 mm plates after 1 day and colonies were screened using selection medium containing 1 mg/mL geneticin. After establishing a stable cell line, the 15-LO cells were cultured in MEM with 10% FBS, 1% 100× non-essential amino acid solution, 10 mM glutamine and 1 mg/mL geneticin.

Western blot analysis. Protein extracts were prepared by lysing either HEK 293 cells or 15-LO cells in sodium dodecyl sulfate-polyacrylamide gel electrophoresis (SDS-PAGE) protein loading buffer (62.5 mM Tris [pH 6.8], 25% glycerol, 2% SDS, 0.1% bromophenol blue, 5% 2-mercaptoethanol). After separation by 10% PAGE, the proteins were transferred to a polyvinylidene difluoride (PVDF) membrane (Immuno-Blot PVDF; Bio-Rad Laboratories), and blocked in 5% dry milk, Tris-buffered saline. The membrane was probed with an antibody specific for 15-LO (Novusbio). Binding of the primary antibody was detected using a goat anti-mouse secondary antibody conjugated to horseradish peroxidase (Novusbio) and visualized by ECL chemiluminescence reaction (Pierce ECL, Thermo Scientific).

Determination of 15-LO Products by UPLC/MS/MS.[62] 15-LO overexpressing cells were harvested and lysed in Tris-HCl (pH 7.4) in the presence of 1% protease inhibitor cocktail (Sigma Aldrich). The residue was vortexed at 10,000 rpm for 10 minutes and the supernatants were incubated with 70 μM arachidonic acid (AA, Nu-Chek Prep) at 37°C for 10 min. The reactions were terminated with 1 volume of methanol followed by TCEP (1.5 mg/mL, Sigma-Aldrich). The samples were stored at room temperature for 90 min. For inhibition studies, incubations with inhibitors were carried out for 10 min on ice prior to the addition of AA. Briefly, 10 μM prostaglandin B_2 (Cayman Chemical) was added as internal standard along with 15 μl of 1M HCl for acidification followed by extraction using C-18 solid phase extraction columns (Thermo Scientific) as per manufacturer's protocol. The eluent in methanol was evaporated to dryness and resuspended in 100 μl methanol. Aliquots (5 μl) were injected on a Waters Acquity C_{18} column (2.1 mm × 50 mm, 1.7-μm particle size) in a Waters Acquity Ultra-Performance

Liquid Chromatography (UPLC) system. HETEs were eluted isocratically with a mixture of acetonitrile, methanol, water and acetic acid (42:25:33:0.007) and detected using MS/MS analysis. Eicosanoids were detected in the negative ion mode by multiple reaction monitoring of *m*/*z* 333 → 235 for PGB_2, *m*/*z* 319 → 115 for 5-HETE, *m*/*z* 319 → 179 for 12-HETE, and *m*/*z* 319 → 219 for 15-HETE. Each experiment was performed with three technical replicates and reproduced independently three times with error bars representing standard deviation from the mean.

Inhibition of Ferroptosis Induced by Gpx4 Inhibition with (1*S*,3*R*)-RSL3. Pfa-1 cells (3,000 in 100 μL) were seeded in 96-well plates and cultured for 6 hours, after which a mixture of linoleic acid (10 μM) and BSA (0.1%) was added and the cells incubated overnight in order to sensitize to ferroptosis. The next day the media was removed, the cells were washed twice with PBS and the cells were suspended in new media for 30 minutes before addition of (*1S,3R*)-RSL3 (100 nM) in a final volume of 100 μl. Cell viability was assessed 6 hours later using the AquaBluer (MultiTarget Pharmaceuticals, LLC) assay according to the manufacturer's instructions. Cell viability was calculated by normalizing the data to untreated controls.

Inhibition of Ferroptosis Induced by* gpx4 *Deletion. Tamoxifen-inducible *Gpx4*$^{-/-}$ Pfa-1 cells[27] (3,000 in 100 μL) were seeded in 96-well plates and cultured for 48 hours in the presence of 1 μM tamoxifen, after which the media was replaced with media containing the test compounds (30 or 100 nM). Cell viability was determined 6 hours after the media change using the Aquabluer assay according to the manufacturer's instructions. Cell viability was calculated by normalizing the data to untreated controls.

Inhibition of Glutamate Toxicity and Cell Death in Mouse Hippocampal Cells. HT22 Cells (30,000 in 100 μL) were seeded in 96-well plates and cultured for 24 hours after which the test compounds were added (100 nM), followed by glutamate (to 5 mM). Cell viability was assessed 10 hours later using AquaBluer. Lipid peroxidation levels were determined in a similar way. Cells (100,000 in 2 mL) were seeded in 6-well plates and glutamate and compounds were added 24 h later for 10 hours. BODIPY-C11$^{581/591}$ (1 μM) was then added for 30 minutes, the cells were trypsinized, washed and resuspended in PBS. Flow cytometry was performed using 488 nm line argon laser for excitation and emission was recorded on channels FL1 at 530 nm and FL2 at 585 nm. Data were collected from at least 30,000 cells. Total glutathione in the cells was measured by the enzymatic method described previously,[66] which is based on the catalytic action of the glutathione reductase system.

2.5 Supporting Information

Select synthetic procedures, inhibited autoxidations of cumene in chlorobenzene and THF in DMSO, and EPR spectra are included in this section. Computational details, GSH levels in HT22 cells and NMR spectra are available in the online version of the manuscript at DOI: 10.1021/acscentsci.7b00028.

2.5.1 Coautoxidations of cumene in chlorobenzene and coautoxidations of THF in DMSO and chlorobenzene.

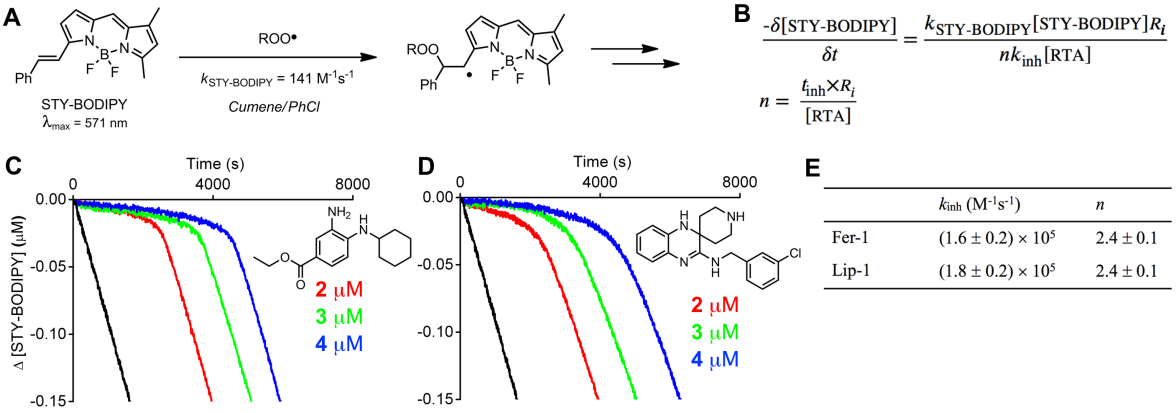

Figure 2.7 Coautoxidations of STY-BODIPY and cumene in chlorobenzene. STY-BODIPY serves as the signal carrier in cumene autoxidations (**A**), enabling determination of rate constants and reaction stoichiometries for reactions of inhibitors with chain-carrying peroxyl radicals (**B**). Coautoxidations of cumene (3.6 M) and STY-BODIPY (10 μM) initiated by AIBN (6 mM) in chlorobenzene at 37 °C (black trace) and inhibited by 2 μM (red trace), 3 μM (green trace), and 4 μM (blue trace) of Fer-1 (**C**) and Lip-1 (**D**). Average inhibition rate constants and stoichiometry summarized in (**E**). Reaction progress was monitored by absorbance at 571 nm (ε = 128,000 M^{-1} cm^{-1}).

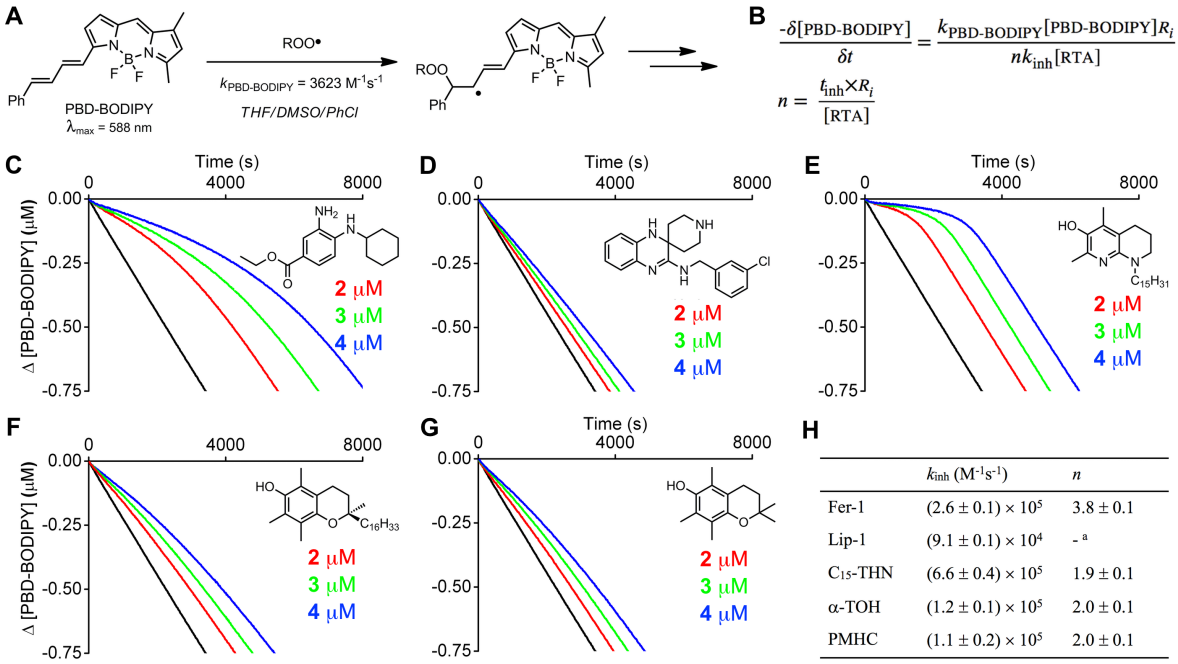

Figure 2.8 Coautoxidations of PBD-BODIPY and THF in DMSO and chlorobenzene. PBDBODIPY serves as the signal carrier in THF autoxidations (**A**), enabling determination of rate constants and reaction stoichiometries for reactions of inhibitors with chain-carrying peroxyl radicals (**B**). Coautoxidations of THF (3.1 M) and PBD-BODIPY (10 μM) initiated by AIBN (6 mM) in DMSO (25 vol%) and chlorobenzene at 37°C (black trace) and inhibited by 2 μM (red trace), 3 μM (green trace), and 4 μM (blue trace) of Fer-1 (**C**), Lip-1 (**D**), C15-THN (**E**), α-TOH (**F**), and PMHC (**G**). Average inhibition rate constants and stoichiometry summarized in (H). Reaction progress was monitored by absorbance at 588 nm (ε = 128,000 M^{-1} cm^{-1}).[a] The stoichiometry could not be determined from the data in panel D and stoichiometry was assumed to be 2 for calculation of k_{inh}.

2.5.2 Experimental procedures

Inhibited autoxidation of cumene in chlorobenzene. These experiments were carried out in a manner similar to that described in our previous work.[a] In brief, cumene was washed thrice with 1 M aqueous NaOH, dried over MgSO4, filtered, distilled under vacuum and purified by percolating through silica, then basic alumina. To a cuvette of 1.25 mL cumene was added 1.18 mL chlorobenzene and the solution equilibrated for 5 minutes

[a] Haidasz, E. A.; Kessel, A. V.; Pratt, D. A. A Continuous Visible Light Spectrophotometric Approach To Accurately Determine the Reactivity of Radical-Trapping Antioxidants. *J. Org. Chem.* **2016**, *81*, 737-744.

at 37°C. The cuvette was blanked and 12.5 μL of 2 mM STY-BODIPY in 1,2,4-trichlorobenzene was added followed by 50 μL of 0.3 M AIBN in chlorobenzene and the solution was thoroughly mixed. After 20 minutes, an aliquot of Lip-1, Fer-1, C15-THN, PMHC or α-TOH stock solution (1 mM) in chlorobenzene was added and the loss of absorbance at 571 nm followed. The inhibition rate constant (k_{inh}) and stoichiometry (n) was determined for each experiment as shown above. Autoxidations were carried out in triplicate.

Inhibited autoxidation of THF in DMSO and chlorobenzene. To a cuvette of 1.19 mL chlorobenzene was added 0.62 mL unstabilized THF and 0.62 mL DMSO and the solution equilibrated for 5 minutes at 37°C. The cuvette was blanked and 12.5 μL of 2 mM PBD-BODIPY in 1,2,4-trichlorobenzene was added followed by 50 μL of 0.3 M AIBN in chlorobenzene and the solution was thoroughly mixed. After 5 minutes, an aliquot of Lip-1, Fer-1, C15-THN, PMHC or α-TOH stock solution (1 mM) in DMSO was added and the loss of absorbance at 588 nm followed. The inhibition rate constant (k_{inh}) and stoichiometry (n) was determined for each experiment as shown above. Autoxidations were carried out in triplicate.

Inhibited autoxidation of styrene for determining KIEs. Lip-1 and Fer-1 stocks (10 mM) were stirred in methanol or methanol-d_4 overnight under N_2 and complete deuterium exchange was confirmed by ^{1}H NMR. Autoxidations of proteated and deuterated RTAs were completed in parallel and identical to styrene autoxidations described in **2.4** with the inclusion of 1% v/v MeOH (HPLC grade) or MeOD prior to blanking the cuvette.

2.5.3 Synthesis of Lip-1.

1-(3'-((3-chlorobenzyl)amino)-1'H-spiro[piperidine-4,2'-quinoxalin]-1-yl)ethanone (*N*-acetyl Lip-1): *N*-acetyl Lip-1 was synthesized by modification of the procedure of Kysil *et. al.*[a] *o*-phenylenediamine (1.081 g, 10 mmol, 1 equiv.) and *N*-acetyl-4-piperidinone (1.412 g, 10 mmol, 1 equiv.) were heated to reflux in 15 mL dry methanol for 4 h under N_2. The reaction mixture was allowed to cool to 50°C, and a solution of TMSCl (1.27 mL, 10 mmol, 1 equiv.) in 7.5 mL dry acetonitrile was added dropwise over 15 min, followed by 1-chloro-3-isocyanomethylbenzene[b] (1.516 g, 10 mmol, 1 eq) in 7.5 mL dry methanol dropwise over 1 h. The reaction mixture was stirred for 4 h at 50°C, cooled, and concentrated *in vacuo*. The residue was triturated in 50 mL dry ether followed by sonication for 10 min. The precipitate was collected by filtration, air dried, and transferred portionwise to 50 mL of water. The mixture was stirred during addition of 1 M aqueous NaOH to pH 9, and extracted with 6 × 50 mL $CHCl_3$. The combined organic layers were washed with brine, dried over $MgSO_4$, filtered and concentrated to yield a brown oil which was purified by silica gel chromatography, 1:5:94 Et_3N:MeOH:CH_2Cl_2. The product was recrystallized from ethanol/hexanes to yield *N*-acetyl Lip-1 as granular crystals (1.53 g, 40%). ^{1}H NMR (400 MHz, DMSO-d_6): δ 7.24-7.36 (m, 4H), 7.16 (t, J = 6.0 Hz, 1H), 6.80 (dd, J = 7.6 Hz, 1.2 Hz, 1H), 6.73 (dd, J = 7.6 Hz, 1.2 Hz, 1H), 6.69 (ddd, J = 7.6 Hz, 1.2 Hz, 1H), 6.54 (ddd, J = 7.6 Hz, 1.2 Hz, 1H), 6.12 (s, 1H), 4.47 (d, J =

---

[a] Kysil, V.; Khvat, A.; Tsirulnikov, S.; Tkachenko, S.; Williams, C.; Churakova, M. & Ivachtchenko, A. General Multicomponent Strategy for the Synthesis of 2-Amino-1,4-diazaheterocycles: Scope, Limitations, and Utility. *Eur. J. Org. Chem.* **2010**, *2010*, 1525– 1543.

[b] Kercher, T.; Rao, C.; Bencsik, J. R.; Josey, J. A. Diversification of the Three-Component Coupling of 2-Aminoheterocycles, Aldehydes, and Isonitriles: Efficient Parallel Synthesis of a Diverse and Druglike Library of Imidazo- and Tetrahydroimidazo[1,2-a] Heterocycles. *J. Comb. Chem.* **2007**, *9*, 1177-1187.

5.6 Hz, 2H), 4.27 (d, *J* = 12.8 Hz, 1H), 3.68 (d, *J* = 12.8 Hz, 1H), 3.43 (t, *J* = 13.2 Hz, 1H), 2.93 (t, *J* = 12.0 Hz, 1H), 2.01 (s, 3H), 1.88 (dt, *J* = 12.8 Hz, 4.4 Hz, 1H) , 1.79 (dt, *J* = 12.8 Hz, 4.8 Hz, 1H), 1.52-1.60 (m, 2H). ^{13}C NMR (100 MHz, DMSO-d_6): δ 168.1, 157.5, 143.0, 134.8, 134.4, 132.7, 130.0, 128.35, 128.31, 127.1, 126.3, 126.0, 122.7, 122.3, 117.9, 113.5, 50.8, 35.4, 31.6, 30.9, 21.3. HRMS (EI) calc. for $C_{21}H_{23}ClN_4O$ [M+] 382.1560; found 382.1530.

***N*-(3-chlorobenzyl)-1'H-spiro[piperidine-4,2'-quinoxalin]-3'-amine (Lip-1):** To a solution of *N*-acetyl Lip-1 (450 mg, 1.18 mmol, 1 equiv.) in 20 mL 99% ethanol was added aqueous KOH (5 mL, 4.0 M) and the mixture heated to reflux for 3 h. The solution was cooled and concentrated *in vacuo*. To the residue was added 10 mL water and the mixture extracted 4 × 25 mL $CHCl_3$. The combined organic layers were washed with brine, dried over $MgSO_4$, filtered and concentrated to yield Lip-1 (380 mg, 95%), which was recrystallized from degassed benzene to yield colourless needles. ^{1}H NMR (400 MHz, DMSO-d_6): δ 7.24-7.35 (m, 4H), 7.13 (t, *J* = 6.4 Hz, 1H), 6.82 (dd, *J* = 7.6 Hz, 1.6 Hz, 1H), 6.69 (dd, *J* = 7.6 Hz, 1.6 Hz, 1H), 6.65 (ddd, *J* = 7.6 Hz, 1.6 Hz, 1H), 6.50 (ddd, *J* = 7.6 Hz, 1.6 Hz, 1H), 5.88 (s, 1H), 4.49 (d, *J* = 6.4 Hz, 2H), 2.88 (t, *J* = 12.0 Hz, 2H), 2.68 (d, *J* = 12.0 Hz, 2H), 2.01 (bs, 1H), 1.75 (dt, *J* = 12.0 Hz, 4.8 Hz, 2H), 1.46 (d, *J* = 12.0 Hz, 2H). ^{13}C NMR (100 MHz, DMSO-d_6): δ 158.4, 143.3, 135.2, 134.7, 132.7, 129.9, 126.9, 126.2, 125.8, 122.4, 122.0, 117.6, 113.6, 50.9, 42.7, 31.9. HRMS (EI) calc. for $C_{19}H_{21}ClN_4$ [M+] 340.1455; found 340.1496.

2.5.4 Generation of nitroxides.

Attempts to independently synthesize the nitroxides derived from Lip-1 and Fer-1 were challenging, and generally lead to intractable mixtures from which a single nitroxide

could not be isolated. For example, UV irradiation of Lip-1 in the presence of dibenzothiophene S-oxide (mild conditions we have recently developed for the synthesis of nitroxides) led to a mixture of at least two nitroxides (Figure 2.9), as well as other (diamagnetic) products.

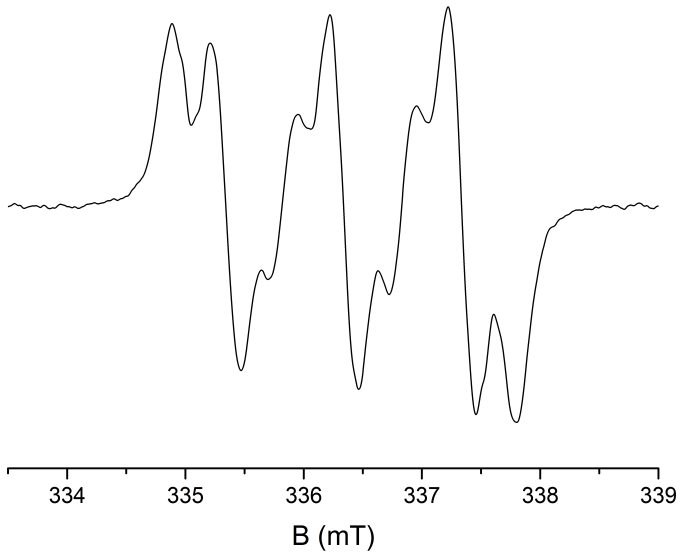

Figure 2.9 EPR spectrum of Lip-1 oxidation products.

2.6 References

[1] Finkel, T.; Holbrook, N. J. Oxidants, Oxidative Stress and the Biology of Ageing. *Nature* **2000**, *408*, 239–247.

[2] Vitale, G.; Salvioli, S.; Franceschi, C. Oxidative Stress and the Ageing Endocrine System. *Nat. Rev. Endocrinol.* **2013**, *9*, 228–240.

[3] Di Paolo, G.; Kim, T.-W. Linking Lipids to Alzheimer's Disease: Cholesterol and Beyond. *Nat. Rev. Neurosci.* **2011**, *12*, 284–296.

[4] Barnham, K. J.; Masters, C. L.; Bush, A. I. Neurodegenerative Diseases and Oxidative Stress. *Nat. Rev. Drug Discov* **2004**, *3*, 205–214.

[5] Benz, C. C.; Yau, C. Ageing, Oxidative Stress and Cancer: Paradigms in Parallax. *Nat. Rev. Cancer* **2008**, *8*, 875–879.

[6] Hussain, S. P.; Hofseth, L. J.; Harris, C. C. Radical Causes of Cancer. *Nat. Rev. Cancer* **2003**, *3*, 276–285.

[7] Dixon, S. J.; Lemberg, K. M.; Lamprecht, M. R.; Skouta, R.; Zaitsev, E. M.; Gleason, C. E.; Patel, D. N.; Bauer, A. J.; Cant- ley, A. M.; Yang, W. S.; Morrison, B.; Stockwell, B. R. Ferrop- tosis: An Iron-Dependent Form of Nonapoptotic Cell Death. *Cell* **2012**, *149*, 1060–1072.

[8] Yang, W. S.; Stockwell, B. R. Ferroptosis: Death by Lipid Peroxidation. *Trends Cell Biol.* **2016**, *26*, 165–176.

[9] Conrad, M.; Angeli, J. P. F.; Vandenabeele, P.; Stockwell, B. R. Regulated Necrosis: Disease Relevance and Therapeutic Opportunities. *Nat. Rev. Drug Discov* **2016**, *15*, 348–366.

[10] Trump, B. F.; Berezesky, I. K.; Chang, S. H.; Phelps, P. C. The Pathways of Cell Death: Oncosis, Apoptosis, and Necrosis. *Toxicol. Pathol.* **1997**, *25*, 82–88.

[11] Edinger, A. L.; Thompson, C. B. Death by Design: Apop- tosis, Necrosis and Autophagy. *Curr. Opin. Cell Biol.* **2004**, *16*, 663–669.

[12] Xie, Y.; Hou, W.; Song, X.; Yu, Y.; Huang, J.; Sun, X.; Kang, R.; Tang, D. Ferroptosis: process and function. *Cell Death Differ.* **2016**, *23*, 369–379.

[13] Gaschler, M. M.; Stockwell, B. R. Lipid Peroxidation in Cell Death. *Biochem. Biophys. Res. Commun.* **2017**, *482*, 419– 425.

[14] Yin, H.; Xu, L.; Porter, N. A. Free Radical Lipid Peroxidation: Mechanisms and Analysis. *Chem. Rev.* **2011**, *111*, 5944–5972.

[15] Porter, N. A. Mechanisms for the Autoxidation of Polyunsaturated Lipids. *Acc. Chem. Res.* **1986**, *19*, 262–268; Pratt, D. A.; Tallman, K. A.; Porter, N. A. Free radical oxidation of polyunsaturated lipids: New mechanistic insights and the development of peroxyl radical clocks. *Acc. Chem. Res.* **2011**, *44*, 458–467.

[16] Haeggström, J. Z.; Funk, C. D. Lipoxygenase and Leukotriene Pathways: Biochemistry, Biology, and Roles in Disease. *Chem. Rev.* **2011**, *111*, 5866–5898.

[17] Girotti, A. W. Lipid Hydroperoxide Generation, Turnover, and Effector Action in Biological Systems. *J. Lipid Res.* **1998**, *39*, 1529–1542.

[18] Friedmann Angeli, J. P.; Schneider, M.; Proneth, B.; Tyurina, Y. Y.; Tyurin, V. A.; Hammond, V. J.; Herbach, N.; Aichler, M.; Walch, A.; Eggenhofer, E.; Basavarajappa, D.; Radmark, O.; Kobayashi, S.; Seibt, T.; Beck, H.; Neff, F.; Esposito, I.; Wanke, R.; Forster, H.; Yefremova, O.; Heinrichmeyer, M.; Bornkamm, G. W.; Geissler, E. K.; Thomas, S. B.; Stockwell, B. R.; O'Donnell, V. B.; Kagan, V. E.; Schick, J. A.; Conrad, M. Inactivation of the ferroptosis regulator Gpx4 triggers acute renal failure in mice. *Nat. Cell. Biol.* **2014,** *16*, 1180-1191.

[19] Skouta, R.; Dixon, S. J.; Wang, J.; Dunn, D. E.; Orman, M.; Shimada, K.; Rosenberg, P. A.; Lo, D. C.; Weinberg, J. M.; Linkermann, A.; Stockwell, B. R. Ferrostatins Inhibit Oxidative Lipid Damage and Cell Death in Diverse Disease Models. *J. Am. Chem. Soc.* **2014**, *136*, 4551–4556.

[20] Nevertheless, the development of these compounds continues. See, e.g. See, e.g. Hofmans, S.; Berghe, T. V.; Devisscher, L.; Hassannia, B.; Lyssens, S.; Joossens, J.;, Van Der Veken, P.; Vandenabeele, P.; Augustyns, K. Novel Ferroptosis Inhibitors with Improved Potency and ADME Properties. *J. Med. Chem.* **2016**, *59*, 2041-2053.

[21] Ingold, K. U.; Pratt, D. A. Advances in Radical-Trapping Antioxidant Chemistry in the 21st Century: a Kinetics and Mechanisms Perspective. *Chem. Rev.* **2014**, *114*, 9022–9046.

[22] Burton, G. W.; Ingold, K. U. Vitamin E: Application of the Principles of Physical Organic Chemistry to the Exploration of Its Structure and Function. *Acc. Chem. Res.* **1986**, *19*, 194–201.

[23] Reddanna, P.; Rao, M. K.; Reddy, C. C. Inhibition of 5-Lipoxygenase by Vitamin-E. *FEBS Lett.* **1985**, *193*, 39–43.

[24] Grossman, S.; Waksman, E. G. New Aspects of the Inhibi tion of Soybean Lipoxygenase by Alpha-Tocopherol. Evidence for the Existence of a Specific Complex. *Int. J. Biochem.* **1984**, *16*, 281–289.

[25] Yang, W. S.; Kim, K. J.; Gaschler, M. M.; Patel, M.; Shchepinov, M. S.; Stockwell, B. R. Peroxidation of Polyunsaturated Fatty Acids by Lipoxygenases Drives Ferroptosis. *Proc. Natl. Acad. Sci. U.S.A.* **2016**, *113*, E4966–E4975.

[26] Ou, Y.; Wang, S.-J.; Li, D.; Chu, B.; Gu, W. Activation of SAT1 engages polyamine metabolism with p53-mediated ferroptotic responses. *Proc. Natl. Acad. Sci. U.S.A.* **2016**, *113*, E6806–E6812.

[27] Seiler, A.; Schneider, M.; Förster, H.; Roth, S.; Wirth, E.; Culmsee, C.; Plesnila, N.; Kremmer, E.; Rådmark, O.; Wurst, W.; Bornkamm, G.; Schweizer, U.; Conrad, M. Glutathione Peroxidase 4 Senses and Translates Oxidative Stress into 12/15-Lipoxygenase Dependent and AIF-Mediated Cell Death. *Cell Metab.* **2008**, *8*, 237-248.

[28] Pratt, D. A.; DiLabio, G. A.; Brigati, G.; Pedulli, G. F.; Valgimigli, L. 5-Pyrimidinols: Novel Chain-Breaking Antioxidants More Effective Than Phenols. *J. Am. Chem. Soc.* **2001**, *123*, 4625–4626.

[29] Wijtmans, M.; Pratt, D. A.; Valgimigli, L.; DiLabio, G. A.; Pedulli, G. F.; Porter, N. A. 6-Amino-3-Pyridinols: Towards Diffusion-Controlled Chain-Breaking Antioxidants. *Angew. Chem. Int. Ed.* **2003**, *42*, 4370–4373.

[30] Valgimigli, L.; Pratt, D. A. Maximizing the Reactivity of Phenolic and Aminic Radical-Trapping Antioxidants: Just Add Nitrogen! *Acc. Chem. Res.* **2015**, *48*, 966–975.

[31] Nam, T.-G.; Rector, C. L.; Kim, H.-Y.; Sonnen, A. F.-P.; Meyer, R.; Nau, W. M.; Atkinson, J.; Rintoul, J.; Pratt, D. A.; Porter, N. A. Tetrahydro-1,8-Naphthyridinol Analogues of Alpha-Tocopherol as Antioxidants in Lipid Membranes and Low-Density Lipoproteins. *J. Am. Chem. Soc.* **2007**, *129*, 10211– 10219.

[32] Li, B.; Harjani, J. R.; Cormier, N. S.; Madarati, H.; Atkinson, J.; Cosa, G.; Pratt, D. A. Besting Vitamin E: Sidechain Substitution Is Key to the Reactivity of Naphthyridinol Antioxidants in Lipid Bilayers. *J. Am. Chem. Soc.* **2013**, *135*, 1394– 1405.

[33] We should note that the Hecht group has extensively studied the somewhat related, but less reactive pyridinol and pyrimidinol derivatives as inhibitors of oxidative stress and associated mitochondrial dysfunction in cell culture. See, e.g. “Mastroeni, D.; Khdour, O. M.; Arce, P. M.; Hecht, S. M.; Coleman, P. D. Novel Antioxidants Protect Mitochondria From the Effects of Oligomeric Amyloid Beta and Contribute to the Maintenance of Epigenome Function. *ACS Chem. Neurosci.* **2015**, *6*, 588–598.; Alam, M. P.; Khdour, O. M.; Arce, P. M.; Chen, Y.; Roy, B.; Johnson, W. G.; Dey, S.; Hecht, S. M. Cytoprotective Pyridinol Antioxidants as Potential Therapeutic Agents for Neurodegenerative and Mitochondrial Diseases. *Bioorg. Med. Chem.* **2014**, *22*, 4935–4947.

[34] Yang, W. S.; SriRamaratnam, R.; Welsch, M. E.; Shimada, K.; Skouta, R.; Viswanathan, V. S.; Cheah, J. H.; Clemons, P. A.; Shamji, A. F.; Clish, C. B.; Brown, L. M.; Girotti, A. W.; Cornish, V. W.; Schreiber, S. L.; Stockwell, B. R. Regulation of Ferroptotic Cancer Cell Death by GPX4. *Cell* **2014,** *156,* 317-331.

[35] Howard, J. A.; Ingold, K. U. The Inhibited Autoxidation Of Styrene: Part I. The Deuterium Isotope Effect For Inhibition By 2, 6-Di-Tert-Butyl-4-Methylphenol. *Can. J. Chem.* **1962**, *40*, 1851–1864.

[36] Haidasz, E. A.; Kessel, A. V.; Pratt, D. A. A Continuous Visible Light Spectrophotometric Approach To Accurately Determine the Reactivity of Radical-Trapping Antioxidants. *J. Org. Chem.* **2016**, *81*, 737-744.

[37] Hanthorn, J. J.; Amorati, R.; Valgimigli, L.; Pratt, D. A. The Reactivity of Air-Stable Pyridine- and Pyrimidine-Containing Diarylamine Antioxidants. *J. Org. Chem.* **2012**, *77*, 6895–6907.

[38] The increase in fluorescence during the inhibited period results from the formation of antioxidant-derived autoxidation products that absorb at this wavelength.

[39] Burton, G. W.; Ingold, K. U. Autoxidation of Biological Molecules. 1. Antioxidant Activity of Vitamin E and Related Chain-Breaking Phenolic Antioxidants in Vitro. *J. Am. Chem. Soc.* **1981**, *103*, 6472–6477.

[40] Montgomery, J. A. Jr.; Frisch, M. J.; Ochterski, J. W.; Petersson, G. A. A complete basis set model chemistry. VI. Use of density functional geometries and frequencies. *J. Chem. Phys.* **1999**, *110*, 2822-2827.

[41] It should be noted that Fer-1 has an ethyl ester as opposed to methyl ester used in the computations.

[42] Valgimigli, L.; Bartolomei, D.; Amorati, R.; Haidasz, E.; Hanthorn, J. J.; Nara, S. J.; Brinkhorst, J.; Pratt, D. A. 3-Pyridinols and 5-Pyrimidinols: Tailor-Made for Use in Synergistic Radical-Trapping Co-Antioxidant Systems. *Beilstein J. Org. Chem.* **2013**, *9*, 2781–2792.

[43] Pratt, D. A.; DiLabio, G. A.; Valgimigli, L.; Pedulli, G. F.; Ingold, K. U. Substituent Effects on the Bond Dissociation Enthalpies of Aromatic Amines. *J. Am. Chem. Soc.* **2002**, *124*, 11085–11092.

[44] *k*p for STY-BODIPY in egg PC liposomes was determined by fitting of α-TOH inhibited autoxidations to the reported *k*inh for α-TOH (5.8 ×10^3 $M^{-1}s^{-1}$, Barclay, L. R. C.; Baskin, K. A.; Dakin, K. A.; Locke, S. J.; Vinqvist, M. R. The Antioxidant Activities of Phenolic Antioxidants in Free Radical Peroxidation of Phospholipid Membranes. *Can. J. Chem.* **1990**, *68*, 2258–2269) and R_i calculated from the inhibition time of PMHC inhibited autoxidations (R_i = (2.6 ±0.1) ×10^{-9} $M^{-1}s^{-1}$), to give k_p = 894 $M^{-1}s^{-1}$.

[45] Niki, E.; Noguchi, N. Dynamics of Antioxidant Action of Vitamin E. *Acc. Chem. Res.* **2004**, *37*, 45–51.

[46] See, *e.g.*, Barclay, L. R. C.; Edwards, C. E.; Vinqvist, M. R. Media Effects on Antioxidant Activities of Phenols and Catechols. *J. Am. Chem. Soc.* **1999**, *121*, 6226–6231.

[47] Litwinienko, G.; Ingold, K. U. Solvent Effects on the Rates and Mechanisms of Reaction of Phenols with Free Radicals. *Acc. Chem. Res.* **2007**, *40*, 222–230.

[48] Abraham, M. H.; Grellier, P. L.; Prior, D.V.; Duce, P. P.; Morris, J. J.; Taylor, P. J. *J. Chem. Soc., Perkin Trans. 2* **1989**, 699.

[49] The α_2^H value of *N*-*t*-butyl-4-*t*-butylaniline was determined by ^{1}H-NMR as described in Abraham, M. H.; Abraham, R. J.; Byrne, J.; Griffith, L. NMR Method for the Determination of Solute Hydrogen Bond Acidity. *J. Org. Chem.* **2006**, *71*, 3389-3394. This model amine was chosen to simplify interpretation of the spectra due to the greater number of interactions possible with the multiple N-H bonds present in both Lip-1 and Fer-1.

[50] Valgimigli, L.; Amorati, R.; Petrucci, S.; Pedulli, G. F.; Hu, D.; Hanthorn, J. J.; Pratt, D. A. Unexpected Acid Catalysis in Reactions of Peroxyl Radicals with Phenols. *Angew. Chem. Int. Ed.* **2009**, *48*, 8348–8351.

[51] Noguchi, N.; Yamashita, H.; Hamahara, J.; Nakamura, A.; Kuhn, H.; Niki, E. The Specificity of Lipoxygenase-Catalyzed Lipid Peroxidation and the Effects of Radical-Scavenging Antioxidants. *Biol. Chem.* **2002**, *383*, 619–626.

[52] Bocan, T. M. A.; Rosebury, W. S.; Mueller, S. B.; Susan Kuchera; Welch, K.; Daugherty, A.; Cornicelli, J. A. A Specific 15-Lipoxygenase Inhibitor Limits the Progression and Monocyte–Macrophage Enrichment of Hypercholesterolemia-Induced Atherosclerosis in the Rabbit. *Atherosclerosis* **1998**, *136*, 203–216.

[53] Lewerenz, J.; Hewett, S. J.; Huang, Y.; Lambros, M.; Gout, P. W.; Kalivas, P. W.; Massie, A.; Smolders, I.; Methner, A.; Pergande, M.; Smith, S. B.; Ganapathy, V.; Maher, P. The Cystine/Glutamate Antiporter System xc- in Health and Disease: From Molecular Mechanisms to Novel Therapeutic Opportunities. *Antioxid. Redox Signal.* **2013,** *18*, 522-555.

[54] Mandal, P. K.; Seiler, A.; Perisic, T.; Kolle, P.; Banjac Canak, A.; Forster, H.; Weiss, N.; Kremmer, E.; Lieberman, M. W.; Bannai, S.; Kuhlencordt, P.; Sato, H.; Bornkamm, G. W.; Conrad, M. System xc- and Thioredoxin Reductase 1 Cooperatively Rescue Glutathione Deficiency. *J. Biol. Chem.* **2010,** *285,* 22244-22253.

[55] Liu, Y.; Wang, W.; Li, Y.; Xiao, Y.; Cheng, J.; Jia, J. The 5-Lipoxygenase Inhibitor Zileuton Confers Neuroprotection against Glutamate Oxidative Damage by Inhibiting Ferroptosis. *Biol. Pharm. Bull.* **2015**, *38*, 1234-1239.

[56] Ingold, K. U. Inhibition of the Autoxidation of Organic Substances in the Liquid Phase. *Chem. Rev.* **1961,** *61*, 563-589.

[57] Burton, G. W.; Traber, M. G.; Acuff, R. V.; Walters, D. N.; Kayden, H.; Hughes, L.; Ingold, K. U. Human plasma and tissue α-tocopherol concentrations in response to supplementation with deuterated natural and synthetic vitamin E. *Am. J. Clin. Nutr.* **1998**, *67*, 669-684.

[58] Panagabko, C.; Morley, S.; Hernandez, M.; Cassolato, P.; Gordon, H.; Parsons, R.; Manor, D.; Atkinson, J. Ligand Specificity in the CRAL-TRIO Protein Family. *Biochemistry* **2003,** *42*, 6467-6474.

[59] Valgimigli, L.; Amorati, R.; Fumo, M. G.; DiLabio, G. A.; Pedulli, G. F.; Ingold, K. U.; Pratt, D. A. The Unusual Reaction of Semiquinone Radicals with Molecular Oxygen. *J. Org. Chem.* **2008**, *73*, 1830-1841.

[60] Haidasz, E. A.; Meng, D.; Amorati, R.; Baschieri, A.; Ingold, K. U.; Valgimigli, L.; Pratt, D. A. Acid Is Key to the Radical-Trapping Antioxidant Activity of Nitroxides. *J. Am. Chem. Soc.* **2016**, *138*, 5290-5298.

[61] Krainz, T.; Gaschler, M. M.; Lim, C.; Sacher, J. R.; Stockwell, B. R.; Wipf, P. A Mitochondrial-Targeted Nitroxide Is a Potent Inhibitor of Ferroptosis. *ACS Cent. Sci.*, **2016**, *2*, 653-659.

[62] Since PD146176 is an arylamine, it may actually inhibit ferroptosis as an RTA and not as an LO inhibitor. The difference in potency between it and Fer-1/Lip-1 may simply reflect its lower RTA activity.

[63] Kagan, V. E.; Mao, G.; Qu, F.; Angeli, J. P. F.; Doll, S.; St Croix, C.; Dar, H. H.; Liu, B.; Tyurin,V. A.; Ritov, V. B.; Kapralov, A. A.; Amoscato, A. A., Jiang, J.; Anthonymuthu, T.; Mohammadyani, D.; Yang, Q.; Proneth, B.; Klein-Seetharaman, J.; Watkins, S.; Bahar, I.; Greenberger, J.; Mallampalli, R.; Stockwell, B. R.; Tyurina, Y. Y.; Conrad, M.; Bayır, H. Oxidized arachidonic and adrenic PEs navigate cells to ferroptosis. *Nat. Chem. Biol.* **2017**, *13*, 81-90.

[64] Yoshida, Y.; Niki, E.; Noguchi, N. Comparative study on the action of tocopherols and tocotrienols as antioxidant: chemical and physical effects. *Chem. Phys. Lipids* **2003**, *123*, 63-75.

[65] Nair, D. G.; Funk, C. D. A cell-based assay for screening lipoxygenase inhibitors. *Prostaglandins and Other Lipid Mediat.* **2009**, *90*, 98-104.

[66] Sato, H.; Shiiya, A.; Kimata, M.; Maebara, K.; Tamba, M.; Sakakura, Y.; Makino, N.; Sugiyama, F.; Yagami, K.; Moriguchi, T.; Takahashi, S.; Bannai, S. Redox Imbalance in Cystine/Glutamate Transporter-deficient Mice *J. Biol. Chem.* **2005**, *280*, 37423-37429.

2.7 Supplementary Results and Discussion

Using the methodologies introduced in the previous sections, we sought to evaluate a small library of hindered aryl amines related to Lip-1 to further study their structure-activity relationship in support of the mechanistic proposals in **Scheme 2.2**, and to use that information in the rational design of superior ferroptosis inhibitors. The reactivity of spiroquinoxalinamines, related aryl amines, and proposed intermediates were evaluated by preparation of the compounds shown in **Figure 2.10**.

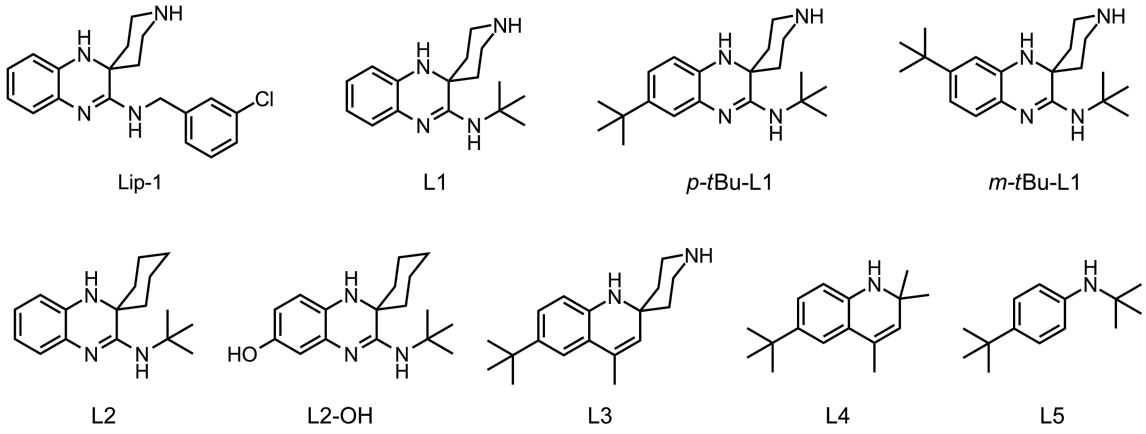

Figure 2.10 Spiroquinoxalinamines synthesized and evaluated in structure-activity relationship study herein.

2.7.1 Synthesis and rationale for spiroquinoxalinamine derivatives

Spiroquinoxalinamines are easily prepared by a one-pot multi-component reaction modeled after the Ugi reaction.[1] The condensation of one equivalent of *ortho*-phenylenediamine with one equivalent of a ketone affords an intermediate imine. The resultant imine is activated with a Lewis acid catalyst (TMSCl) towards attack by an isocyanide nucleophile followed by cyclization and tautomerization to fashion the spiroquinoxalinamines (**Scheme 2.3A**). Lip-1 is synthesized in good yield following basic

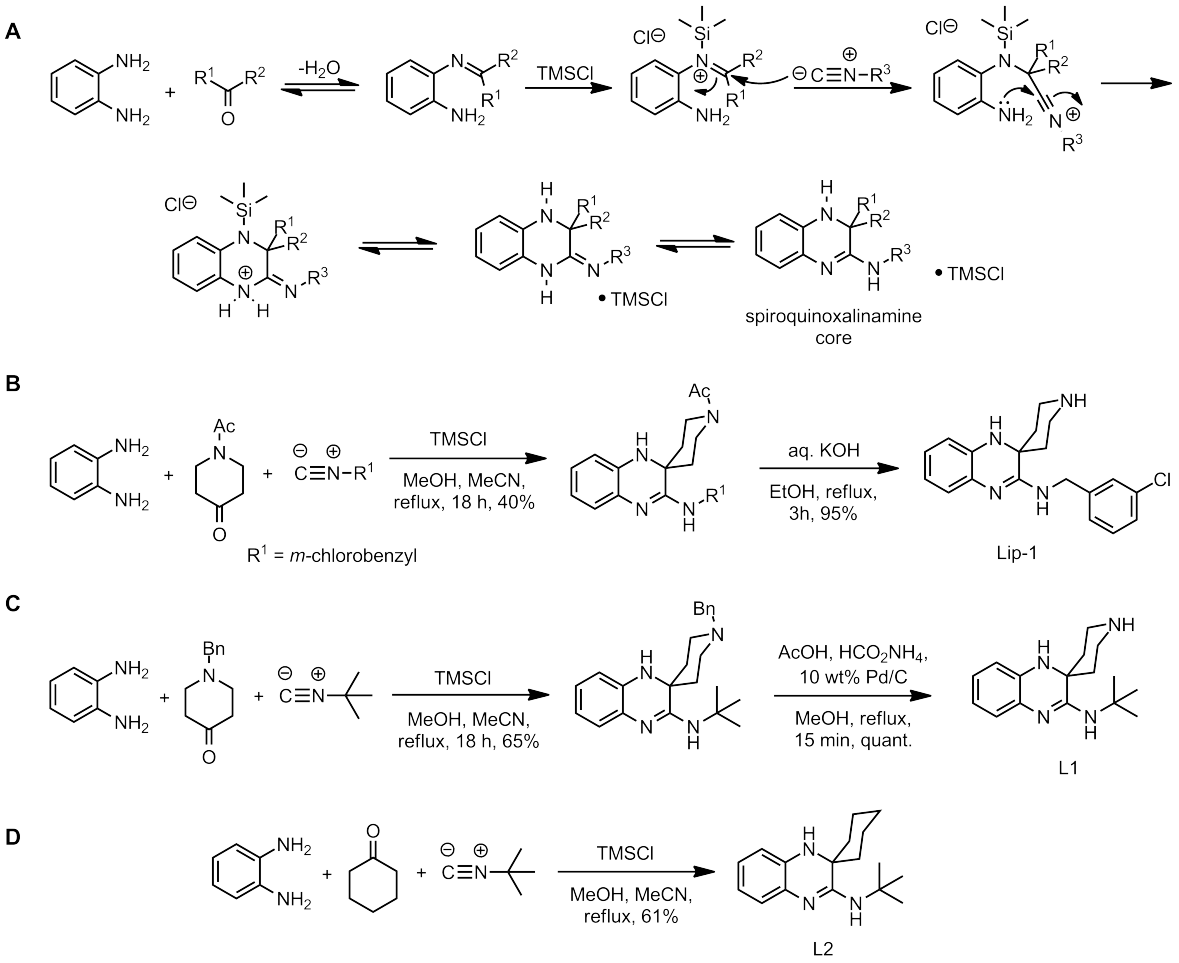

Scheme 2.3 Mechanism and synthesis of spiroquinoxalinamine derivatives. (**A**) Mechanism of the multicomponent reaction between a diamine, ketone, isocyanide, and lewis acid (TMSCl) to afford spiroquinoxalinamines. Synthesis of Lip-1 (**B**), L1 (**C**) and L2 (**D**).

hydrolysis from the multicomponent reaction of *N*-acetyl 4-piperidinone and metachlorobenzylisocyanide (**Scheme 2.3B**).

Substitution was varied on the amidine with a *t*-butyl group to probe the effect of the benzyl group of Lip-1. This modification allowed *N*-benzyl protected 4-piperidinones to be employed in these reactions since there is no benzyl group substitution on the amidine that would be removed by Pd/C hydrogenolysis. However, standard catalytic hydrogenolysis conditions did not result in conversion of starting material. It was hypothesized that poisoning of the palladium catalyst by the substrate aryl amine prevented

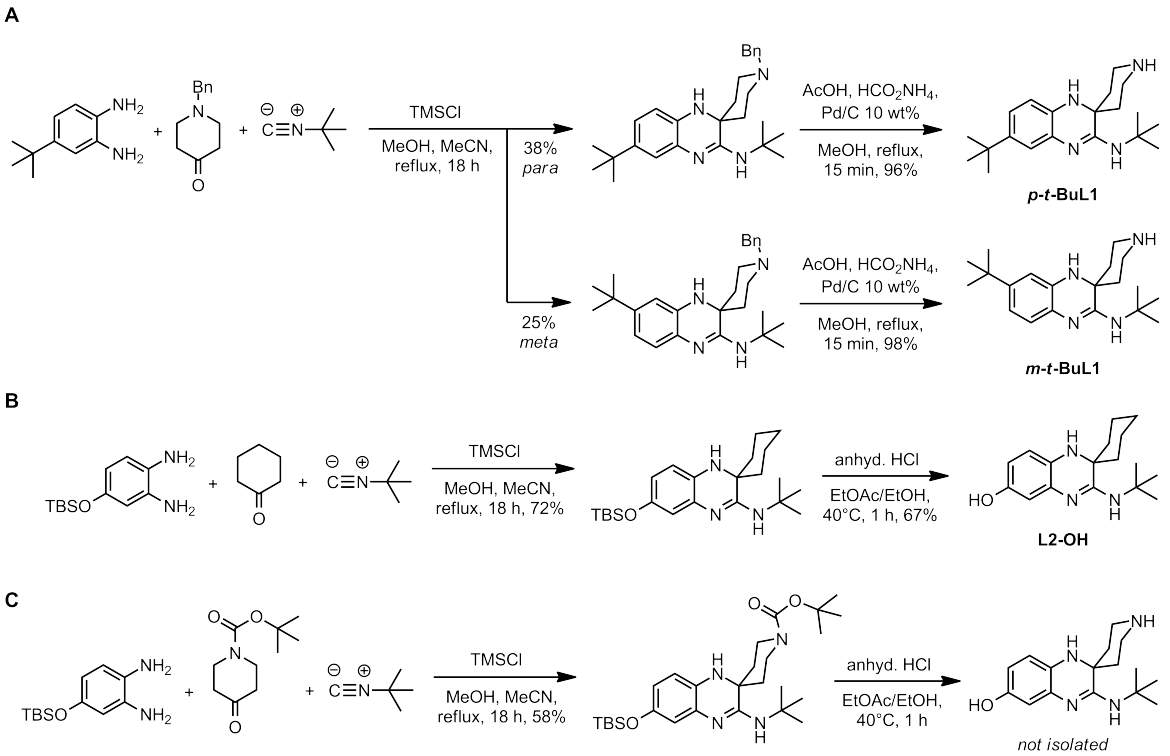

Scheme 2.4 Synthesis of aryl substituted spiroquinoxalinamines: *p*-*t*-Bu-L1 and *m*-*t*-Bu-L1 (**A**), L2-OH (**B**) and attempted synthesis of spiroquinoxalinamine-phenol (**C**).

turnover. This was overcome by the addition of acetic acid to mitigate catalyst inhibition, which rapidly afforded the free piperidine L1 (**Scheme 2.3C**). Notably, the piperidine ring is known to be required for the anti-ferroptotic potency of spiroquinoxalinamines.[2] Accordingly, we prepared the *cyclohexyl* spiroquinoxalinamine L2 (**Scheme 2.3D**) to evaluate the effect of the piperidine N-H on RTA activity.

Previous reports suggested that peroxyl addition onto the aromatic rings of aryl amine (such as diphenylamine)[3] and aryl nitroxide RTAs contributes to diminished stoichiometry by formation of quinone-imine or nitrone type structures, respectively.[4] Thus, we prepared derivatives with the aryl *para* and *meta* positions blocked with *t*-butyl groups (*p*-*t*BuL1 and *m*-*t*BuL1) to prevent ring oxidation. The two *N*-benzyl protected isomers were separated from a single reaction from the diamine 4-(*tert*-butyl)-1,2-diaminobenzene in 3:2 *para*:*meta* ratio. The slight preference for the *para* isomer is likely

owing to the weak electron-donating ability of the *t*-butyl group favouring formation of the *para*-*t*-butyl imine. Catalytic hydrogenolysis afforded the free piperidines (**Scheme 2.4A**).

Given our hypothesis of water addition to the *o*-quinonediimide intermediate in **Scheme 2.2**, **path a**, we envisioned preparation of a spiroquinoxalinamine-phenol. Employing TBS protected 3,4-diaminophenol in the multicomponent reaction afforded the protected spiroquinoxalinamine, which was deprotected by treatment with anhydrous HCl to afford L2-OH (**Scheme 2.4B**). This phenol was observed to be stable for *ca.* one week under ambient conditions, though this could potentially be overcome by storage under inert conditions. No selectivity for the *meta*-TBSO isomer was observed, presumably due to the strong electron-donating ability of the TBSO group to favour *para*-imine formation. The analogous protected piperidine derivatives were also attempted (**Scheme 2.4C**), however, after a one-pot deprotection of both *N*-Boc and O-TBS groups by anhydrous HCl, the product proved difficult to isolate by normal workup procedures owing to the high water-solubility of the compound. Future work could optimize the isolation and investigate the reactivity of these interesting derivatives.

The effect of the amidine moiety was evaluated by preparation of 1,2-dihydroquinolines. Condensation of an aniline with a ketone affords an intermediate imine, which in the presence of a strong acid catalyst is primed for attack by the enol form of a second ketone followed by dehydration to afford dihydroquinolines (**Scheme 2.5A**) in a facile metal-free approach. Thus, two equivalents of acetone are reacted with 4-*t*-butylaniline in the presence of catalytic tosic acid and driven by removal of water to form L4 (**Scheme 2.5C**) in good yield. The procedure was modified to prepare a variant with a spiro-piperidine moiety by sequential condensations: an equivalent of *N*-acetyl-4-

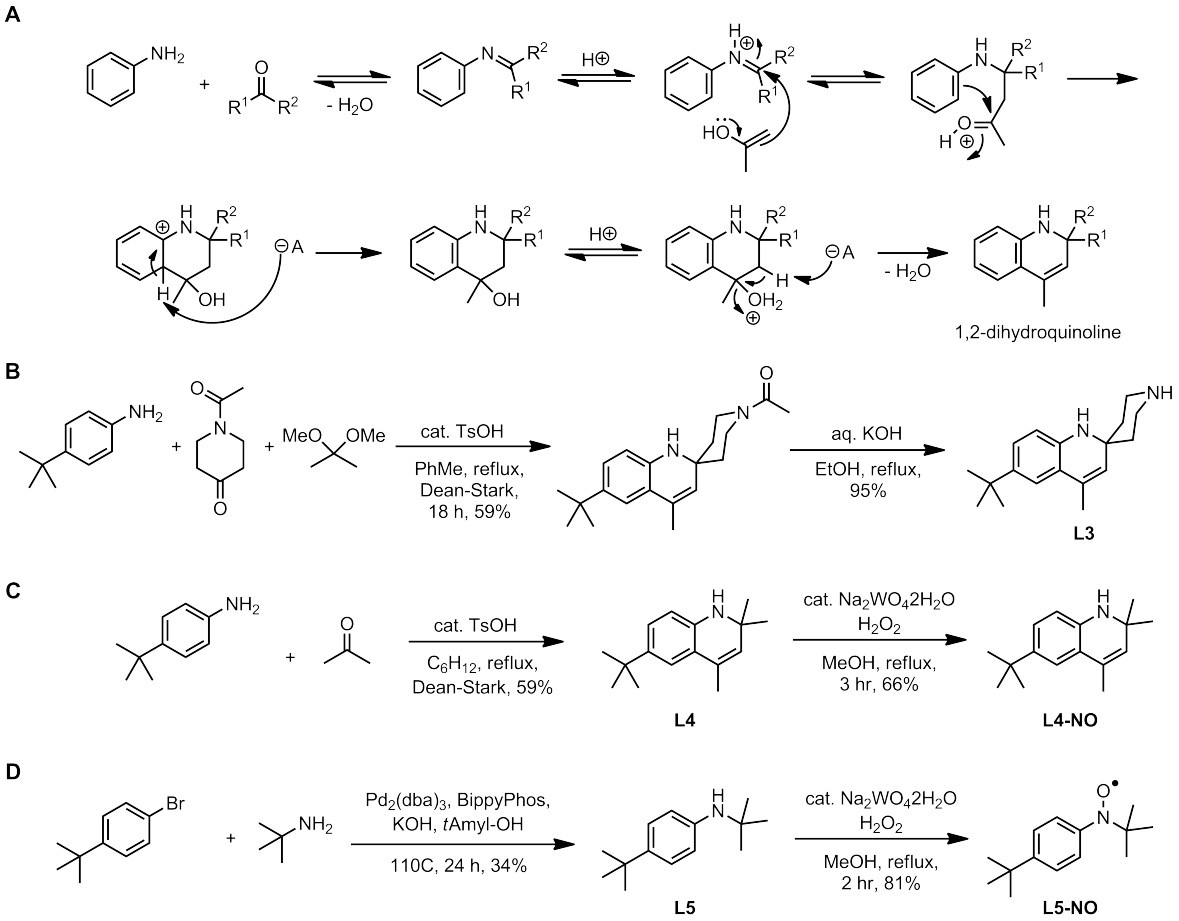

Scheme 2.5 Mechanism and synthesis of dihydroquinolines. Mechanism of dihydroquinoline synthesis by condensation of an aniline with two ketones (**A**). Synthesis of L3 (**B**), L4 and derived nitroxide L4-NO (**C**), and aryl amine L5 and derived nitroxide L5-NO (**D**).

piperidinone was condensed with 4-*tert*-butylaniline first, followed by addition of the acetone equivalent, 2,2-dimethyoxypropane. Basic hydrolysis of the *N*-acetyl group afforded L3 (**Scheme 2.5B**).

The nitroxide derived from L4 was prepared by oxidation with H_2O_2 and catalytic $Na_2WO_4 \bullet 2H_2O$ to fashion L4-NO (**Scheme 2.5C**), which was only moderately stable at room temperature, possibly due to the styryl moiety also present. The stability of the well-known archetype nitroxide, TEMPO, is a result of the steric hindrance and flanking quaternary carbons that preclude α H-atom abstraction and subsequent *N*-oxide formation. Further, ring substitution of *aryl* nitroxides often aid in their isolation. Thus, nitroxide

formation from the precursor of L3 seems possible given it is: a hindered aryl amine; flanked by quaternary carbons, and; has piperidine N-H protected and aryl ring blocked. However, oxidation of L3-NAc and NBz-*p*-*t*BuL1 by conditions above proved difficult to isolate a single product and often resulted in decomposition on silica, on concentration of solvent, or subsequent deprotection. Efforts are ongoing to determine conditions to prepare nitroxides in a milder system that can be directly analyzed.

The simplest hindered alkyl aryl amine derivative envisioned was prepared by a Buchwald-Hartwig cross coupling between *t*-butylamine and 4-*tert*-butyl bromobenzene. The reaction proceeded in a moderate 47% yield owing to the steric bulk of *tert*-butyl amine hindering attack on the Pd(II) complex. This amine proved straightforward to oxidize to the nitroxide by the same conditions as above to provide L5-NO in good yield (**Scheme 2.5D**).

The derivatives prepared here encompass the functional groups present in aryl amines and spiroquinoxalinamines whose reactivity towards peroxyl radicals will be evaluated in homogenous media and biologically relevant systems of: a) non-polar styrene and cumene autoxidations; b) egg PC liposomes; c) competition experiments with a PMHC-conjugated BODIPY in egg PC liposomes; d) buffered aqueous THF co-autoxidations, and; e) cellular models of ferroptosis. The results should guide the rational design of biologically relevant aryl amine RTAs.

2.7.2 RTA activity of spiroquinoxalinamine derivatives

The RTA activity of L1, *p*-*t*BuL1, *m*-*t*BuL1 and L2 in styrene/PBD-BODIPY co-autoxidations was compared with that of Lip-1. The k_{inh} of L1, *p*-*t*Bu-L1 and *m*-*t*Bu-L1 was determined to be similar to Lip-1 at 2 μM, however there is a noticeable lack of dose response in the initial portion of the co-autoxidations (**Figure 2.11**). Furthermore, the stoichiometry of peroxyl radical-trapping could not be determined for any derivative containing a piperidine ring (except Lip-1), suggesting that competing reactions with oxygen may be more favoured with the piperidine moiety.

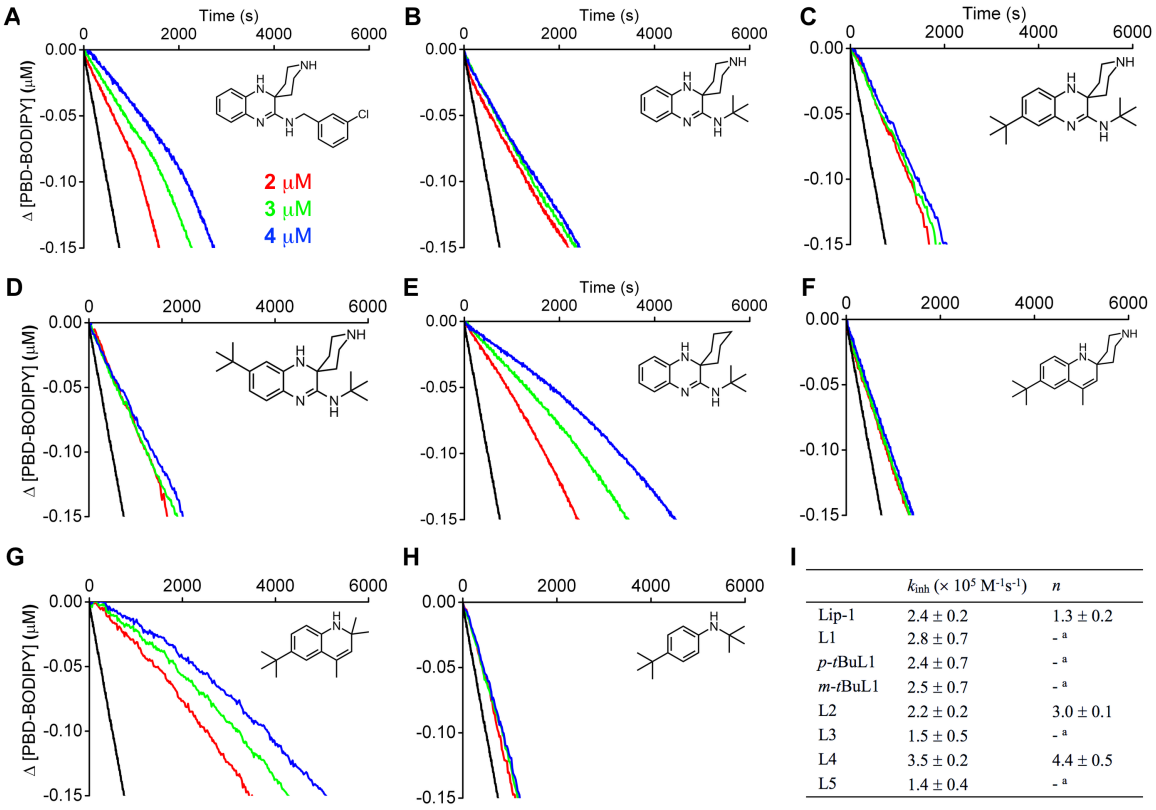

	k_{inh} (× 10^5 $M^{-1}s^{-1}$)	*n*
Lip-1	2.4 ± 0.2	1.3 ± 0.2
L1	2.8 ± 0.7	- [a]
p-*t*BuL1	2.4 ± 0.7	- [a]
m-*t*BuL1	2.5 ± 0.7	- [a]
L2	2.2 ± 0.2	3.0 ± 0.1
L3	1.5 ± 0.5	- [a]
L4	3.5 ± 0.2	4.4 ± 0.5
L5	1.4 ± 0.4	- [a]

Figure 2.11 Co-autooxidations of styrene (4.3 M) and PBD-BODIPY (10 μM) initiated by AIBN (6 mM) in chlorobenzene at 37°C (black trace) and inhibited by 2 μM (red trace), 3 μM (green trace) and 4 μM (blue trace) of Lip-1 (**A**), L1 (**B**), *p*-*t*BuL1 (**C**), *m*-*t*BuL1 (**D**) and L2 (**E**). Average inhibition rate constants and stoichiometry summarized in (**F**). Reaction progress was monitored by absorbance at 591 nm (ε = 139,000 $M^{-1}cm^{-1}$). [a] Stoichiometry could not be determined from the data and *n*=1 was assumed for k_{inh} calculations.

An explanation of these observations may involve the presence of the piperidine functionality, especially since styrene-chlorobenzene mixtures largely do not provide H-bonding interactions for a polar moiety. One could envision an intramolecular H-bond when the piperidine ring adopts a boat conformation (**Figure 2.12** ***a***), or an analogous intermolecular coordination with another RTA molecule. The contribution of these H-bonds at equilibrium could exert a kinetic solvent-like effect that impedes HAT/SPLET from the aniline N-H resulting in a lower k_{inh}. A similar intramolecular H-bond could also be envisioned to form with the amidine N-H (***b***) that could prevent the second radical trapping step or increase opportunity to react with O_2. These explanations are consistent with the greater initial inhibition rate of L2 and L4, lacking the piperidine N-H. Further, it could be envisioned that the amidine *t*-butyl in L1, *m*-*t*Bu-L1 and *p*-*t*Bu-L1 (***c***) sterically impedes approach of a second peroxyl, thereby thereby reducing *n*, and contributes to the lack of clear inflection points. Consistent with this explanation, the effect is not observed

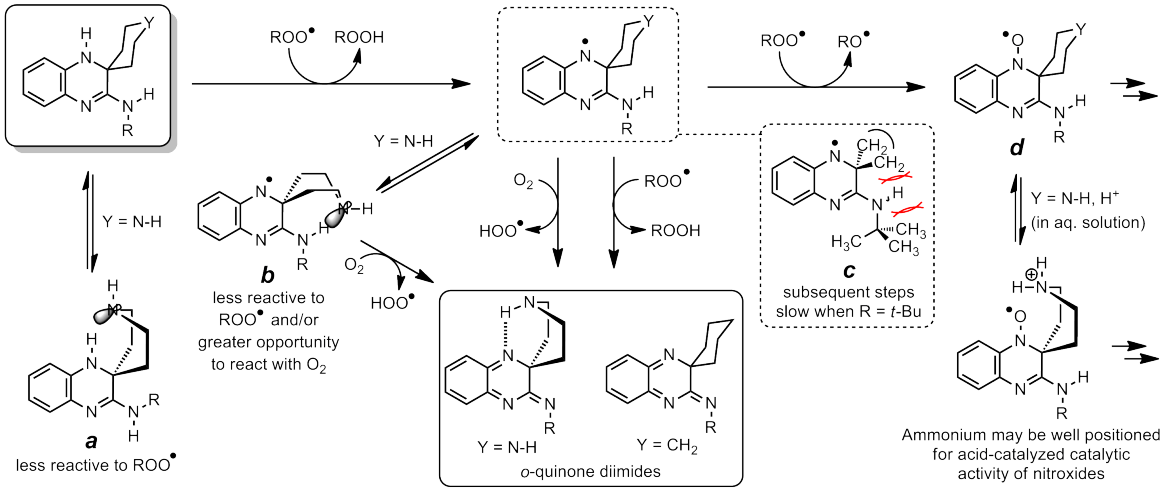

Figure 2.12 When Y = N-H, an intramolecular H-bond from the aniline/amidine N-H (***a, b***) could prevent radical trapping steps analogous to a kinetic solvent effect in H-bond accepting media. This may also allow opportunity to react with O_2 (***b***). Steric bulk around the amidine may prevent approach of a second peroxyl (***c***) reducing stoichiometry or becoming rate limiting. The nitroxides (***d***) could be responsible for the observed catalytic activity.

in Lip-1, which bears a less bulky benzyl group. All of the compounds inhibit autoxidation without clearly returning to uninhibited, suggesting catalytic activity of a persistent species such as the proposed nitroxide (**Figure 2.12** ***d*** and **Scheme 2.2 path b**) may be an intermediate in their mechanism of action.

In cumene autoxidations, the stoichiometry of all compounds was greater than styrene autoxidations, with $n \geq 2$ measured for Lip-1, L1, L2 and L4 (**Figure 2.13**). This can be reasoned, as previously discussed in section **2.3**, by the higher steady state concentration of peroxyl radicals during cumene autoxidation relative to styrene since the termination rate of cumyl peroxyl radicals is much lower than styryl peroxyl radicals. The

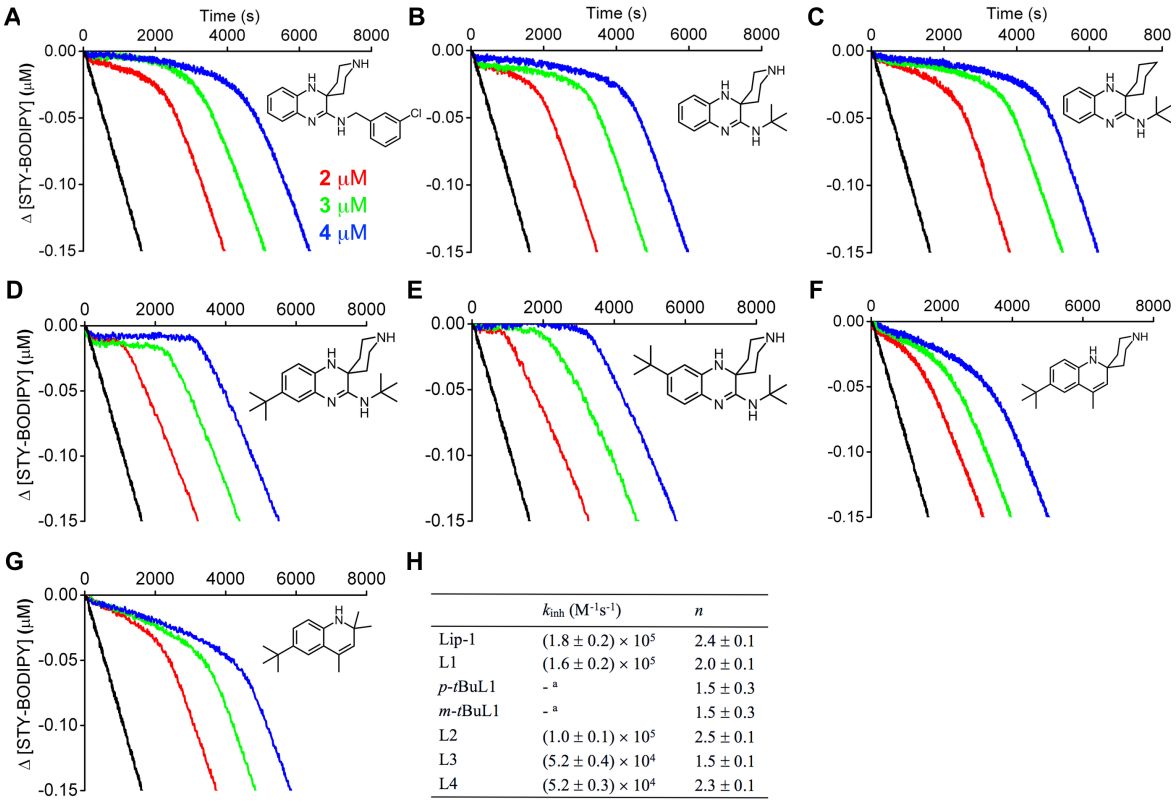

	k_{inh} ($M^{-1}s^{-1}$)	n
Lip-1	$(1.8 \pm 0.2) \times 10^5$	2.4 ± 0.1
L1	$(1.6 \pm 0.2) \times 10^5$	2.0 ± 0.1
p-*t*BuL1	- [a]	1.5 ± 0.3
m-*t*BuL1	- [a]	1.5 ± 0.3
L2	$(1.0 \pm 0.1) \times 10^5$	2.5 ± 0.1
L3	$(5.2 \pm 0.4) \times 10^4$	1.5 ± 0.1
L4	$(5.2 \pm 0.3) \times 10^4$	2.3 ± 0.1

Figure 2.13 Co-autoxidations of cumene (3.6 M) and STY-BODIPY (10 μM) initiated by AIBN (6 mM) in chlorobenzene at 37°C (black trace) and inhibited by 2 μM (red trace), 3 μM (green trace) and 4 μM (blue trace) of Lip-1 (**A**), L1 (**B**), L2 (**C**), *p*-*t*BuL1 (**D**), *m*-*t*BuL1 (**E**), L3 (**F**), and L4 (**G**). Average inhibition rate constants and stoichiometry summarized in (**H**). Reaction progress was monitored by absorbance at 571 nm (ε = 128,000 $M^{-1}cm^{-1}$). [a] k_{inh} greater than can be measured from the data.

higher peroxyl radical concentration effectively reduces competition of the aminyl radical with oxygen, favouring the peroxyl-trapping paths.

Interestingly, the initial rates of *p*-*t*BuL1 and *m*-*t*BuL1 were higher than Lip-1 and L1, suggesting that the weak electron-donating group may favour initial H-atom transfer, however, stoichiometry is markedly reduced. The difference in initial rate and stoichiometry could be explained by partitioning between the two fates of the aminyl radical: if we assume reaction of the intermediate aminyl radical with an alkylperoxyl radical to form a nitroxide (**path a, Scheme 2.2**) is *slower* than formation of the *o*-quinone diimide (**path b**, **Scheme 2.2**), a higher steady state concentration of the aminyl radical—resulting from spiroquinoxalinamines with lower N-H BDEs—may favour **path a** and thus would have reduced stoichiometry (*n* does not reach ~ 2 since the proposed competitive nitroxide formation is not a radical-trapping step). Consistent with this explanation, the dihydroquinoline L4 that has a lower k_{inh} *and* cannot form an *o*-quinone diimide has similar stoichiometry to each of the spiroquinoxalinamines. The lower k_{inh} of L4 is likely due to the lack of the amidine moiety. Alternatively, the difference in stoichiometry could be due to a large difference in rate between the first and second radical trapping steps, and consequently where the inflection point is taken. Both *p*-*t*BuL1 and *m*-*t*BuL1 seem to feature slight retardation in rate after the first major inflection point. The aryl-*t*Bu EDG may stabilize the aminyl radical enough to slow the second radical trapping step relative to L1 or Lip-1.

Liposome autoxidations of the spiroquinoxalinamine derivatives reveal they are great RTAs in this system, trapping more radicals than phenolic RTAs with n>2 for most of the aryl amines (**Figure 2.14**). The *t*-butyl derivatives *p*-*t*BuL1 and *m*-*t*BuL1 both exhibited a higher k_{inh} than Lip-1 and L1, consistent with the weak *t*-butyl EDG reducing N-H BDE. Interestingly, all spiroquinoxalinamines had stoichiometries above 2. Slight variances in n may be a result of subtle electronic and lipophilic differences imparted by aryl and amidine substitution that shift the balance between the two proposed fates of the aminyl radical.

Lack of the piperidine N-H in L2 did not appreciably change n compared to L1,

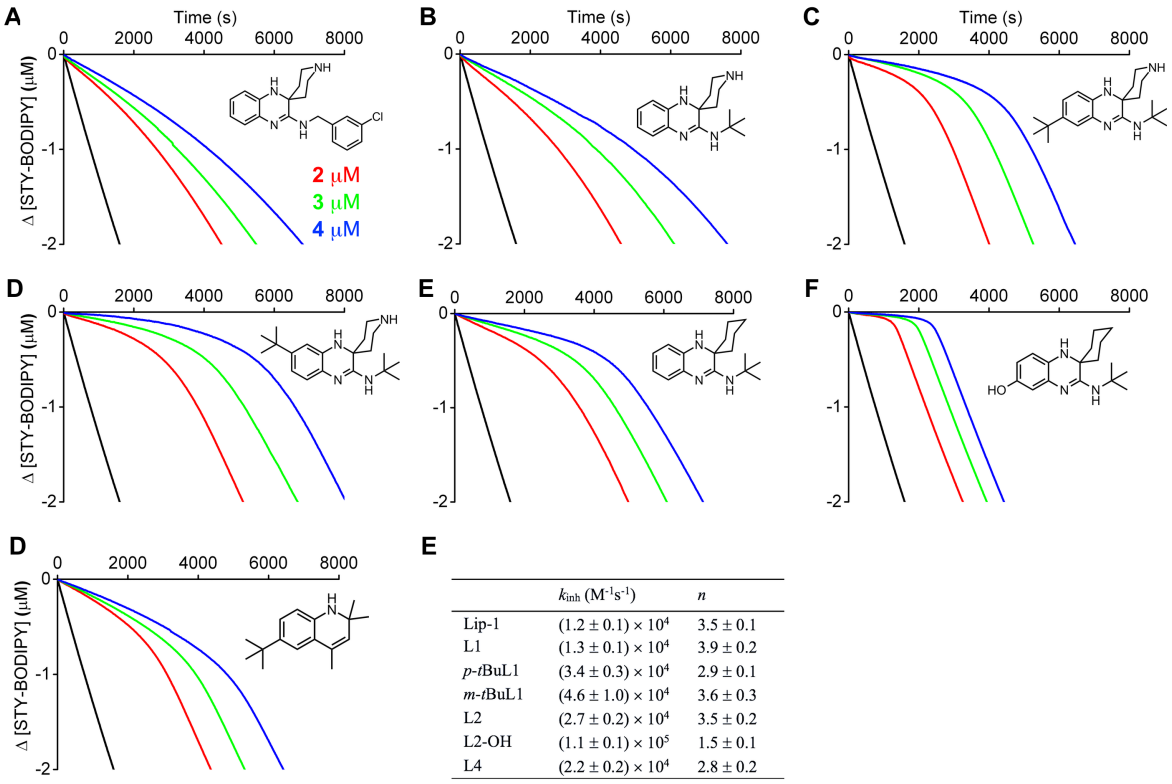

E

	k_{inh} ($M^{-1}s^{-1}$)	n
Lip-1	$(1.2 \pm 0.1) \times 10^4$	3.5 ± 0.1
L1	$(1.3 \pm 0.1) \times 10^4$	3.9 ± 0.2
p-*t*BuL1	$(3.4 \pm 0.3) \times 10^4$	2.9 ± 0.1
m-*t*BuL1	$(4.6 \pm 1.0) \times 10^4$	3.6 ± 0.3
L2	$(2.7 \pm 0.2) \times 10^4$	3.5 ± 0.2
L2-OH	$(1.1 \pm 0.1) \times 10^5$	1.5 ± 0.1
L4	$(2.2 \pm 0.2) \times 10^4$	2.8 ± 0.2

Figure 2.14 Co-autoxidations of egg PC liposomes (1 mM) and STY-BODIPY (8 μM) initiated by MeO-AMVN (200 μM) in pH 7.4 PBS (10 mM) at 37°C (black trace) and inhibited by 2 μM (red trace), 3 μM (green trace) and 4 μM (blue trace) of Lip-1 (**A**), L1 (**B**), *p*-*t*BuL1 (**C**), *m*-*t*BuL1 (**D**), L2 (**E**), L2-OH (**F**) and L4 (**G**). Average inhibition rate constants and stoichiometry summarized in (H). Reaction progress was monitored by absorbance at 565 nm (ε = 123676 $M^{-1}cm^{-1}$).

though the k_{inh} was ~ 2 fold greater. This may be explained by the lack of intramolecular N-H bonds imposing a kinetic solvent-like effect, proposed from and consistent with styrene autoxidations (**Figure 2.12**) since the non-polar environment in liposomes can be analogous to styrene-chlorobenzene.

The phenol derivative L2-OH, which mimics the postulated water addition product to the *o*-quinone diimide, was the fastest spiroquinoxalinamine with k_{inh} similar to the THNs (1.1×10^5 and 9.3×10^4 $M^{-1}s^{-1}$, respectively). This is to be expected given that L2-OH is an electron-rich phenol, and previous work has demonstrated the effect of lowering O-H BDE of phenols with added electron rich nitrogens.[5] Attempts to observe this phenol by direct infusion MS of a THF-buffered H_2O autoxidation of L2 (lacking the phenol -OH) did result in M+16 peaks by ESI+ and APCI+ ionization, however differentiating between the nitroxide/oxoammonium (M+16-1), hydroxylamine (M+16), and the proposed phenol (M+16) cannot be adequately resolved or differentiated by this method. If an authentic standard of the nitroxide/oxoammonium were prepared, MS/MS may reveal unique transitions that could attempt to differentiate the intermediates, presuming the persistence of the species. However, it may also be reasoned that if water addition was kinetically competent and at the root of the increased observed *n* of spiroquinoxalinamines in liposomes, the derivatives *p*-*t*BuL1 and *m*-*t*BuL1 that sterically preclude water addition with an aryl *t*-butyl group would likely have a reduced *n* relative to L1, which is not observed. The difficulty in ruling out water addition is compounded by the fact that O-H PCET is fast and occurs *after* the initial aniline N-H rate-determining step. It should also be noted that an analogous RTA pair is precedented *in vitro* with the hormone melatonin[6]

and its main metabolite, 6-hydroxymelatonin, formed both enzymatically and by reaction of melatonin with •OH.[7]

In lieu of having authentic nitroxides of the spiroquinoxalinamines in hand, two related hindered aryl amine nitroxides related to the spiroquinoxalinamines (L4-NO and L5-NO), in addition to 2,2,6,6-tetramethylpiperidine-1-oxyl (TEMPO) and a lipophilic TEMPO derivative (LONG-TEMPO), were assayed. Both the arylamine-derived nitroxides L4-NO and L5-NO were very competent RTAs, with k_{inh} = (2.8 ± 0.1) × 10^4 $M^{-1}s^{-1}$, n = (0.9 ± 0.1), and k_{inh} = (4.3 ± 0.3) × 10^4 $M^{-1}s^{-1}$, n = (2.2 ± 0.1) respectively. As discussed previously, the nitroxide L4-NO and the parent amine L4 have a similar profile after the initial inhibited period (**Figure 2.6**), providing support for **path b**. The nitroxide L5-NO was very active in liposomes, however, the parent amine was completely ineffective (similarly, the parent amine of TEMPO, TEMPH, is inactive).[a] A possible explanation

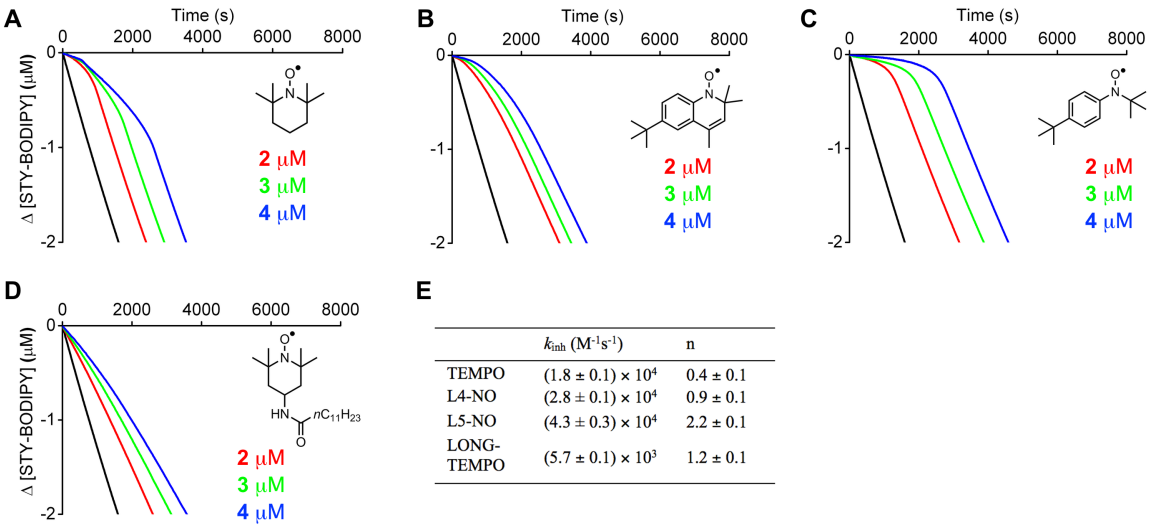

Figure 2.15 Co-autoxidations of egg PC liposomes (1 mM) and STY-BODIPY (8 μM) initiated by MeO-AMVN (200 μM) in pH 7.4 PBS (10 mM) at 37°C (black trace) and inhibited by 2 μM (red trace), 3 μM (green trace) and 4 μM (blue trace) of TEMPO (**A**), L4-NO (**B**), L5-NO (**C**), LONG-TEMPO (**D**). Average inhibition rate constants and stoichiometry summarized in (**E**). Reaction progress was monitored by absorbance at 565 nm (ε = 123676 $M^{-1}cm^{-1}$).

[a] Data not shown.

involves the reduced resonance stabilization of the aminyl radical that is possible in either the dihydroquinolines or spiroquinoxalinamines, but not in L5 or TEMPH as they are not unsaturated bicyclics. Interestingly, TEMPO was very active and exhibited two distinct inhibition phases that are best observed in the 4 μM trace. The second inflection point corresponds to $k_{inh} = (7.1 \pm 0.2) \times 10^3$ $M^{-1}s^{-1}$, $n = 1.5$, for a total of $n = 2$. Future work will investigate this behaviour.

In addition to liposome autoxidations monitored by STY-BODIPY consumption, we also investigated RTA activity by competition experiments with the fluorogenic PMHC-BODIPY conjugate, H_2B-PMHC (**Figure 2.16A**).[8] This probe is quite distinct from STY-BODIPY. Prior to any reaction with peroxyl radicals, photoinduced electron transfer

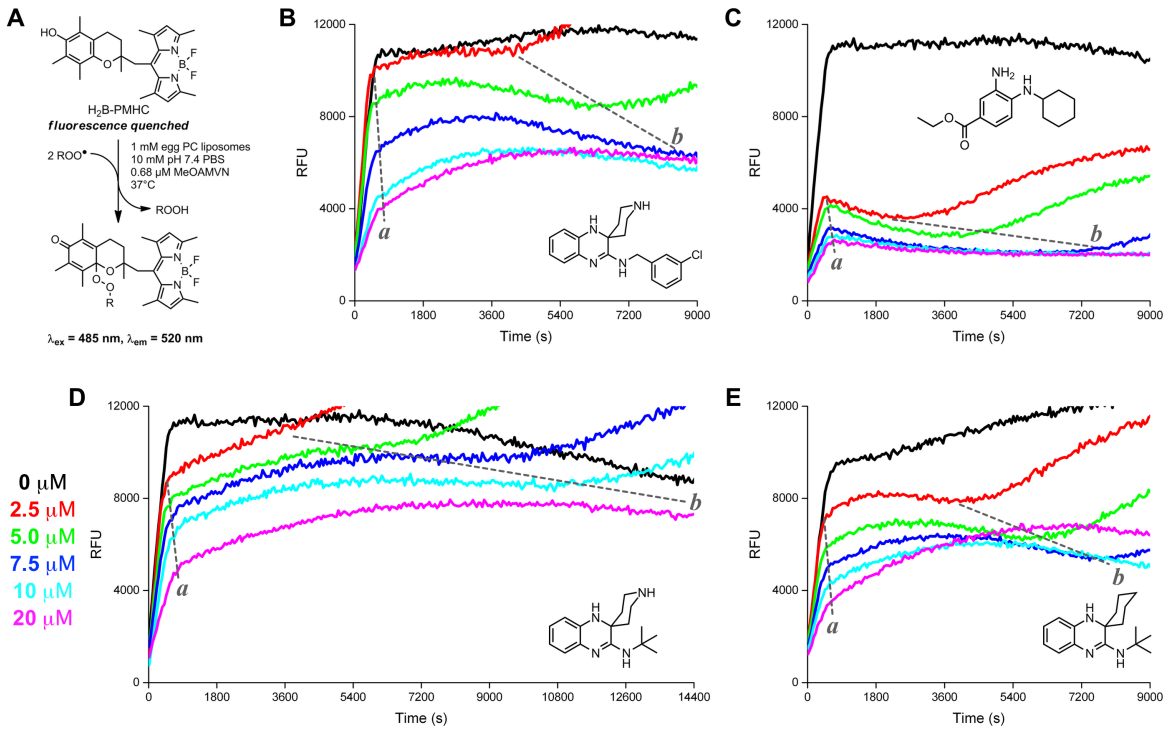

Figure 2.16 Autoxidations of egg PC liposomes (1 mM initiated by 0.68 mM MeOAMVN in 10 mM pH 7.4 PBS at 37°C) inhibited by 0.15 μM H_2B-PMHC (**A**) and RTAs Lip-1 (**B**), Fer-1 (**C**), L1 (**D**) and L2 (**E**). Analogous results obtained for AAPH initiated autoxidations (data not shown).

from the electron rich PMHC moiety completely quenches fluorescence of the probe. The traces resulting from the assay arise from the fluorescence increase that occurs when the quenching is abolished, *i.e.* after the PMHC moiety traps two peroxyl radicals. Reactions without an added RTA rapidly consume the probe after *ca.* 600 s (black traces in **Figure 2.16**) since it is present at a very low concentration (0.15 μM). The RTA being tested must then be able to *compete* with the probe to retard this observed rate. These experiments revealed interesting behaviour of the aminic and aryl nitroxide RTAs that was consistent with the STY-BODIPY co-autoxidations in the *initial* portion of the reactions (before inflection points denoted ***a*** in **Figure 2.16**). Fer-1 retards the initial rate to a greater extent over Lip-1, consistent with their previously determined k_{inh} values of (4.6 *vs.* 1.2) $\times 10^4$ $M^{-1}s^{-1}$, respectively.

After inflection point ***a***, an unexpected *decrease* in fluorescence (*i.e.* a negative rate, best observed in **Figure 2.16C** and **E**) builds in towards another inflection point, ***b***.

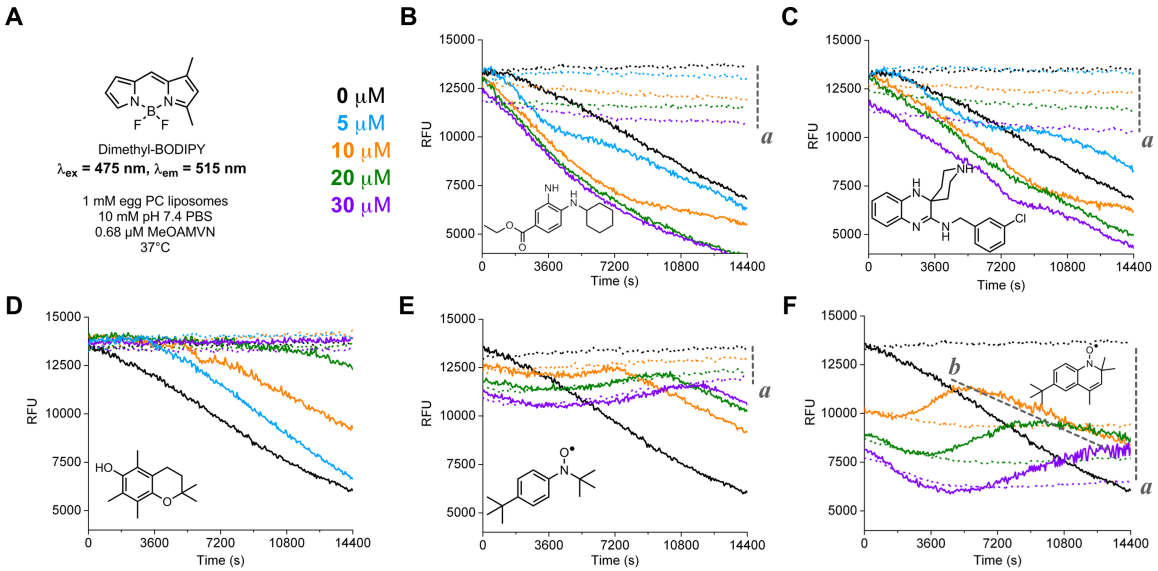

Figure 2.17 Autoxidations of egg PC liposomes (1 mM initiated by 0.68 mM MeOAMVN in 10 mM pH 7.4 PBS at 37°C) with 0.15 μM Dimethyl-BODIPY (**A**) and inhibited by RTAs Fer-1 (**B**), Lip-1 (**C**), PMHC (**D**), L5-NO (**E**) and L4-NO (**F**). Dotted traces lack MeOAMVN initiator. Analogous results obtained for AAPH initiated autoxidations (data not shown).

Based on our understanding of the probe, this implies formation of products able to quench the fluorescence of H_2B-PMHC. To explore this proposition, an experiment with a simple Dimethyl-BODIPY core (**Figure 2.17A**) was used to investigate the behaviour of aminic RTAs and their autoxidation products on the BODIPY core fluorescence in the same liposome system. Dimethyl-BODIPY is natively fluorescent, and upon addition of either Lip-1 or Fer-1, Dimethyl-BODIPY fluorescence was quenched in both non-autoxidizing (dotted traces) and autoxidizing (solid traces) liposomes, a trend indicated by ***a*** in **Figure 2.17.** The model aromatic nitroxides L4-NO and L5-NO exhibited the same behaviour (**Figure 2.17E, F**). As expected, traces from PMHC-inhibited autoxidations never exhibited fluorescence significantly below the untreated control. Not only did L4-NO exhibit the most quenching behaviour, but it also best demonstrated that a nitroxide in this autoxidizing system can enhance BODIPY fluorescence. This enhancement could be due to consumption of the nitroxide, or interactions with the BODIPY core that effectually increases quantum yield. Interestingly, a similar behaviour was also observed in the preceding H_2B-PMHC experiments flanking inflection point ***b*** in **Figure 2.16** of the spiroquinoxalinamines and arylamines under investigation and in each of the nitroxides (**Figure 2.18**).

Since quenching is intrinsically dependent on physical proximity between the BODIPY and an energy-transfer partner, the competition experiments with PMHC-BODIPY cannot be completely reliable for k_{inh} measurements. This is especially so since the preceding experiments with Dimethyl-BODIPY demonstrated that both the parent RTAs and products derived therefrom (*i.e.* mixed nitroxides) can quench fluorescence. We believe this leads to the behaviour after the initial inhibition rates that conclude at inflection point ***a***, and results in a complex behaviour difficult to model. Fortunately, the prior experiments with STY-BODIPY are unaffected by quenching behaviour as they monitor consumption of STY-BODIPY only by absorbance.

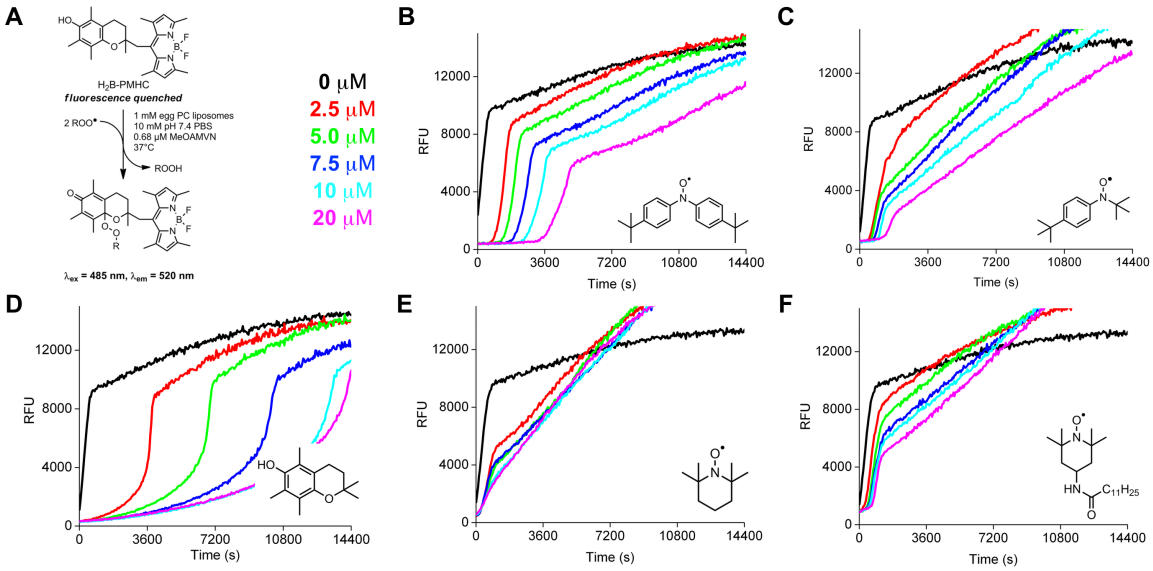

Figure 2.18 Autoxidations of egg PC liposomes (1 mM initiated by 0.68 mM MeOAMVN in 10 mM pH 7.4 PBS at 37°C) inhibited by 0.15 μM PMHC-BODIPY (**A**) and RTAs diaryl-nitroxide (**B**), L5-NO (**C**), PMHC (**D**), TEMPO (**E**) and Long-TEMPO (**F**). Analogous results obtained for AAPH initiated autoxidations (data not shown).

A few conclusions can still be drawn from the data to support invocation of nitroxides in the RTA mechanism of Lip-1 and Fer-1, especially when reinforced by data next obtained in slightly acidic (pH 5.8) and basic (pH 10.8) liposome autoxidations (**Figure 2.19**). We consider these systems especially informative due to recent work from our group improving our understanding of the long known catalytic RTA mechanism for TEMPO. At high temperature, weak acids that are produced from autoxidizing hydrocarbons are proposed to participate in the equilibrium between nitroxide and hydroxylamine radical cation to facilitate catalytic radical trapping through the oxoammonium intermediate.[9] This is consistent with the potency trends we observed in liposome autoxidation inhibited by TEMPO, shown in Figure **Figure 2.19**. An acidic aqueous phase *greatly* favours catalytic behaviour of TEMPO and completely suppresses fluorescence at each concentration in pH 5.8 buffer. Similarly, Fer-1 inhibits best at acidic pH, and both Lip-1 and Fer-1 lose effectiveness at basic pH. We can explain the equal

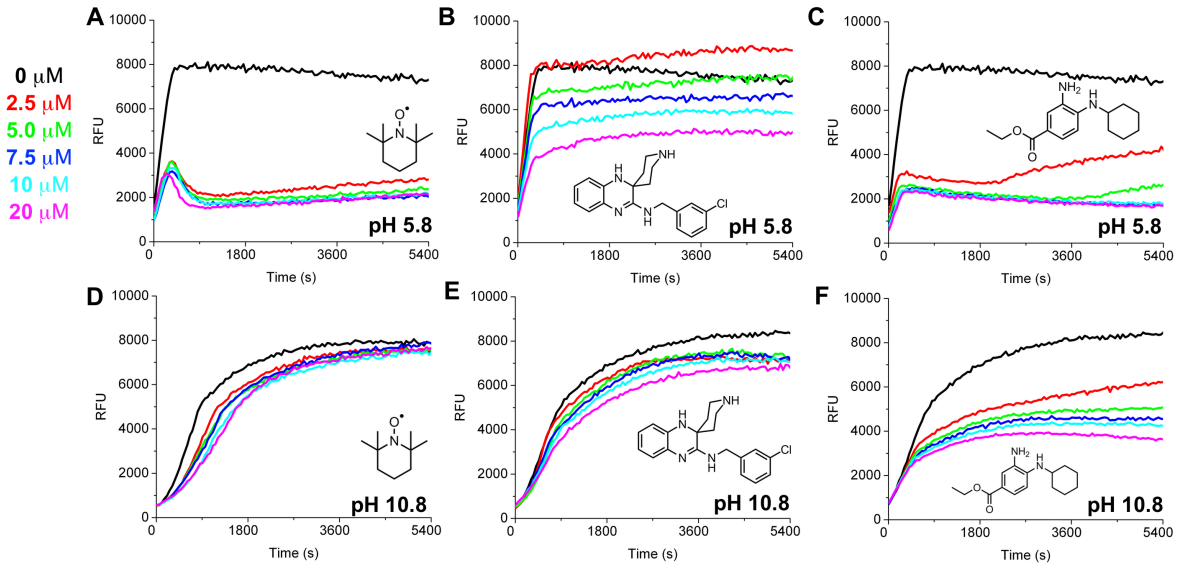

Figure 2.19 Autoxidations of egg PC liposomes (1 mM initiated by 0.68 mM MeOAMVN in 10 mM PBS at pH 5.8 (**A**-**C**) and pH 10.8 (**D**-**F**) at 37°C) inhibited by 0.15 μM PMHC-BODIPY and RTAs TEMPO (**A**,**D**), Lip-1 (**B**,**E**), and Fer-1 (**C**-**F**). Analogous results obtained for AAPH initiated autoxidations (data not shown).

performance of Lip-1 observed between pH 7.4 and 5.8 by either: *i*) the basicity, *i.e.* equilibrium between amine and conjugate acid that may impede acid-catalyzed redox cycling of the nitroxide, or; *ii*) favourable partitioning into the aqueous phase at acidic pH when the piperidine is protonated.

Overall, the common trends of H_2B-PMHC and Dimethyl-BODIPY experiments are quenching (***a***), followed by fluorescence increase (***b***), and the activity-pH trends between spiroquinoxalinamines/ferrostatin-1 and mixed nitroxides. While these experiments could imply a similar fate and/or common intermediate in the mechanism of spiroquinoxalinamine and aromatic amines under investigation, they are far from conclusive and warrant deeper investigation.

2.7.3 Inhibition of RSL3-induced ferroptosis by spiroquinoxalinamine derivatives

With the result of the spiroquinoxalinamine derivatives ability to inhibit lipid autoxidation with similar efficacy to Lip-1, their ability to inhibit RSL3-induced ferroptosis in cells was next evaluated. The model system involves treatment of cells with RSL3, which covalently inhibits the hydroperoxide detoxifying enzyme Gpx4, thereby resulting in an accumulation of lipid hydroperoxides (PUFA-OOH) arising from autoxidation, and leading to ferroptosis (**Figure 2.20A**). RTAs inhibit autoxidation,

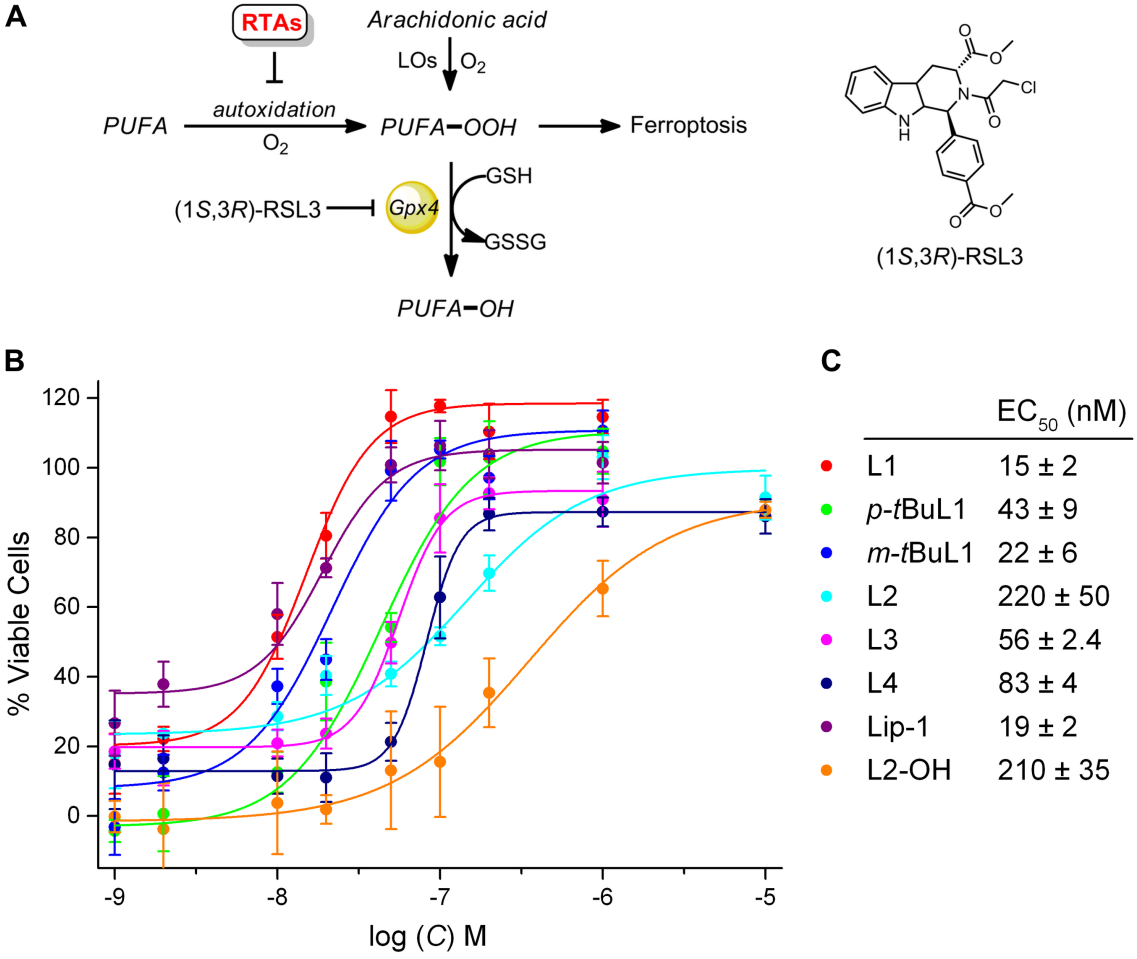

Figure 2.20 Ferroptosis is induced by covalent modification of the enzyme Gpx4 by the small molecule (1*S*,3*R*)-RSL3, leading to accumulation of lipid hydroperoxides (PUFA-OOH) arising from autoxidation (**A**). Spiroquinoxalinamines and the related derivatives rescue Pfa1 cells from ferroptotic death in a dose dependent manner (**B**). Efficacy summarized in (**C**).

thereby preventing ferroptotic cell death.[10]

Lip-1 and L1 were the most potent at subverting ferroptosis with EC_{50} = (19 ± 2) nM and (15 ± 2) nM, respectively. The *t*-butyl modifications in *p*-*t*BuL1 and *m*-*t*BuL1 did not appreciably increase the potency relative to L1, even though their initial rates in liposome autoxidations were *ca.* 3 fold greater. Indeed, even the THNs, which trap less radicals than the aryl-amines but have a much greater k_{inh} in all autoxidation media, have a similar potency to Lip-1. The dihydroquinoline derivative L4 was nearly as potent as Lip-1 (also discussed in section **2.3**). L3 was similarly potent as well, suggesting that indeed many hindered aryl amines are efficacious at subverting ferroptosis. The efficacy of L2 was *ca.* 10 fold less than potent than piperidine derivative L1, consistent with previous reports.[2]

2.8 Conclusions

The key hypothesis of liproxstatin-1 and ferrostatin-1 antioxidant activity has been evaluated. While the corollary of various aryl amines, nitroxides and phenolic antioxidants to subvert ferroptosis and lipid autoxidation—alongside their negligible LOX inhibition activity—has provided evidence for lipid peroxidation being a key contributor of ferroptosis, the fate of nitroxides in the biological milieu remains to be elaborated to exploit their catalytic activity in pursuit of other rationally-designed ferroptosis inhibitors. Towards this goal, future work will extend nitroxide kinetics to EPR, other privileged autoxidation systems, and explore relevant kinetic isotope effects to probe the fate of biologically active catalytic aryl amines and nitroxides.

2.9 Future Work

Decades of research have demonstrated a handful of recurring features of potent, biologically relevant RTAs including: high lipophilicity (for lipid autoxidation); inherent reactivity towards peroxyl radicals, and; ability to regenerate in a catalytic fashion. Given the anti-ferroptotic potency of 'slower' antioxidants that do behave catalytically in liposome autoxidations, such as dihydroquinolines, the question can be raised: are highly reactive RTA's necessarily required? The difference in α-TOH and PMHC illustrates a similar point—reactivity being equal, lipid dynamics is a determinant factor in potency. Thus, there remains considerable motivation for pursuing catalytic antioxidants that balance *in vivo* persistence and bioavailability. Trafficking antioxidants via a protein carrier, namely the tocopherol transport protein, may bridge the divide between RTA efficacy and viable treatments—a strategy realized and invoked in the development of the THNs.

Towards the goal of developing better biologically relevant lipid autoxidation RTAs, we envision an aryl amine antioxidant of the dihydroquinoline structure mapped onto the tocopherol skeleton. These aryl-amine tocopherol derivatives may bind to TTP,

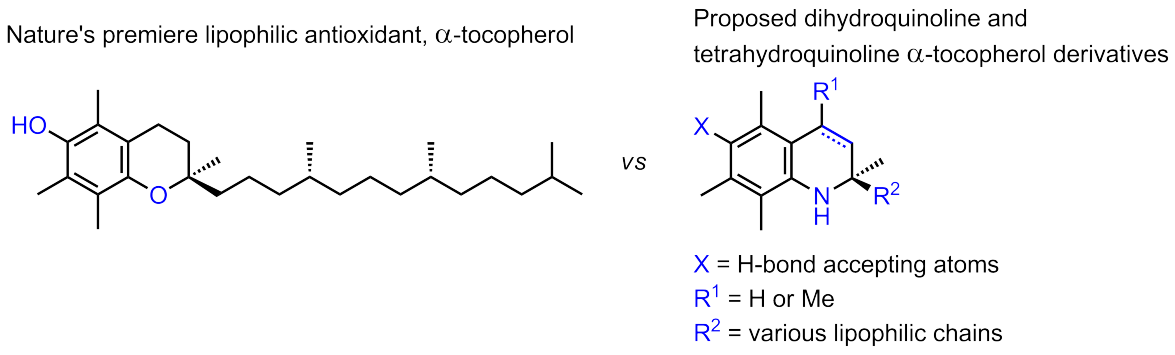

Figure 2.21 Possible dihydroquinoline- and tetrahydroquinoline-derived tocopherol analogues

thereby improving bioavailability. This will not only evaluate the ability of trafficked, catalytic aryl amine antioxidants in disease therapy, but will allow comparison to the potent THNs to further probe the underlying premise, and promise, of antioxidant therapy.

Targeting RTAs to specific subcellular compartments is another strategy used to evade metabolism. MitoQ, a mitochondrially-targeted ubiquinone, is a redox cycling antioxidant that has been shown to rapidly accumulate in the mitochondria. The next chapter will introduce the strategy and design of targeting the THNs to the mitochondria.

2.10 Supplementary Experimental

2.10.1 General

Egg phosphatidylcholine (Sigma-Aldrich) liposomes were prepared as previously described,[11] and liposome preparations and autoxidations employed Chelex® treated PBS (10 mM with 150 mM NaCl) adjusted to the appropriate pH before use. Autoxidations with PBD- or STY-BODIPY and synthesis of Lip-1 were completed as described in Sections **2.4** and **2.5.2**. *t*-butyl isocyanide was synthesized as described in the literature.[12]

2.10.2 Synthesis of spiroquinoxalinamine derivatives.

1-benzyl-*N*-(*tert*-butyl)-1'H-spiro[piperidine-4,2'-quinoxalin]-3'-amine (*NBz*-L1): An oven-dried 100 mL RBF was charged with *o*-phenylenediamine (1.081 g, 10 mmol, 1 eq), methanol (15 mL, dried over 3Å sieves), and *N*-benzyl-4-piperidinone (1.893 g, 10 mmol, 1 eq) and the solution heated to reflux for 3 h under N_2. The reaction mixture was allowed to cool to 50°C, and a solution of TMSCl (1.27 mL, 10 mmol, 1 equiv.) in 7.5 mL dry acetonitrile was added dropwise over 15 min, followed by *t*-butyl isocyanide (0.831 g, 10 mmol, 1 eq) in 7.5 mL methanol dropwise over 1 h. The solution was stirred

overnight, cooled, and concentrated *in vacuo*. The residue was triturated in 50 mL dry ether followed by sonication for 10 min. The precipitate was collected by filtration, air dried, and transferred portionwise to 50 mL of water. The mixture was stirred vigorously during addition of 1 M aqueous NaOH to pH 9, and extracted with 3 × 50 mL $CHCl_3$. The combined organic layers were washed with brine, dried over $MgSO_4$, filtered, concentrated and the residue eluted through a silica gel plug with 1:1 ethyl acetate:hexanes. The eluent was concentrated to yield *NBz*-L1 (2.36 g, 65%) and recrystallized from ethyl acetates/hexanes as granular colourless crystals.

^{1}H NMR (400 MHz, DMSO-d_6): δ 7.63- 7.07 (m, 5H), 6.82 (dd, J = 7.7, 1.4 Hz, 1H), 6.77 (dd, J = 7.6, 1.5 Hz, 1H), 6.67 (td, J = 7.5, 1.5 Hz, 1H), 6.54 (td, J = 7.4, 1.4 Hz, 1H), 5.68 (s, 1H), 5.42 (s, 1H), 3.49 (s, 2H), 2.55 (dt, J = 11.8, 3.2 Hz, 2H), 2.44-2.33 (m, 2H), 1.88 (td, J = 12.6, 4.4 Hz, 2H), 1.49-1.41 (m, 2H), 1.41 (s, 9H). ^{13}C NMR (101 MHz, DMSO-d_6) δ 156.96, 138.67, 134.92, 134.61, 128.76, 128.09, 126.81, 122.60, 121.69, 117.69, 62.18, 51.07, 49.61, 47.28, 30.67, 28.65. HRMS (EI) *m*/*z*: [M^+] calcd for $C_{23}H_{30}N_4$ 362.2470; observed 362.2514.

***N*-(*tert*-butyl)-1'H-spiro[piperidine-4,2'-quinoxalin]-3'-amine** (L1): A 100 mL RBF was flame dried, cooled charged with NBz-L1 (600 mg, 1.66 mmol, 1 eq) and methanol (20 mL) and the solution was sparged with N_2. Pd/C (120 mg, 20% w/w), ammonium formate (522 mg, 8.28 mmol, 5 eq) and acetic acid (95 μL, 1.66 mmol, 1 eq) were added and the mixture was heated to reflux for 10 min, at which point the starting material was consumed (TLC). The reaction mixture was cooled and eluted through a pad of celite with methanol, and the filtrate was concentrated and taken up in water. The pH of the mixture was adjusted to ~ 9 with 1 M NaOH, and extracted with 3 × 15 mL $CHCl_3$.

The combined organic layers were washed exhaustively with water and brine, dried over Na_2SO_4, filtered and concentrated to yield L1 (450 mg, quant.) as a colourless solid that was recrystallized from hexanes as colourless plates.

^{1}H NMR (400 MHz, DMSO-d_6): δ 6.79 (dd, J = 7.6, 1.5 Hz, 1H), 6.77-6.72 (m, 1H), 6.64 (td, J = 7.5, 1.5 Hz, 1H), 6.52 (td, J = 7.4, 1.5 Hz, 1H), 5.76 (s, 1H), 5.29 (s, 1H), 2.84 (td, J = 12.6, 2.4 Hz, 2H), 2.70-2.60 (m, 2H), 1.86 (s, 1H), 1.71 (td, J = 12.5, 4.6 Hz, 2H), 1.41 (s, 9H), 1.42-1.34 (m, 2H). ^{13}C NMR (101 MHz, DMSO-d_6) δ 157.42, 134.96, 134.79, 122.56, 121.74, 117.54, 113.48, 51.00, 50.48, 40.25, 31.70, 28.67. HRMS (EI) *m*/*z*: [M^+] calcd for $C_{16}H_{24}N_4$ 272.2001; observed 272.2031.

1-benzyl-*N*,6'-di-*tert*-butyl-1'H-spiro[piperidine-4,2'-quinoxalin]-3'-amine and **1-benzyl-*N*,7'-di-*tert*-butyl-1'H-spiro[piperidine-4,2'-quinoxalin]-3'-amine** (*NBz-p-t*BuL1 and *NBz-m-t*BuL1): An oven-dried 100 mL RBF was charged with 4-(*t*-butyl) benzene-1,2-diamine (1.00 g, 6.09 mmol, 1 eq), methanol (15 mL, dried over 3Å sieves), and *N*-benzyl-4-piperidinone (1.15 g, 6.1 mmol, 1 eq) and the solution heated to reflux for 4 h under N_2. The reaction mixture was allowed to cool to 50°C, and a solution of TMSCl (0.78 mL, 10 mmol, 1 equiv.) in 7.5 mL dry acetonitrile was added dropwise over 15 min, followed by *t*-butyl isocyanide (0.506 g, 6.09 mmol, 1 eq) in 7.5 mL methanol dropwise over 1 h. The solution was stirred overnight, cooled, and concentrated *in vacuo*. The residue was triturated in 50 mL dry ether followed by sonication for 10 min. The precipitate was collected by filtration, air dried, and transferred portionwise to 50 mL of water. The mixture was stirred vigorously during addition of 1 M aqueous NaOH to pH 9, and extracted with 3 × 50 mL $CHCl_3$. The combined organic layers were washed with brine, dried over $MgSO_4$, filtered, concentrated and the residue eluted through a silica gel

plug with 1:3 ethyl acetate:hexanes. The eluent was concentrated to yield a mixture of regioisomers, which were separated by column chromatography using 1:25:74 Et_3N:E_2O:hexanes to yield *NBz-m-t*BuL1 (0.514 g, 25%)[a] and *NBz-p-t*BuL1 (0.968 g, 38%) as colourless solids.

*NBz-m-t*BuL1. ^{1}H NMR (400 MHz, DMSO-d_6) δ: 7.36-7.21 (m, 5H), 6.87 (d, J = 2.2 Hz, 1H), 6.69 (d, J = 8.0 Hz, 1H), 6.56 (dd, J = 8.1, 2.2 Hz, 1H), 5.62 (br s, 1H), 5.32 (br s, 1H), 3.49 (s, 2H), 2.60-2.51 (m, 2H), 2.44-2.36 (m, 2H), 1.86 (td, J = 12.7, 4.4 Hz, 2H), 1.49-1.42 (m, 2H), 1.39 (s, 9H), 1.23 (s, 9H). ^{13}C NMR (101 MHz, DMSO-d_6) δ 156.44, 144.18, 138.73, 133.88, 132.40, 128.78, 128.10, 126.81, 122.15, 114.47, 110.53, 62.20, 52.22, 50.98, 49.71, 47.28, 33.92, 31.54, 30.88, 28.66. HRMS (EI) m/z: [M^+] calcd for $C_{27}H_{38}N_4$ 418.3096; observed 418.3117. NOE correlation between an aryl C-H doublet (δ 6.87, ^4J = 2.2 Hz) and an aniline N-H identified this isomer as the *meta* isomer.

*NBz-p-t*BuL1. ^{1}H NMR (400 MHz, DMSO-d_6): δ 7.36-7.19 (m, 5H), 6.78 (d, J = 1.9 Hz, 1H), 6.75-6.67 (m, 2H), 5.53 (br s, 1H), 5.36 (br s, 1H), 3.48 (s, 2H), 2.59-2.52 (m, 2H), 2.42-2.31 (m, 2H), 1.85 (td, J = 12.8, 4.6 Hz, 2H), 1.48-1.44 (m, 2H), 1.41 (s, 9H), 1.22 (s, 9H). ^{13}C NMR (100 MHz, DMSO-d_6): δ 157.04, 139.93, 138.70, 134.44, 132.02, 128.76, 128.10, 126.81, 119.51, 118.47, 113.18, 62.19, 51.02, 49.71, 47.30, 33.50, 31.62, 30.67, 28.71. HRMS (EI) m/z: [M^+] calcd for $C_{27}H_{38}N_4$ 418.3096; observed 418.3091.

***N*,7'-di-*tert*-butyl-1'H-spiro[piperidine-4,2'-quinoxalin]-3'-amine** (*m-t*BuL1): A 100 mL RBF was flame dried, cooled and charged with NBz-*m-t*BuL1 (514 mg, 1.10 mmol,[a] 1 eq) and methanol (20 mL) and the vessel was sparged with N_2. Pd/C (51 mg, 10% w/w), ammonium formate (348 mg, 5.52 mmol, 5 eq) and acetic acid (63 μL, 1.10

[a] Coeluted with *N*-benzyl-4-piperidinone starting material; carried onto next reaction.

mmol, 1 eq) were added and the mixture was heated to reflux for 10 min, at which point the starting material was consumed by TLC. The reaction mixture was cooled and eluted through a pad of celite with methanol, and the filtrate was concentrated and taken up in water. The pH of the mixture was adjusted to ~ 9 with 1 M NaOH, and extracted with 3 × 15 mL $CHCl_3$. The combined organic layers were washed with water and brine, dried over Na_2SO_4, filtered and concentrated to yield *m*-*t*BuL1 (460 mg, 96%) as a colourless solid that was recrystallized from ethyl acetate/hexanes as colourless crystals.

^{1}H NMR (400 MHz, DMSO-d_6): δ 6.85 (d, J = 2.1 Hz, 1H), 6.67 (d, J = 8.0 Hz, 1H), 6.54 (dd, J = 8.0, 2.2 Hz, 1H), 5.70 (s, 1H), 5.19 (s, 1H), 2.84 (t, J = 11.6 Hz, 2H), 2.70-2.61 (m, 2H), 1.96 (br s, 1H), 1.71 (td, J = 12.5, 4.5 Hz, 2H), 1.40 (s, 9H), 1.39-1.34 (m, 2H), 1.22 (s, 9H). ^{13}C NMR (101 MHz, DMSO-d_6): δ 156.88, 144.21, 134.20, 132.30, 122.10, 114.28, 110.41, 50.89, 50.54, 40.26, 33.90, 31.85, 31.52, 28.67. HRMS (EI) *m*/*z*: [M^+] calcd for $C_{20}H_{32}N_4$ 328.2627; observed 328.2640.

***N*,6'-di-*tert*-butyl-1'H-spiro[piperidine-4,2'-quinoxalin]-3'-amine** (*p*-*t*BuL1): A 100 mL RBF was flame dried, cooled and charged with NBz-*p*-*t*BuL1 (610 mg, 1.46 mmol, 1 eq) and methanol (20 mL) and the vessel was sparged with N_2. Pd/C (60 mg, 10% w/w), ammonium formate (459 mg, 7.28 mmol, 5 eq) and acetic acid (83 μL, 1.46 mmol, 1 eq) were added and the mixture was heated to reflux for 10 min, at which point the starting material was consumed by TLC. The reaction mixture was cooled and eluted through a pad of celite with methanol, and the filtrate was concentrated and taken up in water. The pH of the mixture was adjusted to ~ 9 with 1 M NaOH, and extracted with 3 × 15 mL $CHCl_3$. The combined organic layers were washed with water and brine, dried over Na_2SO_4,

filtered and concentrated to yield *p*-*t*BuL1 (460 mg, 96%) as a colourless solid that was recrystallized from ethyl acetate/hexanes as colourless crystals.

^{1}H NMR (400 MHz, DMSO-d_6): δ 6.73 (d, J = 1.9 Hz, 1H), 6.70-6.62 (m, 2H), 5.59 (br s, 1H), 5.20 (br s, 1H), 2.79 (td, J = 12.4, 2.4 Hz, 2H), 2.60 (d, J = 13.1 Hz, 2H), 1.85 (br s, 1H), 1.65 (td, J = 12.5, 4.6 Hz, 2H), 1.38 (s, 9H), 1.34 (d, J = 13.1 Hz, 2H), 1.18 (s, 9H). ^{13}C NMR (101 MHz, DMSO-d_6): δ 157.46, 139.78, 134.32, 132.36, 119.47, 118.49, 113.02, 50.94, 50.55, 40.27, 33.49, 31.67, 31.62, 28.72. HRMS (EI) *m*/*z*: [M^+] calcd for $C_{20}H_{32}N_4$ 328.2627; observed 328.2615.

***N*-(*tert*-butyl)-1'H-spiro[cyclohexane-1,2'-quinoxalin]-3'-amine** (L2): An oven-dried 100 mL RBF was charged with *o*-phenylenediamine (1.081 g, 10 mmol, 1 eq), methanol (15 mL, dried over 3Å sieves), and cyclohexanone (0.981 g, 10 mmol, 1 eq) and the solution heated to reflux for 4 h under N_2. The reaction mixture was allowed to cool to 50°C, and a solution of TMSCl (1.27 mL, 10 mmol, 1 equiv.) in 7.5 mL dry acetonitrile was added dropwise over 15 min, followed by *t*-butyl isocyanide (0.831 g, 10 mmol, 1 eq) in 7.5 mL methanol dropwise over 1 h. The solution was stirred overnight, cooled, and concentrated *in vacuo*. The residue was triturated in 50 mL dry ether followed by sonication for 10 min. The precipitate was collected by filtration, air dried, and transferred portionwise to 50 mL of water. The mixture was stirred vigorously during addition of 1 M aqueous NaOH to pH 9, and extracted with 3 × 50 mL $CHCl_3$. The combined organic layers were washed with brine, dried over $MgSO_4$, filtered, concentrated and the residue eluted through a silica gel plug with 1:3 ethyl acetate:hexanes. The eluent was concentrated to yield L2 (1.66 g, 61%), which was recrystallized from ethyl acetate/hexanes as colourless needles.

^{1}H NMR (400 MHz, $CDCl_3$) δ 7.01 (dd, *J* = 7.3, 1.8 Hz, 1H), 6.82-6.71 (m, 2H), 6.59 (dd, *J* = 7.3, 1.7 Hz, 1H), 4.32 (s, 1H), 4.10 (s, 1H), 1.80 (d, *J* = 10.9 Hz, 2H), 1.74-1.54 (m, 4H), 1.46 (s, 9H), 1.42-1.15 (m, 4H). HRMS (EI) *m*/*z*: [M^+] calcd for $C_{17}H_{25}N_3$ 271.2048; observed 271.2034. Spectra matched those reported in the literature.[13]

N-(*tert*-butyl)-6'-((*tert*-butyldimethylsilyl)oxy)-1'H-spiro[cyclohexane-1,2'-quinoxalin]-3'-amine (*L2-OTBS*): An oven-dried 100 mL RBF was charged with 4-((*t*-butyldimethylsilyl)oxy)benzene-1,2-diamine[14] (0.310 g, 1.30 mmol, 1 eq), methanol (8 mL, dried 24-h over 3Å sieves), and cyclohexanone (0.134 mL, 1.30 mmol, 1 eq) and the solution heated to reflux for 3 h under N_2. The reaction mixture was allowed to cool to 50°C, and a solution of TMSCl (0.165 mL, 1.30 mmol, 1 equiv.) in 7.5 mL dry acetonitrile was added dropwise over 15 min, followed by *t*-butyl isocyanide (0.108 g, 1.30 mmol, 1 eq) in 7.5 mL methanol dropwise over 1 h. The solution was stirred overnight, cooled, and concentrated *in vacuo*. The residue was triturated in 50 mL dry ether followed by sonication for 10 min. The precipitate was collected by filtration, air dried, and transferred portionwise to 50 mL of water. The mixture was stirred vigorously during addition of 1 M aqueous NaOH to pH 9, and extracted with 3 × 50 mL $CHCl_3$. The combined organic layers were washed with brine, dried over $MgSO_4$, filtered, concentrated and the residue dry loaded onto a silica gel column. The product was eluted with 1:19:80 triethylamine:diethyl ether:hexanes to yield L2-OTBS (0.372 g, 72%) as a pale solid.

^{1}H NMR (400 MHz, DMSO-d_6): δ 6.63 (d, *J* = 8.2 Hz, 1H), 6.26 (d, *J* = 2.7 Hz, 1H), 6.17 (dd, *J* = 8.2, 2.7 Hz, 1H), 5.32 (s, 2H), 1.67-1.44 (m, 8H), 1.39 (s, 9H), 1.30-1.06 (m, 2H), 0.93 (s, 9H), 0.12 (s, 6H). ^{13}C NMR (101 MHz, DMSO-d_6): δ 158.89, 146.97,

135.89, 129.40, 113.94, 113.52, 112.48, 51.50, 51.00, 30.65, 28.66, 25.65, 24.74, 19.86, 17.83, -4.44. HRMS (EI) *m*/*z*: [M^+] calcd for $C_{23}H_{39}N_3OSi$ 401.2862; observed 401.2834.

3'-(*tert*-butylamino)-1'H-spiro[cyclohexane-1,2'-quinoxalin]-6'-ol (*L2-OH*): A 50 mL RBF was flame dried and charged with L2-OTBS (0.150 g, 0.37 mmol, 1 eq) followed by HCl (5 mL of 6 M prepared from AcCl in 99% EtOH). The solution was heated in a 45°C oil bath for 1 h under N_2. The solution was cooled and diluted with ethyl acetate (25 mL) and washed with portions of saturated aqueous $NaHCO_3$ until gas evolution ceased. The organic layer was washed with brine, dried over Na_2SO_4, filtered and concentrated to yield L2-OH (0.072 g, 67%), which was recrystallized from degassed ethyl acetates/hexanes to yield colourless plates. The solid was stable at ambient conditions for *ca.* 1 week.

^{1}H NMR (300 MHz, DMSO-d_6): δ 8.17 (s, 1H), 6.57 (d, J = 8.2 Hz, 1H), 6.25 (d, J = 2.7 Hz, 1H), 6.10 (dd, J = 8.2, 2.7 Hz, 1H), 5.25 (s, 1H), 5.08 (s, 1H), 1.66-1.40 (m, 8H), 1.39 (s, 9H), 1.37-1.19 (m, 2H). ^{13}C NMR (151 MHz, DMSO-d_6) δ 159.68, 150.01, 136.71, 128.02, 114.54, 110.23, 108.86, 52.10, 51.54, 31.04, 29.14, 25.25, 20.44. HRMS (EI) *m*/*z*: [M^+] calcd for $C_{17}H_{25}N_3O$ 287.1998; observed 287.2011.

1-(6'-(*tert*-butyl)-4'-methyl-1'H-spiro[piperidine-4,2'-quinolin]-1-yl)ethanone (*NAc-L3*): An oven-dried 100 mL RBF, Dean-Stark trap and condenser were assembled hot and cooled under a stream of N_2. The flask was charged with tosic acid dihydrate (*ca.* 20 mg) and dry toluene (25 mL) and heated to vigorous reflux. A solution of 4-*t*-butylaniline (1.16 g, 7.8 mmol, 1 eq.) and N-acetyl-4-piperidinone (1.10 g, 7.8 mmol, 1 eq) in 10 mL dry toluene was added dropwise to the solution at reflux over 15 min and stirred for a further 8 h. The solution was then cooled and transferred into a flame dried sealed

tube with 2,2-dimethoxypropane (1.92 mL, 15.6 mmol, 2 eq) and another portion of tosic acid dihydrate (*ca.* 20 mg). The tube was sealed and heated at 110°C for 5 h, then cooled and concentrated. The residue was taken up in ethyl acetate (100 mL) and washed with 2 × 100 mL saturated aqueous $NaHCO_3$ and brine. The organic layer was dried over $MgSO_4$, filtered, concentrated and the residue purified by silica gel chromatography in 1:19 methanol:methylene chloride to yield NAc-L3 (1.44 g, 59%) as a colourless solid.

^{1}H NMR (400 MHz, DMSO-d_6): δ 7.07 – 6.91 (m, 2H), 6.55 (d, J = 8.9 Hz, 1H), 5.84 (s, 1H), 5.45 (s, 1H), 3.59 – 3.38 (m, 4H), 1.99 (s, 3H), 1.94 (s, 3H), 1.66 – 1.43 (m, 4H), 1.21 (s, 9H). ^{13}C NMR (100 MHz, DMSO-d_6): δ 167.95, 141.40, 137.90, 129.39, 125.42, 125.14, 120.19, 119.72, 112.53, 51.19, 41.03, 38.49, 37.76, 36.12, 33.55, 31.44, 21.27, 18.41. HRMS (EI) *m*/*z*: [M^+] calcd for $C_{20}H_{28}N_2O$ 312.2202; observed 312.2165.

6'-(*tert*-butyl)-4'-methyl-1'H-spiro[piperidine-4,2'-quinoline] (*L3*): A 100 mL RBF was charged with L3-NAc (120 mg, 0.38 mmol, 1 eq), 95% ethanol (15 mL) and KOH (2 mL of 5 M aqueous solution). The solution was sparged with N_2 and heated to reflux for 3 h, then cooled and concentrated. The residue was taken up in methylene chloride (25 mL) and water. The organic layer was washed with 2 × 25 mL water, dried over Na_2SO_4, concentrated and the residue purified by silica gel chromatography in 1:20:79 Et_3N:MeOH:CH_2Cl_2 to yield L3 (98 mg, 95%) as a pale oil, which slowly solidifies.

^{1}H NMR (400 MHz, DMSO-d_6) δ 6.96 – 6.92 (m, 2H), 6.55 (d, J = 8.9 Hz, 1H), 5.77 (s, 1H), 5.45 (s, 1H), 2.97 – 2.84 (m, 2H), 2.84 – 2.72 (m, 2H), 1.93 (d, J = 1.4 Hz, 3H), 1.65 – 1.49 (m, 4H), 1.37 (s, 1H), 1.21 (s, 9H). ^{13}C NMR (151 MHz, DMSO-d_6) δ 141.67, 138.91, 129.99, 126.06, 125.79, 122.87, 120.33, 113.26, 51.04, 40.40, 37.61,

34.08, 31.94, 18.93. HRMS (EI) *m/z*: [M^+] calcd for $C_{18}H_{26}N_2$ [M^+] 270.2096; observed 270.2098.

***N*,4-di-*tert*-butylaniline** (*L5*): An oven-dried 100 mL sealed tube was cooled under a stream of N_2, and *t*-amyl alcohol (10 mL) was added and sparged with N_2 for 10 min. $Pd_2(dba)_3$ (86 mg, 0.09 mmol, 0.01 eq), BippyPhos (191 mg, 0.38 mmol, 0.04 eq), *t*-$BuNH_2$ (19.7 mL, 187.7 mmol, 20 eq), 4-*t*-butyl-bromobenzene (2 g, 9.38 mmol, 1 eq) and KOH (737 mg in 1 mL H_2O, 13.14 mmol, 1.4 eq) were each added in one portion. The tube sparged with N_2, sealed and heated in a 110°C oil bath with vigorous stirring overnight. The mixture was cooled and filtered over celite and washed with methanol. The filtrate was concentrated on a rotovap with dry ice condenser and the residue taken up in DCM (100 mL) and washed twice with H_2O (200 mL). The organic layer was dried over $MgSO_4$, filtered, concentrated, dry loaded onto a minimum of silica, and eluted with 1:3 Et_2O:petroleum ether to yield L5 (913 mg, 47%) as a low melting, colourless solid.

^{1}H NMR (400 MHz, DMSO-d_6) δ 7.06 (dd, *J* = 8.7, 1.5 Hz, 2H), 6.65 (dd, *J* = 8.7, 1.9 Hz, 2H), 4.78 (d, *J* = 3.8 Hz, 1H), 1.26 (s, 9H), 1.21 (s, 9H). ^{13}C NMR (101 MHz, DMSO-d_6) δ 145.08, 138.25, 125.08, 115.65, 50.24, 33.36, 31.40, 29.65. Spectra matched those reported in the literature.[15]

N,4-di-*tert*-butylaniline-*N*-aminoxyl (***L5-NO***): A 100 mL flask was charged with L5 (730 mg, 3.6 mmol, 1 eq) and 10 mL of MeOH. A condenser was affixed and the solution heated to reflux under N_2. Portions of Na_2WO_4•$2H_2O$ (100 uL of 3.5 M in H_2O, 0.36 mmol, 0.1 eq) and H_2O_2 (4.5 mL of 2.5 M prepared in MeOH, 10.7 mmol, 3 eq) were added until the consumption of starting material by TLC. The mixture was cooled, concentrated, and taken up in 100 mL diethyl ether and a minimum of H_2O. The organic

layer was washed with saturated aqueous $NaHCO_3$ × 3, dried over $MgSO_4$, filtrated and concentrated to a residue that was purified by column chromatography in 1:3 diethyl ether:petroleum ether to yield L5-NO (636 mg, 81%) as a red solid.

HRMS (EI) *m*/*z*: [M^+] calcd for $C_{14}H_{22}NO$ 220.1701; observed 220.1675.

2.10.3 PMHC-BODIPY and Dimethyl-BODIPY liposome autoxidations

Solutions of egg PC liposomes (41.5 μL of 20 mM in pH 7.4 PBS), antioxidant (5 μL of appropriate concentration in DMSO), dye (5 μL of 258 uM of either Dimethyl-BODIPY or PMHC-BODIPY in acetonitrile) and 748 μL of PBS were prepared in microcentrifuge tubes, vortexed, and 260 μL×3 aliquots transferred to a 96-well plate (Nunc™ PP, clear). The plate was incubated at 37°C for 5 min, after which 10 μL of either AAPH (73 mM in PBS), MeOAMVN (18.4 mM in acetonitrile) or acetonitrile was added by multichannel pipette and fluorescence was monitored immediately at the appropriate wavelengths.

2.10.4 Inhibition of RSL3-induced ferroptosis.

Pfa-1 cells were cultured at 37°C in 5% CO_2 atmosphere in DMEM containing 10% FBS, 10 mM glutamine, and 1X each of penicillin-streptomycin and non-essential amino acid solutions. 3,000 cells in 100 μL media were seeded in 96-well plates and grown for 18 hours, after which an aliquot of serially diluted antioxidant (10 uL in growth medium without FBS) was added. After 30 min, an aliquot of (1*S*-3*R*)-RLS3 (100 nM in DPBS) was added. The cells were incubated for 6 h followed by determination of cell viability by the AquaBluer (MultiTarget Pharmaceuticals, LLC) assay by replacing media according to the manufacturer's directions.

2.11 Supplementary References

[1] Kysil, V.; Khvat, A.; Tsirulnikov, S.; Tkachenko, S.; Williams, C.; Churakova, M.; Ivachtchenko, A. General Multicomponent Strategy for the Synthesis of 2-Amino-1,4-Diazaheterocycles: Scope, Limitations, and Utility. *Eur. J. Org. Chem.* **2010**, *2010* (8), 1525–1543.

[2] Friedmann Angeli, J. P.; Schneider, M.; Proneth, B.; Tyurina, Y. Y.; Tyurin, V. A.; Hammond, V. J.; Herbach, N.; Aichler, M.; Walch, A.; Eggenhofer, E.; Basavarajappa, D.; Radmark, O.; Kobayashi, S.; Seibt, T.; Beck, H.; Neff, F.; Esposito, I.; Wanke, R.; Forster, H.; Yefremova, O.; Heinrichmeyer, M.; Bornkamm, G. W.; Geissler, E. K.; Thomas, S. B.; Stockwell, B. R.; O'Donnell, V. B.; Kagan, V. E.; Schick, J. A.; Conrad, M. Inactivation of the ferroptosis regulator Gpx4 triggers acute renal failure in mice. *Nat. Cell. Biol.* **2014,** *16* (22), 1180-1191.

[3] Brownlie, I. T.; Ingold, K. U. The Inhibited Autoxidation of Styrene: Part V. The Kinetics and Deuterium Isotope Effect for Inhibition by Diphenylamine, Phenyl-α-Napthylamine, and Phenyl-β-Naphthylamine. *Can J. Chem.* **1966**, *44* (8), 861–868.

[4] Haidasz, E. A.; Shah, R.; Pratt, D. A. The Catalytic Mechanism of Diarylamine Radical-Trapping Antioxidants. *J. Am. Chem. Soc.* **2014**, *136* (47), 16643–16650.

[5] Valgimigli, L.; Pratt, D. A. Maximizing the Reactivity of Phenolic and Aminic Radical-Trapping Antioxidants: Just Add Nitrogen! *Acc. Chem. Res.* **2015**, *48* (4), 966–975.

[6] Scaiano, J. C. Exploratory Laser Flash Photolysis Study of Free Radical Reactions and Magnetic Field Effects in Melatonin Chemistry. *J. Pineal Res.* **1995**, *19* (4), 189–195.

[7] Horstman, J. A.; Wrona, M. Z.; Dryhurst, G. Further Insights Into the Reaction of Melatonin with Hydroxyl Radical. *Bioorg. Chem.* **2002**, *30* (5), 371–382.

[8] [8] Krumoya, K.; Friedland, S.; Cosa, G. How Lipid Unsaturation, Peroxyl Radical Partitioning, and Chromanol Lipophilic Tail Affect the Antioxidant Activity of α-Tocopherol: Direct Visualization via High-Throughput Fluorescence Studies Conducted with Fluorogenic α-Tocopherol Analogues. *J. Am. Chem. Soc.* **2012**, *134* (24), 10102–10113.

[9] Haidasz, E. A.; Meng, D.; Amorati, R.; Baschieri, A.; Ingold, K. U.; Valgimigli, L.; Pratt, D. A. Acid Is Key to the Radical-Trapping Antioxidant Activity of Nitroxides. *J. Am. Chem. Soc.* **2016**, *138* (16), 5290–5298.

[10] Zilka, O.; Shah, R.; Li, B.; Angeli, J. F.; Griesser, M.; Conrad, M.; Pratt, D. A. On the Mechanism of Cytoprotection by Ferrostatin-1 and Liproxstatin-1 and the Role of Lipid Peroxidation in Ferroptotic Cell Death. *ACS Cent. Sci.* **2017**, *3* (3), 232–243.

[11] Li, B.; Harjani, J. R.; Cormier, N. S.; Madarati, H.; Atkinson, J.; Cosa, G.; Pratt, D. A. Besting Vitamin E: Sidechain Substitution Is Key to the Reactivity of Naphthyridinol Antioxidants in Lipid Bilayers. *J. Am. Chem. Soc.* **2013**, *135* (4), 1394–1405.

[12] Gokel, G. W.; Widera, R. P.; Weber, W. P. Phase-Transfer Hofmann Carbylamine Reaction: tert-Butyl Isocyanide. *Org. Synth.* **1976**, *55*, 96.

[13] Kolla, S. R.; Lee, Y. R. EDTA-Catalyzed Synthesis of 3,4-Dihydroquinoxalin-2-Amine Derivatives by a Three-Component Coupling of One-Pot Condensation Reactions in an Aqueous Medium. *Tetrahedron* **2010**, *66* (46), 8938–8944.

[14] Yoshimura, M.; Ono, M.; Matsurnura, K.; Watanabe, H.; Kimura, H.; Cui, M.; Nakamoto, Y.; Togashi, K.; Okamoto, Y.; Ihara, M.; Takahashi, R.; Saji, H. Structure-Activity Relationships and in Vivo Evaluation of Quinoxaline Derivatives for PET Imaging of Beta-Amyloid Plaques. *ACS Med. Chem. Lett.* **2013**, *4* (7), 31–35.

[15] Johnson, A. R.; Cummins, C. C.; Gambarotta, S. (**1998**) *N*-Tert-Alkyl-Anilides as Bulky Anciliary Ligands. In *Inorganic Syntheses*, Vol. 32, pp 123–132. John Wiley & Sons, Inc.: Hoboken, NJ, USA; DOI: 10.1002/9780470132630.ch20

Preface to Chapter 3

Coworker contributions

Animal dissections for determining THN and MitoTHN bioavailability in mice were completed by Prof. Adam Shuhendler. Ron Shah conducted confocal microscopy experiments. Evaluations of MitoTHN binding affinity to α-tocopherol transport protein was completed by undergraduate students Kailey Meehan and Taniya Singh in the lab of our collaborator at Brock University, Prof. Jeffrey Atkinson.

Chapter 3: Targeting Tetrahydronaphthyridinols to the Mitochondria

Mitochondria as we presently know them arose about 2 billion years ago by engulfment of an α-proteobacterium by the progenitor of eukaryotes.[1,2] Their ability to produce ATP through respiration is implicated as the evolutionary driving force for altering the distribution of DNA around these bioenergetic membranes, resulting in the expansion of the genome 200,000-fold.[2] While this symbiosis provides the energetic requirement of higher life, it does so with a much greater requirement of oxygen. Most of the oxygen used by humans is efficiently reduced to water, however, about 2% results in superoxide generation by the mitochondria.[3,4] This constitutes a major homeostatic source of oxidants—a pillar in the free-radical theory of aging.[5,6] Moreover, the relevance of proximal mitochondrial dysfunction has been demonstrated in pathologies such as ischemia reperfusion injury (IRI),[7,8] diabetes,[9] cancer,[10] Mitochondrial Encephalopathy Lactic Acidosis and Stroke-like episodes (MELAS),[11] and neurodegenerative conditions such as Parkinson's[12] and Alzheimer's[13] disease. They also play a central role in maintaining homeostasis by regulating cytosolic calcium,[14] apoptosis,[15] and fatty acid metabolism.

3.1 Introduction

3.1.1 Mitochondrial dysfunction and lipid peroxidation

The downstream effects of elevated levels of intracellular ROS lead to deleterious reactions with proteins, DNA, and importantly, initiation events leading to lipid autoxidation. A cell's remarkable redundancy and self-repair can mitigate minor protein and DNA damage; lipid autoxidation however, is unique in that a single initiation event

triggers an autocatalytic reaction to yield more numerous products than the single initiating species. This can be disastrous in organs with little cellular proliferation, such as in the cardiac and nervous systems. One can envision that elevated ROS generation above 'nominal' levels (*e.g.* 1-5×10^{-10} M for mitochondrial H_2O_2 and superoxide)[16] exponentially increases overall stress to the cell if autoxidation is not curtailed by RTAs such as α-TOH or ubiquinone, or phospholipid GPX (GPX4).

Mitochondrial membranes contain a large amount of polyunsaturated fatty acids susceptible to autoxidation. Phosphatidylcholine and phosphatidylethanolamine account for ~80 mol% of phospholipids and, of the remainder, the majority (~18 mol%) is cardiolipin (**Figure 3.2**).[17] Cardiolipin is of particular interest since it is biosynthesized in the mitochondria and is present in the highest percent composition in mitochondrial over all other membranes, and is implicated in almost every mitochondrial function.[18,19] Importantly, cardiolipin contains *~90%* unsaturated fatty acids,[20] and the acyl chain composition is correlated to age, tissue type and species.[18] Initiation events in these

A

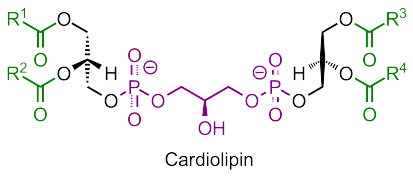

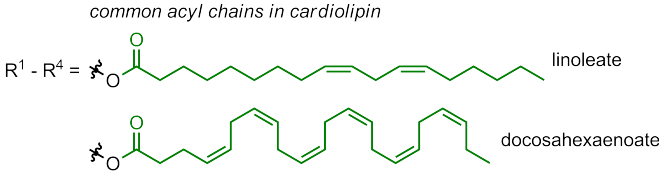

B

Implicated role	Description
Structural	• Conical tertiary structure in the IMM exerts lateral pressure to form cristae
Cofactor of ETC enzymes	• Promotes supercomplex formation and organization of ETC complexes • Anchors cyt *c* , which is highly cationic, in the IMM
Regulation of apoptosis	• Peroxidation results in translocation to the OMM and release of cyt *c*
Acyl chain remodeling	• Differentiation in acyl chains occurs in different species and tissues, and with age, possibly for environmental adaptations
Mitochondrial membrane fusion/fission	• Mitofusin and MitoPLD-mediated fusion involves hydrolysis of cardiolipin to form a fusogenic phosphatidic acid; dysregulation results in fragmented mitochondria

Figure 3.1 (**A**) Structure of cardiolipin and common acyl chains in mammals. (**B**) Various roles of cardiolipin in mitochondrial function.[18,19]

unsaturated fatty acids are similar to any lipid bilayer, either by (superoxide-derived) hydroperoxyl radicals,[21] the action of low-valent iron—or other good one-electron reductants—on peroxides,[22] ionizing radiation, *etc*. Mitochondrial cardiolipin lipid autoxidation results in the same electrophilic aldehydes[23] that adversely affects enzyme activity, energy linked functions, and membrane structure that results in swelling, followed by lysis.[22] Mitochondrial DNA (mtDNA) is particularly susceptible to oxidative stress as it is not protected in histones, nor do the mitochondria possess efficient mtDNA repair systems, each of which contributes to mutation rates over 10-fold higher than in nuclear DNA.[24]

Further, oxidative stress can lead to both mitophagy and the mitochondrial permeability transition (MPT). Mitophagy is a term coined in 2005 for the selective, non-random autophagy of mitochondria by autophagosomes.[25] Oxidative damage is thought to lead to mitophagy through oxidative modification and/or misfolding of proteins from mtDNA mutations, and also through oxidative damage to cardiolipin that subsequently triggers translocation to the outer membrane.[26] These events lead to surface ubiquitination and sequestering via the proautophagic machinery.[27] Dysfunctional mitochondria are also destroyed via the MPT wherein the formation of aqueous pores of up to 1500 Da in size leads to swelling, release of cyt *c* and uncoupling of $\Delta\Psi_m$.[28,29] While the link between autoxidation and mitophagy or MPT remains to be established, it is clear that various oxidative stressors trigger removal of dysfunctional mitochondria and/or pro-apoptotic signaling.

3.1.2 Modelling mitochondrial oxidative stress

The typical model of mitochondrial oxidative stress is by action of the redox cycling molecule *N*,*N*′-dimethyl-4,4′-bipyridinium dichloride, ParaQuat (PQ, **Figure 3.2A**).[30] PQ is a controlled-use herbicide widely used[31] in spite of Parkinsonian-type and lung toxicity effects on humans.[32] The mechanism by which PQ induces oxidative stress is likely due to the ease with which it can be reduced to a species that rapidly reacts with molecular oxygen.[33] Evidence for lipid peroxidation arising from PQ treatment was initially proposed by detection of malondialdehyde in both plants[34] and liver microsomes.[35] More recent research in mice reveal that PQ neurotoxicity leading to Parkinsonian-type pathology correlates well with 4-hydroxy-2-nonenal (4-HNE) formation, another marker for lipid peroxidation, in mouse neurons.[36] PQ's cell uptake is quite low due to its small

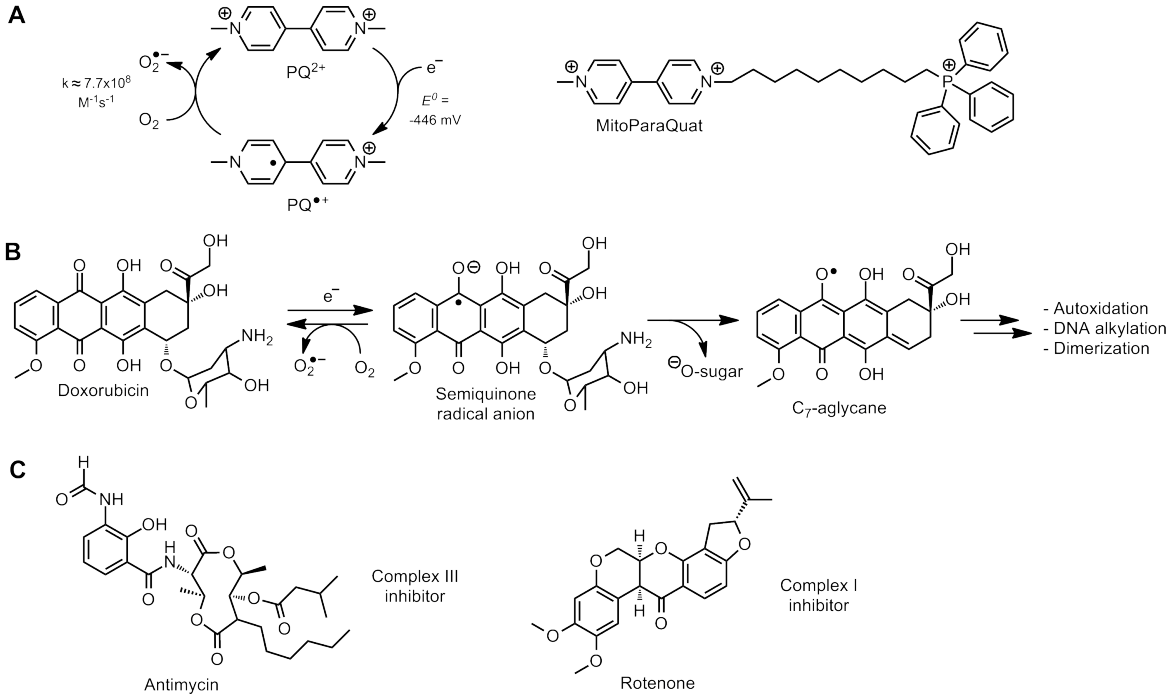

Figure 3.2 One electron redox cycle of ParaQuat (PQ) and MitoParaQuat (MPQ) (**A**) and doxorubicin (DOX) (**B**) that can lead to superoxide generation and lipid autoxidation. ETC inhibitors Antimycin A and Rotenone inhibit Complex III and I, respectively (**C**).

charged structure; a variant was recently prepared with a lipophilic chain (MitoParaquat, MPQ, **Figure 3.2A**) to facilitate cell permeability and more selective mitochondrial delivery for induction of oxidative stress and mitochondrial dysfunction.[37]

Specific inhibitors of ETC complexes have also been identified including Antimycin A, which blocks Complex III at the Q_i site, and rotenone, which blocks Complex I (**Figure 3.2C**). Electron transport is halted through these specific interactions and a buildup of ubisemiquinone (*i.e.* from a high QH_2:Q ratio) leads to generation of superoxide/hydroperoxyl (**Figure 1.3**). Doxorubicin (Adriamycin®) and related anthracycline aminoglycosides are known for their potent antitumor activity resulting from DNA intercalation and cross-linking, however their significant cardiotoxic side effect has led researchers to determine that a significant pro-oxidant effect is also imparted by the quinone moiety. This effect is concentrated in cardiomyocytes due to their numerous mitochondria attracting the lipophilic and positively charged aminoglycoside moiety. The reaction of semiquinone radical with oxygen leads to superoxide generation, or formation of the C_7-aglycane followed by reaction with oxygen can lead to mitochondrial lipid peroxidation (**Figure 3.2B**).[38,39,40]

3.1.3 Mitochondria targeting strategies

Several strategies to deliver pharmacophores to the mitochondria have been developed that target their unique energetic membrane. The protonmotive force (Δp) allows cations that are capable of diffusion across membranes to be attracted into and accumulate in the mitochondria. The Δp imparted by the membrane potential results in ~100-500 fold accumulation relative to the cytoplasm, dictated by the Nernst equation (~10 fold accumulation with every ~60 mV $\Delta\Psi_m$).[41] This allows cationic molecules, including

nanoparticles and functionalized liposomes, to efficiently accumulate in the mitochondria. Also, cationic polypeptides have been developed to target mitochondria that also accumulate independent of the membrane potential.

The triphenylphosphonium (TPP) cation[42] is a commonly employed cationic motif since: *i*) it is excreted in bile and urine without being metabolized;[43] *ii*) it features a diffuse, fixed positive charge, unlike ammonium or guanidinium salts, and; *iii*) it is incapable of redox cycling, as is the case with some alkylated pyridinium cations. However, this methodology is not without disadvantages (**Table 3.1**). Hundreds of bioactive probes, imaging agents, natural products and antioxidants conjugated to TPP cations have recently been exhaustively reviewed.[44] The authors of this review underscore the currently unmet

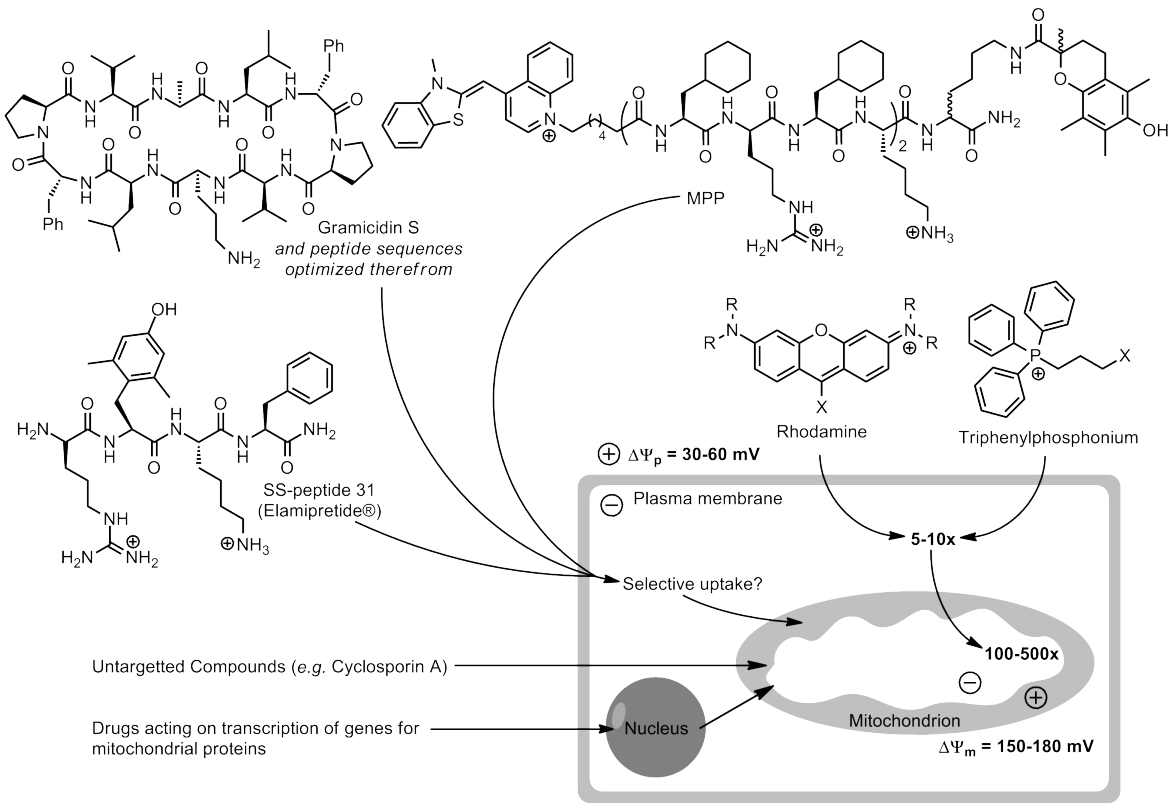

Figure 3.3 Common strategies to target pharmacophores to mitochondria. Adapted from reference 41.

need for careful clinical evaluations of this methodology; nevertheless, the scope of these compounds is only growing, in part due to the often observed elevated Ψ_m in cancer cells (*i.e.* > 60 mV $\Delta\Psi_m$)[45] that imparts a distinct target otherwise unexploited by current chemotherapy, and the somewhat controversial success of MitoQ (discussed in **3.2.7**).

Table 3.1 Advantages and disadvantages of current mitochondrial targeting strategies.[41,52]

Targetting method	Advantages	Disadvantages
Triphenyl-phosphonium (TPP)	• Rapid uptake due to fixed positive charge • Lower doses resulting from efficient accumulation • Reduced toxicity towards electroneutral cellular compartments • Ease of preparation • Facilitates targeting of hydrophobic pharmacophores	• Electrostatics contribute to depolarization of membrane • Chaotropic (detergent-like) toxicity to membranes • Organ non-specific; tendency to accumulate in cells/tissues with numerous mitochondria • Preferential accumulation near the negative matrix face of inner membrane *vs.* outer membrane
SS and MPP peptides	• Reduced toxicity *vs.* TPP • Presumed to be independent of membrane potential	• Slower incorporation relative to TPP • Broader intracellular distribution • Difficult and/or costly to prepare
Nanoparticles	• Highly functionalizable surface with fluorescent probes, magnetization, and bioactive compounds • Better stability and controlled release relative to liposomes	• Difficult and/or costly to prepare • Limited biocompatibility demonstrated *in vivo* • Biodegradable polymers required
Liposomes	• Delivery of hydrophobic and hydrophilic payload mixtures	• Desired small liposome size difficult to achieve; polydispersity of large liposomes • Still requires functionalization (*e.g.* with stearyl TTP) to target mitochondria and escape endocytosis

The Szeto-Schiller (SS) peptides[46] are thought to bind specifically to cardiolipin *via* electrostatic interactions of the cationic amino and guanidinium groups with the anionic groups of cardiolipin, resulting in accumulation of 1000 to 5000-fold over the cytosol. The lead compound SS-31 (Elampretide™/Bendavia™) is multimodal: it targets a 2,6-dimethyltyrosine residue to effect antioxidant activity[47] and it stabilizes native cardiolipin-cyt *c* interactions by sitting on top of the anionic phosphoglycerol. It is this specific binding to cardiolipin that is proposed to promote the desired electron transfer role of cyt *c* instead of cyt *c* unfolding into cyt *c* peroxidase, thereby maximizing electron transfer

during oxidative phosphorylation resulting in greater ATP production and minimal cardiolipin peroxidation.[48,49] Hemigramicidin-based[50] and other cationic mitochondrial penetrating peptides (MPPs)[51] thought to bind to targets in the mitochondria have also been developed. There is speculation that the overarching transport mechanism of both MPPs and SS-peptides are identical to cationic molecules.[41] Nanoparticles have also been successfully evaluated, though they have demonstrated limited biocompatibility *in vivo*.[52]

3.1.4 Methods used to evaluate mitochondrial uptake of small molecules

The minute size and delicate structure of mitochondria prevent the direct measurement of a membrane potential with microelectrodes, thus indirect methods have been used to verify both that mitochondria feature electrochemical gradient and that amphipathic cations are in fact electrophoretically attracted into the mitochondria. This is complicated by depolarization of Ψ_m and subsequent release of compounds that occurs upon (even rapid) cellular fractionation attempts.[53]

Preliminary research by Skulachev *et al.* validated that respiring mitochondria maintain a potential difference by using the apparatus shown in **Figure 3.4**.[54,55] A semipermeable phospholipid membrane (circled blue in **A**) separates two solutions and allows ions that are sufficiently amphipathic to equilibrate across the apparatus membrane. The choice of penetrating ion is such that they do not induce conductance for other ions present in the test incubation mixture (*e.g.* by chelating metal ions). Such penetrating anions and cations have been screened and prominently include triphenylmethyl phosphonium ($TPMP^+$), tetraphenyl borate (TPB^-), and dibenzyldimethyl ammonium (DDA^+) (**Figure 3.4B**). The conductance recorded across the apparatus membrane then depends only the concentration-dependent diffusion of the penetrating ion, which is

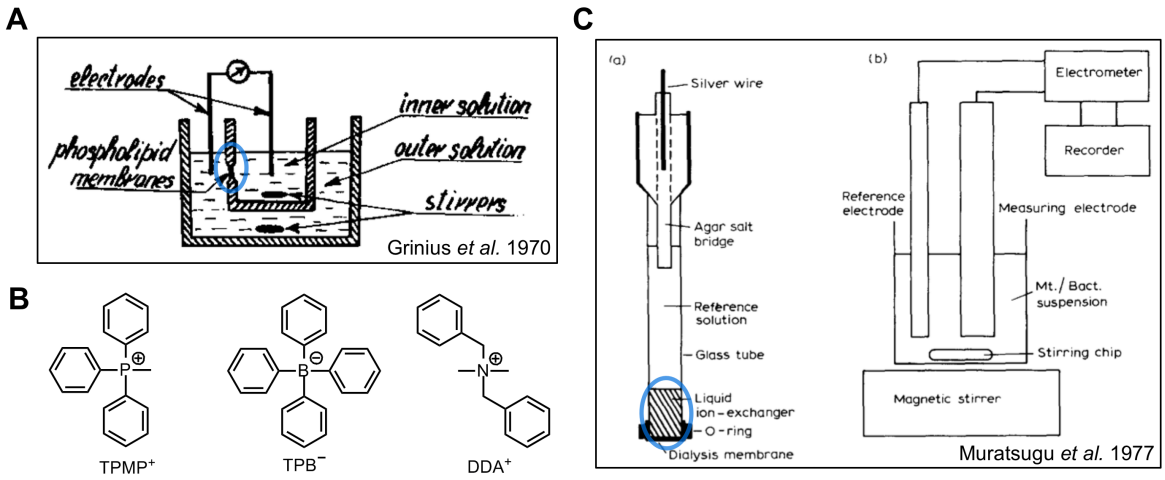

Figure 3.4 Apparatus (**A** and **C**) used to verify and evaluate electrophoretic accumulation of ions (**B**) across charged subcellular organelles. Images reproduced from references 55 and 56.

standardized to allow kinetic measurements. Penetrating cations added to a solution of mitochondria brought about the same changes accompanying native cations such as Ca^{2+} and K^{+}, all in accordance with a negatively charged inner matrix. Importantly, uptake of these cations brought about acidification of the test solution, implying the electric field is maintained by actively pumping protons out of the mitochondria to compensate for cation accumulation.[54]

This methodology was adapted to replace the phospholipid membrane with other ion-selective mediums inside of a probe, namely an immiscible organic solution,[56] and a PVC-based membrane.[57,58] In the former method, a dichloroethane solution of the penetrating ion DDA^{+} and counterion TPB^{-} are separated from the test media by a cellulose dialysis membrane (circled blue in **Figure 3.4C**). A potential difference is then generated when mitochondria are introduced into the test solution such that DDA^{+} was assumed to be drawn into the mitochondria. This method is amenable to any penetrating ion, though it is unclear why the counterion TPB^{-} is required in the test solution. The requirement for TPB^{-} was overcome however by impregnating NaTPB into a non-

penetrating PVC membrane[57] in place of the dialysis membrane as in **Figure 3.4C,** omitting the organic solution. This has become the common apparatus of convenience for measuring uptake of cations into cellular and subcellular compartments.[59,121]

The chemiosmotic theory was further corroborated using radioisotope labeling of penetrating cations. This methodology is less quantitative as it requires cell fractionation before scintillation counting. Nevertheless, isotope detection of any manner in the mitochondrial fraction is excellent evidence for the uptake of payloads in the mitochondria. Common isotopes used are ^{3}H and ^{18}F incorporated into TPP.[60] This methodology has detected up to half the dosed amount of MitoQ,[69] discussed in **3.1.6**, in the mitochondria.

The most prominent modern technique to evaluate mitochondrial uptake involves direct cell imaging with confocal microscopy. This requires the molecule of interest to be inherently fluorescent or tagged with a fluorophore.[61] The live cells are stained with a mitochondrially-targeted fluorescent probe with a different emission wavelength from the test compound that allows successive images to be superimposed to evaluate co-localization.[62] This is the method most amenable to laboratories since the equipment is widely available. Of note, tetramethylrhodamine methyl ester (TMRM) is widely used in fluorescence imaging as a measure of membrane potential.[63]

3.1.5 Probes for sensing mitochondrial lipid peroxidation

While numerous probes are purported to selectively visualize ROS (*e.g.* H_2O_2, superoxide) in mitochondria,[64,65] only a few lipid peroxidation probes have been prepared: MitoPerOx,[66] MitoDPPP,[67] and Mito-BODIPY-TOH[68] (Figure 3.5). Shioji's MitoDPPP is based on phosphine reactivity towards hydroperoxides, thus it suffers from sluggish reactivity and poor sensitivity that has prevented widespread adoption of its use. Murphy's MitoPerOx is based on the methodology of C11-BODIPY, thus it exhibits very rapid reactivity towards peroxyl radicals and at low nM concentration. Cosa's Mito-BODIPY-TOH is itself an RTA. Other RTAs compete with the PMHC moiety to retard the rate of fluorescence increase, rather than the former two dyes that are employed as 'endpoint' dyes. Our efforts to prepare our own version of a mitochondrially targeted BODIPY are described in section **3.2.2**.

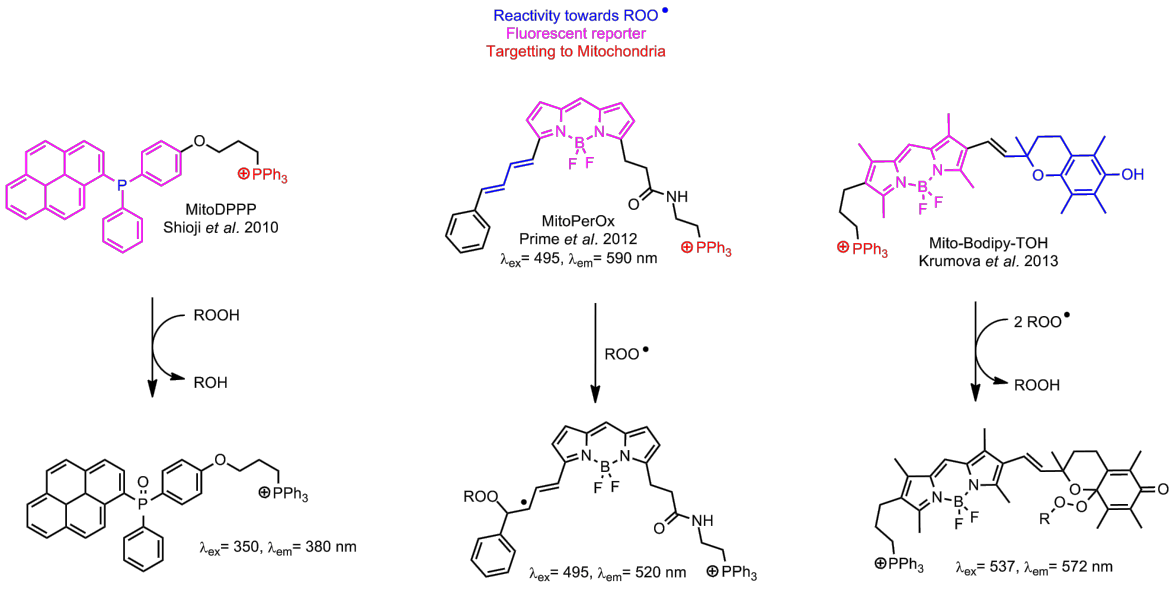

Figure 3.5 Lipid peroxidation probes targeted to the mitochondria.

3.1.6 Mitochondrially-targeted antioxidants

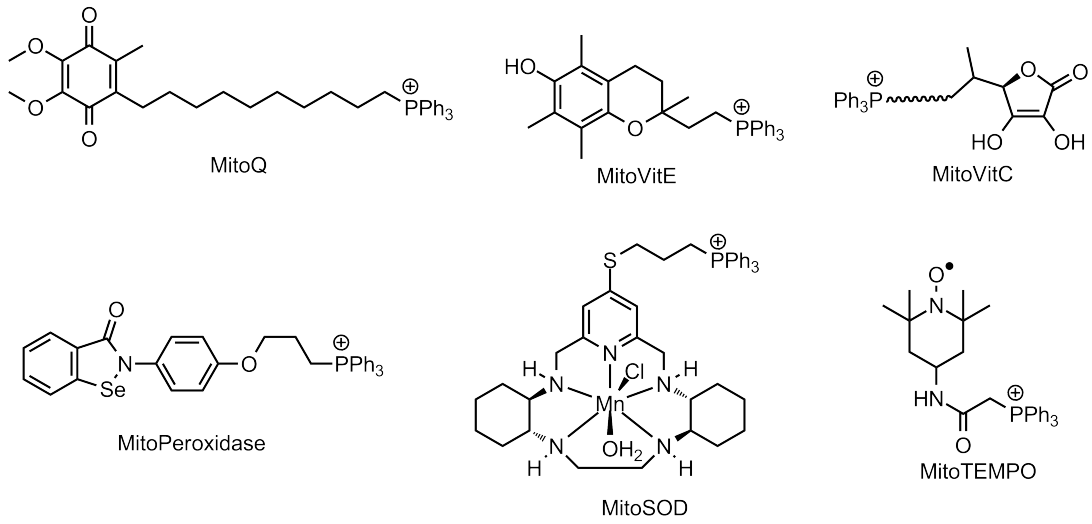

Figure 3.6 Prominent mitochondrially-targeted TPP-based antioxidants.

The concept of mitochondrially-targeted antioxidants follows in the wake of mitochondrially-targeted ubiquinone (MitoQ, **Figure 3.6**), developed by the Murphy group over the past few decades.[69] MitoQ is regarded as the lead candidate in ameliorating mitochondrial oxidative stress, and has enjoyed a plethora of success in small animal and *in vitro* models,[70] including ischemia reperfusion injury,[71] hypertension,[72] and sepsis.[73] In humans however, there has been limited success in combating neurodegenerative disease such as Parkinson's disease, likely due to the neuronal loss suffered prior to any clinical presentation, or to insufficient delivery across the blood-brain barrier.[74] Indeed, many of the positive effects in humans have been protective and mildly restorative, rather than fully reversing a condition.[75] Alongside MitoQ, the Murphy group has prepared analogous compounds including MitoVitE,[76] MitoVitC,[77] MitoSOD,[78] MitoPeroxidase[79] among others. Most compounds have demonstrated some success *in vitro*, though interestingly none have been as successful as MitoQ.[75]

Careful investigations of both MitoVitE and MitoQ have revealed that while *in vitro* experiments suggest they ameliorate oxidative stress, cell and animal experiments reveal proapoptotic properties that increase oxidative stress to the cell. It has been demonstrated that MitoVitE depletes intracellular ATP, which is selectively cytotoxic to cancer cells,[80,81] and the effects are vastly increased when the carbon chain is lengthened to increase lipophilicity.[82] Similarly, the redox cycling of MitoQ has been demonstrated to exert proxidant effects in endothelial cells that adversely alter bioenergetics[83] and can lead to apoptosis.[84] Further work disclosed dysregulation of calcium levels.[85] These results have been addressed by demonstrating that the protective effects occur *in vivo* at much lower concentration than those required to model dysfunction.[86] This highlights the careful scrutiny and judgment researchers must practice interpreting results in the field of mitochondrial dysfunction.

3.1.7 Mitochondrial dysfunction in ferroptosis

The recent discovery of ferroptosis,[87] a novel, regulated necrotic mode of cell death (**Figure 1.12**) was determined to involve the degeneration of mitochondria,[87,88,89,90] however *without* significant mitochondrial ROS production. This conclusion is supported on the basis of several experiments that demonstrate:

i) cells treated with erastin do not exhibit significant increase in MitoSOX fluorescence (a purportedly superoxide-selective mitochondrial probe);[87]

ii) cells treated with RSL3 exhibit C11-BODIPY fluorescence early in ferroptosis induction without significant increase in MitoPerOx fluorescence (a mitochondrial lipid peroxidation-selective probe),[90] and;

iii) ferroptotic cell death induced by each of erastin, RSL3, BSO and *Gpx4*$^{-/-}$ knockout was rescued by decyl-Q—a non-targeted lipophilic antioxidant—with 100-fold *greater* potency over MitoQ—the analogous mitochondrially targeted antioxidant.

These observations are at odds with numerous recent reports including: a mitochondrially-targeted nitroxide inhibiting ferroptosis,[91] the observation of oxidized cardiolipin accumulating in *Gpx4* knockout mouse kidney,[90] the report of BID (a pro-apoptotic protein that translocates to mitochondria)[92] knockout or inhibition preventing ferroptotic cell death,[93] the report of the mitochondrial CDGSH iron sulfur domain 1 (CISD1) stabilization inhibiting ferroptosis,[94] and the depletion of ubiquinone inducing ferroptosis.[95] Each of these reports suggests some contribution of intramitochondrial lipid peroxidation (autoxidation) or mitochondrial dysfunction contributing to ferroptotic cell death. Careful experimentation by Angeli *et al.* has shown rupture of the outer mitochondrial membrane (OMM) by transmission electron microscopy within 1 hour of ferroptosis induction by RSL3, which the authors suggest may "*possibly [mark] the point of no return in ferroptosis.*" [90] Furthermore, the authors address that while MitoQ putatively localizes in the matrix face of the inner mitochondrial membrane (IMM), (mitochondrial) GPX4 is in the intermembrane space. This may explain why MitoQ exhibits poor anti-ferroptotic activity, since it would be sequestered from propagating lipid peroxyls in the OMM.[90] The rupture event is likely not related to a MPT pore since cyclosporine A, an inhibitor of MPT pore formation, does not sensitize cells towards or against ferroptosis.[87] Lastly, careful analysis of MitoPerOx *vs.* C11-BODIPY flow cytometry histograms in RSL3 treated cells do demonstrate a 3-fold distinct fluorescence

increase concomitant with the *ca.* 10-fold increase in C11-BODIPY over 3 hours, while a known mitochondrial peroxidation initiator was not reported under identical conditions to determine if 3-fold fluorescence increase of MitoPerOx was significant.[90]

Recent work in our group has implicated lipid autoxidation in ferroptosis.[96,97,98] Given that GPX4 is accepted as the key ferroptotic regulator,[99] it follows that the cellular compartments with the greatest potential for lipid peroxidation, such as mitochondrial membranes, would be kinetically predisposed to peroxidation when GPX4 activity ceases. Yet as previously introduced, evidence for this proposal has suggested the opposite, that mitochondrial peroxidation is not as significant.[87,90] We suggest that a mitochondrially targeted antioxidant other than MitoQ may uncover different results. Accepting the explanation of Angeli *et al.* that MitoQ may not co-localize with mitochondrial GPX (and by extension, propagating mitochondrial lipid peroxyls), it is nevertheless unsurprising that treatment with MitoQ is ineffective at modulating ferroptosis given that MitoQ possesses equivalent inherent reactivity to coenzyme-Q. The preparation and evaluation of mitochondrially-targeted THNs (a MitoTHN) of unparalleled RTA activity—described next—will attempt to address these unanswered questions to clarify the relationship between the mitochondria, lipid autoxidation, and GPX4 in the ferroptotic mode of cell death. Moreover, the MitoTHNs may hold promise for any other pathology in which mitochondrial oxidative stress is suggested. Towards this goal, we advance development of our THN repertoire to biodistribution studies in mice.

3.2 Results and Discussion

3.2.1 Synthesis of mitochondrially targeted tetrahydronaphthyridinols (Mito-THNs)

Previous work in our group has optimized the synthesis of the THN core to take advantage of a simple alkylation of **1** (**Scheme 3.1**) with a desired side chain that allows access to THNs with a wide variety of lipophilicity. We envisioned compounds structurally similar to MitoQ, putatively delivering the THN to mitochondria with a TPP moiety.

Our initial strategy to introduce the mitochondria targeting side chain in one step with 1-bromo-8-triphenylphosphoniumoctane bromide proved challenging as the choice of base and/or forcing conditions led to significant ylide formation. A two-step approach was then envisioned involving alkylation of **1** with bis-terminally substituted bromoalkanes. Such compounds would then provide access to a variety of mitochondrially-targeted motifs at the terminal position of the alkyl side chain, such as TPP incorporation.

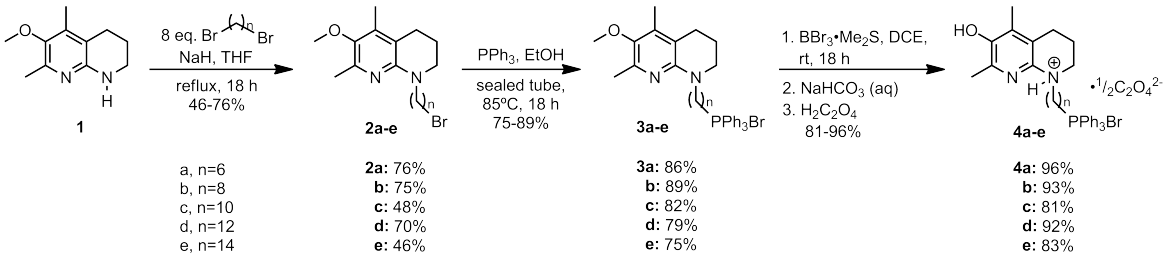

Scheme 3.1 Synthesis of mitochondrially-targeted THNs (MitoTHNs, **4**).

Alkylation of **1** with 1,*n*-dibromo-*n*-alkanes successfully provided side-chains of *n* = 6, 8, 10, 12 and 14 carbons (**Scheme 3.1**). Intermediates **2a-e** were obtained in good yields when four equivalents of the dibromoalkane were used to disfavor the double substitution product. Longer sidechains proved difficult to push to completion, and reaction times greater than 48 h decreased yields, presumably due to formation of

quaternary ammonium salts of **1**. The final products were observed to decompose upon storage, presumably due to the presence of both nucleophilic and electrophilic sites on the molecule. The primary halides were thus carried through to subsequent reactions with haste. Substitution of the halide with triphenylphosphine proceeded cleanly in polar solvents such as acetonitrile and ethanol, though similar to the alkylation reactions, longer chain lengths required longer reaction times and greater equivalents of triphenylphosphine. A physical characteristic of the longer chain alkyl-triphenylphosphonium salts is the formation of foams upon concentration. This was evident in each of the intermediates **3a-e** and problematic since the foams collapse and gum when exposed to moisture. Nevertheless, the solid foams were stable under nitrogen at room temperature and transferring with anhydrous methylene chloride for subsequent steps was effective.

Demethylation was facile utilizing similar conditions to those previously developed for the THNs. BBr_3•Me_2S complex was effective in deprotection of the methylated phenol without *N*-dealkylation, consistent with the optimized lipophilic THN syntheses.[100] The issue of boron contamination of the final product was revealed during preliminary attempts at isolating the predicted addition salt with oxalic acid, which initially failed to produce homogenous solids. Heating a solution of the product in methanol treated with excess oxalic acid at 50°C during slow rotary evaporation was effective at isolating the product, presumably via azeotropic removal of $B(OR)_3$ formed upon reaction of the excess BBr_3 or the phenoxyl boronate esters with water in the quench and workup. The resultant residues could then be purified by column chromatography allowing storage of the solid at -20°C. Inert conditions were still necessary due to the hygroscopic nature of the phosphonium salts, evident even as oxalate addition products.

3.2.2 Synthesis of a mitochondrially-targeted peroxidation probe

Alongside our recent work monitoring hydrocarbon autoxidations with STY- and PBD-BODIPY,[101] we decided to synthesize a mitochondrially targeted BODIPY probe for sensing live-cell mitochondrial lipid peroxidation. We opted to connect the alkyl chain before assembly of the BODIPY core, as shown in the retrosynthesis in **Scheme 3.2**, to minimize the steps after forming the BODIPY core – a problem we identified with Murphy's MitoPerOx.

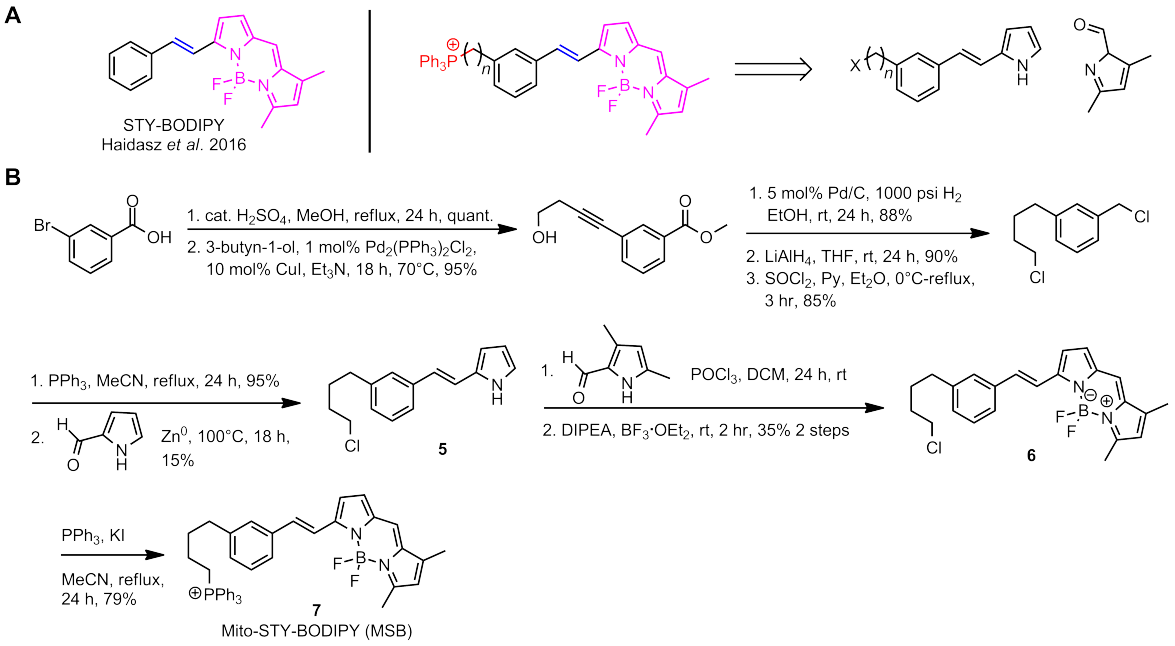

Scheme 3.2 Retrosynthesis (**A**) and synthesis (**B**) of MitoSTY-BODIPY (MSB, **7**).

The key styryl pyrrole **5** was prepared by a Wittig reaction with a benzyl chloride and a pyrrole aldehyde. Nucleophilic attack of **5** onto another pyrrole aldehyde activated with $POCl_3$ followed by elimination upon addition of DIPEA provided the dipyromethene scaffold *in situ* before addition of BF_3 diethyl etherate to fashion BODIPY intermediate **6**. Substitution with triphenylphosphine afforded the desired MitoSTY-BODIPY (MSB) **7**. With MSB and a small library of MitoTHNs in hand, their reactivity could be investigated.

3.2.3 MitoTHNs are equivalently potent to THNs in both homogeneous and heterogeneous media

The THNs were rationally designed to maximize the RTA activity of phenols resulting in k_{inh} of 8.8×10^7 $M^{-1}s^{-1}$ measured by oxygen uptake during the inhibited autoxidation of styrene.[102] These rates are faster than can be measured by co-autoxidation of PBD-BODIPY with styrene, and thus THNs completely inhibit the co-autoxidation resulting in a zero slope.[96] As shown in **Figure 3.7B**, the co-autoxidation of PBD-BODIPY with styrene is completely inhibited by each of the MitoTHNs, similar to C_{15}-THN, indicating that the inherent reactivity and stoichiometry of the THNs is not greatly affected by the triphenylphosphonium moiety.

The reactivity of the MitoTHNs in liposome autoxidations was evaluated next.

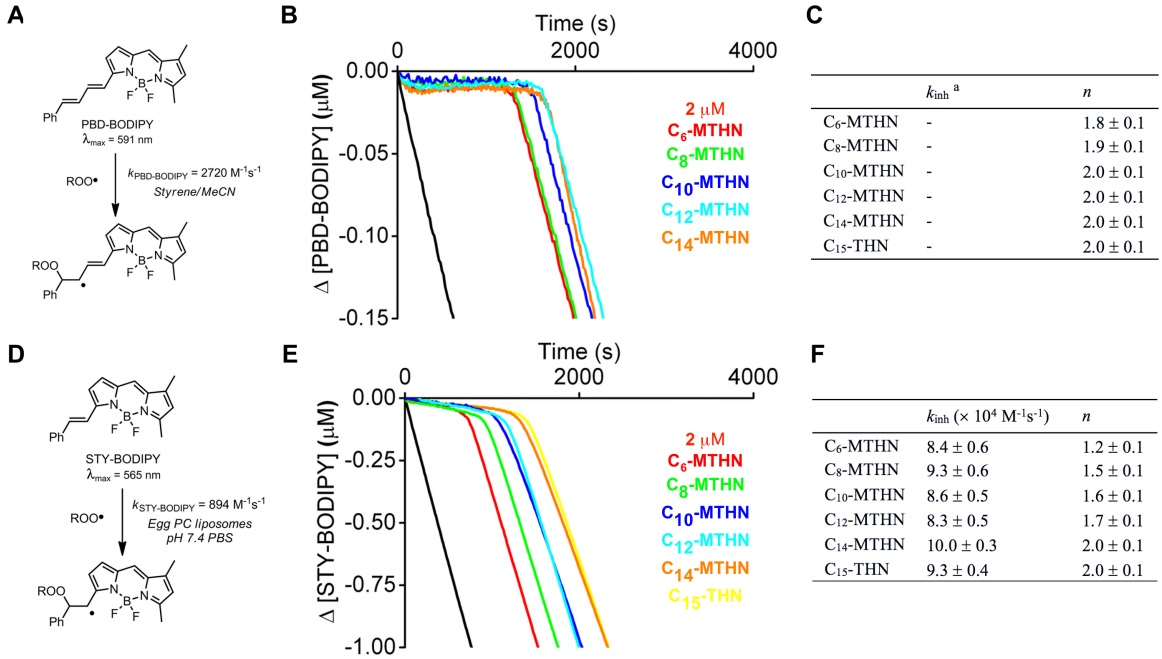

	k_{inh} [a]	n
C_6-MTHN	-	1.8 ± 0.1
C_8-MTHN	-	1.9 ± 0.1
C_{10}-MTHN	-	2.0 ± 0.1
C_{12}-MTHN	-	2.0 ± 0.1
C_{14}-MTHN	-	2.0 ± 0.1
C_{15}-THN	-	2.0 ± 0.1

	k_{inh} ($\times 10^4$ $M^{-1}s^{-1}$)	n
C_6-MTHN	8.4 ± 0.6	1.2 ± 0.1
C_8-MTHN	9.3 ± 0.6	1.5 ± 0.1
C_{10}-MTHN	8.6 ± 0.5	1.6 ± 0.1
C_{12}-MTHN	8.3 ± 0.5	1.7 ± 0.1
C_{14}-MTHN	10.0 ± 0.3	2.0 ± 0.1
C_{15}-THN	9.3 ± 0.4	2.0 ± 0.1

Figure 3.7 The inherent RTA activity of the THNs translates to MitoTHNs in organic solution autoxidations (Panels **A-C**, 4.3 M styrene in acetonitrile, initiated by 6 mM AIBN at 37°C) and in heterogeneous egg phosphatidylcholine lipid bilayer autoxidations (Panels **D-F**, 1 mM liposomes in 10 mM pH 7.4 PBS, initiated by 0.2 mM MeOAMVN at 37°C).

Effective inhibition rate constants of (8.3-10.0)×10^4 $M^{-1}s^{-1}$ were determined, each similar to C_{15}-THN at 9.3×10^4 $M^{-1}s^{-1}$ (**Figure 3.7E**). The stoichiometry of the MitoTHNs increased with increasing side chain length from ~1 for C_6 to ~2 for C_{14}. This is consistent with the trend previously observed for a series of THNs of varying lipophilicity,[100] where shorter sidechain THNs have a reduced stoichiometry that approaches a maximum by increasing lipophilicity. This trend has been attributed to greater partitioning into the aqueous phase of the heterogeneous media when the chain length is not long enough to impart sufficient hydrophobicity to favour the non-polar lipid phase. The free THN in the aqueous phase may then undergo deleterious electron transfer reactions with O_2— presumably via the aryloxide. C_{14}-MitoTHN provides the greatest performance in liposomes with n = 2, which suggests it is the best candidate for cell and animal studies. We next evaluated cytotoxicity of the prepared MitoTHNs.

3.2.4 Cytotoxicity of MitoTHNs

The cytotoxicity of the MitoTHNs was investigated in HEK293 cells. TC_{50} increased with chain length from (18 ± 1.4) μM for C_6 up to (1.7 ± 0.2) μM for C_{14} MTHN. These values are consistent with reported observations of $MitoQ_{10}$, where in cell culture concentrations of up to 1 μM are well tolerated, and effects on membrane potential, respiration rate or LDH release begin at 10 μM.[78] Rigorous studies on similar effects of the

Table 3.2 Cytotoxicity of MitoTHNs in HEK293 cells. Compounds were incubated for 22 h and viability determined using the AquaBluer assay.

Compound	TC_{50} (μM)
C_6-MitoTHN	18.1 ± 1.4
C_8-MitoTHN	19.9 ± 1.9
C_{10}-MitoTHN	5.9 ± 0.3
C_{12}-MitoTHN	2.5 ± 0.4
C_{14}-MitoTHN	1.7 ± 0.2

MitoTHNs on respiration rate, LDH release, *etc.* remain for future investigations. To determine if MitoTHNs, or other RTAs, sensitize mitochondrially-stressed cells towards or against cell death, we next conducted a viability screen with two mitochondrial oxidative stress initiators and various RTAs.

3.2.5 Towards rescue of mitochondrial oxidative stress-induced apoptosis

Cells treated with either MitoParaquat (MPQ) or doxorubicin (DOX) exhibit a slight sensitization to cell death with increasing concentrations of MitoTHN, or decyl-TPP. More importantly however, none of the antioxidant treatments result in greater viability than initiator alone—rather, increasing RTA concentration tends to result in cell death that is roughly the product of the individual toxicity of the RTA and either DOX or MPQ (left to right across **Figure 3.8**).

The anti-mitotic mechanism of action of DOX is presumably concomitant with the experimentally desired pro-oxidant effects, which may explain the lack of any rescuing

% Viability

MPQ (uM)	C10-TPPBr (uM)						C12-MTHN (uM)						PMC (uM)						Lip-1 (uM)					
	0	0.008	0.04	0.2	1	5	0	0.008	0.04	0.2	1	5	0	0.008	0.04	0.2	1	5	0	0.008	0.04	0.2	1	5
0	100	94	74	55	50	0	106	110	105	93	54	41	100	100	85	99	95	90	105	110	103	95	84	44
16	95	64	47	38	32	0	88	91	78	73	48	31	87	87	84	103	103	96	93					
31	81	60	48	37	41	0	90	76	68	61	44	31	77	79	78	86	79	75	88					
63	72	56	44	42	39	0	77	71	68	43	38	25	70	68	73	80	87	79	92	90	83	71	53	25
125	64	54	43	35	33	-1	61	62	61	44	29	21	64	82	72	76	67	70	71	76	68	56	38	24
250	53	48	44	30	25	0	62	50	48	48	34	11	64	82	65	69	68	65	68	66	58	49	33	20
500	50	37	36	36	29	0	38	41	31	36	25	15	52	67	42	60	47	49	49	51	49	47	20	22
1000	38	45	39	32	21	0	34	33	28	23	26	8	34	36	32	40	36	42	33	38	40	25	28	18

% Viability

DOX (uM)	C10-TPPBr (uM)						C12-MTHN (uM)						PMC (uM)						Lip-1 (uM)					
	0	0.008	0.04	0.2	1	5	0	0.008	0.04	0.2	1	5	0	0.008	0.04	0.2	1	5	0	0.008	0.04	0.2	1	5
0	100	96	63	46	35	0	80	74	62	63	45	27	100	97	95	88	83	87	97	103	106	85	80	69
0.8	89	78	52	32	26	0	65	68	48	48	36	24	76	81	71	78	67	72	83	81	82	69	61	28
1.6	84	70	53	26	26	0	55	57	41	29	24	26	55	58	61	73	66	68	75	70	75	74	58	29
3.1	67	61	54	47	39	0	55	52	35	30	21	18	58	59	54	65	57	51	53	57	58	49	45	19
6.3	61	61	50	50	34	0	59	52	31	38	22	18	37	33	41	44	39	37	47	38	45	41	34	19
12.5	54	45	41	35	25	0	47	42	34	32	21	11	36	35	38	37	36	36	35	35	34	36	34	17
25	40	43	37	15	17	0	30	24	15	18	15	5	33	36	32	35	40	35	35	41	30	29	23	14
50	47	35	29	26	13	1	25	20	17	17	14	2	17	26	24	29	30	27	34	33	25	24	26	12

Figure 3.8 MTHNs and RTAs do not rescue MEF cells treated with mitochondrial oxidative stress initiators MitoParaquat (MPQ, Top) and doxorubicin (DOX, bottom) from cell death.

effect by the RTAs. Similarly, apoptosis may also arise from superoxide toxicity by MPQ treatment before sufficient propagation of lipid autoxidation. For the case of MPQ, a cell line overexpressing SOD may be sufficient to prevent apoptosis during the course of the experiment. This may permit any lipid autoxidation to propagate since SOD is sequestered from lipids, and may allow any effect of chain breaking RTAs against mitochondrial lipid peroxidation to be resolved.

We next evaluated MitoTHNs in live cell models of oxidative stress using MSB, which importantly enables comparison of mitochondrially-targeted and non-targeted antioxidants since mitochondria are not isolated from cells prior to analysis.

3.2.6 Towards monitoring mitochondrial lipid peroxidation using MitoSTY-BODIPY

To evaluate the efficacy of MitoTHNs in their putative role of inhibiting mitochondrial lipid peroxidation, we investigated the use of MSB in live cell populations.

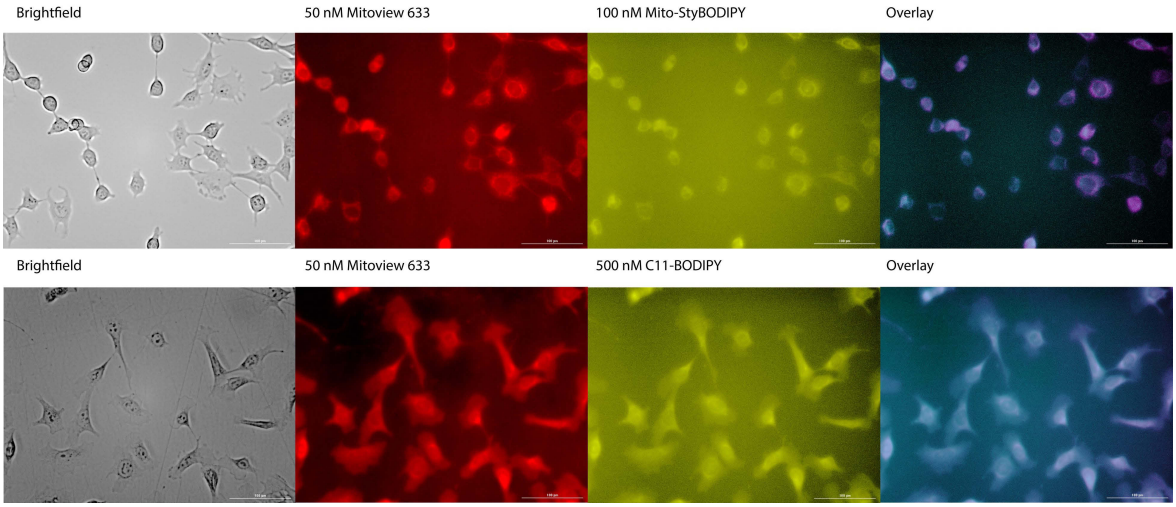

Figure 3.9 MSB localizes in the mitochondria. Pfa-1 cells were stained with the mitochondrial dye MitoView 633 and either MSB (top row) or C11-BODIPY (bottom row). The overlay represents areas of colocalization in purple.

We first ensured that the dye is present in the mitochondria by co-staining cells with MSB and MitoView 633. As expected, MSB has a significant overlap in fluorescence (**Figure 3.9**), whereas C11-BODIPY, the non-targeted lipid peroxidation probe, exhibits very little co-localization. This confirms MSB is present in the mitochondria.

We next attempted the precedented methodology of C11-BODIPY[103] using our prepared MSB probe by administering oxidative stress initiators to cells followed by MSB at the endpoint of an experiment to evaluate lipid peroxidation inhibition by RTAs. Flow cytometry is an ideal and reliable method of evaluating efficacy since a large population of live cells is tested.

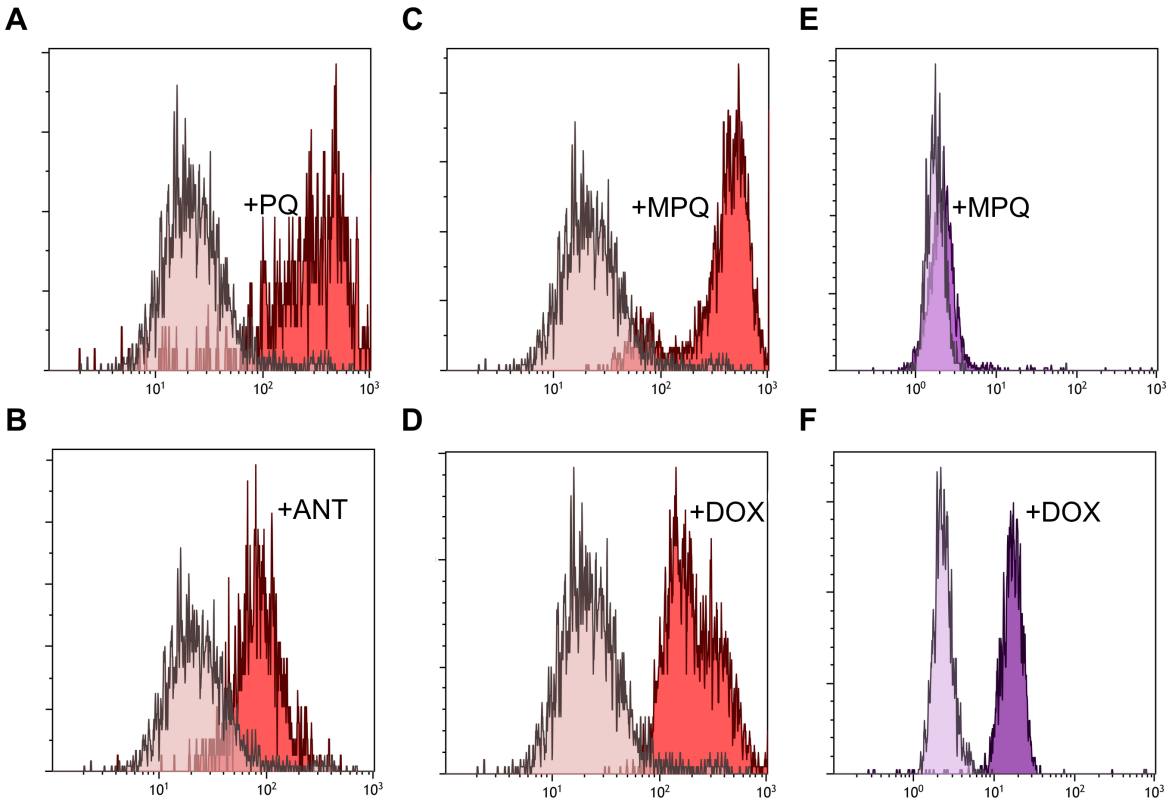

Figure 3.10 Mitochondrial initiators cause lipid peroxidation measured by MSB (FL2; untreated ▭, treated with initiator ▭) and C11-BODIPY (FL1; untreated ▭, treated with initiator ▭). Pfa-1 cells were treated with PQ (**A**, 1 mM, 22 h), ANT (**B**, 100 µM, 22 h), MPQ (**C** and **E**, 250 µM, 5 h), or DOX (**D** and **F**, 10 µM, 4 h), followed by MSB (250 nM, 30 min) or C11-BODIPY (1 µM, 30 min).

After optimizing concentration and initiation time, we observed an increase in MSB fluorescence with DOX, MPQ, ANT and PQ treatment varying from *ca.* 5-fold for ANT to 10-fold for PQ and MPQ (**Figure 3.10A-D**). While no reports of flow cytometry measurements with MitoPerOx have been reported, our measurements with MSB are comparable with a past report of *ca.* 5-fold enhancement of MitoPerOx fluorescence measured by confocal microscopy in a Parkinson's disease model of human neuroblasts challenged with 100 μM 6-hydroxydopamine for 3 h.[104] Similarly, a 2-3 fold enhancement of MitoPerOx fluorescence measured by confocal microscopy is observed in *Asperigillus fumigatus* treated with various antifungals.[105] The enhancement we observe is also much greater than the 1.25 fold fluorescence enhancement of MitoPerOx in 500 μM H_2O_2 treated HEK293 cells for 90 minutes measured in a custom flow cell fluorimeter and by confocal microscopy.[66]

Treatment of cells with MPQ did not appreciably increase C11-BODIPY fluorescence (**Figure 3.10E**), implying MSB is reporting on peroxidation arising from a location distinct from the non-targeted lipid C11-BODIPY probe, and that the peroxidation effects do not extend significantly to other lipid membranes of the cell under these conditions. In comparison, DOX treatment caused significant change in C11-BODIPY fluorescence (**Figure 3.10F**), suggesting that under these conditions, oxidants either leak out to other compartments, or incomplete mitochondrial accumulation of DOX results in non-mitochondrial initiation events—consistent with the lack of a distinct targeting moiety of DOX. However, the *ca.* 10-fold increase we observe with DOX treatment is an order of magnitude less than the well-known cell-wide lipid peroxidation initiator diethylmaleate (which increases C11-BODIPY fluorescence ~100-fold, discussed in section **3.2.8**). PQ

was observed to require at least 22 h to result in a significant MSB fluorescence increase, which is consistent with the increased potency of MPQ that is proposed to arise from greater lipophilicity and cellular uptake relative to PQ.[37] PQ and ANT were not investigated further as they required 24-hour incubations in this assay, which is undesirable for THN stability as the half-life is on the order of days in aerated hydrocarbons due to the electron rich nature of the phenol.[106]

The MSB fluorescence increase with treatment by all of DOX, MPQ and PQ, suggest that MSB is reporting on mitochondrial oxidative stress, however cytosolic ROS levels should also be compared under our experimental conditions to attain a measure of kinetics of cytosolic ROS levels that theoretically lead to the membrane peroxidation measured by MSB. Further, we acknowledge controls of RTA-alone treatment should be investigated to reveal potential pro-oxidant effects of the RTAs themselves.

With the appropriate positive controls established, an initial antioxidant screen was explored using MPQ and DOX initiators. However, to our disappointment, no significant effect on MSB fluorescence was observed when cells were co-incubated with mitochondrial stress initiators and a MitoTHN or THN.[a] We acknowledge that MitoQ, MitoVitE and decyl-TPP were not used as controls in this context to date.

While no suppression of MSB fluorescence was observed, this does not necessarily imply the MitoTHNs are not inhibiting mitochondrial lipid peroxidation. The effect of MitoTHNs could be more brief than which can be resolved by flow cytometry, *i.e.* the RTAs may be consumed during the 4-5 hours of incubation prior to application of the probe. This would result in indistinguishable measurements to the positive control. Further,

[a] Data not shown.

the greater reactivity of MitoTHNs implies they will be preferentially oxidized in the presence of the other lipophilic antioxidants present in mitochondria (*i.e.* ubiquinone, tocopherol). This explanation is consistent with the limited published experiments suggesting MitoPerOx fluorescence is suppressed with a mitochondrial antioxidant. For example, both MitoC and MitoQ were shown to be effective (at high micromolar concentrations) at preventing MitoPerOx fluorescence in isolated mitochondria only for the duration of a 10-12 *minute* experiment.[65,77] No other mitochondrial antioxidants have been reported to inhibit the fluorescence of MitoPerOx. To address the hypothesis that MitoTHNs are rapidly consumed, we attempted to administer the antioxidant to cells after administering either MPQ or DOX, then testing co-autoxidation with the probe directly thereafter. While some inhibitory effect of MitoTHNs and non-targeted antioxidants was observed,[a] at best only two-fold suppression relative to positive control was measured, with results difficult to reproduce. We would expect closer to complete suppression (*i.e.* 5 to 10-fold based on geometric mean of histograms of positive and negative controls) if the MitoTHN were being co-autoxidized with MSB in light of their behaviour in liposome autoxidations and the potency of THNs relative to other antioxidants. The irreproducibility likely arises from unpredictable damage and dynamics associated with ongoing mitochondrial oxidative stress and difficulty associated with monitoring kinetics of this manner by flow cytometry. Similarly, an alternate explanation for the lack of inhibitory effect on MSB fluorescence could be that the proapoptotic- and/or promitophagic-signaling cascade that occurs during mitochondrial oxidative stress has progressed too far before application of the mitochondrial RTA.

[a] Data not shown.

The sensitivity of MSB could be improved with a phenylbutadiene substituent on the probe, similar to C11-BODIPY and MitoPerOx, as we can predict the phenylallyl-like radical derived from peroxyl radical addition is more stable than a benzyl-like radical derived from peroxyl radical addition to MSB. Indeed, as other researchers have reported, the C11-BODIPY phenylbutadiene moiety is more sensitive to peroxidation over common unsaturated lipids, and the phenylbutadiene tends to overestimate 'oxidative stress' and underestimate antioxidant effectiveness in cells.[107] Thus a styryl C-H with a k_p closer to bisallylic C-H of lipids may be the preferable choice[101] in this context. Also, a longer phosphonium alkyl chain on MSB may aid in performance by disfavouring equilibrium into the aqueous phase, though MitoPerOx and MitoDPPP are quite similar in size to MSB.

Another important consideration for the assay is the requirement of up to three distinct treatments containing the triphenylphosphonium moiety. While 100 nM of either MitoPerOx[66,104] or MSB (**Figure 3.9**) is sufficient for confocal microscopy experiments, 2.5-fold higher concentration of MSB is required to achieve the requisite signal response by flow cytometry. Moreover, the initiators MPQ and PQ are present in the 0.1-5.0 mM concentration range, and antioxidants themselves are also present in the high nanomolar range. The effect on mitochondrial membrane potential when high concentrations of these large molecules with fixed positive charges should be carefully considered. The MitoTHNs are generally cytotoxic above *ca.* 2 μM. The combination of the various exogens may contribute to significant membrane depolarization, which is well precedented as a toxic effect of triphenylphosphonium salts, in addition to chaotropic effects on membranes. The dissipation of the electrochemical gradient would limit respiratory activity and thus the production of ROS in the assay, and concomitant disruption of mitochondrial membrane

integrity would lead to cell death before effects of peroxidation would be apparent. MSB is required at 250 nM to achieve the requisite response by flow cytometry, which is similar to 100 nM commonly reported with MitoPerOx employed in confocal microscopy experiments.

It is possible that superoxide generation in the mitochondria by the chosen initiators does not result in significant lipid peroxidation, and instead SOD activity rapidly mitigates the produced superoxide. If this were the case, the observed fluorescence increase could be due to partitioning of the probe into the aqueous phase resulting in reaction with hydroperoxyl radicals. Lipophilic RTAs would then appear to be ineffective since they would not be co-autoxidizing with the probe. Partitioning of short chain phosphonium salts has precedence in the C_6-C_{14} MitoTHN stoichiometry trend from the foregoing liposome autoxidation data.

Another consideration for the MitoTHN RTAs is the pH differences between mitochondrial compartments. If the MitoTHN has significant partitioning into the internal matrix, which is favoured by the negative potential (~ -160 mV) that attracts the phosphonium moiety, there would be a greater concentration of the tetrahydronapthyridinol-derived anion (phenoxide) since the matrix actively maintains a slight basic internal pH (~8). Moreover, it is known that concomitant H+ extrusion occurs with the uptake of penetrating cations, likely to maintain the membrane potential, which may further increase pH.[42] Electron transfer chemistry of the phenoxide, or single electron transfer from the phenol to O_2 (**Scheme 1.6**) may degrade the active antioxidant and thereby preclude effectiveness in the lipid.

The combined results of using MSB and flow cytometry suggest that obtaining unambiguous evidence for mitochondrial antioxidant efficacy by this method is too convoluted by cellular dynamics, the degrees of freedom of cellular mitochondria under significant oxidative stress over the time course of the experiment. Indeed, similar experiments sensing mitochondrial lipid peroxidation by flow cytometry have no precedence in the literature. Instead, methods supporting efficacy of mitochondrial antioxidants are overwhelmingly obtained either *via* confocal microscopy or in isolated mitochondria. This does raise the question of efficacy of these compounds in relevant cell assays, especially since microscopy techniques are inherently biased against large sample sizes and isolated mitochondria lack interaction with their intrinsic host cell. Nevertheless, future work will explore confocal microscopy as a technique to demonstrate proof of concept of the MitoTHNs in relevant cell models. We next sought to evaluate if MTHNs could rescue cells from RSL3-induced ferroptosis.

3.2.7 Medium-chain length MTHNs are mediocre ferroptosis inhibitors

The medium chain C_8- and C_{10}-MitoTHNs were able to partially rescue cells from ferroptotic cell death (**Figure 3.11**), exhibiting potency on the order of the premiere ferroptosis inhibitors Fer-1, Lip-1 and C_{15}-THN.[96] However, unlike these ferroptosis inhibitors, the MitoTHNs plateaued at rescuing ~70% of cell viability, and the trend observed on increasing lipophilicity of MitoTHNs to the chain length of C_{12} only rescued cells to 40% viability, while C_{14}-MitoTHN did not exhibit any protective effect. This is an unexpected result given only a slight difference of chain length.

An explanation for the longer chain C_{12}- and C_{14}-MitoTHNs having little effect on ferroptosis could lie in the kinetics of apoptotic over ferroptotic cell death pathways when mitochondrial function is perturbed by the chaotropic effects of lipophilic phosphonium cations[108],[109] such as the long chain MitoTHN. Evaluating lipid peroxidation with C11-BODIPY in addition to viability data above would help to evaluate the hypothesis, as

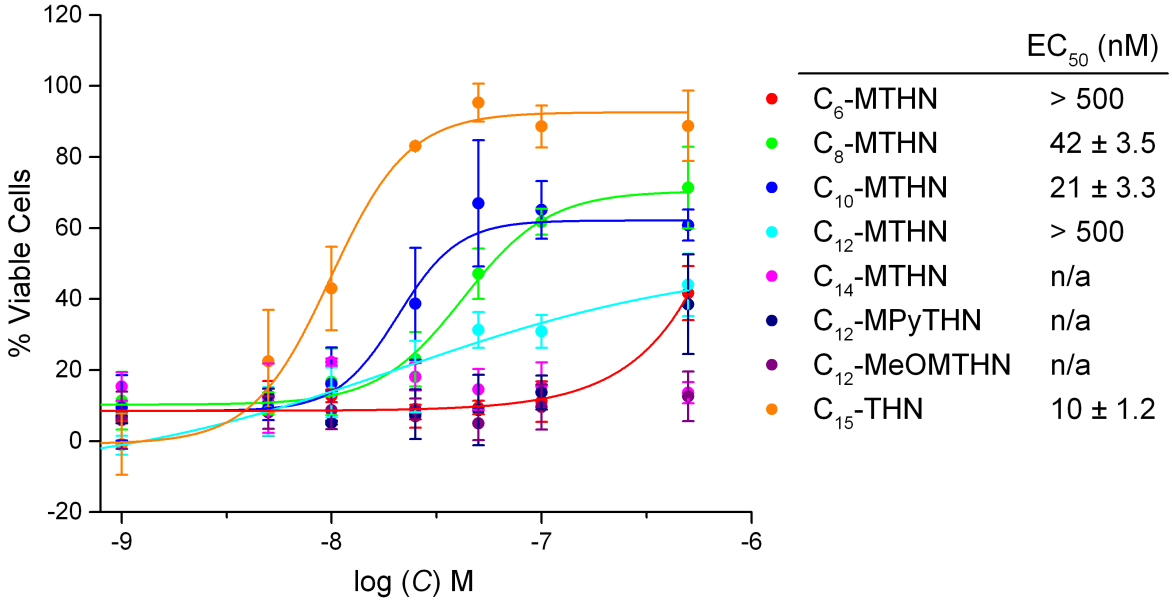

Figure 3.11 Medium-chain length MTHNs partially rescue cells from ferroptosis induced by RSL3 (100 nM) in Pfa-1 MEFs.

would measurement of apoptotic signals such as caspase activity and LDH activity as a measure of mitochondrial function. One explanation for the short chain MitoTHNs only rescuing viability to ~70% could be related to the increase in oxidative stress/superoxide production that occurs in cancer cells treated with MitoQ. This hypothesis remains to be investigated using confocal microscopy and MSB.

An alternative explanation to the observation of both MitoTHN and MitoQ[90] inhibit ferroptosis with less efficacy over their untargeted versions may involve the hormetic behaviour of mitochondria, termed mitohormesis,[110,111,112] a well-established hypothesis in medicine. Its application to free radical theories of diseases and aging stipulates that low amounts of oxidative stress products are required for upregulation of antioxidant response elements (AREs) from nuclear transcription.[111,113] The best-studied hormetic response involves the KEAP1/Nrf2/AGE signaling network, wherein the KEAP1 Nrf2 complex is natively targeted for ubiquitin-mediated destruction. However, upon reaction of cysteine-rich KEAP1 with electrophiles such as aldehydes that can arise from lipid peroxidation, the complex dissociates and Nrf2 is then free to translocate to the nucleus. Nrf2 then binds to promoter regions for AREs, of which there are hundreds (*e.g.* quinone oxidoreductase-1, heme oxygenase-1, and ferritin heavy chain-1) thereby increasing antioxidant defenses in response to either transient or persistent oxidative stress.[114,115,116] The mitochondrial pool of Nrf2 is tethered to the outer mitochondrial membrane with PGAM5.[117,118] If a MitoTHN is genuinely effective at preventing lipid peroxidation in the mitochondria, the KEAP1 redox sensitive response element would *not* be activated early in ferroptosis induction and thus cells would be sensitized towards ferroptosis arising from (extramitochondrial) iron catalysis and lipid autoxidation. Indeed, Nrf2 knockdown sensitizes cells towards, and

overexpression away from, ferroptosis.[119] Furthermore, Stockwell's group initially reported that cells treated with erastin increase the ATP/viable cells ratio ~ 2-fold, which may suggest a hormetic response to the erastin insult. This explanation could also contribute to why the medium-chain MitoTHNs can only rescue cells to 70% viability. The sensitization caused by the MitoTHNs to various ferroptotic triggers will be investigated in the future in an effort to uncover any synergistic effects.

If MitoTHNs do inhibit the mitochondrially-regulated antioxidant defenses of the cell, this manner of intervention could represent a distinctive axis of pharmacological cancer therapy where cells may be sensitized to ferroptosis/apoptosis by inhibiting this mitohormetic defense with a very potent mitochondrial antioxidant, thereby preventing a cancer cell's response mechanisms to environmental oxidative stresses such as ischemia or exogenous chemotherapy such as doxorubicin. This idea is distinct from the conventional approach in chemotherapy to avoid antioxidants in an effort to retain the proxidant effects of doxorubicin or radiation therapy. However, MitoQ has also been proposed in this context as it has often been reported that MitoQ is selectively toxic to cancer cells over healthy cells,[120] however this is presumed to arise from the increase in stress experienced by the cell.[108]

Another comparison that should be drawn relates to the binding effectiveness of the long chain phosphonium salts to the mitochondria, which the Murphy group has previously investigated with the MitoQ core and various lengths of the side chain.[121] The ion-selective probe methodology revealed that the uptake/incorporation of long chain phosphonium salts into the mitochondria depends on chain length. The authors demonstrated that a chain of 15 carbons results in nearly complete mitochondrial incorporation (84%, 4.2 μM of a 5.0 μM solution) upon addition of mitochondria (**Figure 3.12B**), whereas the chain length in common MitoQ—the commercialized variant—has a 10 carbon chain and exhibits only about 50% incorporation (2.6 μM of a 5 μM solution). Applying these known incorporation trends for may offer insight into the MitoTHN ferroptosis inhibition trend we observe since C_{10}- and C_{14}-MitoTHN are quite similar in both size and polarity to $MitoQ_{10}$ and $MitoQ_{15}$ (**Figure 3.12A**). $MitoQ_{10}$ rescues RSL3-induced ferroptosis with EC_{50} *ca.* 200 nM,[90] consistent with and within an order of the similarly sized C_8- and C_{10}-MitoTHN at EC_{50} = 42 and 21 nM respectively. It is curious that $MitoQ_{15}$ was not tested under the same

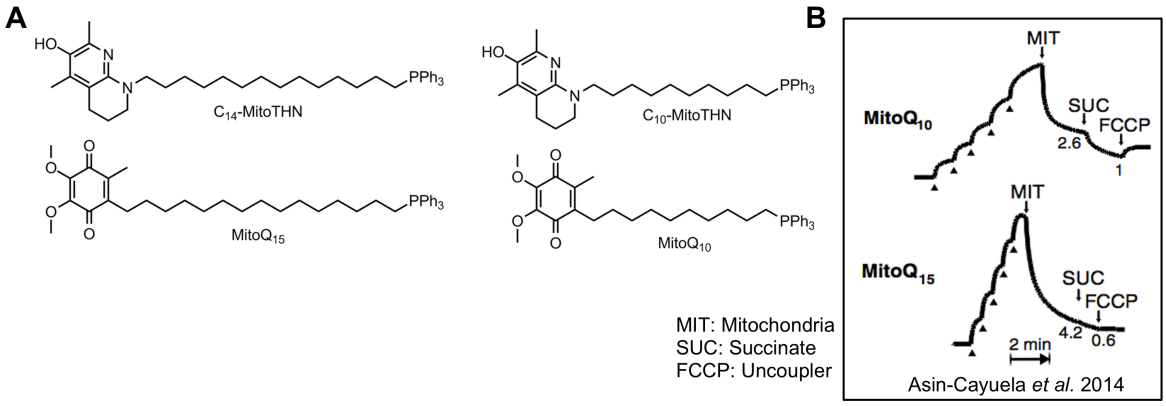

Figure 3.12 C_{10}- and C_{14}-MitoTHN are similar in physical size to $MitoQ_{10}$ and $MitoQ_{15}$, respectively (**A**). In isolated mitochondria, chain length affects the extent of incorporation. Approximately 50% (2.6 of 5 μM) of $MitoQ_{10}$ and 84% (4.2 of 5 μM) of $MitoQ_{15}$ incorporate in non-energized mitochondria, increasing to 72% and 96% respectively, upon establishment of a membrane potential with succinate (**B**). Image reproduced from Asin-Cayuela *et al.* 2014.[121]

conditions, since it has superior mitochondrial incorporation increasing from 84% to 96% when a membrane potential is established and further that it has been reported in only one other publication from the Hecht group[122] to date. As $MitoQ_{15}$ is very similar in size to C_{14}-MitoTHN, we can predict a similarly high incorporation of C_{14}-MitoTHN. Accepting that any conclusions on this comparison are purely speculative given that $MitoQ_{15}$ is not prevalent in the literature in any context beyond the two reports, this may suggest that alkyl phosphonium chain lengths that are too long and incorporate to a great extent in both energized and non-energized mitochondria may not be viable compounds for treatment of mitochondrial dysfunctions. Murphy's initial publication on $MitoQ_{15}$ evaluates the various chain lengths at preventing MDA accumulation in isolated mitochondria,[121] a technique that cannot corroborate the observed trend with the viability of the mitochondria, *i.e.* MDA accumulation may be low due because of mitochondrial dysfunction. The Hecht group employed a oxygen-sensitive fluorescent microplate assay (BD Oxygen Biosensor plate) to uncover an oxygen consumption trend consistent with the Murphy group report; again however, cell viability was not corroborated and dose-dependent toxicity cannot be ruled out for the trends observed in either publication.

This builds to a final point related to the known accumulation trends of the $MitoQ_{5\text{-}15}$ variants that may be inferred from where the fraction of dosed compound that is not accumulated in the mitochondria is expected to reside. For example, if 50% of a medium chain phosphonium salt (*e.g.* $MitoQ_{10}$ or C_{10}-MitoTHN) is extramitochondrial, then we may expect this fraction to be effective at preventing lipid peroxidation in any other cell membrane, much like the non-targeted THNs[96] or decyl-Q.[90] This is consistent with the comparable efficacy of C_8- or C_{10}-MitoTHN (42 and 21 nM, respectively) to the

non-targeted C_{12}- and C_{15}-THN (13 and 50 nM, respectively).[96] Thus, the mitochondrial-targeted antioxidants may rescue cells from ferroptosis simply by virtue of their extra-mitochondrial lipid RTA activity, and not by a manner related to the mitochondria at all. Relating this back to one of our original goals of determining mitochondrial contribution of ferroptosis, we may not be able to confirm or rule out mitochondrial peroxidation from the results herein or the work of Angeli *et al.* that employed MitoQ.

3.2.8 MitoTHNs significantly inhibit DEM-induced lipid peroxidation

More information was gleaned when the MitoTHNs were assayed in a model of oxidative stress involving depletion of glutathione by diethyl maleate (DEM) treatment, which rapidly conjugates with the free thiol of glutathione. It is regarded as a harsh method

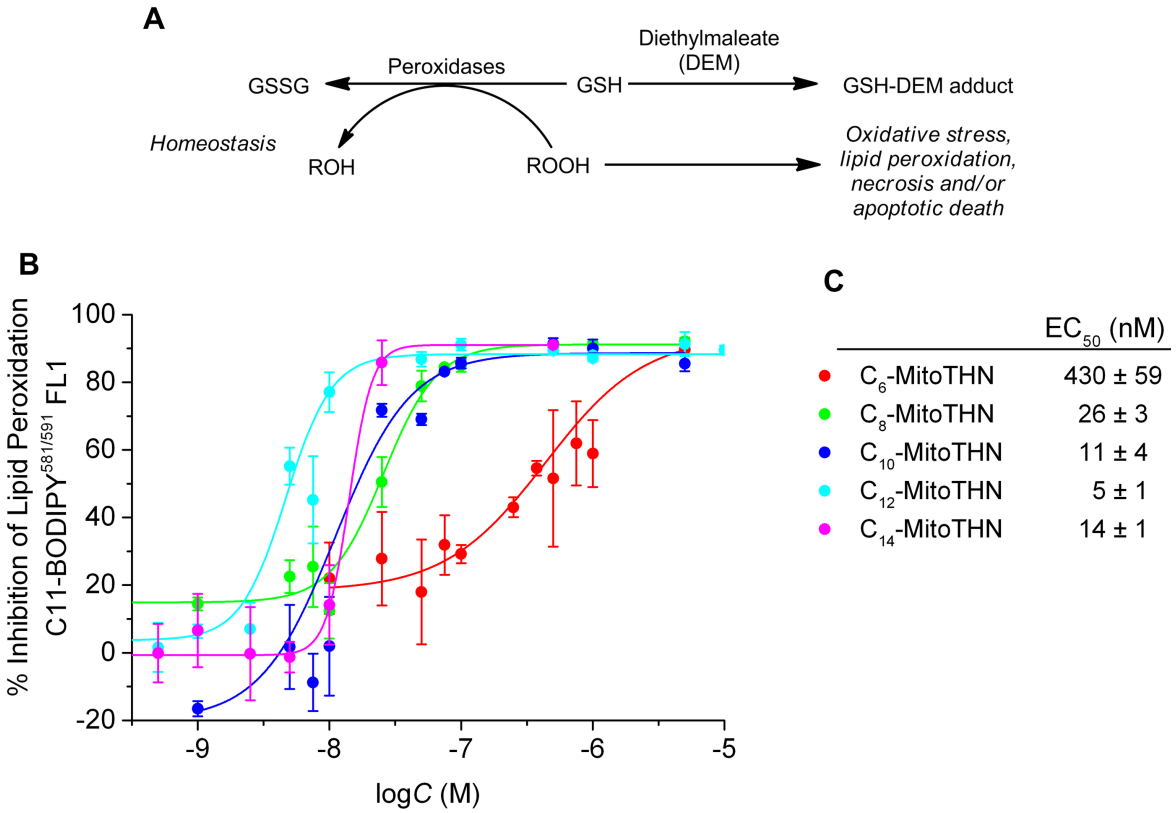

Figure 3.13 MTHNs are highly effective inhibitors of lipid peroxidation initiated by 2 hours of 9 mM DEM treatment in HEK293 cells measured by C11-BODIPY.

of GSH depletion (compared to erastin, for example) since protein thiols are likely modified as well. However, the onset of oxidative stress is very rapid, ~1 hour for significant lipid peroxidation by measurement of C11-BODIPY fluorescence, and is followed by necrotic and/or apoptotic cell death. The MitoTHNs were remarkably effective at prevent lipid peroxidation with low nM potency, however the data is not corroborated by cell viability. Thus while lipid peroxidation may by inhibited, the cell populations may be apoptotic or necrotic. The data also suggest the MitoTHNs of at least 8-carbons are highly effective at preventing lipid peroxidation, and that the reduced efficacy of C_{12}- and C_{14}-MitoTHN with RSL3 treatment is likely not caused by experimental factors such as: significant binding to serum albumins present in the cell culture medium, which is precedented to lower the available concentration of long chain alkyl phosphonium salts (*e.g.* $MitoQ_{10}$)[123] in media.

Future work will corroborate and build on these results by assaying MitoTHN efficacy in other models of oxidative stress, including GSH depletion by erastin treatment, *Gpx4*-inducible knockout cells and buthionine sulfoxamine treatment.

3.2.9 Long chain MTHNs bind to human α-tocopherol transport protein

The binding affinities of the MitoTHNs to hTTP were evaluated by a competitive displacement assay using NDB-Toc (**Figure 3.14A**).[124] NBD-Toc features a NBD-fluorophore at the terminal position of the phytyl sidechain of α-TOH. Fluorescence of NBD is quenched in the unbound state by the chromanol moiety that functions as a FRET partner with NBD. In the protein-bound state, the chromanol moiety is sequestered in the binding pocket and thus NBD-Toc fluorescence is restored. This approach was previously used to assay the THNs.[100]

The titration of NBD-Toc/hTTP with test compounds produced the binding curves shown in **Figure 3.14B**, which enable derivations of the effective dissociation constant, $K_{d,eff}$, to be measured from fitting data to a one-site bimolecular association model.[100] In these experiments, α-TOH binds to hTTP with $K_{d,eff}$ = (0.22 ± 0.05) μM.[a] The results demonstrate a sidechain dependence of binding, where the short C_6-MitoTHN had $K_{d,eff}$ = (15 ± 6) μM, with binding efficacy increasing to (0.56 ± 0.06) μM for C_{14}-MitoTHN,

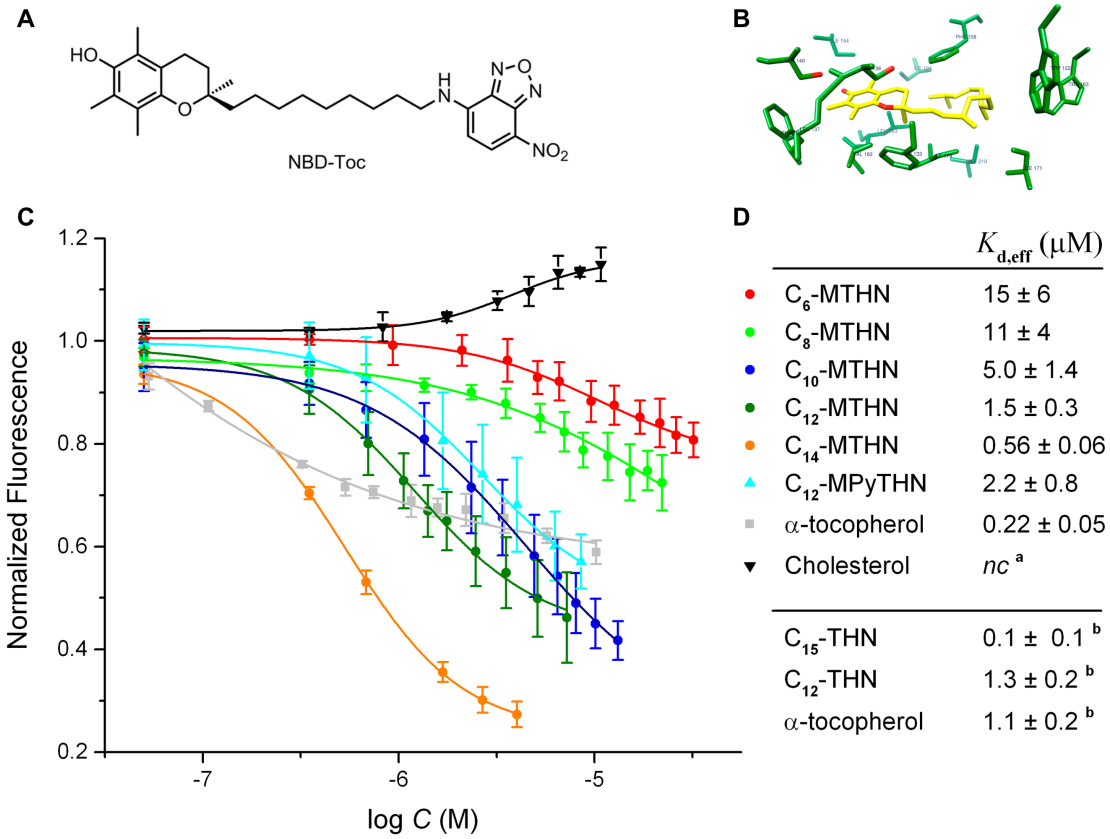

Figure 3.14 The fluorescent α-TOH analogue NBD-Toc (**A**) binds to the active side of hTTP (crystal structure with native ligand α-TOH shown)[125] (**B**) and is titrated with test molecules to produce titration curves (**C**) allowing determination of the effective dissociation constant, $K_{d,eff}$ (**D**), for binding to hTTP (1 μM NBD-Toc and 0.5 μM hTTP in SET buffer).
[a] Non-competitive with NBD-Toc. [b] Values from reference 100.

[a] The variance between $K_{d,eff}$ of α-TOH obtained here and in reference 100 is attributed to the assay conditions and $K_{d,eff}$ should be compared relative to α-TOH within each experiment.

which is about two-fold *less* effective than α-TOH (**Figure 3.14C**). In comparison, C_{15}-THN has about ten-fold *greater* binding efficacy relative to α-TOH,[100] which has been attributed to a strong H-bond between the tertiary amine of the THN and Ser-136 of hTTP,[126] and mirroring the farnesyl sidechain of α-TOH. The difference between MitoTHN and THN binding affinities can presumably be attributed to the large triphenylphosphonium moiety, which must be solvent exposed when bound.

A protein binding affinity similar to α-TOH is desirable such that it can be competitive with the native ligand, while not so strong as to preclude the efficient dissociation that allows trafficking into a bilayer. Thus, the long-chain MitoTHNs hold the same promise as lipophilic THNs for the transport and concomitant protection by hTTP from rapid metabolism. We next sought to evaluate if the promising results of THN affinity to hTTP would be born out *in vivo* by determining biodistribution of both the THNs and MitoTHNs in mice.

3.2.10 THNs and MitoTHNs are broadly bioavailable among tissues

A biodistribution assay was designed wherein two species of mice were

Table 3.3 Comparison of tissue bioavailability of α-TOH (in rats)[127] and THNs (in mice).

	αTOH[127] **24h**	C_{15}-THN **2 h**		C_{15}-THN **24 h**		C_{14}-MTHN **2 h**		C_{14}-MTHN **24 h**	
Tissue	nmol/g or mL	nmol/ g or mL	% of α-TOH 24 h	nmol/ g or mL	% of α-TOH 24 h	nmol/ g or mL	% of α-TOH 24 h	nmol/ g or mL	% of α-TOH 24 h
Liver	110	17±8.5	**15**	0.32±0.09	**0.3**	19±5.3	**17**	0.82±0.87	**0.7**
Lung	50	0.45±0.61	**0.9**	0.16±0.19	**0.3**	5.1±3.5	**10**	0.26±0.13	**0.5**
Heart	15	0.10±0.08	**0.7**	0.11±0.13	**0.7**	15±10	**100**	0.70±0.69	**4.6**
Spleen	95	0.17±0.09	**0.2**	0.06±0.03	**0.06**	4.6±3.3	**4.8**	2.3±1.1	**2.4**
Whole Blood	45[†]	0.56±0.28	**1.2**	0.011± 0.012	**0.02**	1.7±1.1	**3.7**	0.25±0.06	**0.6**

administered a single dose of THN or MitoTHN by gavage. The mice were sacrificed, dissected and the compounds quantified by LC-MS/MS (**Figure 3.15** and **Figure 3.16**).

In general, the THNs have between 0.2-5.0% of the bioavailability of α-TOH[127] after 24 h (**Table 3.3**), though the comparison is rough since the species of mice and rat may not express or require equivalent levels of tocopherol transport protein. Nevertheless, the relatively low values relative to α-TOH could be explained by the contribution of a number of factors. The extraction protocol of α-TOH (Burton *et al.*) had been well established[128] and employs mechanical wet tissue homogenization followed by an extraction with SDS detergent and heptane. In comparison, the THN extraction protocol employed herein involved flash freezing and grinding tissue in liquid nitrogen followed by probe sonication in MeOH/$CHCl_3$. The employment of a detergent in the former method combined with mechanical homogenization can be predicted to disrupt cellular bilayers more efficiently than grinding frozen tissue followed by relatively gentle probe sonication in the latter method.

The oxidizability of the THNs relative to α-TOH can be predicted to reduce stability under ambient conditions, such as during the extraction procedure, leading to degradation of the analyte. The samples were treated with formic acid during concentration of $CHCl_3$ to ensure minimal oxidation after this step. The effectiveness of the THNs in cellular models with 24-hour incubation periods is notably much lower than with shorter (1-4 hr) incubations, suggesting degradation may occur *in vivo* as well and contribute to the reduced bioavailability.

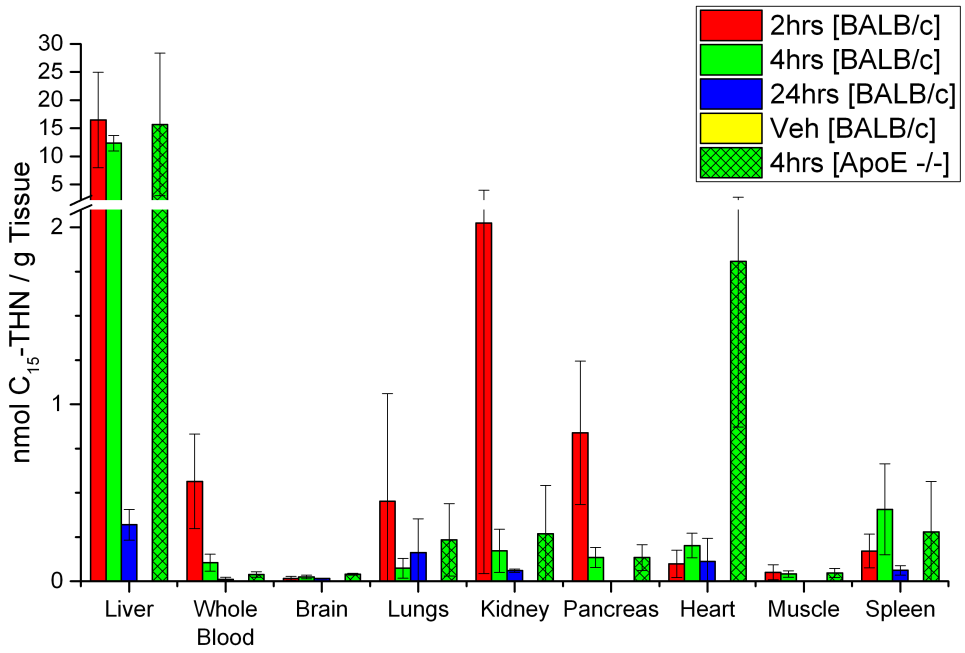

Figure 3.15 Biodistribution of C_{15}-THN in BALB/c and ApoE$^{-/-}$ mice after 2, 4 and 24 h of a single 2 mg dose by gavage.

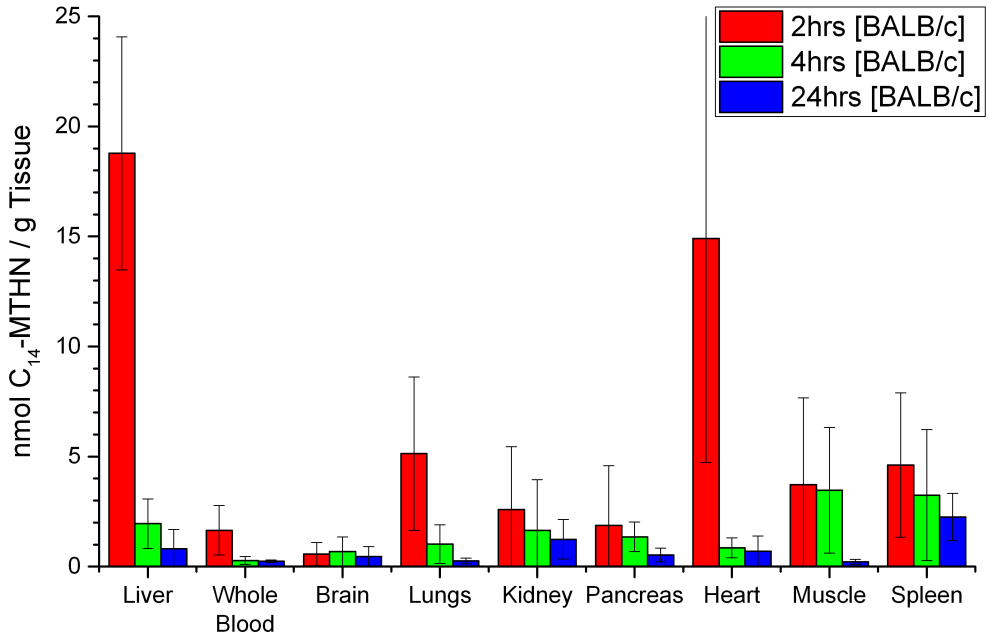

Figure 3.16 Biodistribution of C_{14}-MitoTHN in BALB/c mice after 2, 4 and 24 h of a single 2 mg dose by gavage.

Another notable difference in the experiment of Burton *et al.* was the use of protected α-TOH in a ratio of 1.376:1 α-tocopherol acetate:free phenol. The ester modification is generally thought to increase the bioavailability of α-TOH *in vivo*, however previous work has demonstrated that any effect is largely dosage medium dependent: there is no difference in bioavailability observed between acetate and phenol when administered in solid chow; the acetate is slightly favoured when administered in an oily medium.[127] It was hypothesized that ester hydrolysis is fast in the small intestine relative to oxidation of the free phenols. This effect may have contributed to the THN bioavailability given that it was administered in sunflower oil as the free phenol. Administering the acetate form may be a worthwhile modification in future experiments given the greater reactivity of THNs relative to α-TOH. Nevertheless, the trends suggest that THNs are indeed trafficked through animals in a manner similar to α-TOH.

Given that the THNs are effective at subverting oxidative stress in ferroptosis models in the tens of nanomolar range, the concentrations in the tissues above can be predicted to be well within the effective range of the antioxidant,[a] though the cell density is notably much greater in tissues relative to *ex vivo* assays. Whether this translates to an effective therapy in animal and other cellular disease models, however, remains to be determined.

[a] The concentration ranges of THNs quantified in the biodistribution assay are in nmol/**g,** which should be considered as ~ 1000 fold higher when comparing to efficacy in cellular (*e.g.* ferroptosis inhibition) assays, where lipophilic RTAs are effective in the low nmol/**L** range.

3.3 Future work

While unambiguous evidence for the efficacy of the MitoTHNs in preventing mitochondrial lipid peroxidation currently eludes us, we have learned from viability assays that TPP salts may not be the ideal targeting moiety to traffic the RTAs. Their ability to decouple the ETC and chaotropic effects suggest that alternative strategies may allow their efficacy to be evaluated rather than relying solely on electrophoretic accumulation of TPP if the goal of targeting mitochondria is to preserve their function. These could include a targeting peptide sequence like the SS series or exploiting a native transporter such as carnitine acetyl transferase by forming the carnitine ester of a THN. Both of these methods may enrich the mitochondria without the effects of the TPP moiety. The use of TPP for cancer chemotherapeutics is less problematic since preventing cellular proliferation is ultimately desired. Future work will also investigate MitoVitE and MitoQ in comparison to the MitoTHNs, especially in light of the cytotoxic behaviour we and others have observed and the known ability of MitoVitE and MitoQ to selectively kill cancer cells.

The results of the biodistribution assay suggest that THNs are broadly bioavailable, though experimental limiting factors may have prevented accurate quantification given that the THNs were detected at ~1% that of α-TOH as reported in the literature. C_{15}-THN was not detected to great extent in the brain, one of the organs of particular significance in Parkinson's and Alzheimer's disease. While this result may be genuine, the THNs are much more reactive to ambient conditions than α-TOH and this may represent an experimental limitation for quantification by this method. An alternative strategy we envision for demonstrating THN bioavailability involves radiolabelling with ^{124}I, which allows imaging in real time over several days (^{124}I $t_{½}$ = 4.2 d) via PET imaging. One could

envision the terminal position of a THN being radiolabelled by an expedient Finkelstein reaction with a $M^{124}I$ salt.

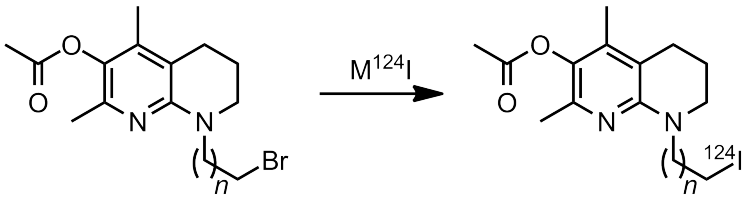

The dysfunctional phenotype of mitochondria is well documented in many degenerative pathologies discussed previously including cancer, diabetes, and neurodegeneration. Researchers in these fields often consider whether genetic mutations cause tumorogenesis (such as in RAS or P53 tumor suppressor) or neurodegeneration, or if these mutations are secondary to mitochondrial dysfunction.[129,130] The latter case is supported by the work of Otto Warburg, who originally found that cancer cell mitochondria were largely inactive. Instead, elevated lactate production indicated fermentation was their major metabolic pathway over respiration (The Warburg effect) and that this phenotype was a result of dysfunctional mitochondria. Later, researchers discovered the vast collection of somatic cell mutations, which shifted the opinion of many from cancer being metabolic in origin, as the Warburg effect implies, to one being a result of these nuclear mutations since the mutations veritably result in uncontrolled proliferation and metastasis. This likely contributes to why antioxidants have not been successful in many clinical trials (not limited to cancer), as antioxidants do not address the fundamental metabolic (*e.g.* epigenetic) changes that occur in dysfunctional mitochondria.[131] However, the outlook for targeting the mitochondria in this context cannot be overstated if the underlying pathology indeed emanates from mitochondrial origin rather than downstream effects. Given that RTAs do not reverse oxidative damage that has accumulated, fruitful

research efforts would benefit from being guided by the potential of antioxidants in preventative over palliative contexts.

3.4 Experimental

3.4.1 General

MeOTHN (**1**)[100] and MPQ[37] were synthesized by literature methods. Antimycin A (Sigma), doxorubicin (Sigma), Paraquat (Sigma), MitoView 633 (Biotium) and C11-BODIPY (Sigma) were obtained from commercial sources. Zinc was activated by treatment with 2% HCl, filtration, and the solid washed with water, ethanol, and diethyl ether followed by drying in a 100ºC oven overnight. Autoxidations were completed as described in section **2.4**, and ferroptosis inhibition assay was completed as described in section **2.10.4**. Binding studies of MTHNs to TTP were completed as described in reference 100.

3.4.2 MitoTHN syntheses

In a flame-dried 2-neck 100 mL RBF, NaH (60 wt%, 47 mg, 1.17 mmol, 1.5 eq) was triturated with hexanes and decanted. To the residue was added dry THF (8 mL) followed by **1** (150 mg, 0.78 mmol, 1 eq) and the appropriate dibromoalkane (4-8 eq). The flask was fitted with a condenser and purged with N_2, and the mixture heated to reflux for 18 h under nitrogen. The mixture was then cooled, quenched with *ca.* 1 mL MeOH and concentrated *in vacuo*. The residue was taken up with 15 mL diethyl ether and 15 mL water, and the aqueous layer extracted with 3 x 25 mL diethyl ether. The combined organic layers were dried over anhydrous $MgSO_4$, filtered and concentrated *in vacuo* to yield a colourless oil which was purified on silica gel prepared in 1:99 Et_3N:petroleum ether. The excess dibromoalkane is recovered by elution with petroleum ether (500 mL) followed by 1:9 Et_2O:petroleum ether (500 mL) to elute the alkylated THN as a colourless oil. The

product was used promptly in the subsequent reaction as it was observed to decompose when stored.

MeOTHNC6Br **2a** (76%). ^{1}H NMR (400 MHz, $CDCl_3$): δ 3.62 (s, 3H), 3.57-3.53 (m, 2H), 3.41 (t, *J* = 6.9 Hz, 2H), 3.28-3.23 (m, 2H), 2.58 (t, *J* = 6.5 Hz, 2H), 2.32 (s, 3H), 2.07 (s, 3H), 1.94-1.83 (m, 4H), 1.63-1.57 (m, 2H), 1.54-1.44 (m, 2H), 1.40-1.30 (m, 2H).[a]

MeOTHNC8Br **2b** (75%). ^{1}H NMR (600 MHz, $CDCl_3$) δ 3.62 (s, 3H), 3.56 – 3.51 (m, 2H), 3.40 (t, *J* = 6.9 Hz, 2H), 3.28 – 3.24 (m, 2H), 2.58 (t, *J* = 6.5 Hz, 2H), 2.32 (s, 3H), 2.07 (s, 3H), 1.95 – 1.89 (m, 2H), 1.88 – 1.81 (m, 2H), 1.58 – 1.52 (m, 2H), 1.46 – 1.39 (m, 2H), 1.37 – 1.27 (m, 6H). ^{13}C NMR (101 MHz, $CDCl_3$) δ: 151.82, 145.71, 144.34, 137.80, 113.46, 60.59, 48.63, 47.55, 34.20, 33.00, 29.41, 28.88, 28.31, 27.16, 27.11, 24.99, 22.11, 19.28, 11.87. HRMS (ESI+/Q-TOF) *m*/*z*: [M+H] calcd for $C_{19}H_{32}BrN_2O$ 383.1698; observed 383.1725.

MeOTHNC10Br **2c** (48%). ^{1}H NMR (600 MHz, $CDCl_3$) δ 3.61 (s, 3H), 3.56 – 3.52 (m, 2H), 3.40 (t, *J* = 6.9 Hz, 2H), 3.28 – 3.24 (m, 2H), 2.58 (t, *J* = 6.5 Hz, 2H), 2.32 (s, 3H), 2.07 (s, 3H), 1.94 – 1.89 (m, 2H), 1.88 – 1.81 (m, 2H), 1.59 – 1.51 (m, 2H), 1.45 – 1.39 (m, 2H), 1.36 – 1.26 (m, 10H). ^{13}C NMR (151 MHz, $CDCl_3$) δ 151.80, 145.69, 144.30, 137.81, 113.45, 60.60, 48.61, 47.52, 34.24, 32.98, 29.40, 28.87, 28.30, 27.13, 27.09, 24.98, 22.08, 19.28, 11.87. HRMS (ESI+/Q-TOF) *m*/*z*: [M+H] calcd for $C_{21}H_{36}BrN_2O$ 411.2011; observed 411.2018.

To a solution of alkylated MeOTHN **2a-e** (0.5 mmol, 1 eq) in 2 mL 99% EtOH in a sealed tube was added triphenylphosphine (262 mg, 1 mmol, 2 eq). The tube was purged with nitrogen, sealed, and heated in a 90ºC oil bath in the dark for 24-48 h until starting

[a] Rapid decomposition of the C6 primary halide (specifically) prevented the acquisition of a ^{13}C spectrum and HRMS.

material was consumed as determined by TLC. The solution was allowed to cool, then concentrated *in vacuo* and purified by silica gel chromatography using 1:19-1:9 MeOH:CH_2Cl_2 to yield the triphenylphosphonium bromide **3a-e** as a colourless and hygroscopic foam.

MeOTHNC6PPh_3Br **3a** (86%). ^{1}H NMR (400 MHz, $CDCl_3$) δ 7.88-7.64 (m, 15H), 3.85-3.75 (m, 2H), 3.59 (s, 3H), 3.49-3.46 (m, 2H), 3.24-3.17 (m, 2H), 2.55 (t, *J* = 6.5 Hz, 2H), 2.23 (s, 3H), 2.05 (s, 3H), 1.90-1.84 (m, 2H), 1.72-1.57 (m, 4H), 1.53-1.43 (m, 2H), 1.35-1.25 (m, 2H). ^{13}C NMR (151 MHz, DMSO-d_6) δ 150.98, 144.35, 143.73, 137.34, 134.88 (d, *J* = 3.0 Hz), 133.57 (d, *J* = 10.0 Hz), 130.23 (d, *J* = 12.3 Hz), 118.58 (d, *J* = 85.7 Hz), 113.17, 60.03, 47.68, 46.86, 29.65 (d, *J* = 4.4 Hz), 26.12, 25.63, 24.14, 21.74 (d, *J* = 4.4 Hz), 21.38, 20.11 (d, *J* = 49.8 Hz), 19.02, 11.48. ^{31}P NMR (121 MHz, DMSO-d_6) δ 25.27. HRMS (ESI+/Q-TOF) *m*/*z*: [M^+] calcd for $C_{35}H_{42}N_2OP$ 537.3035; observed 537.3042.

MeOTHNC8PPh_3Br **3b** (89%). ^{1}H NMR (600 MHz, $CDCl_3$) δ 7.79 – 7.72 (m, 9H), 7.68 – 7.63 (m, 6H), 3.69 – 3.59 (m, 2H), 3.54 (s, 3H) 3.49 – 3.38 (m, 2H), 3.18 (t, *J* = 5.5 Hz, 2H), 2.51 (t, *J* = 6.5 Hz, 2H), 2.22 (s, 3H), 2.00 (s, 3H), 1.88 – 1.81 (m, 2H), 1.61 – 1.51 (m, 4H), 1.43 (p, *J* = 7.1 Hz, 2H), 1.25 – 1.13 (m, 6H). ^{13}C NMR (151 MHz, $CDCl_3$) δ 151.57, 145.27, 144.04, 137.65, 135.05 (d, *J* = 2.9 Hz), 133.59 (d, *J* = 9.9 Hz), 130.51 (d, *J* = 12.5 Hz), 118.24 (d, *J* = 85.9 Hz), 113.44, 60.45, 48.46, 47.39, 30.35 (d, *J* = 15.5 Hz), 29.08, 28.97, 26.90, 26.88 (d, *J* = 3.8 Hz), 24.76, 22.72 (d, *J* = 53.4 Hz), 22.58, 21.81, 19.07, 11.73. HRMS (ESI+/Q-TOF) *m*/*z*: [M^+] calcd for $C_{37}H_{46}N_2OP$ 565.3348; observed 565.3367.

MeOTHNC10PPh$_3$Br **3c** (82%). ^{1}H NMR (600 MHz, $CDCl_3$) δ 7.80 – 7.73 (m, 9H), 7.68 – 7.64 (m, 6H), 3.69 – 3.61 (m, 2H), 3.54 (s, 3H), 3.49 – 3.43 (m, 2H), 3.22 – 3.17 (m, 2H), 2.52 (t, *J* = 6.6 Hz, 2H), 2.24 (s, 3H), 2.01 (s, 3H), 1.85 (t, *J* = 5.9 Hz, 2H), 1.60 – 1.52 (m, 4H), 1.50 – 1.44 (m, 2H), 1.25 – 1.10 (m, 10H). ^{13}C NMR (151 MHz, $CDCl_3$) δ 151.62, 145.35, 144.05, 137.62, 135.05 (d, *J* = 3.1 Hz), 133.61 (d, *J* = 9.9 Hz), 130.51 (d, *J* = 12.5 Hz), 118.27 (d, *J* = 85.8 Hz), 113.38, 60.46, 48.50, 47.38, 30.39 (d, *J* = 15.5 Hz), 29.43, 29.35, 29.15, 29.11, 27.00 (d, *J* = 2.2 Hz), 24.79, 22.75 (d, *J* = 52.5 Hz), 22.60, 22.59, 21.84, 19.09, 11.74. ^{31}P NMR (121 MHz, DMSO-d_6) δ 25.27. HRMS (ESI+/Q-TOF) *m*/*z*: [M^+] calcd for $C_{39}H_{50}N_2OP$ 593.3661; observed 593.3630.

MeOTHNC12PPh$_3$Br **3d** (79%). ^{1}H NMR (600 MHz, $CDCl_3$) δ 7.88 – 7.80 (m, 6H), 7.80 – 7.75 (m, 3H), 7.73 – 7.66 (m, 6H), 3.59 (s, 3H), 3.53 – 3.49 (m, 2H), 3.24 (t, *J* = 5.5 Hz, 2H), 2.56 (t, *J* = 6.6 Hz, 2H), 2.29 (s, 3H), 2.05 (s, 3H), 1.93 – 1.87 (m, 2H), 1.61 – 1.56 (m, 4H), 1.54 – 1.48 (m, 2H), 1.30 – 1.13 (m, 16H). ^{13}C NMR (151 MHz, $CDCl_3$) δ 151.80, 145.58, 144.21, 137.74, 135.00 (d, *J* = 3.0 Hz), 133.83 (d, *J* = 10.0 Hz), 130.56 (d, *J* = 12.4 Hz), 118.63 (d, *J* = 85.6 Hz), 113.47, 60.58, 48.65, 47.48, 30.42 (d, *J* = 15.5 Hz), 29.70, 29.67, 29.65, 29.61, 29.37, 29.29, 27.20 (d, *J* = 8.7 Hz), 24.95, 22.57 (d, *J* = 4.5 Hz), 22.03, 19.24, 11.84. ^{31}P NMR (121 MHz, DMSO-d_6) δ 25.27. HRMS (ESI+/Q-TOF) *m*/*z*: [M^+] calcd for $C_{41}H_{54}N_2OP$ 621.3974; observed 621.3981.

To a solution of MeOTHN-PPh$_3$Br **3a-e** (0.4 mmol, 1 eq) in 8 mL dry CH_2Cl_2 was added BBr_3•Me_2S (500 mg, 1.6 mmol, 4 eq). The flask was purged with nitrogen and stirred for 18 h at reflux. The reaction mixture was then cooled in an ice bath and transferred to a separatory funnel with 5 mL of cold saturated sodium bicarbonate and 5 mL water. The funnel was shaken until gas evolution ceased and then the aqueous layer

was extracted with 3 x 10 mL CH_2Cl_2. The combined organic layers were dried over anhydrous $MgSO_4$ and filtered. To the filtrate was added 250 mL methanol and oxalic acid (50 mg, 0.4 mmol, 1 eq) and heated at 50ºC on a rotovap under sufficient reduced pressure to slowly remove methanol over *ca.* 2 h. The residue was dissolved in 5 mL CH_2Cl_2 and diethyl ether was added until saturated. This solution was subsequently added dropwise to excess diethyl ether and the resultant precipitate was isolated either by filtration (C_6- and C_8-MitoTHNs) or by centrifugation in Pyrex tubes (C_{10}-, C_{12}-, and C_{14}-MitoTHN) followed by decanting. The precipitation procedure was repeated once and the solid was dried *in vacuo*. If required, the protonated material can be purified by silica gel chromatography using 1:9 MeOH:CH_2Cl_2 followed by precipitation from diethyl ether as above.[a]

C6MTHN **4a** (96%). ^{1}H NMR (600 MHz, DMSO-d_6) δ 7.92-7.71 (m, 16H*), 3.57-3.49 (m, 2H), 3.25-3.14 (m, 2H), 2.56 (t, J = 6.2 Hz, 2H), 2.21 (s, 3H), 2.03 (s, 3H), 1.86-1.77 (m, 2H), 1.54-1.24 (m, 8H). ^{13}C NMR (151 MHz, DMSO-d_6) δ: 161.38, 139.91, 134.98 (d, J = 3.0 Hz), 133.62 (d, J = 10.0 Hz), 130.31 (d, J = 12.4 Hz), 122.46, 118.62 (d, J = 85.7 Hz), 48.43, 47.52, 40.06, 29.78, 29.67, 25.93, 25.60, 24.09, 21.78 (d, J = 4.3 Hz), 21.12, 20.21 (d, J = 49.7 Hz), 12.37. * +D_2O, 15H. HRMS (ESI+/Q-TOF) m/z: [M^+] calcd for $C_{34}H_{40}N_2OP$ 523.2878; observed 523.2874.

C8MTHN **4b** (93%). ^{1}H NMR (600 MHz, DMSO-d_6) δ 7.91 – 7.73 (m, 16H*), 3.58 – 3.48 (m, 2H), 3.34 – 3.29 (m, 2H), 2.60 (t, J = 6.4 Hz, 2H), 2.32 (s, 3H), 2.10 (s, 3H), 1.86 – 1.81 (m, 2H), 1.56 – 1.41 (m, 6H), 1.30 – 1.18 (m, 6H). ^{13}C NMR (151 MHz, DMSO-d_6) δ 161.40, 140.24, 135.37 (d, J = 3.0 Hz), 134.02 (d, J = 10.1 Hz), 130.71 (d, J

[a]We attribute the increased integration of the ^{1}H triphenylphosphonium peaks in some of the final THNs to slight radical cation formation supressing the heteroaryl methyl ^{1}H resonances relative to aromatic C-H peaks. ^{31}P NMR confirmed a single phosphorous species in all cases.

= 12.3 Hz), 122.84, 119.01 (d, *J* = 85.6 Hz), 49.41, 48.36, 30.34 (d, *J* = 16.6 Hz), 29.09, 28.63, 26.49 (d, *J* = 21.7 Hz), 24.23, 22.23 (d, *J* = 4.4 Hz), 20.80 (d, *J* = 8.0 Hz), 20.44, 13.28. * +D_2O, 15H. HRMS (ESI+/Q-TOF) *m*/*z*: [M^+] calcd for $C_{36}H_{44}N_2OP$ 523.2878; observed 523.2874.

C10MTHN **4c** (81%). ^{1}H NMR (600 MHz, DMSO-d_6) δ 7.91 – 7.74 (m, 16H*), 3.58 – 3.51 (m, 2H), 3.46 (t, *J* = 7.2 Hz, 2H), 3.23 (t, *J* = 5.4 Hz, 2H), 2.56 (t, *J* = 6.3 Hz, 2H), 2.24 (s, 3H), 2.03 (s, 3H), 1.84 – 1.78 (m, 2H), 1.54 – 1.39 (m, 6H), 1.29 – 1.13 (m, 10H). ^{13}C NMR (151 MHz, DMSO-d_6) δ 162.17, 147.71, 140.25, 135.36 (d, *J* = 3.0 Hz), 134.01 (d, *J* = 10.2 Hz), 130.70 (d, *J* = 12.5 Hz), 122.86, 119.01 (d, *J* = 85.7 Hz), 115.95, 49.07, 48.02, 40.28, 30.34, 30.23, 29.32, 29.26, 29.17, 28.58, 26.75, 26.54, 24.41, 22.19 (d, *J* = 4.5 Hz), 21.28, 20.58 (d, *J* = 49.8 Hz), 17.41, 15.63, 12.94. * +D_2O, 15H. HRMS (ESI+/Q-TOF) *m*/*z*: [M^+] calcd for $C_{38}H_{48}N_2OP$ 579.3504; observed 579.3539.

C12MTHN **4d** (92%). ^{1}H NMR (600 MHz, DMSO-d_6) δ 7.92 – 7.75 (m, 16H*), 3.57 – 3.52 (m, 4H), 3.38 – 3.32 (m, 2H), 2.63 (t, *J* = 6.4 Hz, 2H), 2.36 (s, 3H), 2.13 (s, 3H), 1.90 – 1.81 (m, 2H), 1.54 – 1.41 (m, 6H), 1.28 – 1.17 (m, 14H). ^{13}C NMR (151 MHz, DMSO-d_6) δ 162.46, 147.63, 139.99, 137.80, 136.93, 136.38, 134.88 (d, *J* = 3.0 Hz), 133.59 (d, *J* = 10.2 Hz), 130.23 (d, *J* = 12.4 Hz), 118.60 (d, *J* = 85.6 Hz), 114.91, 48.53, 47.43, 29.82 (d, *J* = 16.7 Hz), 29.01, 28.97, 28.88 (d, *J* = 5.9 Hz), 28.77, 28.74, 28.13, 26.34, 26.14, 24.05, 21.76, 21.73, 21.05, 20.15 (d, *J* = 49.8 Hz), 17.54, 12.37. * +D_2O, 15H. HRMS (ESI+/Q-TOF) *m*/*z*: [M^+] calcd for $C_{40}H_{52}N_2OP$ 607.3817; observed 607.3843.

C14MTHN **4e** (83%). ^{1}H NMR (600 MHz, DMSO-d_6) δ 7.93 – 7.88 (m, 4H), 7.84 – 7.75 (m, 12H*), 3.62 – 3.56 (m, 2H), 3.51 (t, *J* = 7.4 Hz, 2H), 3.27 (t, *J* = 5.5 Hz, 2H),

2.58 (t, J = 6.5 Hz, 2H), 2.29 (s, 3H), 2.06 (s, 3H), 1.87 – 1.80 (m, 2H), 1.55 – 1.40 (m, 6H), 1.32 – 1.12 (m, 20H). ^{13}C NMR (151 MHz, DMSO-d_6) δ 162.10, 152.34, 147.40, 139.97, 134.87 (d, J = 3.0 Hz), 133.59 (d, J = 10.1 Hz), 130.22 (d, J = 12.4 Hz), 125.42, 118.59 (d, J = 85.6 Hz), 115.21, 48.63, 47.51, 29.82 (d, J = 16.6 Hz), 29.04, 29.01, 28.90, 28.86, 28.79, 28.73, 28.13, 26.30, 26.10, 24.01, 21.74 (d, J = 4.4 Hz), 20.93, 20.15 (d, J = 49.8 Hz), 17.25, 12.46. * +D_2O, 11H. HRMS (ESI+/Q-TOF) m/z: [M^+] calcd for $C_{42}H_{56}N_2OP$ 635.4130; observed 635.4144.

3.4.3 MitoSTY-BODIPY synthesis

Methyl-3-bromobenzoate. A 1 L RBF was charged with 3-bromobenzoic acid (20 g, 99.5 mmol, 1 eq.) followed by methanol (300 mL) and sulfuric acid (6 mL). The flask was fitted with a condenser and heated to reflux with vigorous stirring overnight. The mixture was cooled, quenched with saturated aqueous $NaHCO_3$ and concentrated *in vacuo*. The residue was taken up in water (200 mL) and extracted with 3 × 100 mL ethyl acetate. The combined organic layers were washed with brine, dried over $MgSO_4$, filtered and concentrated *in vacuo* to yield methyl-3-bromobenzoate as a pale, fragrant oil (21.3 g, quant.).

^{1}H NMR (300 MHz, $CDCl_3$) δ: 8.20 (dd, J = 1.8, 1.6 Hz, 1H), 7.98 (ddd, J = 7.8, 1.6, 1.1 Hz, 1H), 7.70 (ddd, J = 8.0, 2.0, 1.1 Hz, 1H), 7.34 (dd, J = 7.9 Hz, 1H), 3.94 (s, 3H). Spectra matched those reported in the literature.[132]

Methyl 3-(4-hydroxybut-1-yn-1-yl)benzoate. Methyl-3-bromobenzoate (9.00 g, 41.8 mmol, 1 eq) was charged in a flame dried sealed tube followed by but-3-yn-1-ol (4.4 g, 62.8 mmol, 1.5 eq) and Et_3N (80 mL). The solution was sparged with N_2 for 10 min followed by addition of $Pd(PPh_3)_4$ (0.483 g, 0.42 mmol, 0.01 eq) and finely ground CuI

(0.8 g, 4.2 mmol, 0.1 eq). The vessel was sealed and heated with vigorous stirring in a 70°C oil bath overnight, cooled, filtered over celite and the filter cake rinsed with ethyl acetate. The filtrate was concentrated and the residue was extracted from 100 mL water with 3 × 100 mL ethyl acetate. The combined organic layers were washed with water, brine, dried over $MgSO_4$, concentrated, dry loaded onto a minimum of silica, and purified by flash chromatography using a gradient of 1:9 to 3:1 EtOAc:hexanes to yield methyl 3-(4-hydroxybut-1-yn-1-yl)benzoate (8.12 g, 95%) as a pale oil.

^{1}H NMR (300 MHz, $CDCl_3$) δ: 8.09 (t, *J* = 1.6 Hz, 1H), 7.96 (dt, *J* = 7.9, 1.4 Hz, 1H), 7.58 (dt, *J* = 7.7, 1.4 Hz, 1H), 7.37 (t, *J* = 7.8, 1H), 3.92 (s, 3H), 3.83 (t, *J* = 6.3 Hz, 2H), 2.70 (t, *J* = 6.3 Hz, 2H). Spectra matched those reported in the literature.[133]

Methyl 3-(4-hydroxybutyl)benzoate. A Parr reactor was charged with methyl 3-(4-hydroxybut-1-yn-1-yl)benzoate (3.00 g, 14.7 mmol, 1 eq) and ethanol (10 mL). The solution was purged with N_2 for 5 min, Pd/C (150 mg, 5 wt%) was added and the vessel sealed. H_2 was introduced at *ca.* 1000 psi and the reaction stirred at ambient temperature overnight. The mixture was filtered over celite and concentrated to yield methyl 3-(4-hydroxybutyl)benzoate (3.04 g, quant.) of sufficient purity.

^{1}H NMR (300 MHz, $CDCl_3$) δ 7.86 – 7.78 (m, 2H), 7.38 – 7.27 (m, 2H), 3.88 (s, 3H), 3.63 (t, *J* = 6.3 Hz, 2H), 2.66 (t, *J* = 7.5 Hz, 2H), 1.81 – 1.49 (m, 5H). Spectra matched those reported in the literature.[133]

4-(3-(hydroxymethyl)phenyl)butan-1-ol. A 100 mL RBF was charged lithium aluminum hydride (0.91 g, 24 mmol, 2 eq) followed by dry THF (30 mL) and cooled in an ice bath under N_2. A solution of 3-(4-hydroxybutyl)benzoate (2.5 g, 12 mmol, 1 eq) in 10 mL dry THF was added dropwise to the suspension over 30 minutes, and allowed to stir at

ambient temperature overnight. The Feiser workup procedure was used to obtain 4-(3-(hydroxymethyl)phenyl)butan-1-ol (2.0 g, 92%) as colourless oil.

^{1}H NMR (300 MHz, $CDCl_3$) δ: 7.31 – 7.23 (m, 1H), 7.20 – 7.14 (m, 2H), 7.13 – 7.07 (m, 1H), 4.64 (s, 2H), 3.63 (t, *J* = 6.4 Hz, 2H), 2.63 (t, *J* = 7.4 Hz, 2H), 1.72 (br s, 2H), 1.73 – 1.52 (m, 4H). ^{13}C NMR (151 MHz, $CDCl_3$) δ 142.62, 137.67, 128.92, 128.74, 128.63, 126.33, 46.48, 45.00, 35.09, 32.21, 28.60. HRMS (EI) *m*/*z*: [M-H_2O] calcd for $C_{11}H_{14}O$ 162.1045; observed 162.1058.

1-(4-chlorobutyl)-3-(chloromethyl)benzene. A dry 100 mL RBF was charged with 4-(3-(hydroxymethyl)phenyl)butan-1-ol (1.5 g, 13.9 mmol, 1 eq) and dry dichloromethane (20 mL) followed by pyridine (0.56 mL, 6.9 mmol 0.5 eq) and the solution cooled in an ice bath. $SOCl_2$ (3.02 mL, 41.6 mmol, 3 eq) was slowly added to the cooled solution, and the mixture allowed to warm to ambient temperature, then heated to reflux for 2 hours. The mixture was cooled, quenched with saturated aqueous sodium bicarbonate and washed with 2 × 25 mL water. The organic layer was dried over $MgSO_4$ and eluted over a short plug of silica with diethyl ether and concentrated to yield 1-(4-chlorobutyl)-3-(chloromethyl)benzene (2.55 g, 85%) as a pale yellow oil.

^{1}H NMR (300 MHz, $CDCl_3$) δ: 7.33 – 7.26 (m, 1H), 7.25 – 7.20 (m, 2H), 7.15 (dt, *J* = 7.3, 1.7 Hz, 1H), 4.58 (s, 2H), 3.56 (t, *J* = 6.3 Hz, 2H), 2.66 (t, *J* = 7.1 Hz, 2H), 1.81 (m, 4H). ^{13}C NMR (151 MHz, $CDCl_3$) δ 142.87, 141.02, 128.70, 127.92, 127.22, 124.61, 65.60, 62.96, 35.72, 32.47, 27.68. HRMS (EI) *m*/*z*: [M+] calcd for $C_{11}H_{14}Cl_2$ 216.0473; observed 216.0474.

3-(4-chlorobutyl)benzyl)triphenylphosphophonium chloride. A flame dried sealed tube was charged with 1-(4-chlorobutyl)-3-(chloromethyl)benzene (1.5 g, 6.91 mmol, 1

eq), triphenylphosphine (1.81 g, 6.91 mmol, 1 eq) and dry acetonitrile (30 mL) and the solution purged with N_2 for 5 min. The tube was sealed and heated in the dark in an 85°C oil bath overnight. The solution was cooled, concentrated and the residue taken up in a minimum of dichloromethane. The solution was added dropwise to an excess of cold diethyl ether. A white precipitate was collected by filtration to yield 3-(4-chlorobutyl)benzyl)triphenylphosphophonium chloride (2.92 g, 88%) of sufficient purity.

^{1}H NMR (300 MHz, $CDCl_3$) δ: 7.81 – 7.72 (m, 9H), 7.69 – 7.59 (m, 6H), 7.09 – 7.00 (m, 2H), 6.97 – 6.90 (m, 1H), 6.90 – 6.85 (m, 1H), 5.48 (d, J = 14.4 Hz, 2H), 3.47 (t, J = 6.4 Hz, 2H), 2.42 (t, J = 7.5 Hz, 2H), 1.70 – 1.42 (m, 4H). ^{13}C NMR (151 MHz, $CDCl_3$) δ 142.50 (d, J = 3.5 Hz), 134.79 (d, J = 3.1 Hz), 134.40 (d, J = 9.8 Hz), 131.57 (d, J = 5.6 Hz), 130.05 (d, J = 12.5 Hz), 129.08 (d, J = 5.6 Hz), 128.78 (d, J = 3.5 Hz), 128.43 (d, J = 3.9 Hz), 127.31 (d, J = 8.8 Hz), 118.15 (d, J = 85.5 Hz), 44.92, 34.65, 31.84, 30.75 (d, J = 46.2 Hz), 28.34. HRMS (ESI+/Q-TOF) m/z: [M^+] calcd for $C_{29}H_{29}ClP$ 443.1695; observed 443.1708.

(*E*)-2-(3-(4-chlorobutyl)styryl)-1H-pyrrole **5**. A 100 mL RBF was charged with 3-(4-chlorobutyl)benzyl)triphenylphosphophonium chloride (2.5 g, 5.21 mmol, 1 eq), 1H-pyrrole-2-carbaldehyde (1.29 g, 5.21 mmol, 1 eq) and activated zinc (0.34 g, 5.21 mmol, 1 eq). The solids were slowly stirred under N_2 in a 100°C oil bath overnight. The thick, homogenous slurry was cooled until it could be diluted in dichloromethane (*ca.* 100 mL) and the mixture was filtered over celite. The filtrate was washed with 2 × 100 mL H_2O, dried over $MgSO_4$, filtered, concentrated and dry loaded onto a minimum of silica and purified by flash chromatography with a gradient of 1:9 to 1:1 dichloromethane:petroleum ether to yield **5** (200 mg, 15%) as a colourless solid.

^{1}H NMR (300 MHz, DMSO-d_6) δ: 11.13 (br s, 1H), 7.29 – 7.26 (m, 1H), 7.26 – 7.22 (m, 1H), 7.09 – 6.97 (m, 2H), 6.89 – 6.75 (m, 2H), 6.31 – 6.19 (m, 1H), 6.06 (dt, J = 3.4, 2.4 Hz, 1H), 3.67 (t, J = 6.2 Hz, 2H), 2.61 (t, J = 7.1 Hz, 2H), 1.80 – 1.63 (m, 4H). ^{13}C NMR (151 MHz, DMSO-d_6) δ 142.77, 138.13, 130.87, 129.30, 127.28, 125.96, 123.69, 122.84, 120.29, 120.04, 109.68, 109.60, 45.87, 34.75, 32.07, 28.64. HRMS (EI) *m*/*z*: [M+] calcd for $C_{16}H_{18}ClN$ 259.1128; observed 259.1119.

(*E*)-7-(3-(4-chlorobutyl)styryl)-5,5-difluoro-1,3-dimethyl-5H-dipyrrolo[1,2-c:2',1'-f][1,3,2]diazaborinin-4-ium-5-uide **6**. A flame dried 100 mL RBF was charged with (*E*)-2-(3-(4-chlorobutyl)styryl)-1H-pyrrole (180 mg, 0.69 mmol, 1 eq), 3,5-dimethyl-1H-pyrrole-2-carbaldehyde (85 mg, 0.69 mmol, 1 eq) and dry dichloromethane (50 mL). To the solution was added phosphorous oxychloride (71 μL, 0.76 mmol, 1.07 eq) dropwise over *ca.* 1 min, and the solution stirred in the dark at ambient temperature overnight. Dry diisopropylethylamine (483 μL, 2.77 mmol, 4 eq) was added slowly and the solution stirred for 10 min until the evolved gas dissipated. BF_3 diethyl etherate (500 μL) was added dropwise over *ca.* 1 min and stirred in the dark at ambient temperature for 2 h. The reaction mixture was then concentrated, dry loaded onto a minimum of silica, and eluted over a short silica plug with DCM. The filtrate was concentrated and dry loaded onto a minimum of silica and purified by flash chromatography with a gradient of 1:4 to 2:3 dichloromethane:petroleum ether to yield **6** (100 mg, 35%) as a bronze solid.

^{1}H NMR (400 MHz, Acetone-d_6) δ: 7.68 – 7.60 (m, 1H), 7.54 – 7.49 (m, 2H), 7.50 – 7.43 (m, 2H), 7.36 (t, J = 8.1 Hz, 1H), 7.23 (dt, J = 7.5, 1.4 Hz, 1H), 7.15 (d, J = 4.4 Hz, 1H), 7.08 (d, J = 4.4 Hz, 1H), 6.28 (s, 1H), 3.65 (t, J = 6.2 Hz, 2H), 2.73 (t, J = 7.1 Hz, 2H), 2.57 (s, 3H), 2.31 (s, 3H), 1.90 – 1.77 (m, 4H). ^{13}C NMR (151 MHz, DMSO-d_6) δ

158.58, 152.33, 143.42, 142.59, 136.08, 135.94, 134.70, 134.51, 129.15, 129.07, 129.02, 126.84, 124.42, 123.66, 120.16, 118.02, 115.70, 45.10, 34.06, 31.56, 28.09, 14.54, 10.96. ^{19}F NMR (377 MHz, DMSO-d_6) δ: -143.06 (dd, J = 67.2, 33.2 Hz). HRMS (ESI+/Q-TOF) m/z: [M+Na] calcd for $C_{23}H_{24}N_2NaClBF_2$ 435.1587; observed 435.1574.

(*E*)-5,5-difluoro-1,3-dimethyl-7-(3-(4-(triphenylphosphonio)butyl)styryl)-5H-dipyrrolo[1,2-c:2',1'-f][1,3,2]diazaborinin-4-ium-5-uide **7**. A flame dried 10 mL RBF was charged with (*E*)-7-(3-(4-chlorobutyl)styryl)-5,5-difluoro-1,3-dimethyl-5H-dipyrrolo[1,2-c:2',1'-f][1,3,2]diazaborinin-4-ium-5-uide (81 mg, 0.195 mmol, 1 eq), triphenylphosphine (256 mg, 0.977 mmol, 5 eq), potassium iodide (32 mg, 0.195 mmol, 1 eq) and dry acetonitrile (5 mL). The flask was fitted with a condenser and purged with N_2, and heated to reflux in the dark overnight. The solution was cooled and concentrated *in vacuo*, dry loaded onto a minimum of silica and purified by flash chromatography eluting with a gradient of 1:50 to 1:9 methanol:dichloromethane to yield **7** (117 mg, 79%) as a purple solid, which was stored at -20ºC in the dark.

^{1}H NMR (600 MHz, Acetone-d_6) δ 7.97 – 7.91 (m, 9H), 7.82 – 7.77 (m, 6H), 7.61 – 7.51 (m, 3H), 7.47 (s, 1H), 7.44 (d, J = 7.8 Hz, 1H), 7.32 (t, J = 7.6 Hz, 1H), 7.19 – 7.16 (m, 2H), 7.11 (d, J = 4.2 Hz, 1H), 6.30 (s, 1H), 3.78 – 3.72 (m, 2H), 2.77 (t, J = 7.5 Hz, 2H), 2.57 (s, 3H), 2.32 (s, 3H), 2.02 – 1.95 (m, 2H), 1.88 – 1.80 (m, 2H). ^{13}C NMR (151 MHz, Acetone-d_6) δ: 159.93, 154.00, 144.50, 143.19, 137.69, 136.60, 136.21, 135.94 (d, J = 2.8 Hz), 134.72 (d, J = 10.2 Hz), 131.22 (d, J = 12.5 Hz), 129.98 (d, J = 26.6 Hz), 129.74, 127.90, 127.84, 125.93, 125.88, 124.19, 123.99, 121.05, 119.70, 119.58 (d, J = 86.1 Hz), 116.29, 35.06, 32.54 (d, J = 16.4 Hz), 22.37, 22.19 (d, J = 45.4 Hz), 15.01,

11.29. ^{19}F NMR (377 MHz, Acetone-d_6) δ -143.09 (dd, J = 66.1, 33.1 Hz). HRMS (ESI+/Q-TOF) m/z: [M^+] calcd for $C_{41}H_{39}N_2PBF_2$ 639.2912; observed 639.2919.

3.4.4 Inhibition of mitochondrial lipid peroxidation in live cells using MSB.

Pfa-1 MEF cells (100,000 in 1 mL) were plated in 12-well plates for 18 hours. The cells were washed once with DPBS and the media exchanged with media containing the appropriate concentration of MPQ, DOX, PQ or ANT, then treated with an aliquot (1 μL in DMSO) of antioxidant or DMSO. The cells were incubated for the appropriate amount of time (4-5 hours for MPQ and DOX, 24 hours for ANT and PQ), followed by addition of MSB (2 μL of 125 μM DMSO solution) or C11-BODIPY (2 μL of 500 μM DMSO solution) for 30 min. The cells were washed once with DPBS, treated with trypsin, and suspended in clear media without FBS for flow cytometry analysis.

3.4.5 Inhibition of mitochondrial oxidative stress-induced apoptosis by MTHNs.

Pfa-1 MEF cells (10,000 in 100 μL) were plated in 96-well plates for 12 hours. The media was then exchanged with 100 μL media serially diluted from the appropriate concentrations of initiator and either with or without FBS. The appropriate antioxidant was added (0.8 μL in DMSO) and cells were incubated for 20 h. The media was then exchanged and viability determined with the Aquabluer assay.

3.4.6 Confocal microscopy

Pfa-1 MEF cells were plated in 12-well plates and grown overnight. Cells were treated with MitoView 633 and either C11-BODIPY or MSB at the indicated

concentrations for 30 minutes prior to visualization in an incubated Biotek plate reader/imager.

3.4.7 Bioavailability of THNs and MitoTHNs

BALB/c (~20 g, normal diet) and ApoE$^{-/-}$ (~100 g, high calorie diet) mice were acclimated for one week after delivery from a commercial source. A 20 mg/mL solution of C_{15}-THN or C_{14}-MitoTHN was prepared in 5% DMSO in sunflower oil, and shaken before administration by gavage for a 100 mg/kg dose. Four mice were chosen for each time point at 2, 4 and 24 h; the mouse was anesthetised and incised, blood was drawn from the heart and treated with EDTA, and the carcass was perfused with saline supplemented with ascorbic acid. The tissues were immediately harvested, weighed wet, flash frozen in liquid nitrogen, and stored at -80°C until analysis. Each tissue was transferred to a mortar with liquid nitrogen, ground under liquid nitrogen, and the frozen residue quickly transferred to 2:1 $CHCl_3$:MeOH (50 mg tissue or μL blood per mL extraction solution) in a Falcon tube on ice. The mixture was sonicated for 30 s with a probe sonicator (Hielscher UP100H), treated with 0.2 volume of 5% aqueous NaCl, vortexed and 80% of the organic layer transferred to test tubes. Each solution was immediately treated with 10 μL of 2% v/v formic acid in methanol. The test tubes were concentrated by centrivap at 40°C and the residue triturated in 250 μL of methanol. The mixture was taken up through a 0.45 μm syringe filter and 90 μL of the filtrate transferred to an HPLC vial insert followed by 10 μL of internal standard in methanol. The compounds were quantified by UPLC-ESI$^+$-MS/MS with an Acquity UPLC BEH C18, 130Å, 1.7 μm, 2.1 mm X 50 mm column: C_{15}-THN was quantified by using C_{10}-MeOTHN (1 μM) as internal standard eluting with 90:10:0.04 MeOH:H_2O:formic acid at 0.2 mL/min for 15 min; C_{14}-MTHN was quantified using C_6-

MeOMTHN as internal standard eluting with 90:10:0.04 MeOH:H_2O:formic acid at 0.2 mL/min for 15 min. Vehicle control tissue samples were assayed first, then standard curves were prepared in the vehicle control samples to compensate for slight matrix effects. Concentrations are reported as the average ± standard deviation from the mean of $n = 4$ mice. A single mouse for C_{14}-MTHN exhibited signs of distress and an abnormally high concentration of compound in the lung and was excluded from the dataset.

3.5 References

[1] Friedman, J. R.; Nunnari, J. Mitochondrial Form and Function. *Nature* **2014**, *505* (7483), 335–343.

[2] Lane, N.; Martin, W. The Energetics of Genome Complexity. *Nature* **2010**, *467* (7318), 929–934.

[3] Davies, K. J. Oxidative Stress: the Paradox of Aerobic Life. *Biochem. Soc. Symp.* **1995**, *61*, 1–31.

[4] Murphy, M. P. How Mitochondria Produce Reactive Oxygen Species. *Biochem. J.* **2009**, *417* (1), 1–13.

[5] Muller, F. The Nature and Mechanism of Superoxide Production by the Electron Transport Chain: Its Relevance to Aging. *J. Am. Aging Assoc.* **2000**, *23* (4), 227–253.

[6] Ruggiero, F. M.; Cafagna, F.; Petruzzella, V.; Gadaleta, M. N.; Quagliariello, E. Lipid Composition in Synaptic and Nonsynaptic Mitochondria From Rat Brains and Effect of Aging. *J. Neurochem.* **1992**, *59* (2), 487–491.

[7] McCord, J. M. Free Radicals and Myocardial Ischemia: Overview and Outlook. *Free Radic. Biol. Med.* **1988**, *4* (1), 9–14.

[8] Arai, M.; Imai, H.; Koumura, T.; Yoshida, M.; Emoto, K.; Umeda, M.; Chiba, N.; Nakagawa, Y. Mitochondrial Phospholipid Hydroperoxide Glutathione Peroxidase Plays a Major Role in Preventing Oxidative Injury to Cells. *J. Biol. Chem.* **1999**, *274* (8), 4924–4933.

[9] Green, K.; Brand, M. D.; Murphy, M. P. Prevention of Mitochondrial Oxidative Damage as a Therapeutic Strategy in Diabetes. *Diabetes* **2004**, *53* (Suppl 1), S110–S118.

[10] Seyfried, T. N.; Flores, R. E.; Poff, A. M.; D'Agostino, D. P. Cancer as a Metabolic Disease: Implications for Novel Therapeutics. *Carcinogenesis* **2014**, *35* (3), 515–527.

[11] Goto, Y.; Nonaka, I.; Horai, S. A Mutation in the $tRNA^{Leu(UUR)}$ Gene Associated with the MELAS Subgroup of Mitochondrial Encephalomyopathies. *Nature* **1990**, *348*, 651–653.

[12] Beal, M. F. Mitochondria, Oxidative Damage, and Inflammation in Parkinson's Disease. *Ann. N. Y. Acad. Sci.* **2003**, *991*, 120–131.

[13] Cadonic, C.; Sabbir, M. G.; Albensi, B. C. Mechanisms of Mitochondrial Dysfunction in Alzheimer's Disease. *Mol. Neurobiol.* **2016**, *53*, 6078−6090.

[14] Giorgi, C.; Agnoletto, C.; Bononi, A.; Bonora, M.; De Marchi, E.; Marchi, S.; Missiroli, S.; Patergnani, S.; Poletti, F.; Rimessi, A.; Suski, J. M.; Wieckowski, M. R.; Pinton, P. Mitochondrial Calcium Homeostasis as Potential Target for Mitochondrial Medicine. *Mitochondrion* **2012**, *12* (1), 77–85.

[15] Zamzami, N.; Kroemer, G. The Mitochondrion in Apoptosis: How Pandora's Box Opens. *Nat. Rev. Mol. Cell Biol.* **2001**, *2* (1), 67–71.

[16] Cadenas, E.; Davies, K. Mitochondrial Free Radical Generation, Oxidative Stress, and Aging. *Free Radic. Biol. Med.* **2000**, *29* (3-4), 222–230.

[17] Daum, G. Lipids of Mitochondria. *Biochim. Biophys. Acta* **1985**, *822* (1), 1–42.

[18] Houtkooper, R. H.; Vaz, F. M. Cardiolipin, the Heart of Mitochondrial Metabolism. *Cell. Mol. Life Sci.* **2008**, *65* (16), 2493–2506.

[19] Maguire, J. J.; Tyurina, Y. Y.; Mohammadyani, D.; Kapralov, A. A.; Anthonymuthu, T. S.; Qu, F.; Amoscato, A. A.; Sparvero, L. J.; Tyurin, V. A.; Planas-Iglesias, J.; He, R.-R.; Klein-Seetharaman, J.; Bayir, H.; Kagan, V. E. Known Unknowns of Cardiolipin Signaling: the Best Is Yet to Come. *Biochim. Biophys. Acta* **2017**, *1862* (1), 8–24.

[20] Schlame, M.; Rüstow, B. Lysocardiolipin Formation and Reacylation in Isolated Rat Liver Mitochondria. *Biochem. J.* **1990**, *272* (3), 589–595.

[21] McCord, J. M. Superoxide Dismutase, Lipid Peroxidation, and Bell-Shaped Dose Response Curves. *Dose Resp.* **2008**, *6* (3), 223–238.

[22] Bindoli, A. Lipid Peroxidation in Mitochondria. *Free Radic. Biol. Med.* **1988**, *5* (4), 247–261.

[23] Liu, W.; Porter, N. A.; Schneider, C.; Brash, A. R.; Yin, H. Formation of 4-Hydroxynonenal From Cardiolipin Oxidation: Intramolecular Peroxyl Radical Addition and Decomposition. *Free Radic. Biol. Med.* **2011**, *50* (1), 166–178.

[24] Tuppen, H. A. L.; Blakely, E. L.; Turnbull, D. M.; Taylor, R. W. Mitochondrial DNA Mutations and Human Disease. *Biochim. Biophys. Acta* **2010**, *1797* (2), 113–128.

[25] Lemasters, J. J. Selective Mitochondrial Autophagy, or Mitophagy, as a Targeted Defense Against Oxidative Stress, Mitochondrial Dysfunction, and Aging. *Rejuvenation Res.* **2005**, *8* (1), 3–5.

[26] Li, X.-X.; Tsoi, B.; Li, Y.-F.; Kurihara, H.; He, R.-R. Cardiolipin and Its Different Properties in Mitophagy and Apoptosis. *J. Histochem. Cytochem.* **2015**, *63* (5), 301–311.

[27] Georgakopoulos, N. D.; Wells, G.; Campanellal, M. The Pharmacological Regulation of Cellular Mitophagy. *Nat. Chem. Biol.* **2017**, *13* (2), 136–146.

[28] He, L. H.; Lemasters, J. J. Regulated and Unregulated Mitochondrial Permeability Transition Pores: a New Paradigm of Pore Structure and Function? *FEBS Lett.* **2002**, *512* (1-3), 1–7.

[29] Nakagawa, T.; Shimizu, S.; Watanabe, T.; Yamaguchi, O.; Otsu, K.; Yamagata, H.; Inohara, H.; Kubo, T.; Tsujimoto, Y. Cyclophilin D-Dependent Mitochondrial Permeability Transition Regulates Some Necrotic but Not Apoptotic Cell Death. *Nature* **2005**, *434* (7033), 652–658.

[30] Castello, P. R.; Drechsel, D. A.; Patel, M. Mitochondria Are a Major Source of Paraquat-Induced Reactive Oxygen Species Production in the Brain. *J. Biol. Chem.* **2007**, *282* (19), 14186–14193.

[31] Paraquat Information Centre Home Page. http://www.paraquat.com (accessed July 20, 2017), ©2017 Paraquat Information Center on behalf of Syngenta Crop Protection AG.

[32] Berry, C.; La Vecchia, C.; Nicotera, P. Paraquat and Parkinson's Disease. *Cell Death Differ.* **2010**, *17*, 1115–1125.

[33] Michaelis, L.; Hill, E. S. The Viologen Indicators. *J. Gen. Physiol.* **1933**, *16* (6), 859–873.

[34] Dodge, A. D.; Harris, N.; Baldwin, B. C. The Mode of Action of Paraquat and Diquat. *Biochem. J.* **1970**, *118* (3), 43P–44P.

[35] Bus, J. S.; Aust, S. D.; Gibson, J. E. Superoxide- and Singlet Oxygen-Catalyzed Lipid Peroxidation as a Possible Mechanism for Paraquat (Methyl Viologen) Toxicity. *Biochem. Biophys. Res. Commun.* **1974**, *58* (3), 749–755.

[36] McCormack, A. L.; Atienza, J. G.; Johnston, L. C.; Andersen, J. K.; Vu, S.; Di Monte, D. A. Role of Oxidative Stress in Paraquat-Induced Dopaminergic Cell Degeneration. *J. Neurochem.* **2005**, *93* (4), 1030–1037.

[37] Robb, E. L.; Gawel, J. M.; Aksentijević, D.; Cochemé, H. M.; Stewart, T. S.; Shchepinova, M. M.; Qiang, H.; Prime, T. A.; Bright, T. P.; James, A. M.; Shattock, M. J.; Senn, H. M.; Hartley, R. C.; Murphy, M. P. Selective Superoxide Generation Within Mitochondria by the Targeted Redox Cycler MitoParaquat. *Free Radic. Biol. Med.* **2015**, *89*, 883–894.

[38] Myers, C. E.; McGuire, W. P.; Liss, R. H.; Ifrim, I.; Grotzinger, K.; Young, R. C. Adriamycin: the Role of Lipid Peroxidation in Cardiac Toxicity and Tumor Response. *Science* **1977**, *197* (4299), 165–167.

[39] Keizer, H. G.; Pinedo, H. M.; Schuurhuis, G. J.; Joenje, H. Doxorubicin (Adriamycin): a Critical Review of Free Radical-Dependent Mechanisms of Cytotoxicity. *Pharmac. Ther.* **1990**, *47* (2), 219–231.

[40] Sato, S.; Iwaizumi, M.; Handa, K.; Tamura, Y. Electron Spin Resonance Study on the Mode of Generation of Free Radicals of Daunomycin, Adriamycin, and Carboquone in NAD(P)H-Microsome System. *Gann* **1977**, *68* (5), 603–608.

[41] Smith, R. A. J.; Hartley, R. C.; Cochemé, H. M.; Murphy, M. P. Mitochondrial Pharmacology. *Trends Pharmacol. Sci.* **2012**, *33* (6), 341–352.

[42] Bakeeva, L. E.; Grinius, L. L.; Jasaitis, A. A.; Kuliene, V. V.; Levitsky, D. O.; Liberman, E. A.; Severina, I. I.; Skulachev, V. P. Conversion of Biomembrane-Produced Energy Into Electric Form. II. Intact Mitochondria. *Biochim. Biophys. Acta* **1970**, *216* (1), 13–21.

[43] Li, Y.; Zhang, H.; Fawcett, J. P.; Tucker, I. G. Effect of Cyclosporin A on the Pharmacokinetics of Mitoquinone (MitoQ10), a Mitochondria-Targeted Antioxidant, in Rat. *Asian J. Pharm. Sci.* **2010**, *5* (3), 106–113.

[44] Zielonka, J.; Joseph, J.; Sikora, A.; Hardy, M.; Ouari, O.; Vasquez-Vivar, J.; Cheng, G.; Lopez, M.; Kalyanaraman, B. Mitochondria-Targeted Triphenylphosphonium-Based Compounds: Syntheses, Mechanisms of Action, and Therapeutic and Diagnostic Applications. *Chem. Rev.* **2017**, *117* (15), 10043–10120.

[45] Chen, L. B. Mitochondrial Membrane Potential in Living Cells. *Ann. Rev. Cell Biol.* **1988**, *4*, 155–181.

[46] Szeto, H. H. First-in-Class Cardiolipin-Protective Compound as a Therapeutic Agent to Restore Mitochondrial Bioenergetics. *Br. J. Pharmacol.* **2014**, *171* (8), 2029–2050.

[47] Zhao, K. S.; Zhao, G. M.; Wu, D. L.; Soong, Y.; Birk, A. V.; Schiller, P. W.; Szeto, H. H. Cell-Permeable Peptide Antioxidants Targeted to Inner Mitochondrial Membrane Inhibit Mitochondrial Swelling, Oxidative Cell Death, and Reperfusion Injury. *J. Biol. Chem.* **2004**, *279* (33), 34682–34690.

[48] Birk, A. V.; Liu, S.; Soong, Y.; Mills, W.; Singh, P.; Warren, J. D.; Seshan, S. V.; Pardee, J. D.; Szeto, H. H. The Mitochondrial-Targeted Compound SS-31 Re-Energizes Ischemic Mitochondria by Interacting with Cardiolipin. *J. Am. Soc. Nephrol.* **2013**, *24* (8), 1250–1261.

[49] Birk, A. V.; Chao, W. M.; Bracken, C.; Warren, J. D.; Szeto, H. H. Targeting Mitochondrial Cardiolipin and the Cytochrome C/Cardiolipin Complex to Promote Electron Transport and Optimize Mitochondrial ATP Synthesis. *Br. J. Pharmacol.* **2014**, *171* (8), 2017–2028.

[50] Hoye, A. T.; Davoren, J. E.; Wipf, P.; Fink, M. P.; Kagan, V. E. Targeting Mitochondria. *Acc. Chem. Res.* **2008**, *41* (1), 87–97.

[51] Horton, K. L.; Stewart, K. M.; Fonseca, S. B.; Guo, Q.; Kelley, S. O. Mitochondria-Penetrating Peptides. *Chem. Biol.* **2008**, *15* (4), 375–382.

[52] Pathak, R. K.; Kolishetti, N.; Dhar, S. Targeted Nanoparticles in Mitochondrial Medicine. *WIREs Nanomed. Nanobiotechnol.* **2014**, *7* (3), 315–329.

[53] Smith, R. A. J.; Adlam, V. J.; Blaikie, F. H.; Manas, A.-R. B.; Porteous, C. M.; James, A. M.; Ross, M. F.; Logan, A.; Cochemé, H. M.; Trnka, J.; Prime, T. A.; Abakumova, I.; Jones, B. A.; Filipovska, A.; Murphy, M. P. Mitochondria-Targeted Antioxidants in the Treatment of Disease. *Ann. N. Y. Acad. Sci.* **2008**, *1147* (1), 105–111.

[54] Bakeeva, L. E.; Grinius, L. L.; Jasaitis, A. A.; Kuliene, V. V.; Levitsky, D. O.; Liberman, E. A.; Severina, I. I.; Skulachev, V. P. Conversion of Biomembrane-Produced Energy Into Electric Form. II. Intact Mitochondria. *Biochim. Biophys. Acta* **1970**, *216* (1), 13–21.

[55] Grinius, L. L.; Jasaitis, A. A.; Kadziauskas, Y. P.; Liberman, E. A.; Skulachev, V. P.; Topali, V. P.; Tsofina, L. M.; Vladimirova, M. A. Conversion of Biomembrane-Produced Energy Into Electric Form. I. Submitochondrial Particles. *Biochim. Biophys. Acta* **1970**, *216* (1), 1–12.

[56] Muratsugu, M.; Kamo, N.; Kurihara, K.; Kobatake, Y. Selective Electrode for Dibenzyl Dimethyl Ammonium Cation as Indicator of the Membrane Potential in Biological Systems. *Biochim. Biophys. Acta* **1977**, *464* (3), 613–619.

[57] Kamo, N.; Muratsugu, M.; Hongoh, R.; Kobatake, Y. Membrane Potential of Mitochondria Measured with an Electrode Sensitive to Tetraphenyl Phosphonium and Relationship Between Proton Electrochemical Potential and Phosphorylation Potential in Steady State. *J. Membrane Biol.* **1979**, *49* (2), 105–121.

[58] Shinbo, T.; Kamo, N.; Kurihara, K.; Kobatake, Y. A PVC-Based Electrode Sensitive to DDA+ as a Device for Monitoring the Membrane Potential in Biological Systems. *Arch. Biochem. Biophys.* **1978**, *187* (2), 414–422.

[59] Davey, G. P.; Tipton, K. F.; Murphy, M. P. Uptake and Accumulation of 1-Methyl-4-Phenylpyridinium by Rat Liver Mitochondria Measured Using an Ion-Selective Electrode. *Biochem. J.* **1992**, *288* (2), 439–443.

[60] Murphy, M. P. Targeting Antioxidants to Mitochondria by Conjugation to Lipophilic Cations. In *Drug-Induced Mitochondrial Dysfunction*; Dykens, J. A., Will, Y., Eds.; John Wiley & Sons, Inc., 2008; pp 575–587.

[61] Cottet Rousselle, C.; Ronot, X.; Leverve, X.; Mayol, J. F. Cytometric Assessment of Mitochondria Using Fluorescent Probes. *Cytometry Part A* **2011**, *79A* (6), 405–425.

[62] Dunn, K. W.; Kamocka, M. M.; McDonald, J. H. A Practical Guide to Evaluating Colocalization in Biological Microscopy. *Am. J. Physiol., Cell Physiol.* **2011**, *300* (4), C723–C742.

[63] Scaduto, R. C., Jr.; Grotyohann, L. W. Measurement of Mitochondrial Membrane Potential Using Fluorescent Rhodamine Derivatives. *Biophys. J.* **1999**, *76* (1), 469–477.

[64] Xu, Z.; Xu, L. Fluorescent Probes for the Selective Detection of Chemical Species Inside Mitochondria. *Chem. Commun.* **2016**, *52* (6), 1094–1119.

[65] Dikalov, S. I.; Harrison, D. G. Methods for Detection of Mitochondrial and Cellular Reactive Oxygen Species. *Antioxid. Redox Signal.* **2014**, *20* (2), 372–382.

[66] Prime, T. A.; Forkink, M.; Logan, A.; Finichiu, P. G.; McLachlan, J.; Li Pun, P. B.; Koopman, W. J. H.; Larsen, L.; Latter, M. J.; Smith, R. A. J.; Murphy, M. P. A Ratiometric Fluorescent Probe for Assessing Mitochondrial Phospholipid Peroxidation Within Living Cells. *Free Radic. Biol. Med.* **2012**, *53* (3), 544–553.

[67] Shioji, K.; Oyama, Y.; Okuma, K.; Nakagawa, H. Synthesis and Properties of Fluorescence Probe for Detection of Peroxides in Mitochondria. *Bioorg. Med. Chem. Lett.* **2010**, *20* (13), 3911–3915.

[68] Krumova, K.; Greene, L. E.; Cosa, G. Fluorogenic α-Tocopherol Analogue for Monitoring the Antioxidant Status Within the Inner Mitochondrial Membrane of Live Cells. *J. Am. Chem. Soc.* **2013**, *135* (45), 17135–17143.

[69] Kelso, G. F.; Porteous, C. M.; Coulter, C. V.; Hughes, G.; Porteous, W. K.; Ledgerwood, E. C.; Smith, R. A. J.; Murphy, M. P. Selective Targeting of a Redox-Active Ubiquinone to Mitochondria Within Cells: Antioxidant and Antiapoptotic Properties. *J. Biol. Chem.* **2001**, *276* (7), 4588–4596.

[70] Smith, R. A. J.; Murphy, M. P. Animal and Human Studies with the Mitochondria-Targeted Antioxidant MitoQ. *Ann. N. Y. Acad. Sci.* **2010**, *1201* (1), 96–103.

[71] Adlam, V. J.; Harrison, J. C.; Porteous, C. M.; James, A. M.; Smith, R. A. J.; Murphy, M. P.; Sammut, I. A. Targeting an Antioxidant to Mitochondria Decreases Cardiac Ischemia-Reperfusion Injury. *FASEB J* **2005**, *19* (9), 1088–1095.

[72] Graham, D.; Huynh, N. N.; Hamilton, C. A.; Beattie, E.; Smith, R. A. J.; Cochemé, H. M.; Murphy, M. P.; Dominiczak, A. F. Mitochondria-Targeted Antioxidant $MitoQ_{10}$ Improves Endothelial Function and Attenuates Cardiac Hypertrophy. *Hypertension* **2009**, *54* (2), 322–328.

[73] Lowes, D. A.; Webster, N. R.; Murphy, M. P.; Galley, H. F. Antioxidants That Protect Mitochondria Reduce Interleukin-6 and Oxidative Stress, Improve Mitochondrial Function, and Reduce Biochemical Markers of Organ Dysfunction in a Rat Model of Acute Sepsis. *Br J Anaesth* **2013**, *110* (3), 472–480.

[74] Snow, B. J.; Rolfe, F. L.; Lockhart, M. M.; Frampton, C. M.; O'Sullivan, J. D.; Fung, V.; Smith, R. A. J.; Murphy, M. P.; Taylor, K. M. A Double-Blind, Placebo-Controlled Study to Assess the Mitochondria-Targeted Antioxidant MitoQ as a Disease-Modifying Therapy in Parkinson's Disease. *Movement Disord.* **2010**, *25* (11), 1670–1674.

[75] MitoQ Home Page. https://www.mitoq.com/ (accessed July 20, 2017). ©2017 MITOQ.

[76] Smith, R. A. J.; Porteous, C. M.; Coulter, C. V.; Murphy, M. P. Selective Targeting of an Antioxidant to Mitochondria. *Eur. J. Biochem.* **1999**, *263* (3), 709–716.

[77] Finichiu, P. G.; Larsen, D. S.; Evans, C.; Larsen, L.; Bright, T. P.; Robb, E. L.; Trnka, J.; Prime, T. A.; James, A. M.; Smith, R. A. J.; Murphy, M. P. A Mitochondria-Targeted Derivative of Ascorbate: MitoC. *Free Radic. Biol. Med.* **2015**, *89*, 668–678.

[78] Kelso, G. F.; Maroz, A.; Cochemé, H. M.; Logan, A.; Prime, T. A.; Peskin, A. V.; Winterbourn, C. C.; James, A. M.; Ross, M. F.; Brooker, S.; Porteous, C. M.; Anderson, R. F.; Murphy, M. P.; Smith, R. A. J. A Mitochondria-Targeted Macrocyclic Mn(II) Superoxide Dismutase Mimetic. *Chem. Biol.* **2012**, *19* (10), 1237–1246.

[79] Filipovska, A.; Kelso, G. F.; Brown, S. E.; Beer, S. M.; Smith, R. A. J.; Murphy, M. P. Synthesis and Characterization of a Triphenylphosphonium-Conjugated Peroxidase Mimetic. Insights Into the Interaction of Ebselen with Mitochondria. *J. Biol. Chem.* **2005**, *280* (25), 24113–24126.

[80] Neuzil, J.; Dong, L.-F.; Ramanathapuram, L.; Hahn, T.; Chladova, M.; Wang, X.-F.; Zobalova, R.; Prochazka, L.; Gold, M.; Freeman, R.; Turanek, J.; Akporiaye, E. T.; Dyason, J. C.; Ralph, S. J. Vitamin E Analogues as a Novel Group of Mitocans: Anti-Cancer Agents That Act by Targeting Mitochondria. *Mol. Aspects Med.* **2007**, *28* (5-6), 607–645.

[81] Cheng, G.; Zielonka, J.; McAllister, D. M.; Mackinnon, A. C.; Joseph, J.; Dwinell, M. B.; Kalyanaraman, B. Mitochondria-Targeted Vitamin E Analogs Inhibit Breast Cancer Cell Energy Metabolism and Promote Cell Death. *BMC Cancer* **2013**, *13* (1), 285.

[82] Dong, L.-F.; Jameson, V. J. A.; Tilly, D.; Cerny, J.; Mahdavian, E.; Marín-Hernández, A.; Hernández-Esquivel, L.; Rodríguez-Enríquez, S.; Stursa, J.; Witting, P. K.; Stantic, B.; Rohlena, J.; Truksa, J.; Kluckova, K.; Dyason, J. C.; Ledvina, M.; Salvatore, B. A.; Moreno-Sánchez, R.; Coster, M. J.; Ralph, S. J.; Smith, R. A. J.; Neuzil, J. Mitochondrial Targeting of Vitamin E Succinate Enhances Its Pro-Apoptotic and Anti-Cancer Activity via Mitochondrial Complex II. *J. Biol. Chem.* **2011**, *286* (5), 3717–3728.

[83] Fink, B. D.; O'Malley, Y.; Dake, B. L.; Ross, N. C.; Prisinzano, T. E.; Sivitz, W. I. Mitochondrial Targeted Coenzyme Q, Superoxide, and Fuel Selectivity in Endothelial Cells. *PLoS ONE* **2009**, *4* (1).

[84] Doughan, A. K.; Dikalov, S. I. Mitochondrial Redox Cycling of Mitoquinone Leads to Superoxide Production and Cellular Apoptosis. *Antioxid. Redox Signal.* **2007**, *9* (11), 1825–1836.

[85] Leo, S.; Szabadkai, G.; Rizzuto, R. The Mitochondrial Antioxidants $MitoE_2$ and $MitoQ_{10}$ Increase Mitochondrial Ca^{2+} Load Upon Cell Stimulation by Inhibiting Ca^{2+} Efflux From the Organelle. *Ann. N. Y. Acad. Sci.* **2008**, *1147* (1), 264–274.

[86] Reily, C.; Mitchell, T.; Chacko, B. K.; Benavides, G. A.; Murphy, M. P.; Darley-Usmar, V. M. Mitochondrially Targeted Compounds and Their Impact on Cellular Bioenergetics. *Redox Biology* **2013**, *1* (1), 86–93.

[87] Dixon, S. J.; Lemberg, K. M.; Lamprecht, M. R.; Skouta, R.; Zaitsev, E. M.; Gleason, C. E.; Patel, D. N.; Bauer, A. J.; Cantley, A. M.; Yang, W. S.; Morrison, B., III; Stockwell, B. R. Ferroptosis: an Iron-Dependent Form of Nonapoptotic Cell Death. *Cell* **2012**, *149* (5), 1060–1072.

[88] Yagoda, N.; Rechenberg, von, M.; Zaganjor, E.; Bauer, A. J.; Yang, W. S.; Fridman, D. J.; Wolpaw, A. J.; Smukste, I.; Peltier, J. M.; Boniface, J. J.; Smith, R.; Lessnick, S. L.; Sahasrabudhe, S.; Stockwell, B. R. RAS-RAF-MEK-Dependent Oxidative Cell Death Involving Voltage-Dependent Anion Channels. *Nature* **2007**, *447* (7146), 864–868.

[89] Seiler, A.; Schneider, M.; Foerster, H.; Roth, S.; Wirth, E. K.; Culmsee, C.; Plesnila, N.; Kremmer, E.; Rådmark, O.; Wurst, W.; Bornkamm, G. W.; Schweizer, U.; Conrad, M. Glutathione Peroxidase 4 Senses and Translates Oxidative Stress Into 12/15-Lipoxygenase Dependent- and AIF-Mediated Cell Death. *Cell Metab.* **2008**, *8* (3), 237–248.

[90] Friedmann Angeli, J. P.; Schneider, M.; Proneth, B.; Tyurina, Y. Y.; Tyurin, V. A.; Hammond, V. J.; Herbach, N.; Aichler, M.; Walch, A.; Eggenhofer, E.; Basavarajappa, D.; Rådmark, O.; Kobayashi, S.; Seibt, T.; Beck, H.; Neff, F.; Esposito, I.; Wanke, R.; Förster, H.; Yefremova, O.; Heinrichmeyer, M.; Bornkamm, G. W.; Geissler, E. K.; Thomas, S. B.; Stockwell, B. R.; O'Donnell, V. B.; Kagan, V. E.; Schick, J. A.; Conrad, M. Inactivation of the Ferroptosis Regulator Gpx4 Triggers Acute Renal Failure in Mice. *Nat. Cell Biol.* **2014**, *16* (12), 1180–1191.

[91] Krainz, T.; Gaschler, M. M.; Lim, C.; Sacher, J. R.; Stockwell, B. R.; Wipf, P. A Mitochondrial-Targeted Nitroxide Is a Potent Inhibitor of Ferroptosis. *ACS Cent. Sci.* **2016**, *2* (4), 653–659.

[92] Tobaben, S.; Grohm, J.; Seiler, A.; Conrad, M.; Plesnila, N.; Culmsee, C. Bid-Mediated Mitochondrial Damage Is a Key Mechanism in Glutamate-Induced Oxidative Stress and AIF-Dependent Cell Death in Immortalized HT-22 Hippocampal Neurons. *Cell Death Differ.* **2010**, *18* (2), 282–292.

[93] Neitemeier, S.; Jelinek, A.; Laino, V.; Hoffmann, L.; Eisenbach, I.; Eying, R.; Ganjam, G. K.; Dolga, A. M.; Oppermann, S.; Culmsee, C. BID Links Ferroptosis to Mitochondrial Cell Death Pathways. *Redox Biol.* **2017**, *12*, 558–570.

[94] Yuan, H.; Li, X.; Zhang, X.; Kang, R.; Tang, D. CISD1 Inhibits Ferroptosis by Protection Against Mitochondrial Lipid Peroxidation. *Biochem. Biophys. Res. Commun.* **2016**, *478* (2), 838–844.

[95] Shimada, K.; Skouta, R.; Kaplan, A.; Yang, W. S.; Hayano, M.; Dixon, S. J.; Brown, L. M.; Valenzuela, C. A.; Wolpaw, A. J.; Stockwell, B. R. Global Survey of Cell Death Mechanisms Reveals Metabolic Regulation of Ferroptosis. *Nat. Chem. Biol.* **2016**, *12* (7), 497–503.

[96] Zilka, O.; Shah, R.; Li, B.; Angeli, J. F.; Griesser, M.; Conrad, M.; Pratt, D. A. On the Mechanism of Cytoprotection by Ferrostatin-1 and Liproxstatin-1 and the Role of Lipid Peroxidation in Ferroptotic Cell Death. *ACS Cent. Sci.* **2017**, *3* (3), 232–243.

[97] Angeli, J. P. F.; Shah, R.; Pratt, D. A.; Conrad, M. Ferroptosis Inhibition: Mechanisms and Opportunities. *Trends Pharmacol. Sci.* **2017**, *38* (5), 489–498.

[98] Shah, R.; Margison, K.; Pratt, D. The Potency of Diarylamine Radical-Trapping Antioxidants As Inhibitors of Ferroptosis Underscores the Role Of Autoxidation in the Mechanism of Cell Death. *ACS Chem. Biol.* **2017**, *Just Accepted*, DOI: 10.1021/acschembio.7b00730.

[99] Yang, W. S.; SriRamaratnam, R.; Welsch, M. E.; Shimada, K.; Skouta, R.; Viswanathan, V. S.; Cheah, J. H.; Clemons, P. A.; Shamji, A. F.; Clish, C. B.; Brown, L. M.; Girotti, A. W.; Cornish, V. W.; Schreiber, S. L.; Stockwell, B. R. Regulation of Ferroptotic Cancer Cell Death by GPX4. *Cell* **2014**, *156* (1-2), 317–331.

[100] Li, B.; Harjani, J. R.; Cormier, N. S.; Madarati, H.; Atkinson, J.; Cosa, G.; Pratt, D. A. Besting Vitamin E: Sidechain Substitution Is Key to the Reactivity of Naphthyridinol Antioxidants in Lipid Bilayers. *J. Am. Chem. Soc.* **2013**, *135* (4), 1394–1405.

[101] Haidasz, E. A.; Van Kessel, A. T. M.; Pratt, D. A. A Continuous Visible Light Spectrophotometric Approach to Accurately Determine the Reactivity of Radical-Trapping Antioxidants. *J. Org. Chem.* **2016**, *81* (3), 737–744.

[102] Pratt, D. A.; DiLabio, G. A.; Brigati, G.; Pedulli, G. F.; Valgimigli, L. 5-Pyrimidinols: Novel Chain-Breaking Antioxidants More Effective Than Phenols. *J. Am. Chem. Soc.* **2001**, *123*, 4625−4626.

[103] Pap, E. H.; Drummen, G. P.; Winter, V. J.; Kooij, T. W.; Rijken, P.; Wirtz, K. W.; Op den Kamp, J. A.; Hage, W. J.; Post, J. A. Ratio-Fluorescence Microscopy of Lipid Oxidation in Living Cells Using C11-BODIPY$^{581/591}$. *FEBS Lett.* **1999**, *453* (3), 278–282.

[104] Solesio, M. E.; Prime, T. A.; Logan, A.; Murphy, M. P.; del Mar Arroyo-Jimenez, M.; Jordán, J.; Galindo, M. F. The Mitochondria-Targeted Anti-Oxidant MitoQ Reduces Aspects of Mitochondrial Fission in the 6-OHDA Cell Model of Parkinson's Disease. *Biochim. Biophys. Acta* **2013**, *1832* (1), 174–182.

[105] Shekhova, E.; Kniemeyer, O.; Brakhage, A. A. Induction of Mitochondrial ROS Production by Itraconazole, Terbinafine and Amphotericin B as a Mode of Action Against *Aspergillus Fumigatus*. *Antimicrob. Agents Chemother.* **2017**, DOI: 10.1128/AAC.00978-17.

[106] Wijtmans, M.; Pratt, D. A.; Valgimigli, L.; DiLabio, G. A.; Pedulli, G. F.; Porter, N. A. 6-Amino-3-Pyridinols: Towards Diffusion-Controlled Chain-Breaking Antioxidants. *Angew. Chem. Int. Ed.* **2003**, *42* (36), 4370–4373.

[107] MacDonald, M. L.; Murray, I. V. J.; Axelsen, P. H. Mass Spectrometric Analysis Demonstrates That BODIPY 581/591 C11 Overestimates and Inhibits Oxidative Lipid Damage. *Free Radic. Biol. Med.* **2007**, *42* (9), 1392–1397.

[108] Trnka, J.; Elkalaf, M.; Andel, M. Lipophilic Triphenylphosphonium Cations Inhibit Mitochondrial Electron Transport Chain and Induce Mitochondrial Proton Leak. *PLoS ONE* **2015**, *10* (4).

[109] Khailova, L. S.; Nazarov, P. A.; Sumbatyan, N. V.; Korshunova, G. A.; Rokitskaya, T. I.; Dedukhova, V. I.; Antonenko, Y. N.; Skulachev, V. P. Uncoupling and Toxic Action of Alkyltriphenylphosphonium Cations on Mitochondria and the Bacterium Bacillus Subtilis as a Function of Alkyl Chain Length. *Biochemistry Mosc.* **2015**, *80* (12), 1589–1597.

[110] Tapia, P. C. Sublethal Mitochondrial Stress with an Attendant Stoichiometric Augmentation of Reactive Oxygen Species May Precipitate Many of the Beneficial Alterations in Cellular Physiology Produced by Caloric Restriction, Intermittent Fasting, Exercise and Dietary Phytonutrients: "'Mitohormesis'" for Health and Vitality. *Medical Hypotheses* **2006**, *66* (4), 832–843.

[111] Ristow, M. Unraveling the Truth About Antioxidants: Mitohormesis Explains ROS-Induced Health Benefits. *Nature Med.* **2014**, *20* (7), 709–711.

[112] Yun, J.; Finkel, T. Mitohormesis. *Cell Metab.* **2014**, *19* (5), 757–766.

[113] Ristow, M.; Schmeisser, K. Mitohormesis: Promoting Health and Lifespan by Increased Levels of Reactive Oxygen Species (ROS). *Dose Resp.* **2014**, *12*, 288–341.

[114] Taguchi, K.; Motohashi, H.; Yamamoto, M. Molecular Mechanisms of the Keap1–Nrf2 Pathway in Stress Response and Cancer Evolution. *Genes Cells* **2011**, *16* (2), 123–140.

[115] Holmström, K. M.; Kostov, R. V.; Dinkova-Kostova, A. T. The Multifaceted Role of Nrf2 in Mitochondrial Function. *Curr Opin Toxicol* **2016**, *1*, 80–91.

[116] Piantadosi, C. A.; Suliman, H. B. Mitochondrial Transcription Factor a Induction by Redox Activation of Nuclear Respiratory Factor 1. *J. Biol. Chem.* **2006**, *281* (1), 324–333.

[117] Shih-Ching Lo, M. H. PGAM5 Tethers a Ternary Complex Containing Keap1 and Nrf2 to Mitochondria. *Exp. Cell Res.* **2008**, *314* (8), 1789–1803.

[118] Plafker, K. S.; Plafker, S. M. The Ubiquitin-Conjugating Enzyme UBE2E3 and Its Import Receptor Importin-11 Regulate the Localization and Activity of the Antioxidant Transcription Factor NRF2. *Mol. Biol. Cell* **2015**, *26* (2), 327–338.

[119] Sun, X.; Ou, Z.; Chen, R.; Niu, X.; Chen, D.; Kang, R.; Tang, D. Activation of the P62-Keap1-NRF2 Pathway Protects Against Ferroptosis in Hepatocellular Carcinoma Cells. *Hepatology* **2016**, *63* (1), 173–184.

[120] Kalyanaraman, B.; Kalivendi, S. Methods for Reducing Anthracycline-Induced Toxicity. US Patent Office, US 2008/032940 A1. **2008**.

[121] Asin-Cayuela, J.; Manas, A.-R. B.; James, A. M.; Smith, R. A. J.; Murphy, M. P. Fine-Tuning the Hydrophobicity of a Mitochondria-Targeted Antioxidant. *FEBS Lett.* **2004**, *571* (1-3), 9–16.

[122] Duveau, D. Y.; Arce, P. M.; Schoenfeld, R. A.; Raghav, N. Synthesis and Characterization of mitoQ and Idebenone Analogues as Mediators of Oxygen Consumption in Mitochondria. *Bioorg. Med. Chem.* **2010**, *18* (17), 6429–6441.

[123] Smith, R.; Kelso, G. F.; James, A. M.; Murphy, M. P. Targeting Coenzyme Q Derivatives to Mitochondria. *Meth. Enzymol.* **2004**, *382*, 45–67.

[124] Nava, P.; Cecchini, M.; Chirico, S.; Gordon, H.; Morley, S.; Manor, D.; Atkinson, J. Preparation of Fluorescent Tocopherols for Use in Protein Binding and Localization with the Alpha-Tocopherol Transfer Protein. *Bioorg. Med. Chem.* **2006**, *14* (11), 3721–3736.

[125] Min, K. C.; Kovall, R. A.; Hendrickson, W. A. Crystal Structure of Human α-Tocopherol Transfer Protein Bound to Its Ligand: Implications for Ataxia with Vitamin E Deficiency. *Proc. Natl. Acad. Sci. USA* **2003**, *100* (25), 14713–14718.

[126] Nam, T.-G.; Rector, C. L.; Kim, H.-Y.; Sonnen, A. F.-P.; Meyer, R.; Nau, W. M.; Atkinson, J.; Rintoul, J.; Pratt, D. A.; Porter, N. A. Tetrahydro-1,8-Naphthyridinol Analogues of Alpha-Tocopherol as Antioxidants in Lipid Membranes and Low-Density Lipoproteins. *J. Am. Chem. Soc.* **2007**, *129* (33), 10211–10219.

[127] Burton, G. W.; Ingold, K. U.; Foster, D. O.; Cheng, S. C.; Webb, A.; Hughes, L. Comparison of Free α-Tocopherol and α-Tocopheryl Acetate as Sources of Vitamin E in Rats and Humans. *Lipids* **1988**, *23* (9), 834–840.

[128] Burton, G. W.; Webb, A.; Ingold, K. U. A Mild, Rapid, and Efficient Method of Lipid Extraction for Use in Determining Vitamin-E Lipid Ratios. *Lipids* **1985**, *20* (1), 29–39.

[129] Heiden, M. G. V.; Cantley, L. C.; Thompson, C. B. Understanding the Warburg Effect: the Metabolic Requirements of Cell Proliferation. *Science* **2009**, *324* (5930), 1029–1033.

[130] Seyfried, T. N.; Flores, R. E.; Poff, A. M.; D'Agostino, D. P. Cancer as a Metabolic Disease: Implications for Novel Therapeutics. *Carcinogenesis* **2014**, *35* (3), 515–527.

[131] Seyfried, T. N. Cancer as a Mitochondrial Metabolic Disease. *Front Cell Dev Biol* **2015**, *3*, 43.

[132] Hirashima, S.-I.; Nobuta, T.; Tada, N.; Miura, T.; Itoh, A. Direct Aerobic Photo-Oxidative Synthesis of Aromatic Methyl Esters From Methyl Aromatics via Dimethyl Acetals. *Org. Lett.* **2010**, *12* (16), 3645–3647.

[133] Kirkman, J. K.; Lindell, S. D.; Maechling, S.; Slawin, A. M. Z.; Moody, C. J. Synthesis of 3-(Carboxyarylalkyl)Imidazo[2,1-f][1,2,4]Triazines as Potential Inhibitors of AMP Deaminase. *Org. Biomol. Chem.* **2008**, *6* (23), 4452–4459.

Appendix 1: NMR Spectra for Chapter 2

The following appendix contains NMR spectra for the new compounds used in the SAR study in Chapter 2, Section **2.7**-**2.10**.

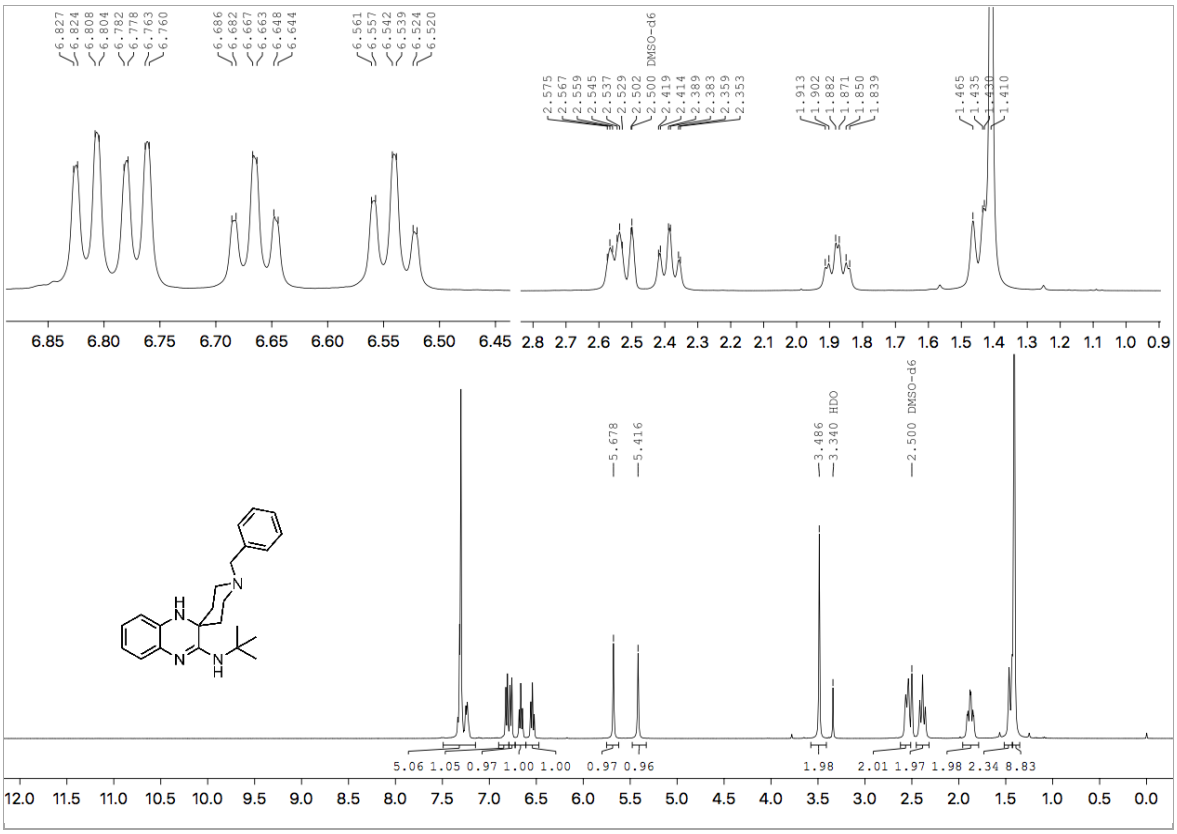
6.827
6.824
6.808
6.804
6.782
6.778
6.763
6.760
6.686
6.682
6.667
6.663
6.648
6.644
6.561
6.557
6.542
6.539
6.524
6.520
2.575
2.567
2.559
2.545
2.537
2.529
2.502
2.500 DMSO-d6
2.419
2.414
2.389
2.383
2.359
2.353
1.913
1.902
1.882
1.871
1.850
1.839
1.465
1.435
1.430
1.410
5.678
5.416
3.486
3.340 HDO
2.500 DMSO-d6
5.06 1.05 0.97 1.00 1.00 0.97 0.96
1.98
2.01 1.97 1.98 2.34 8.83

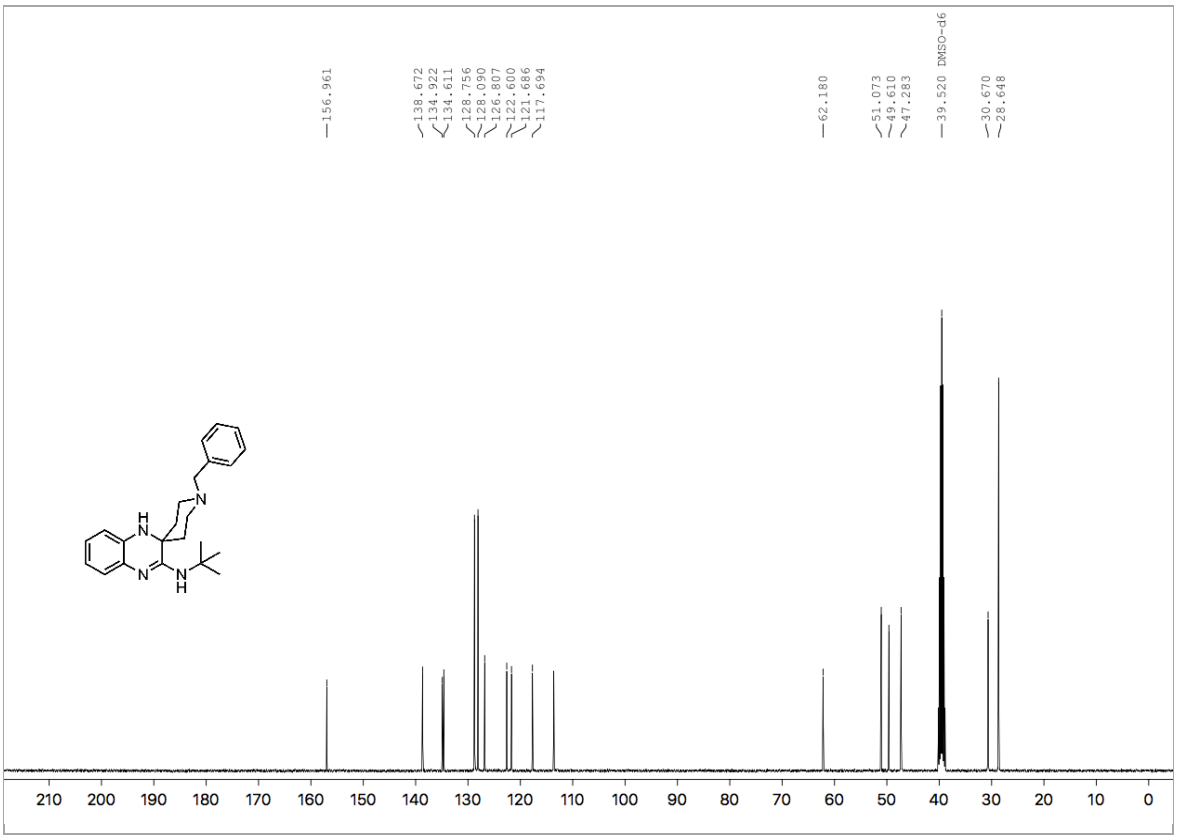
156.961
138.672
134.922
134.611
128.756
128.090
126.807
122.600
121.686
117.694
62.180
51.073
49.610
47.283
39.520 DMSO-d6
30.670
28.648

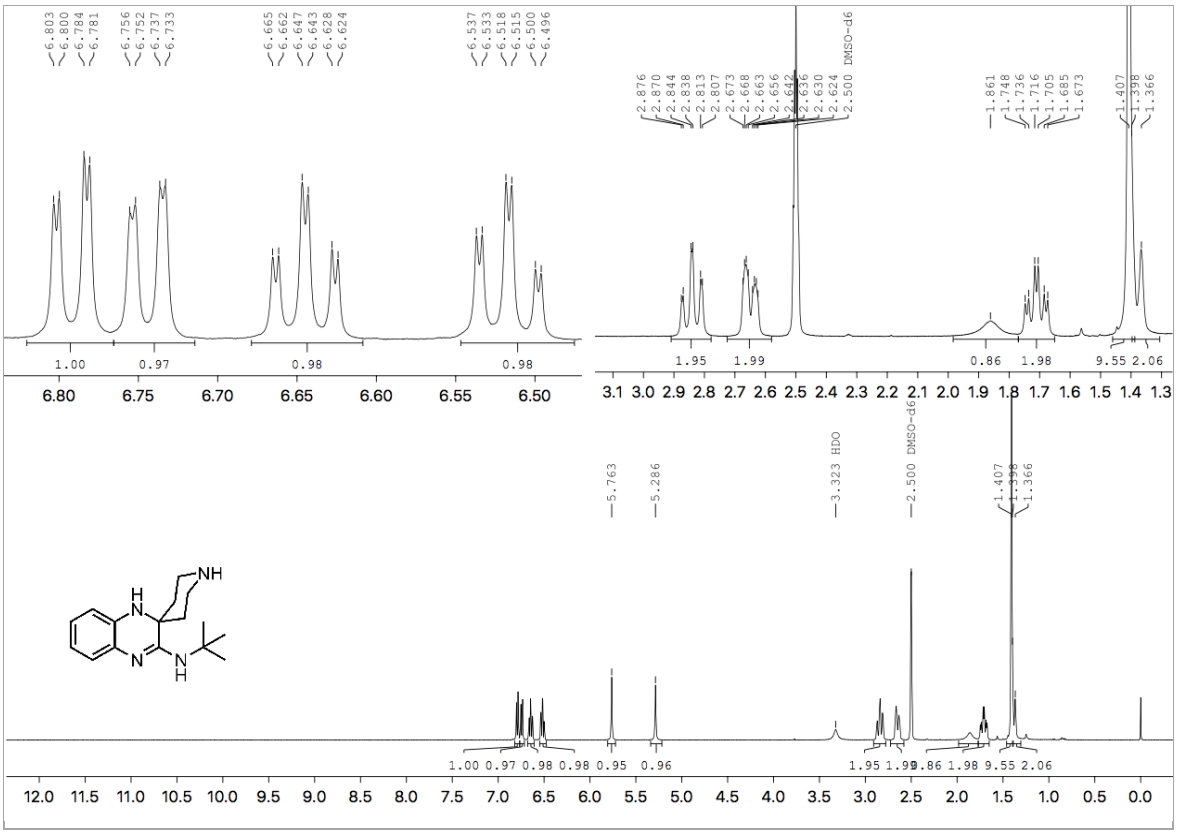
6.803
6.800
6.784
6.781
6.756
6.752
6.737
6.733
6.665
6.662
6.647
6.643
6.628
6.624
6.537
6.533
6.518
6.515
6.500
6.496
2.876
2.870
2.844
2.838
2.813
2.807
2.673
2.668
2.663
2.656
2.642
2.636
2.630
2.624
2.500 DMSO-d6
1.861
1.748
1.736
1.716
1.705
1.685
1.673
1.407
1.398
1.366
1.00 0.97 0.98 0.98
1.95 1.99 0.86 1.98 9.55 2.06
5.763
5.286
3.323 HDO
2.500 DMSO-d6
1.407
1.398
1.366
1.00 0.97 0.98 0.98 0.95 0.96
1.95 1.99 0.86 1.98 9.55 2.06
NH
H
N
N
H

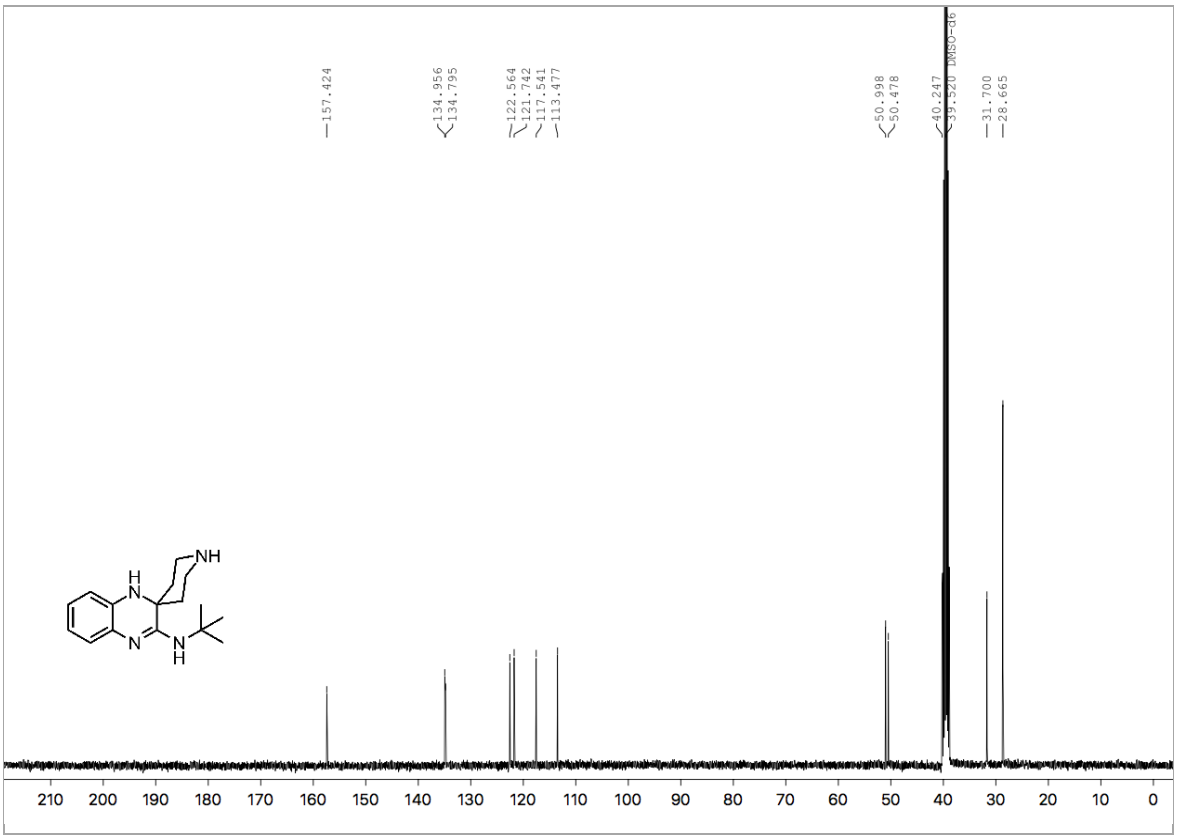
157.424
134.956
134.795
122.564
121.742
117.541
113.477
50.998
50.478
40.247
39.520 DMSO-d6
31.700
28.665
NH
H
N
N
H

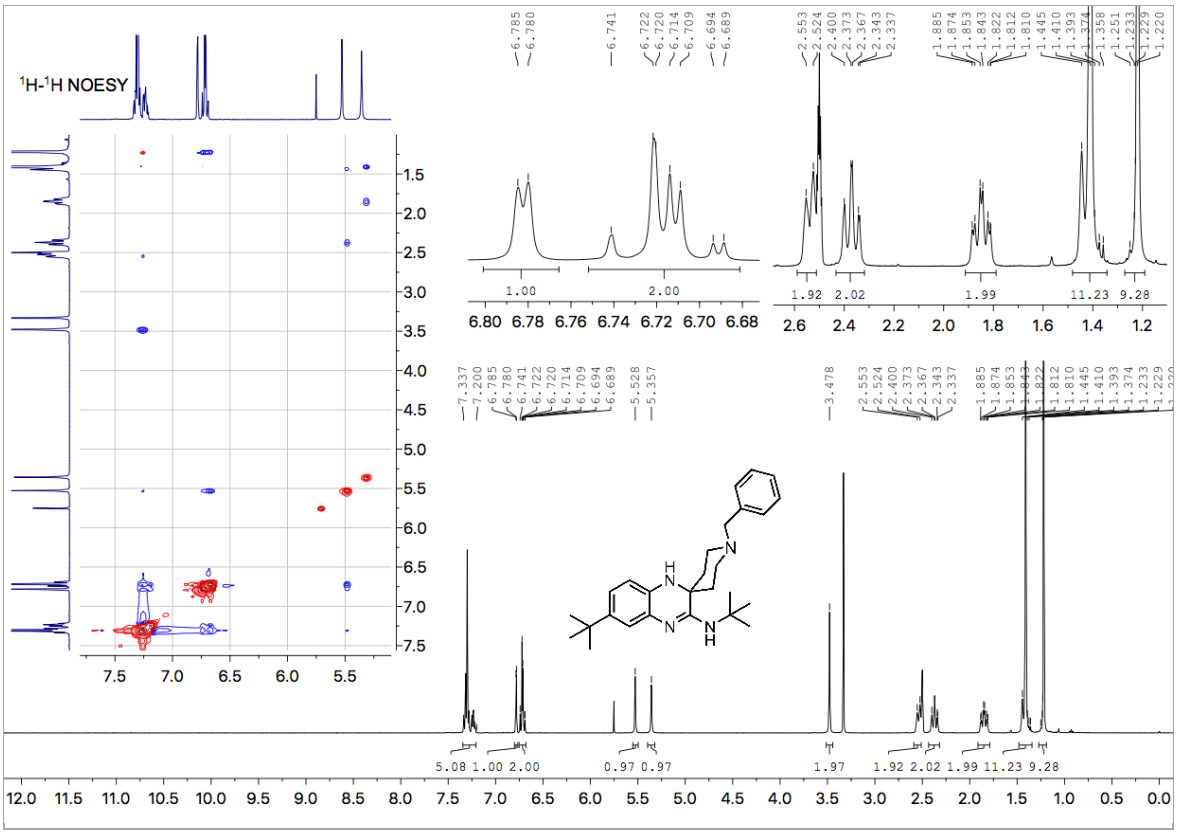
^{1}H-^{1}H NOESY

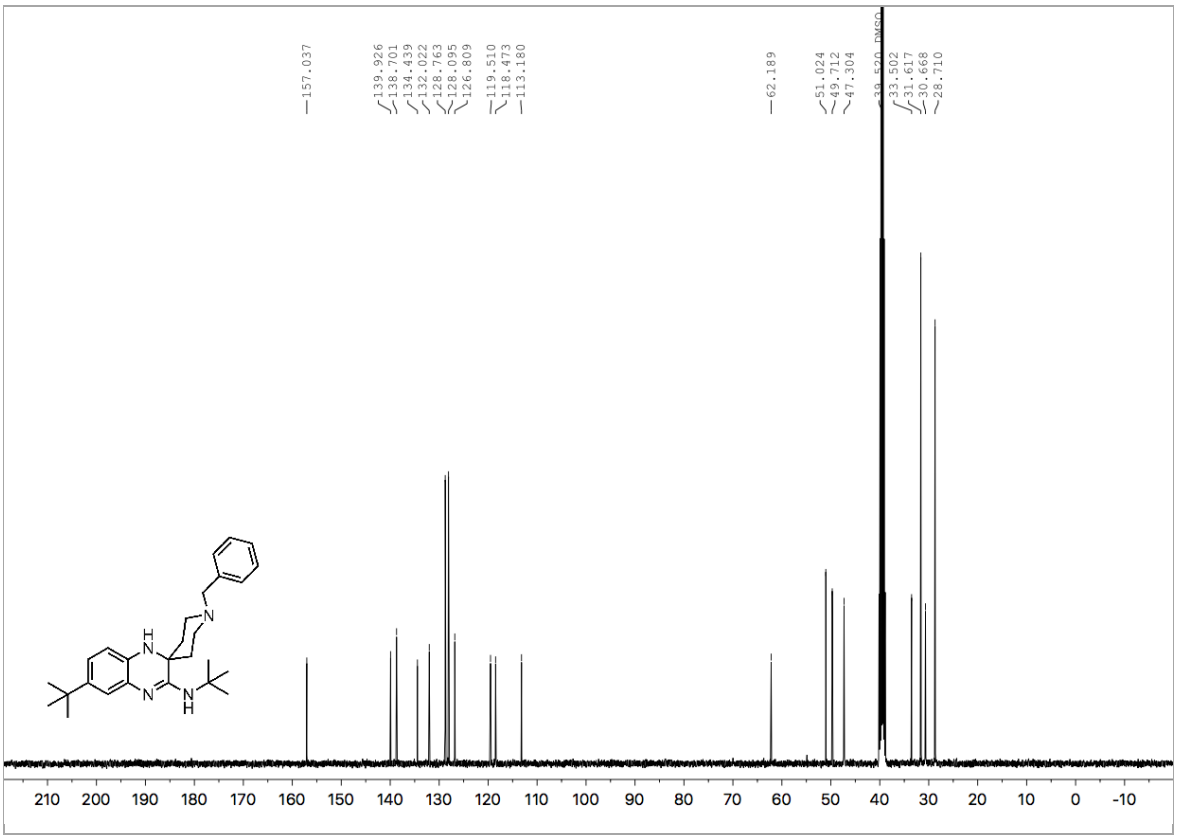

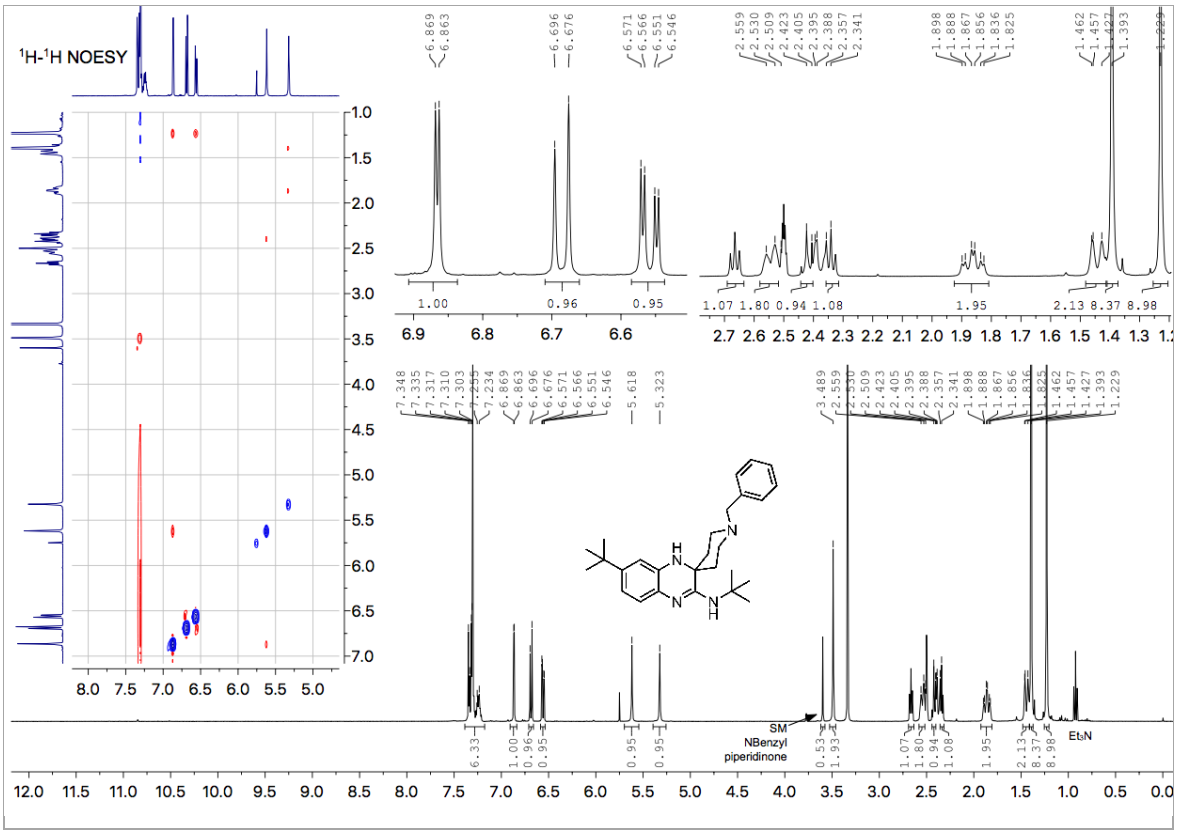
^{1}H-^{1}H NOESY
SM
NBenzyl
piperidinone
Et$_3$N

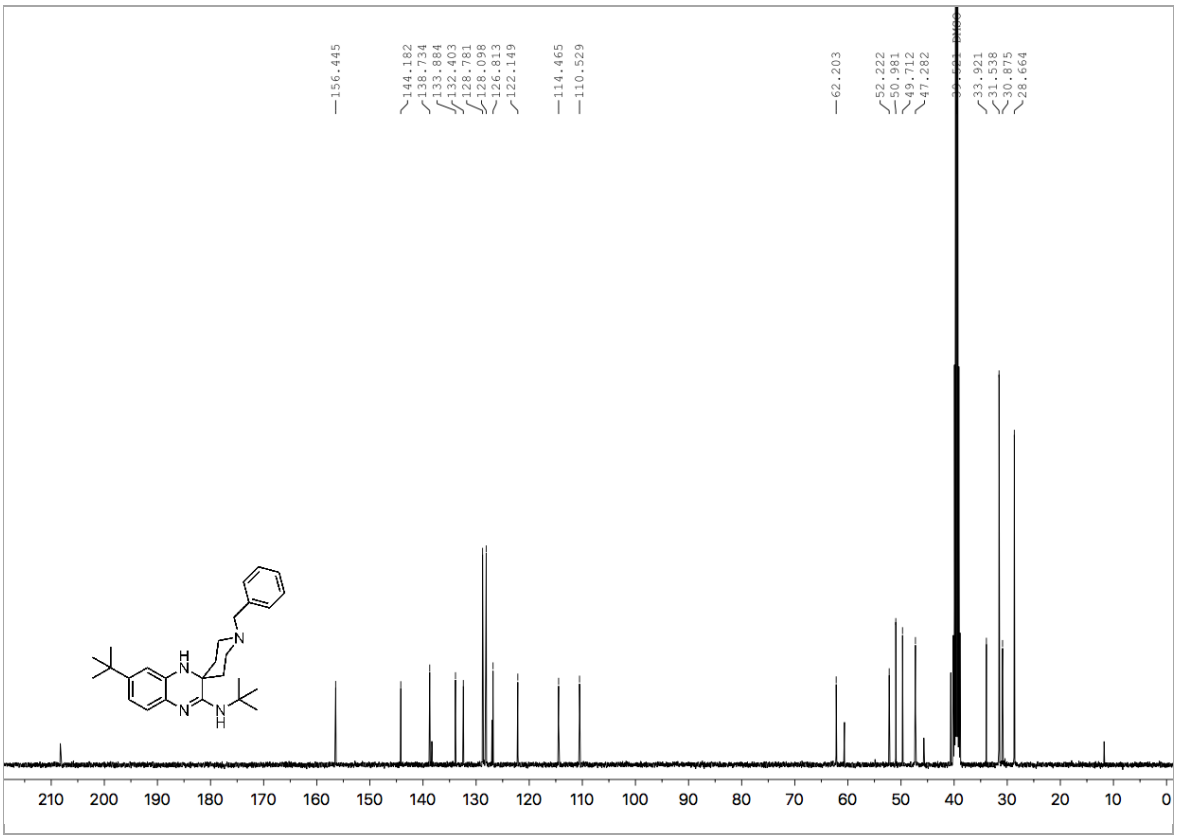

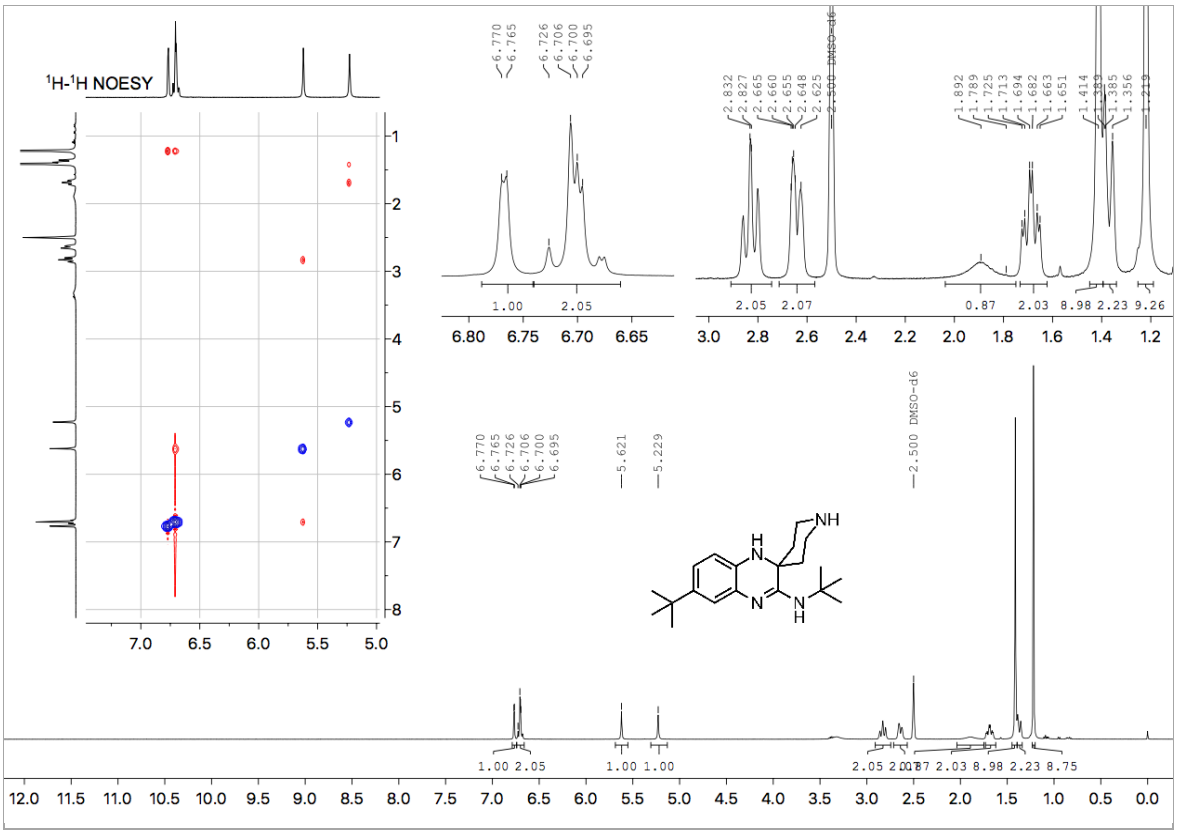
^{1}H-^{1}H NOESY
6.770
6.765
6.726
6.706
6.700
6.695
2.832
2.827
2.665
2.660
2.655
2.648
2.625
2.500 DMSO-d6
1.892
1.789
1.725
1.713
1.694
1.682
1.663
1.651
1.414
1.385
1.356
1.219
1.00 2.05
2.05 2.07
0.87 2.03 8.98 2.23 9.26
5.621
5.229
1.00 1.00
2.05 2.07 2.03 8.98 2.23 8.75
NH
H
N
N
H

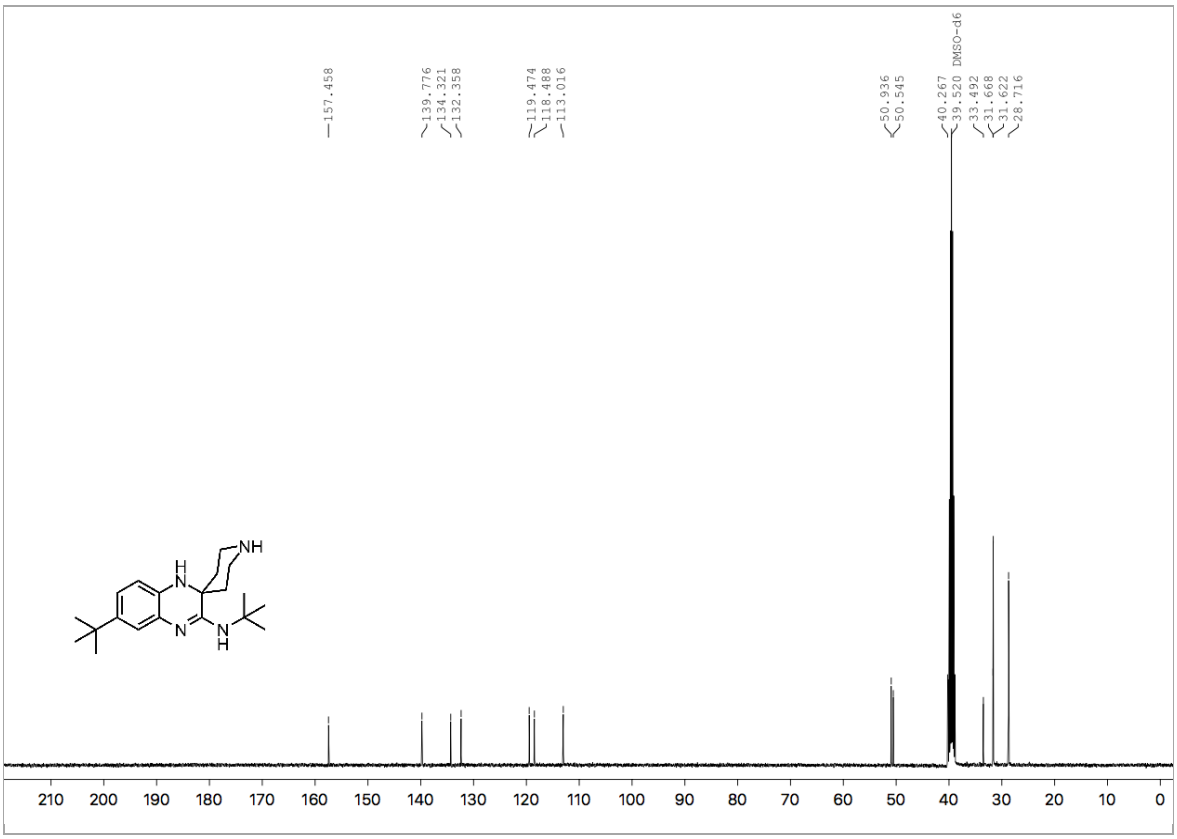
157.458
139.776
134.321
132.358
119.474
118.488
113.016
50.936
50.545
40.267
39.520 DMSO-d6
33.492
31.668
31.622
28.716
NH
H
N
N
H

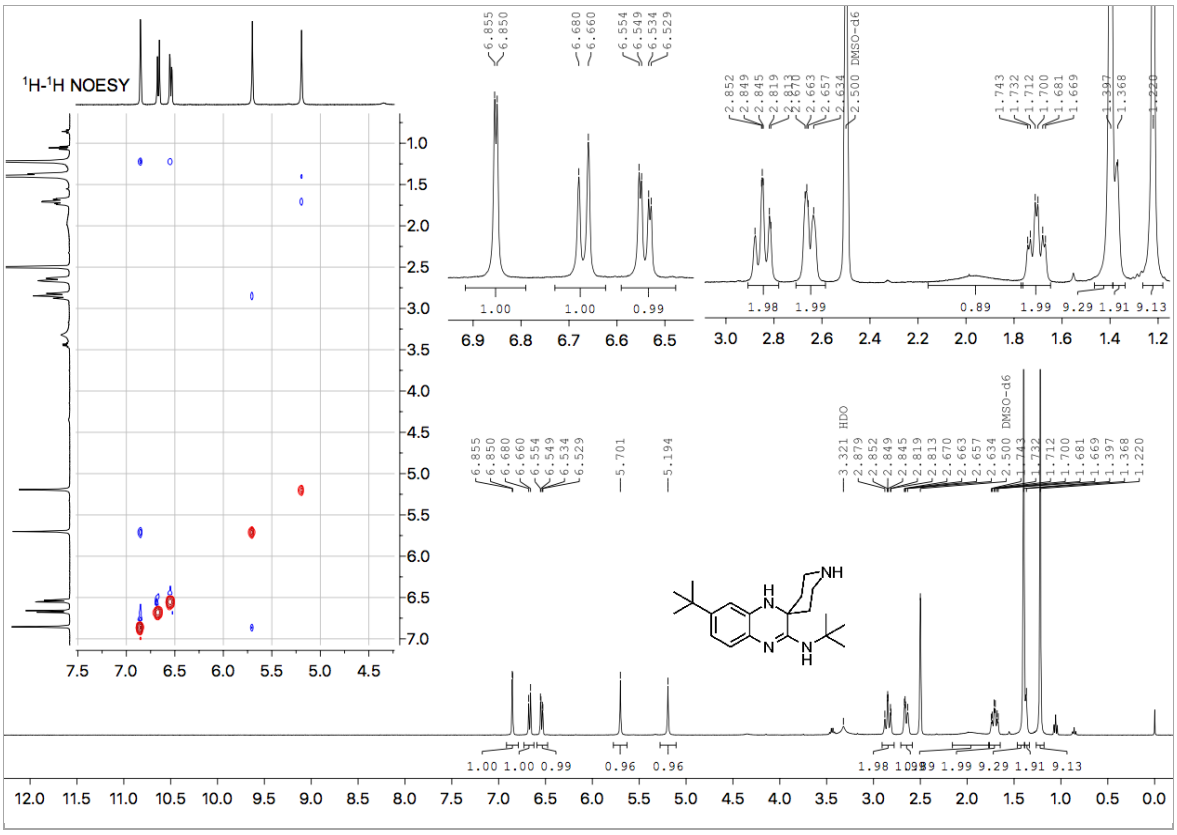
^{1}H-^{1}H NOESY
DMSO-d6
HDO

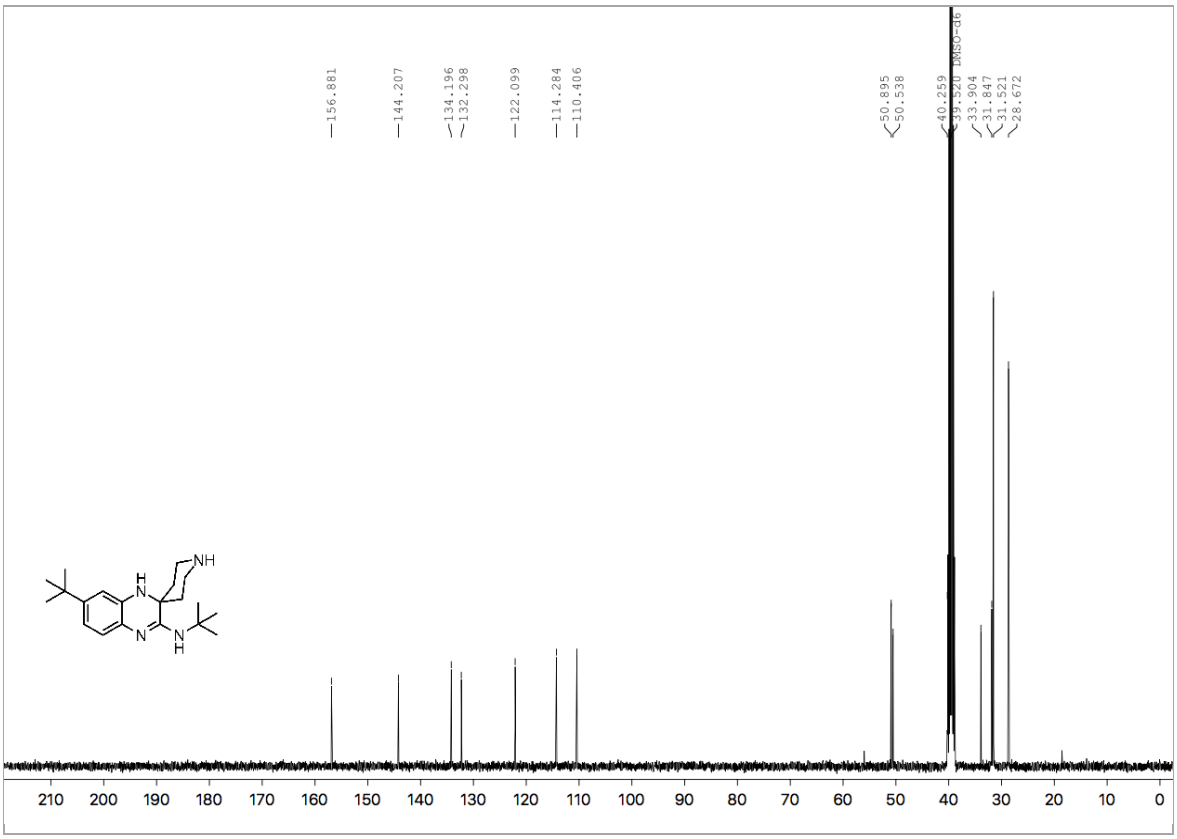
DMSO-d6

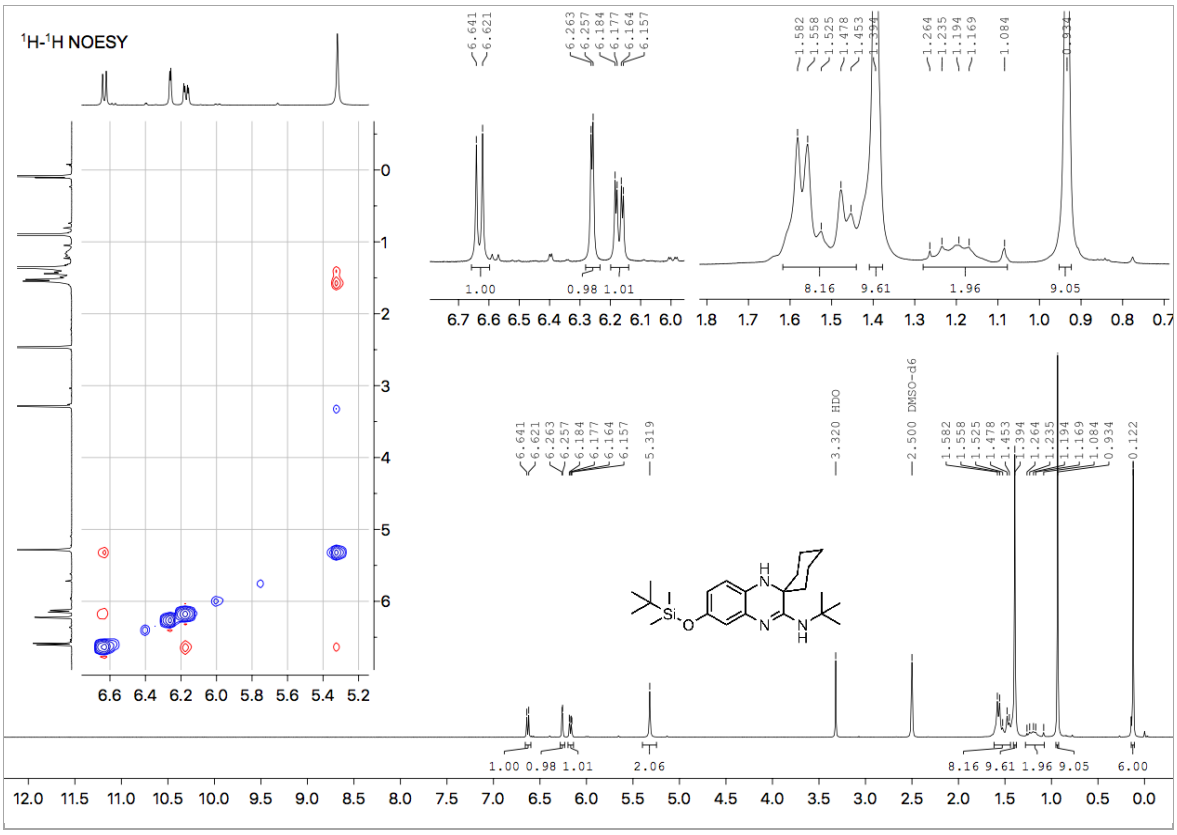
^{1}H-^{1}H NOESY
6.641
6.621
6.263
6.257
6.184
6.177
6.164
6.157
1.582
1.558
1.525
1.478
1.453
1.394
1.264
1.235
1.194
1.169
1.084
0.934
1.00
0.98 1.01
8.16
9.61
1.96
9.05
5.319
3.320 HDO
2.500 DMSO-d6
0.122
2.06
6.00

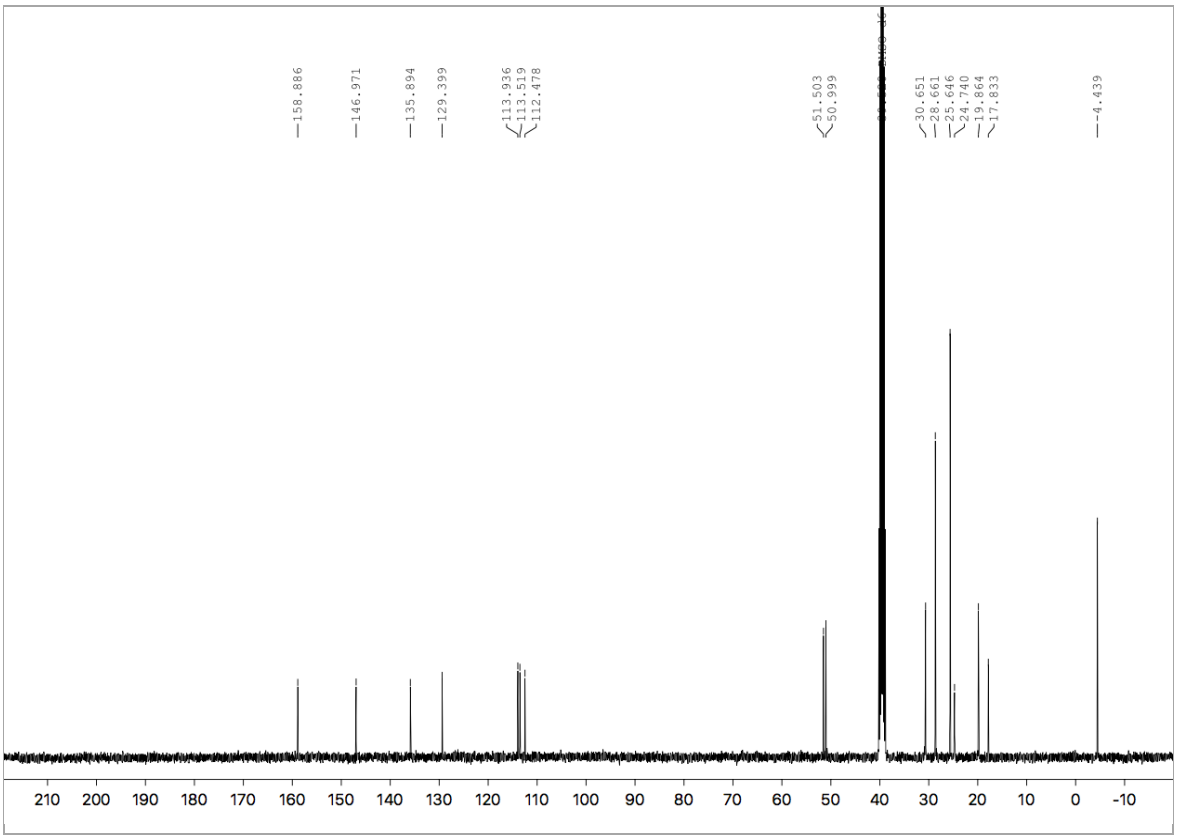
158.886
146.971
135.894
129.399
113.936
113.519
112.478
51.503
50.999
30.651
28.661
25.646
24.740
19.864
17.833
-4.439

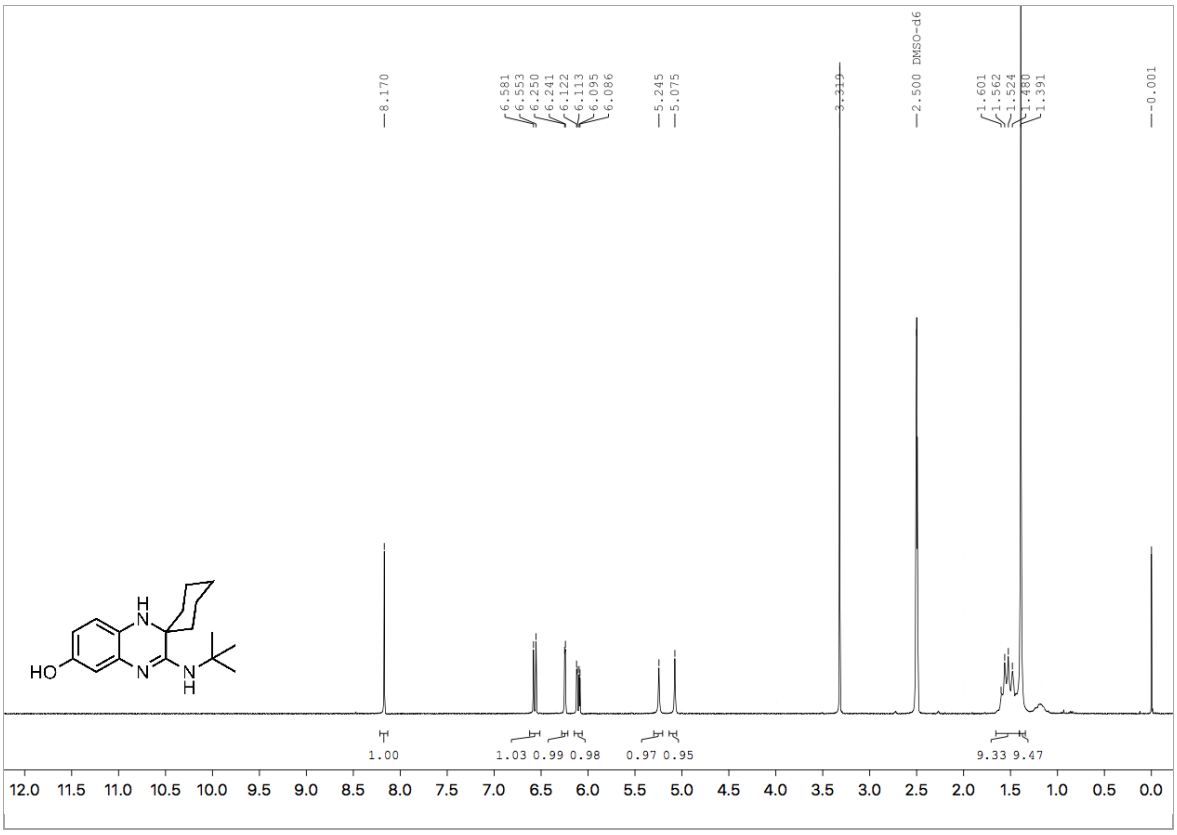
8.170
6.581
6.553
6.250
6.241
6.122
6.113
6.095
6.086
5.245
5.075
3.319
2.500 DMSO-d6
1.601
1.562
1.524
1.480
1.391
0.001
1.00
1.03 0.99 0.98
0.97 0.95
9.33 9.47
HO
N
H
N
N
H

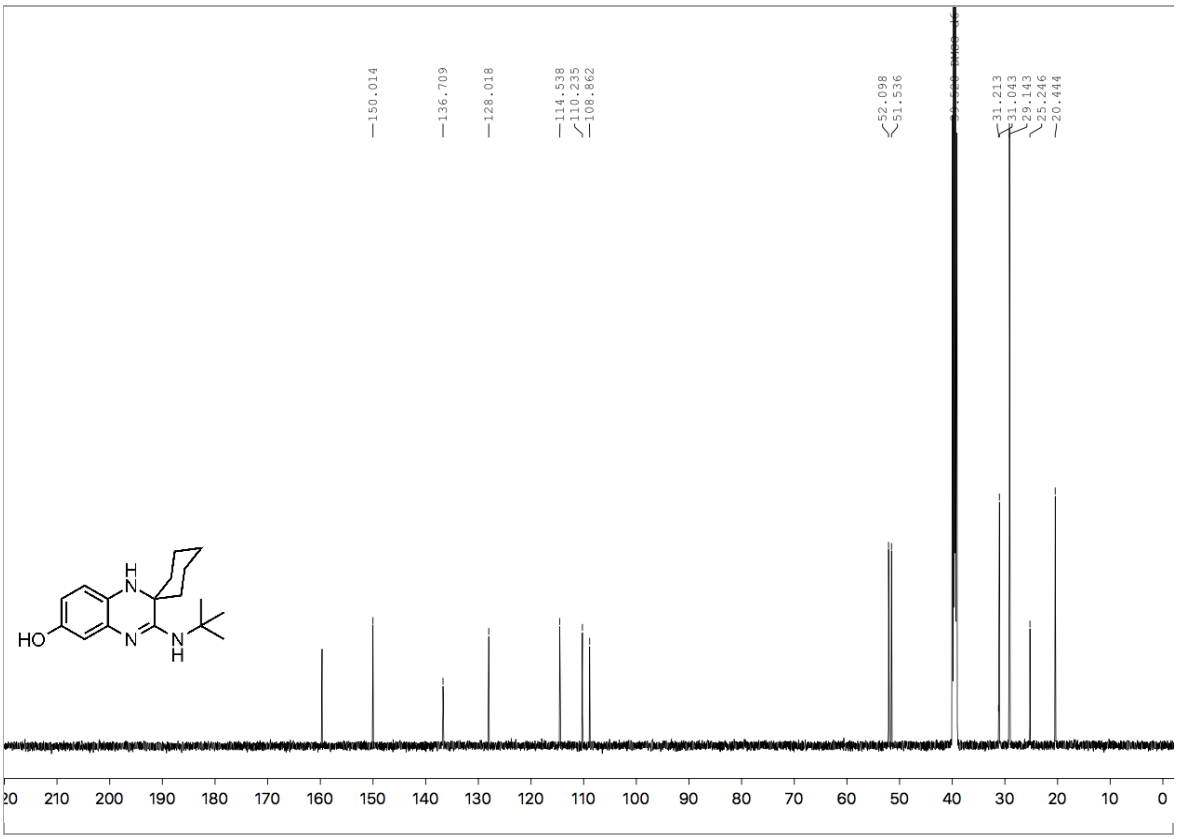
150.014
136.709
128.018
114.538
110.235
108.862
52.098
51.536
39.506 DMSO-d6
31.213
31.043
29.143
25.246
20.444
HO
N
H
N
N
H

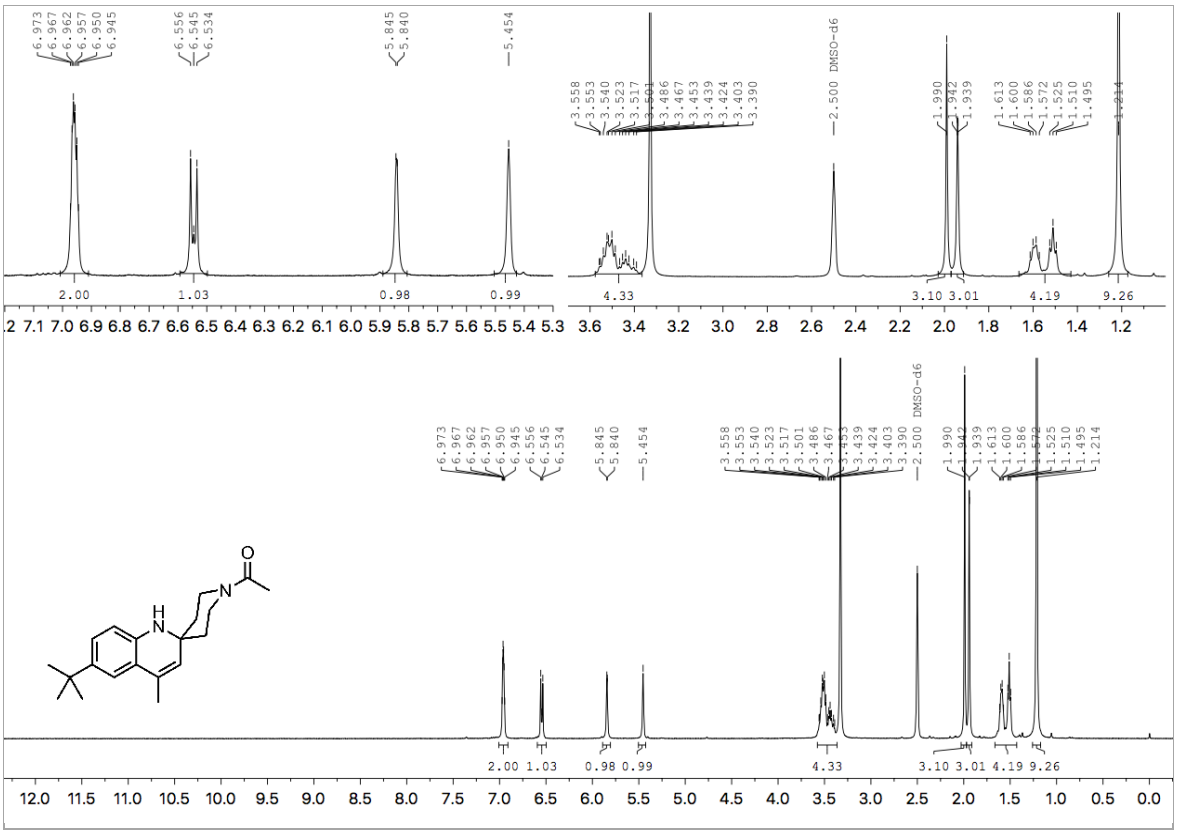
6.973
6.967
6.962
6.957
6.950
6.945
6.556
6.545
6.534
5.845
5.840
5.454
3.558
3.553
3.540
3.523
3.517
3.501
3.486
3.467
3.453
3.439
3.424
3.403
3.390
2.500 DMSO-d6
1.990
1.942
1.939
1.613
1.600
1.586
1.572
1.525
1.510
1.495
1.214
2.00 1.03 0.98 0.99
4.33
3.10 3.01 4.19 9.26

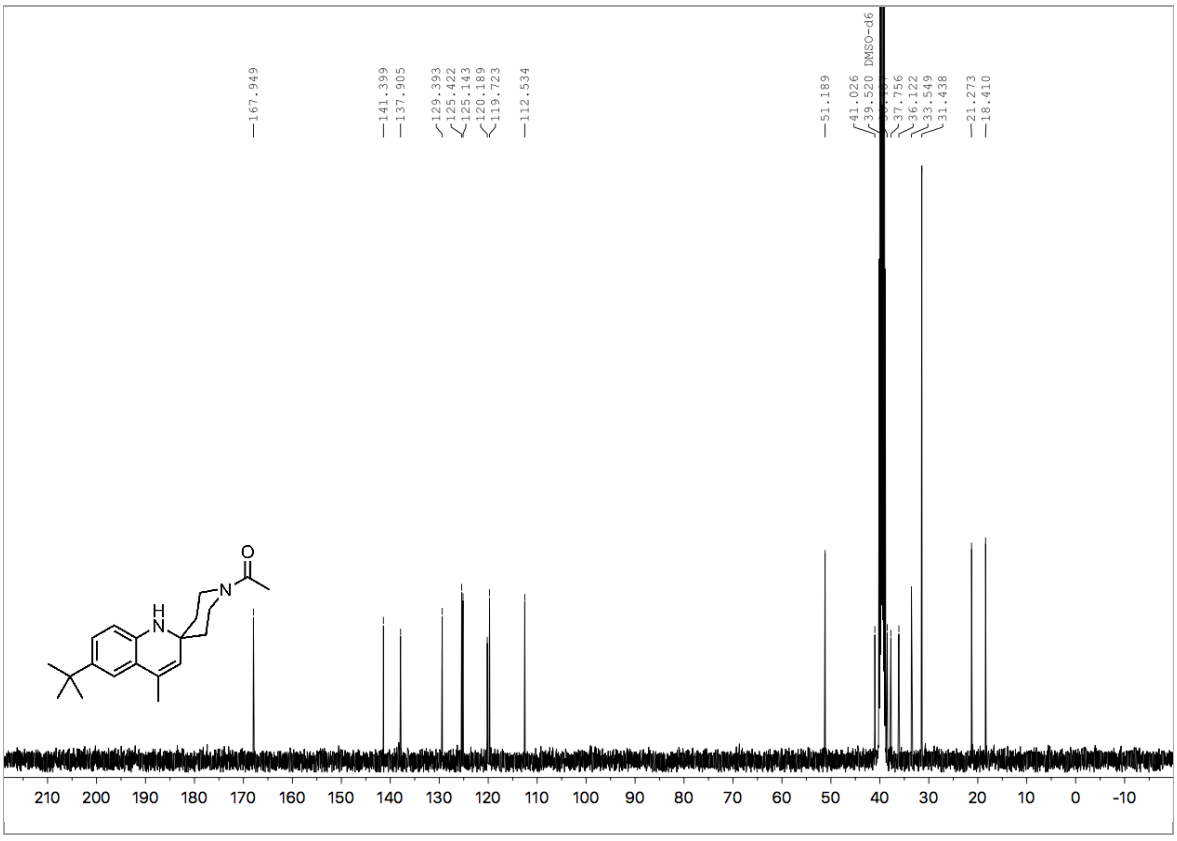
167.949
141.399
137.905
129.393
125.422
125.143
120.189
119.723
112.534
51.189
41.026
39.520 DMSO-d6
37.756
36.122
33.549
31.438
21.273
18.410

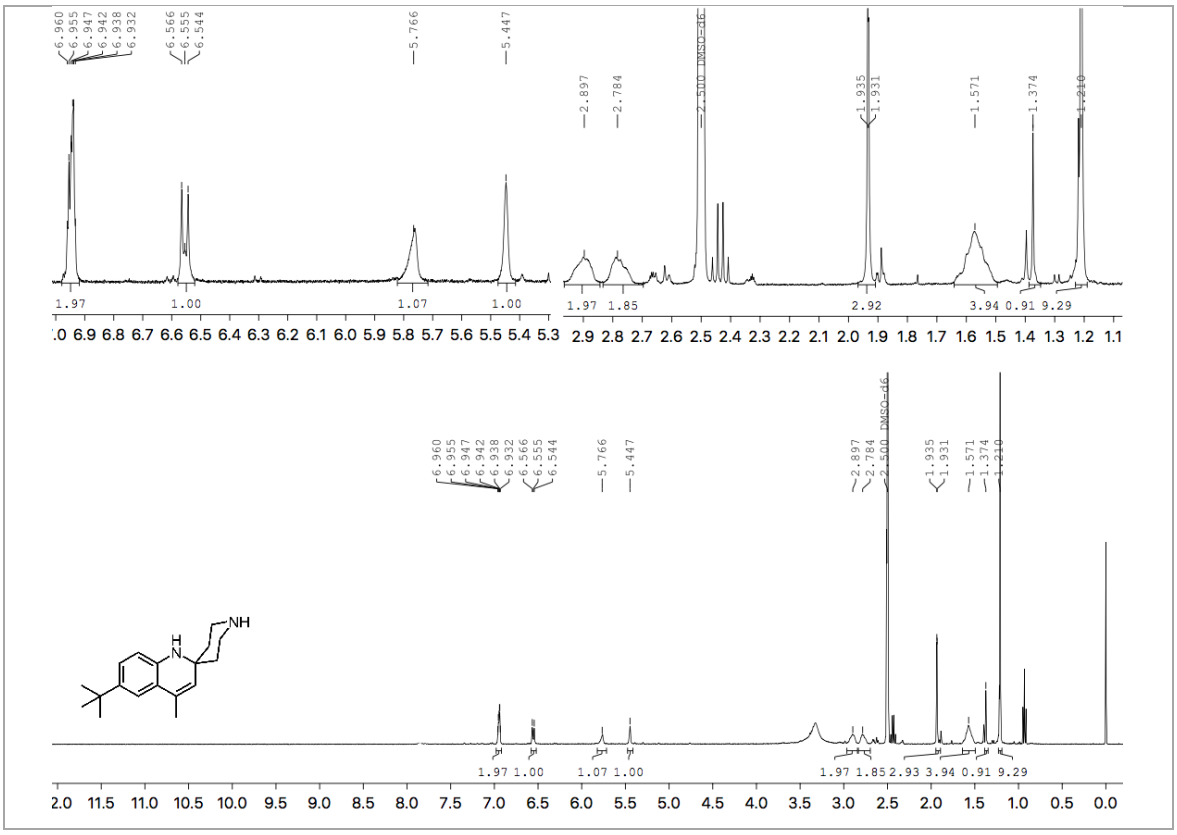
6.960
6.955
6.947
6.942
6.938
6.932
6.566
6.555
6.544
5.766
5.447
2.897
2.784
2.510 DMSO-d6
1.935
1.931
1.571
1.374
1.210
NH
H
N
1.97 1.00 1.07 1.00 1.97 1.85 2.92 3.94 0.91 9.29

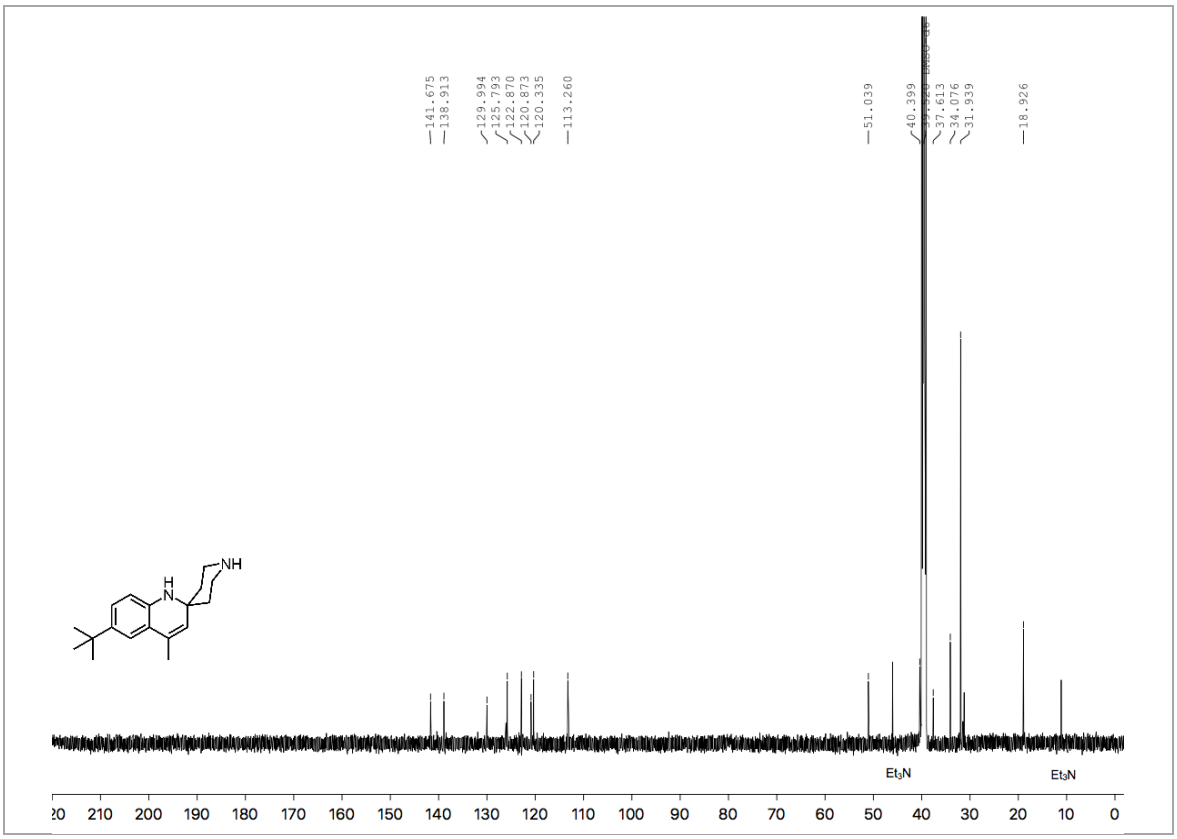
141.675
138.913
129.994
125.793
122.870
120.873
120.335
113.260
51.039
40.399
37.613
34.076
31.939
18.926
NH
H
N
Et3N
Et3N

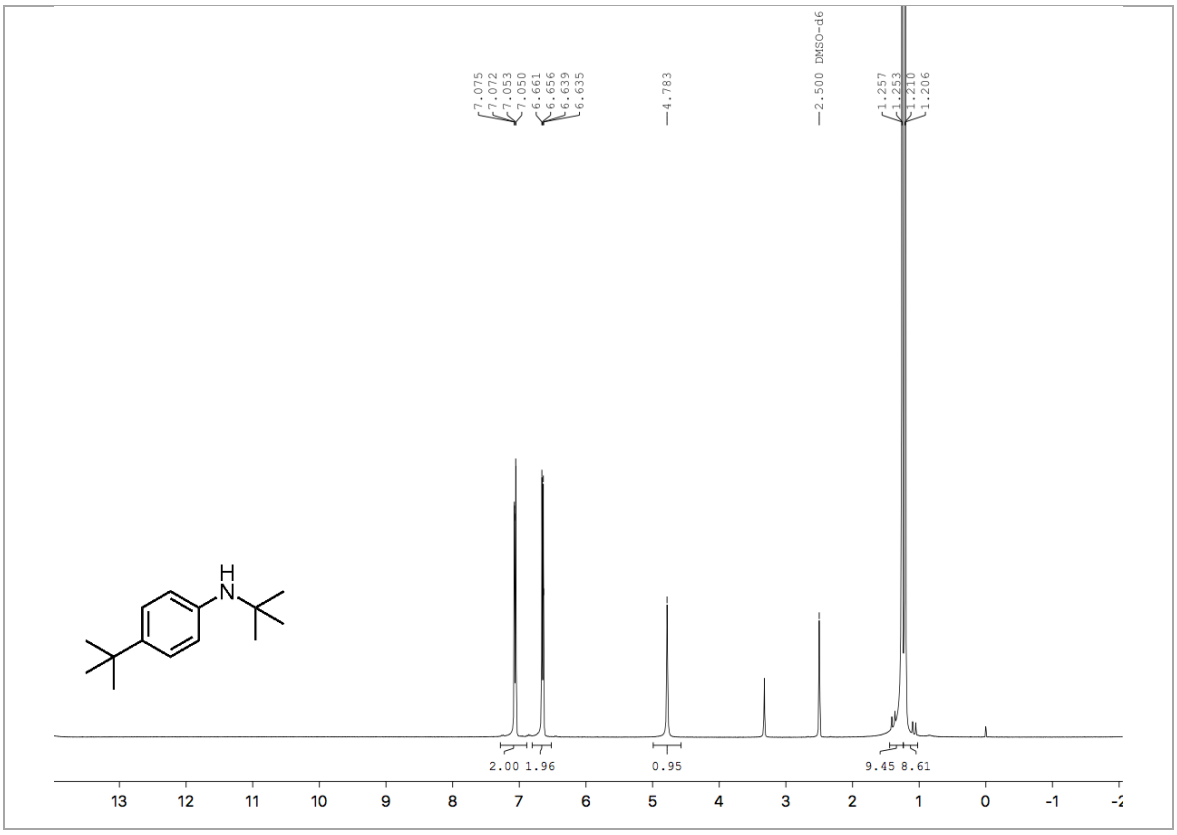
7.075
7.072
7.053
7.050
6.661
6.656
6.639
6.635
4.783
2.500 DMSO-d6
1.257
1.253
1.210
1.206
2.00 1.96
0.95
9.45 8.61
13 12 11 10 9 8 7 6 5 4 3 2 1 0 -1

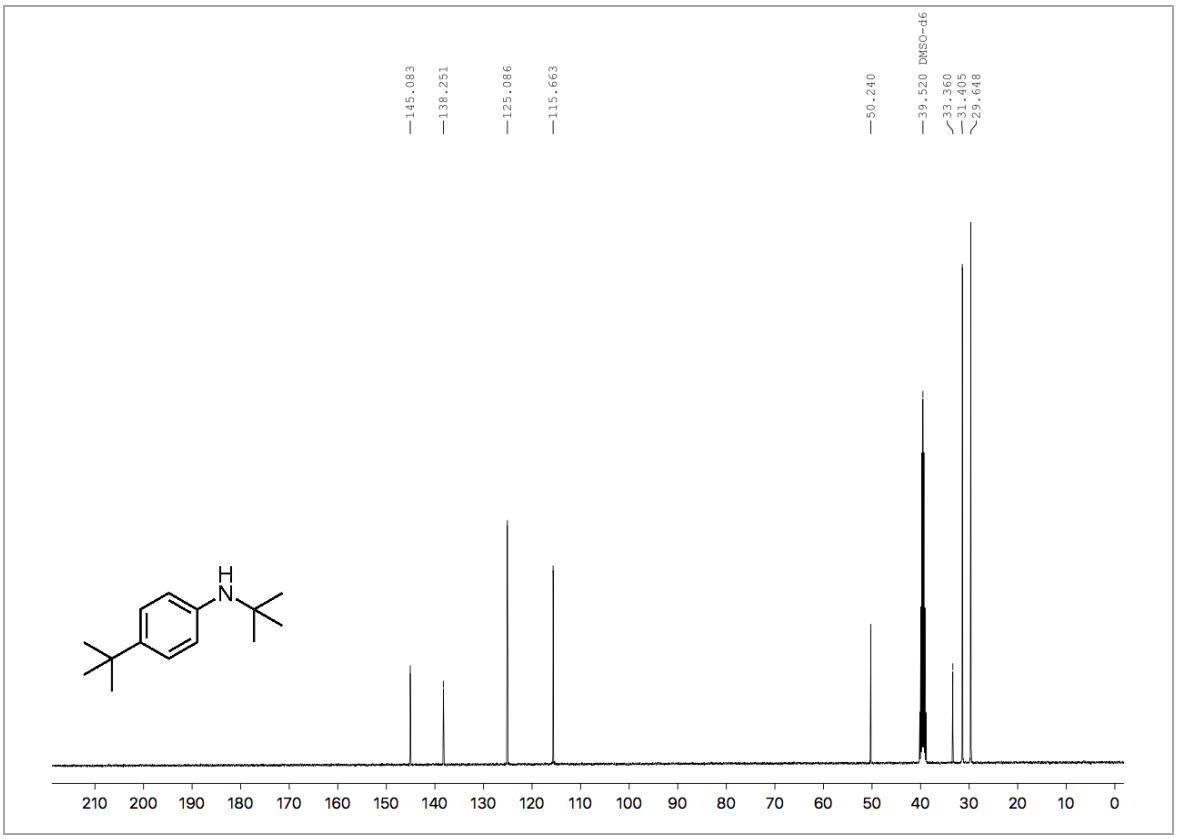
145.083
138.251
125.086
115.663
50.240
39.520 DMSO-d6
33.360
31.405
29.648
210 200 190 180 170 160 150 140 130 120 110 100 90 80 70 60 50 40 30 20 10 0

Appendix 2: NMR Spectra for Chapter 3

The following appendix contains NMR spectra for the new compounds in Chapter 3.

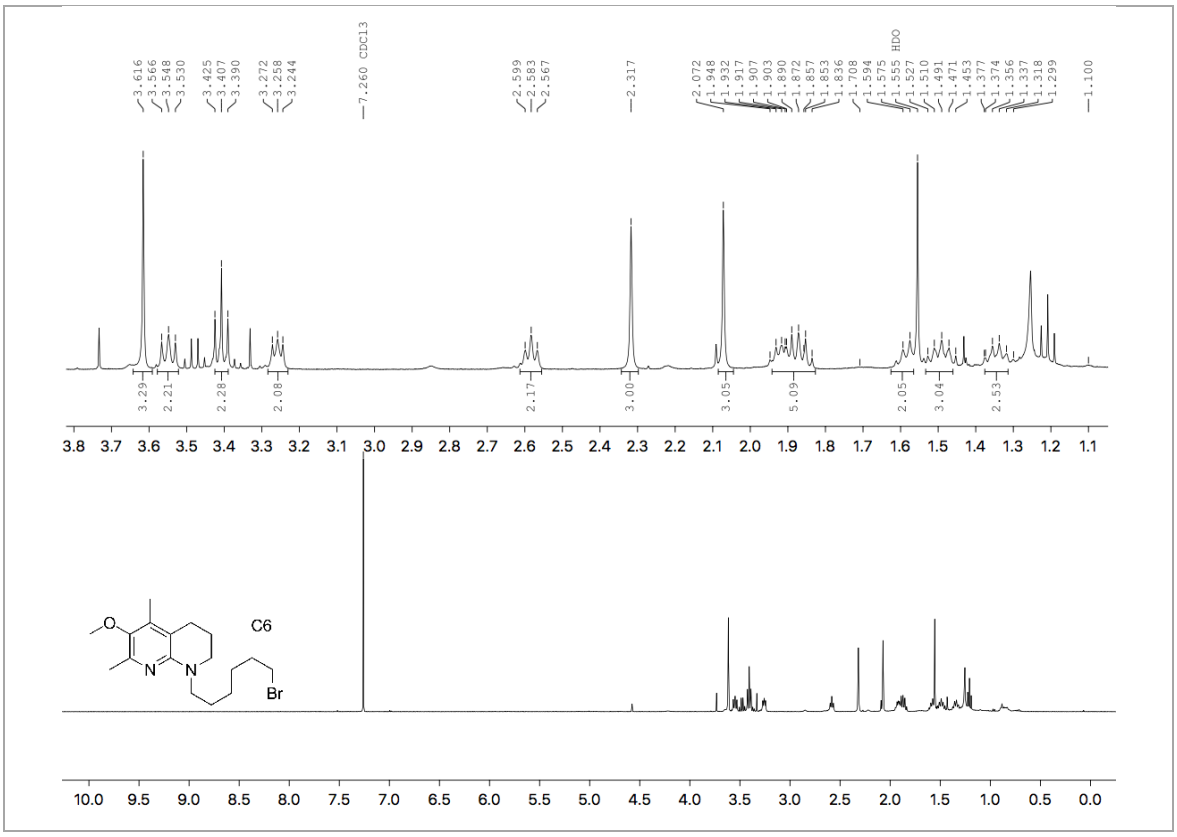
3.616
3.566
3.548
3.530
3.425
3.407
3.390
3.272
3.258
3.244
7.260 CDCl3
2.599
2.583
2.567
2.317
2.072
1.948
1.932
1.917
1.907
1.903
1.890
1.872
1.857
1.853
1.836
1.708
1.594
1.575
1.555
HDO
1.527
1.510
1.491
1.471
1.453
1.377
1.374
1.356
1.337
1.318
1.299
1.100
3.29
2.21
2.28
2.08
2.17
3.00
3.05
5.09
2.05
3.04
2.53
C6
O
N
N
Br

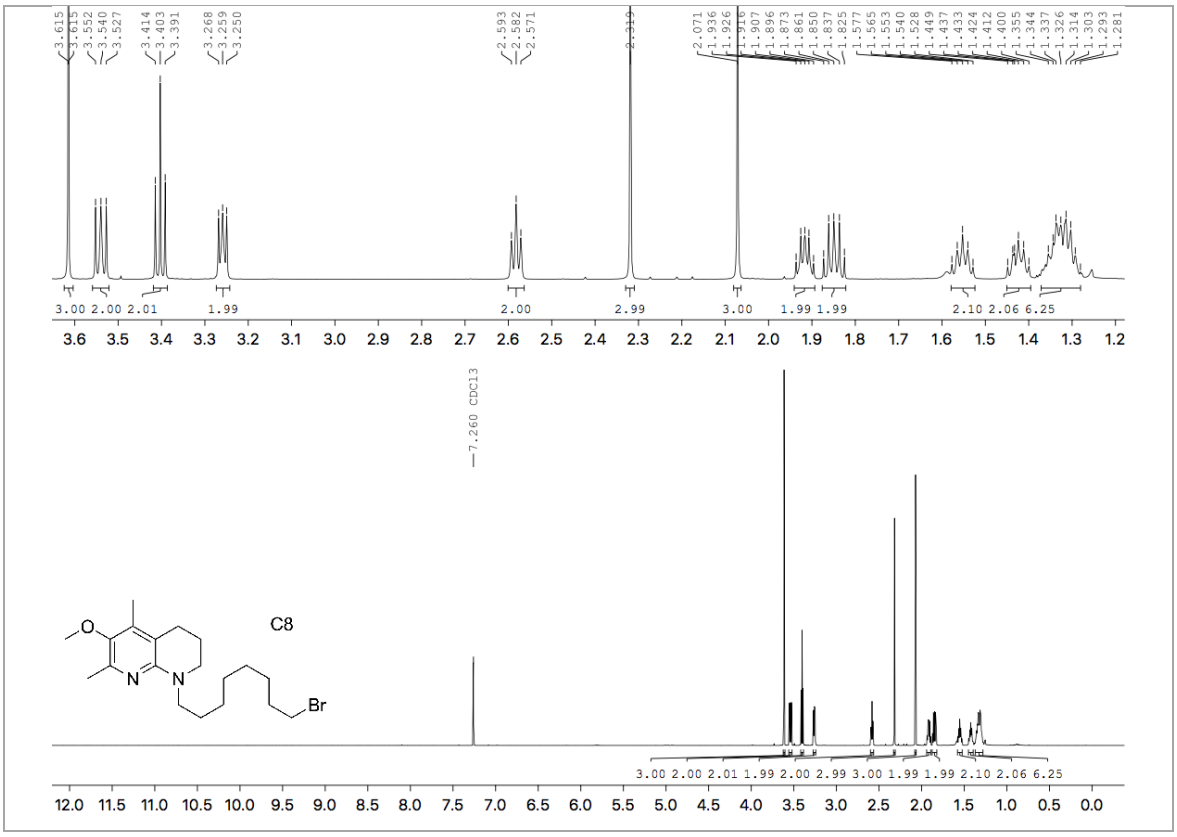
3.615
3.552
3.540
3.527
3.414
3.403
3.391
3.268
3.259
3.250
2.593
2.582
2.571
2.319
2.071
1.936
1.926
1.916
1.907
1.896
1.873
1.861
1.850
1.837
1.825
1.577
1.565
1.553
1.540
1.528
1.449
1.437
1.433
1.424
1.412
1.400
1.355
1.344
1.337
1.326
1.314
1.303
1.293
1.281
3.00 2.00 2.01 1.99 2.00 2.99 3.00 1.99 1.99 2.10 2.06 6.25
7.260 CDCl3
C8
O
N
N
Br
3.00 2.00 2.01 1.99 2.00 2.99 3.00 1.99 1.99 2.10 2.06 6.25

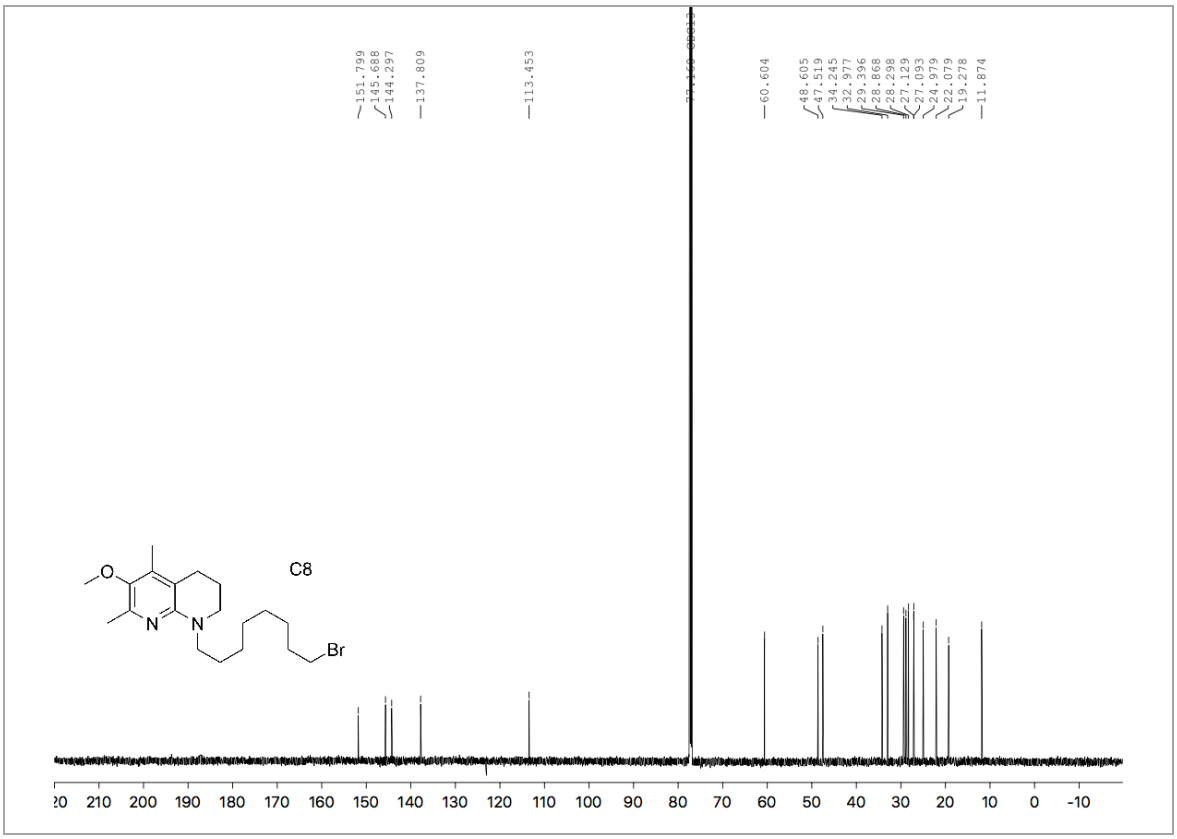
151.799
145.688
144.297
137.809
113.453
77.160 CDCl3
60.604
48.605
47.519
34.245
32.977
29.396
28.868
28.298
27.129
27.093
24.979
22.079
19.278
11.874
C8
O
N
N
Br

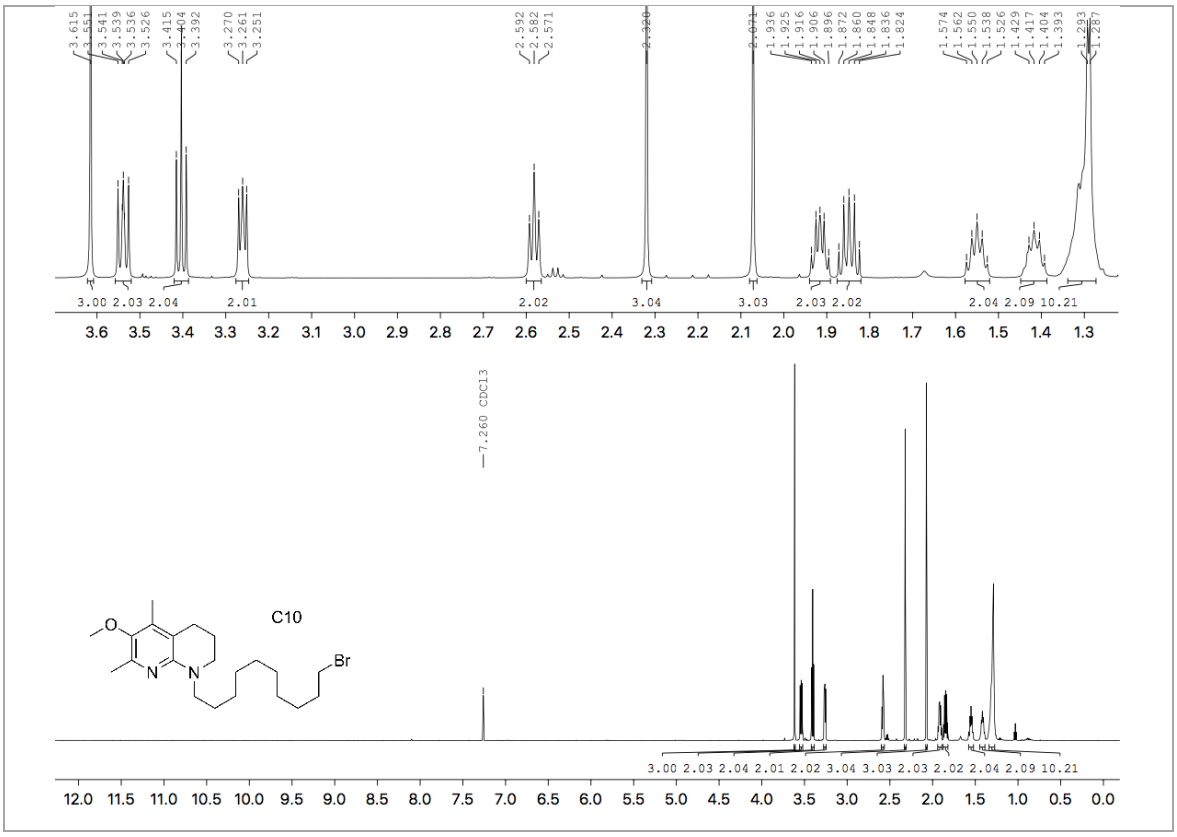
3.615
3.541
3.539
3.536
3.526
3.415
3.404
3.392
3.270
3.261
3.251
2.592
2.582
2.571
2.320
2.071
1.936
1.925
1.916
1.906
1.896
1.872
1.860
1.848
1.836
1.824
1.574
1.562
1.550
1.538
1.526
1.429
1.417
1.404
1.393
1.293
1.287
3.00 2.03 2.04 2.01 2.02 3.04 3.03 2.03 2.02 2.04 2.09 10.21
7.260 CDCl3
C10
Br
3.00 2.03 2.04 2.01 2.02 3.04 3.03 2.03 2.02 2.04 2.09 10.21

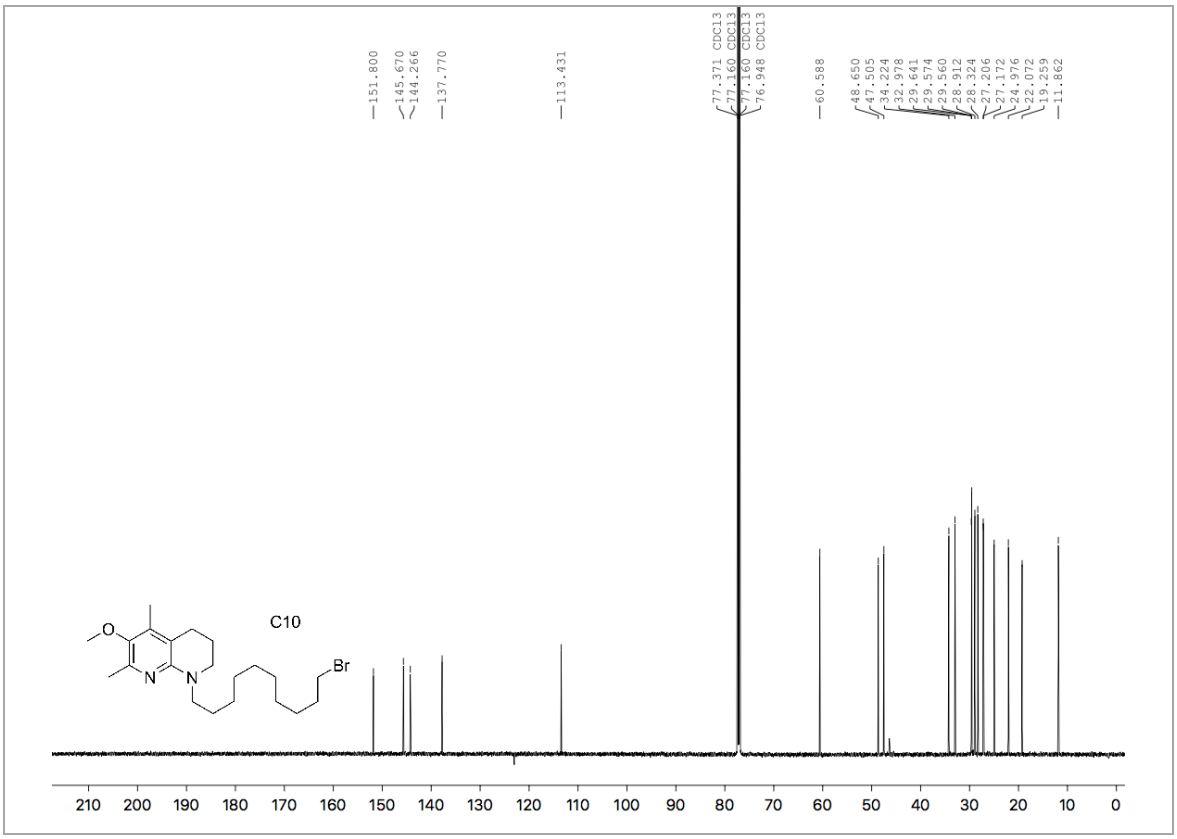
151.800
145.670
144.266
137.770
113.431
77.371 CDCl3
77.160 CDCl3
76.948 CDCl3
60.588
48.650
47.505
34.224
32.978
29.641
29.574
29.560
28.912
28.324
27.206
27.172
24.976
22.072
19.259
11.862
C10
Br

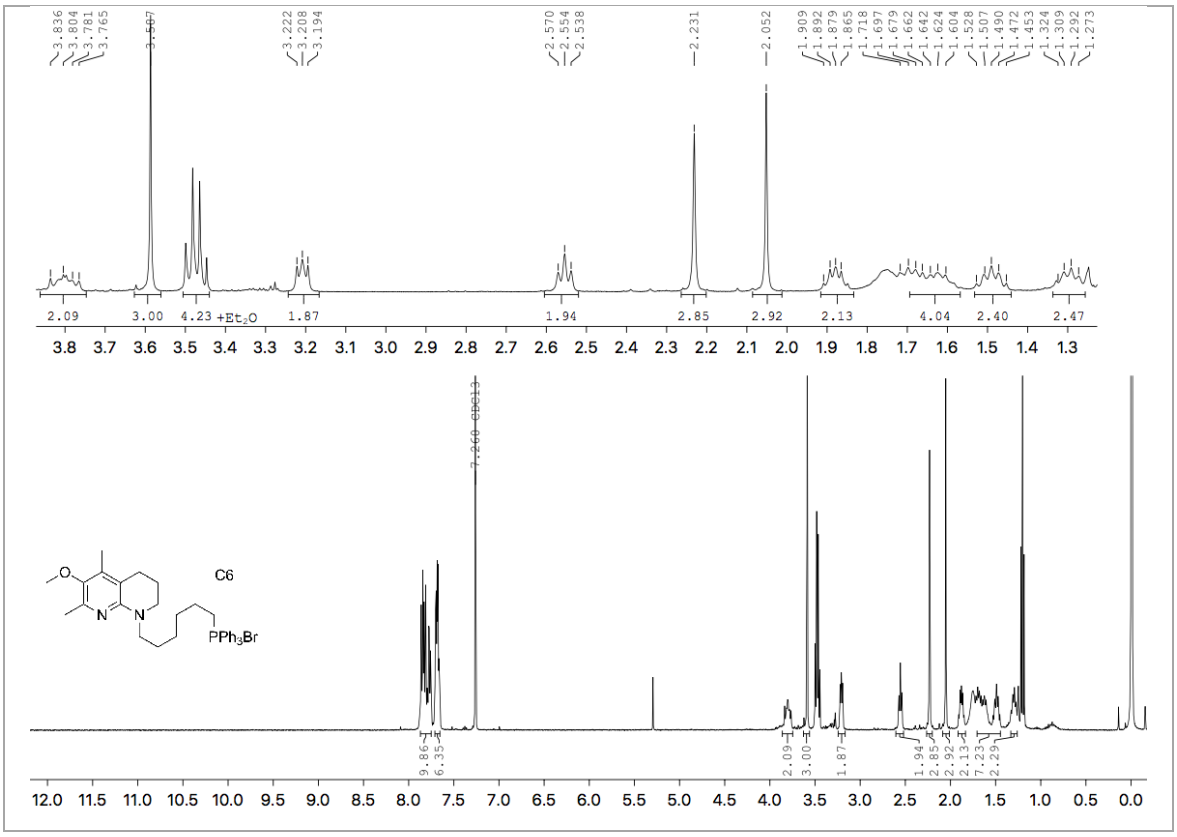
3.836
3.804
3.781
3.765
3.567
3.222
3.208
3.194
2.570
2.554
2.538
2.231
2.052
1.909
1.892
1.879
1.865
1.718
1.697
1.679
1.662
1.642
1.624
1.604
1.528
1.507
1.490
1.472
1.453
1.324
1.309
1.292
1.273
2.09
3.00
4.23 +Et2O
1.87
1.94
2.85
2.92
2.13
4.04
2.40
2.47
7.260
C6
PPh3Br
9.86
6.35
2.09
3.00
1.87
1.94
2.85
2.92
2.13
7.23
2.29

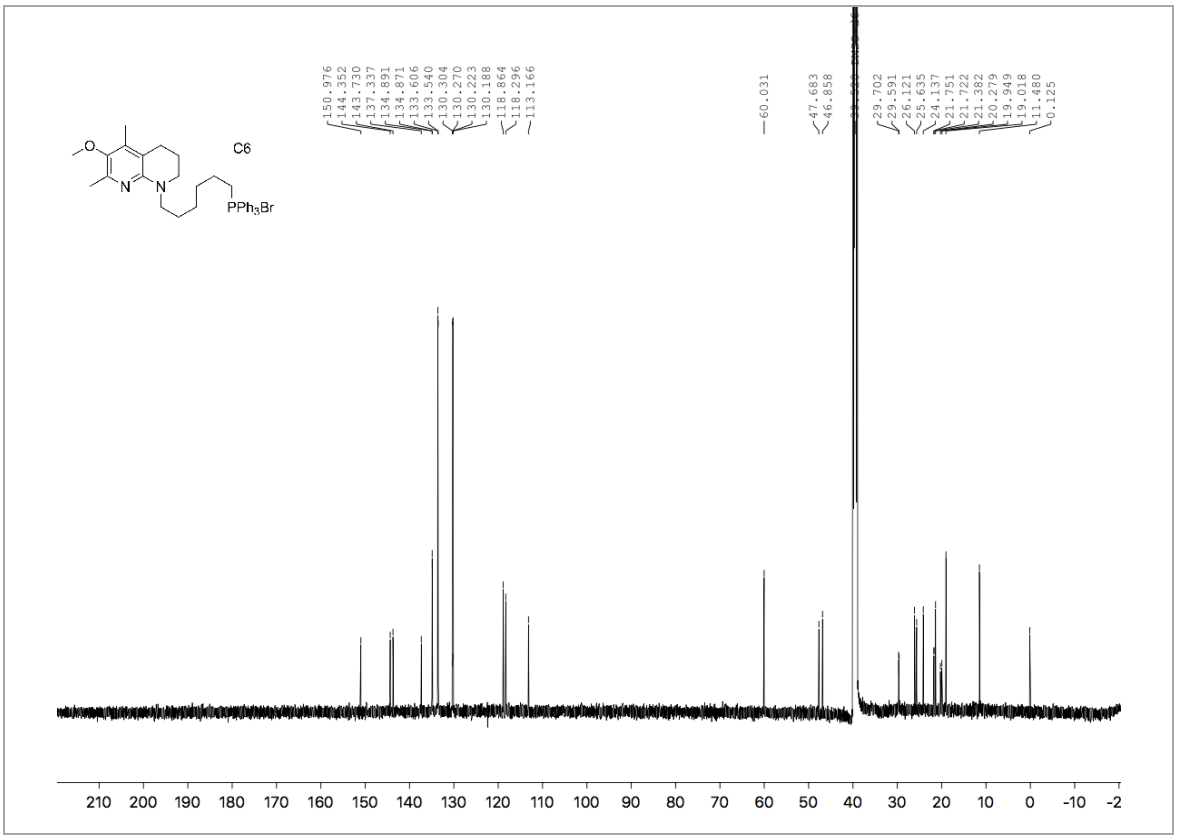
150.976
144.352
143.730
137.337
134.891
134.871
133.606
133.540
130.304
130.270
130.223
130.188
118.864
118.296
113.166
60.031
47.683
46.858
29.702
29.591
26.121
25.635
24.137
21.751
21.722
21.382
20.279
19.949
19.018
11.480
0.125
C6
PPh3Br

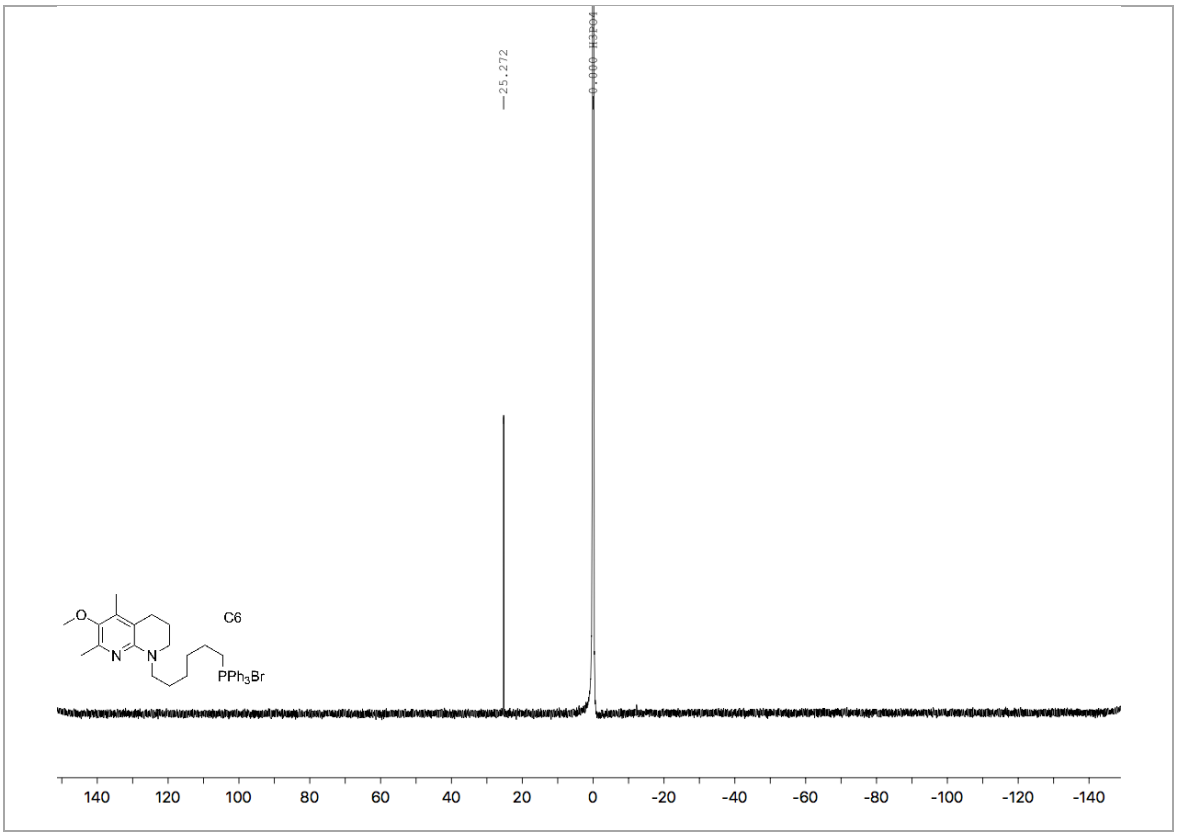
25.272
0.000
C6
PPh3Br
140
120
100
80
60
40
20
0
-20
-40
-60
-80
-100
-120
-140

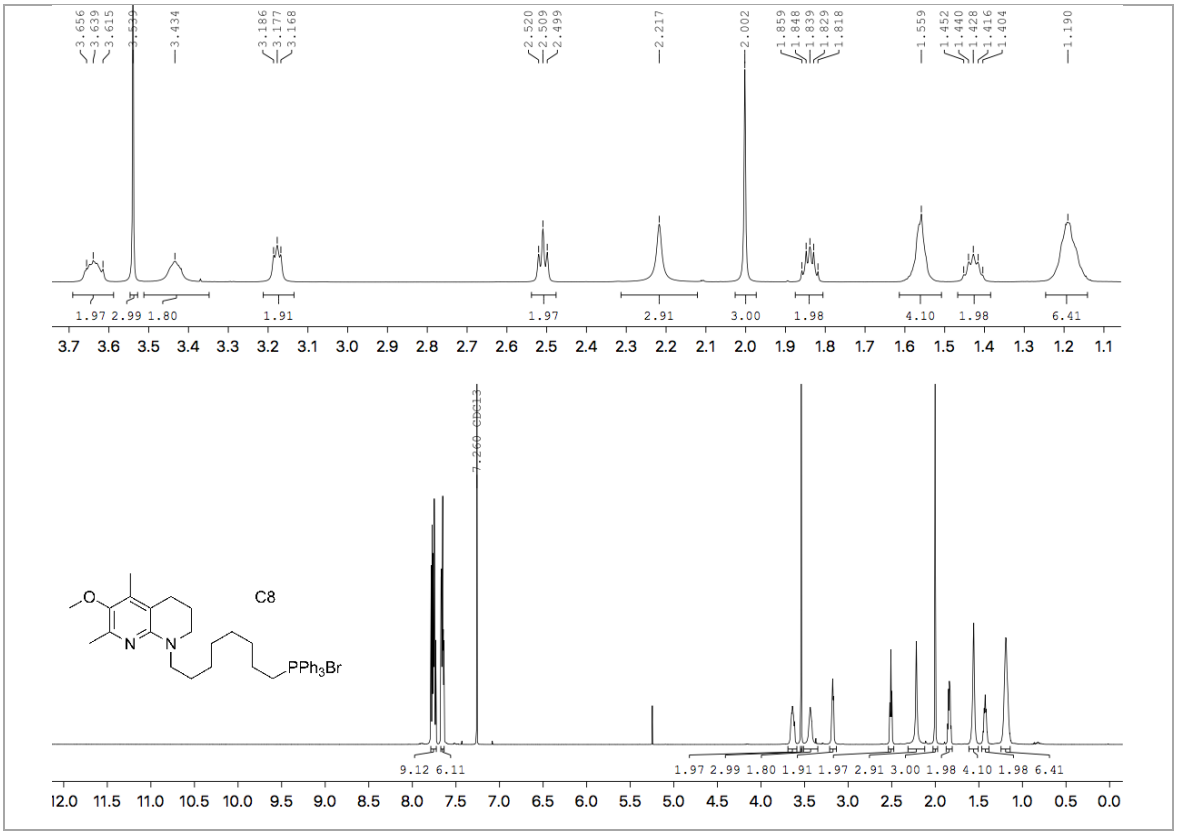
3.656
3.639
3.615
3.539
3.434
3.186
3.177
3.168
2.520
2.509
2.499
2.217
2.002
1.859
1.848
1.839
1.829
1.818
1.559
1.452
1.440
1.428
1.416
1.404
1.190
1.97 2.99 1.80
1.91
1.97
2.91
3.00
1.98
4.10
1.98
6.41
7.260 CDCl3
C8
PPh3Br
9.12 6.11
1.97 2.99 1.80 1.91 1.97 2.91 3.00 1.98 4.10 1.98 6.41

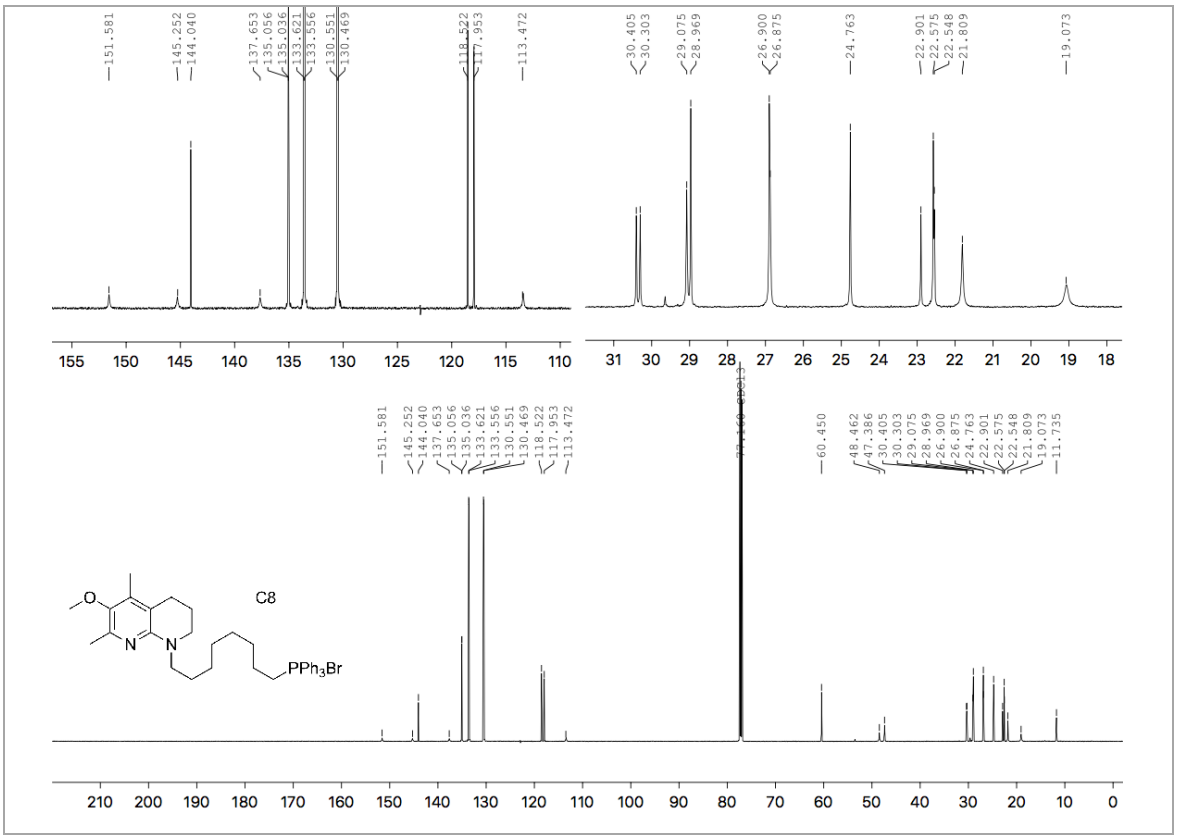
151.581
145.252
144.040
137.653
135.056
135.036
133.621
133.556
130.551
130.469
118.522
117.953
113.472
30.405
30.303
29.075
28.969
26.900
26.875
24.763
22.901
22.575
22.548
21.809
19.073
77.160 CDCl3
60.450
48.462
47.386
11.735
C8
PPh3Br

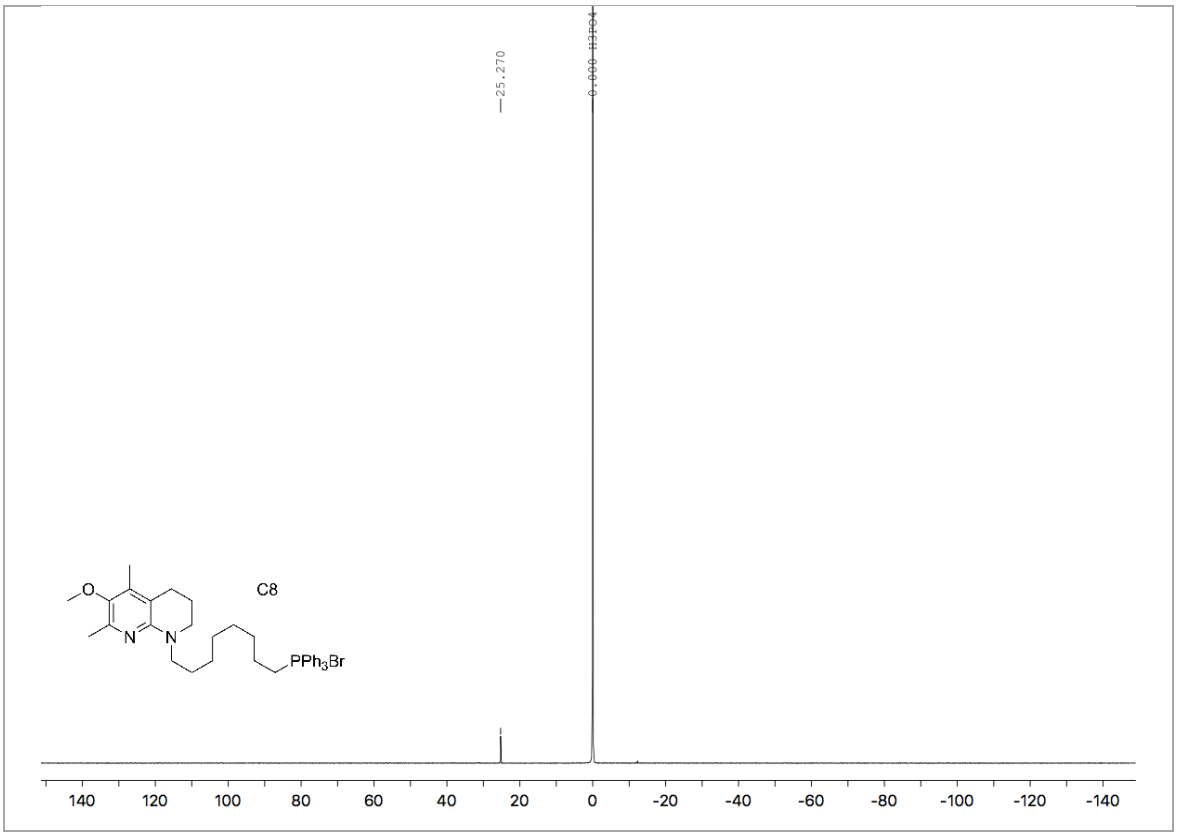
25.270
0.000
C8
O
N
N
PPh3Br
140
120
100
80
60
40
20
0
-20
-40
-60
-80
-100
-120
-140

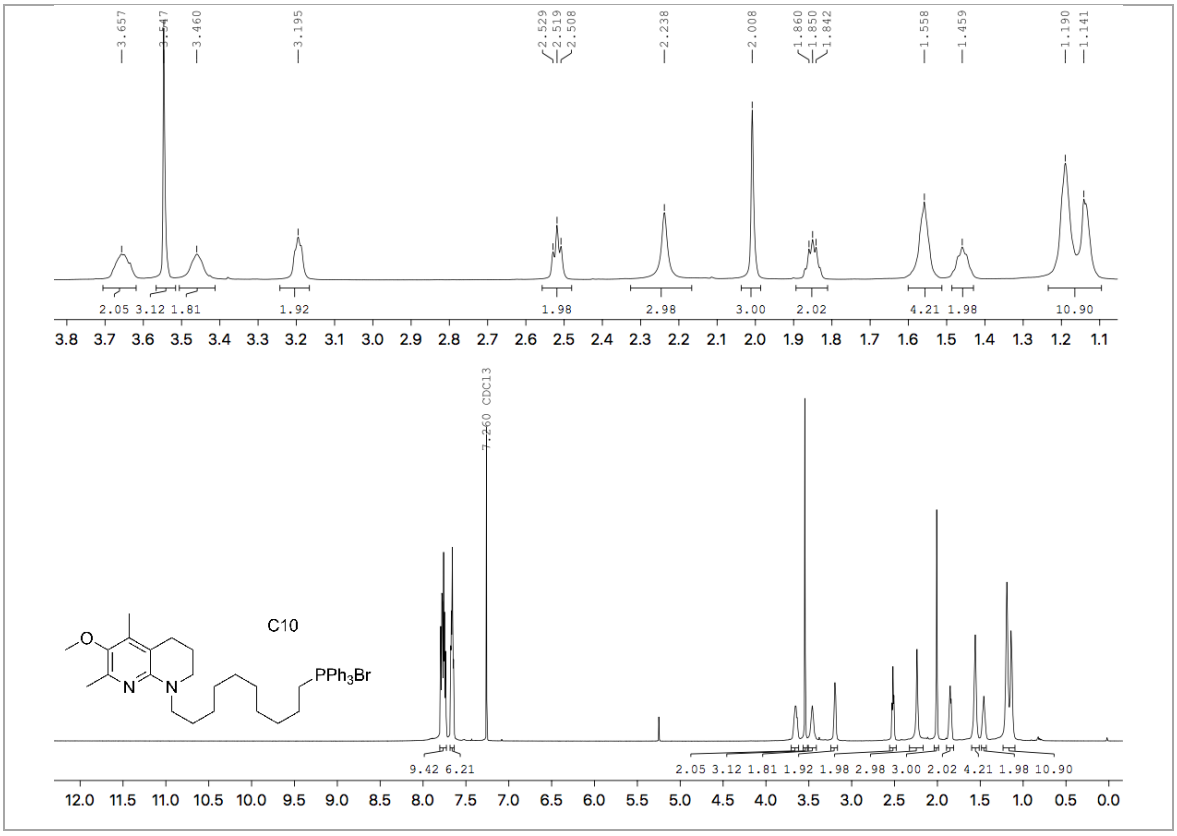
3.657
3.547
3.460
3.195
2.529
2.519
2.508
2.238
2.008
1.860
1.850
1.842
1.558
1.459
1.190
1.141
2.05 3.12 1.81
1.92
1.98
2.98
3.00
2.02
4.21 1.98
10.90
7.260 CDCl3
C10
PPh3Br
9.42 6.21
2.05 3.12 1.81 1.92 1.98 2.98 3.00 2.02 4.21 1.98 10.90

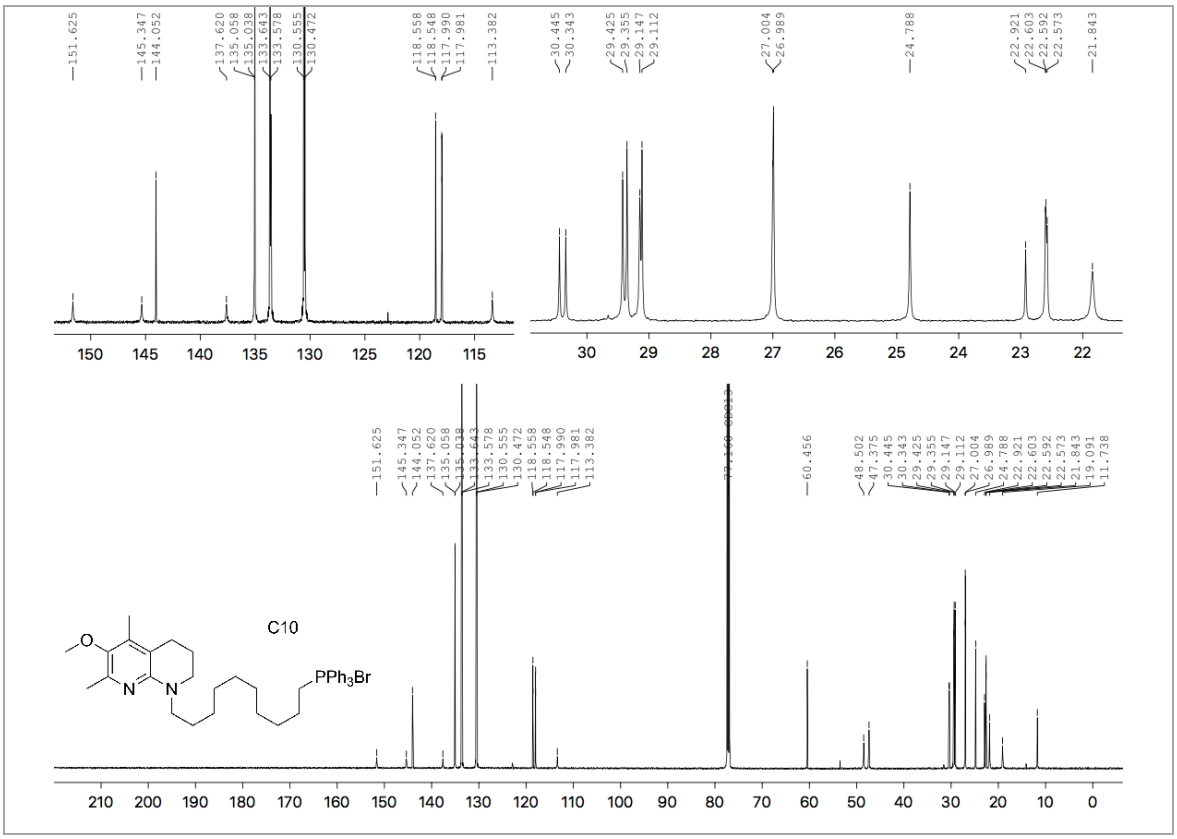
151.625
145.347
144.052
137.620
135.058
135.038
133.643
133.578
130.555
130.472
118.558
118.548
117.990
117.981
113.382
30.445
30.343
29.425
29.355
29.147
29.112
27.004
26.989
24.788
22.921
22.603
22.592
22.573
21.843
60.456
48.502
47.375
19.091
11.738
C10
PPh3Br

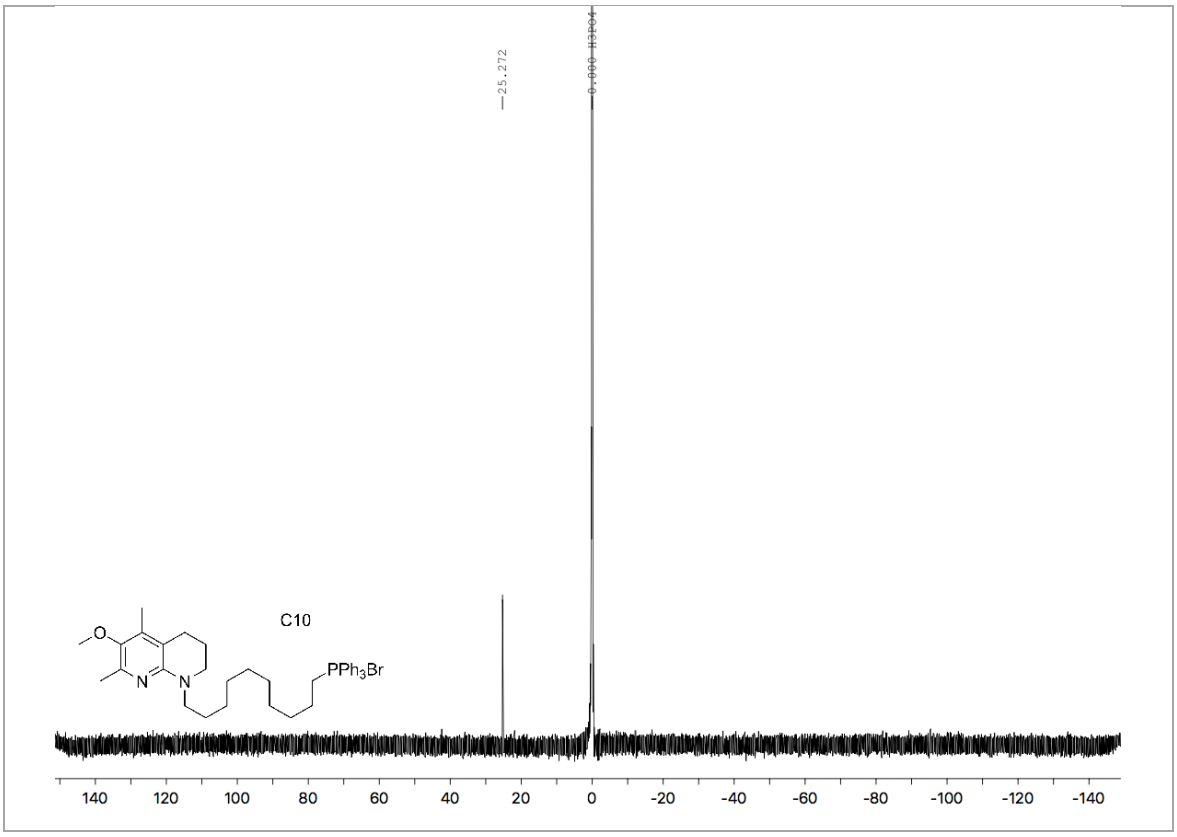
25.272
0.000
C10
PPh3Br
O
N
N
140
120
100
80
60
40
20
0
-20
-40
-60
-80
-100
-120
-140

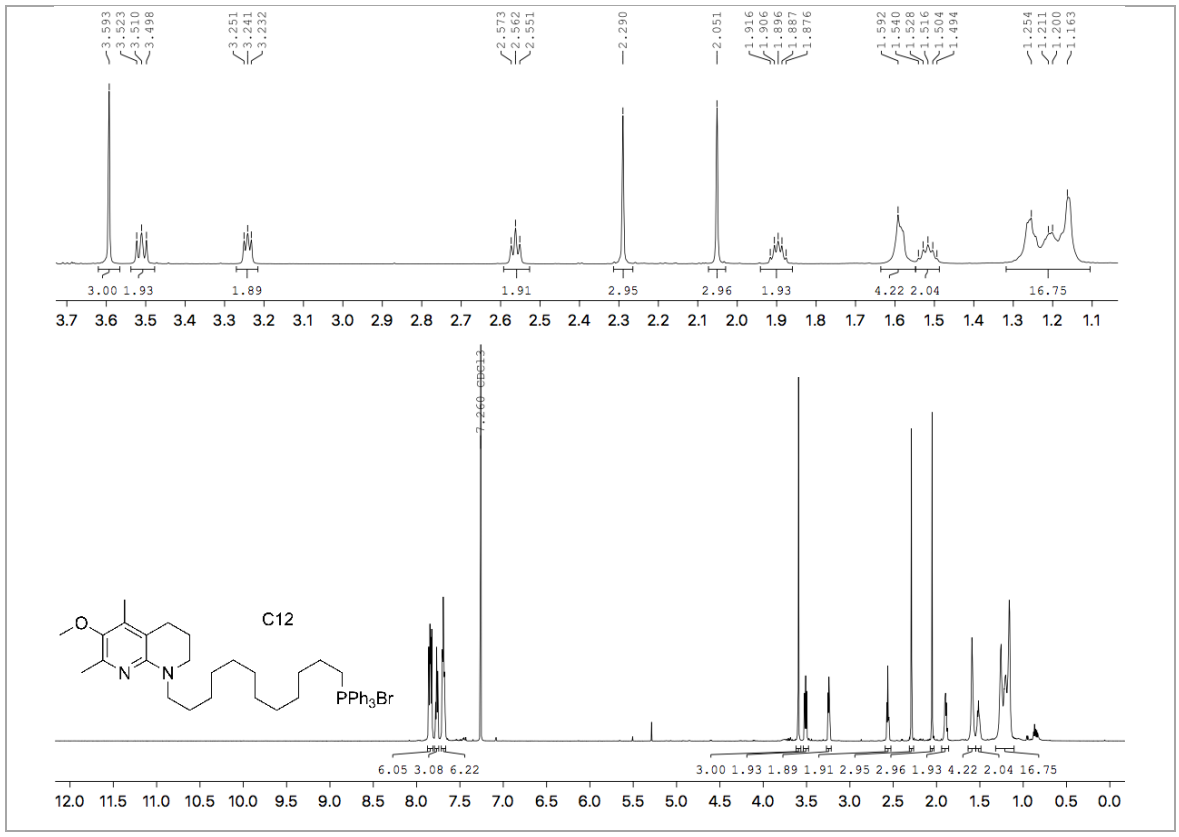
3.593
3.523
3.510
3.498
3.251
3.241
3.232
2.573
2.562
2.551
2.290
2.051
1.916
1.906
1.896
1.887
1.876
1.592
1.540
1.528
1.516
1.504
1.494
1.254
1.211
1.200
1.163
3.00 1.93 1.89 1.91 2.95 2.96 1.93 4.22 2.04 16.75
7.260
C12
PPh3Br
6.05 3.08 6.22
3.00 1.93 1.89 1.91 2.95 2.96 1.93 4.22 2.04 16.75

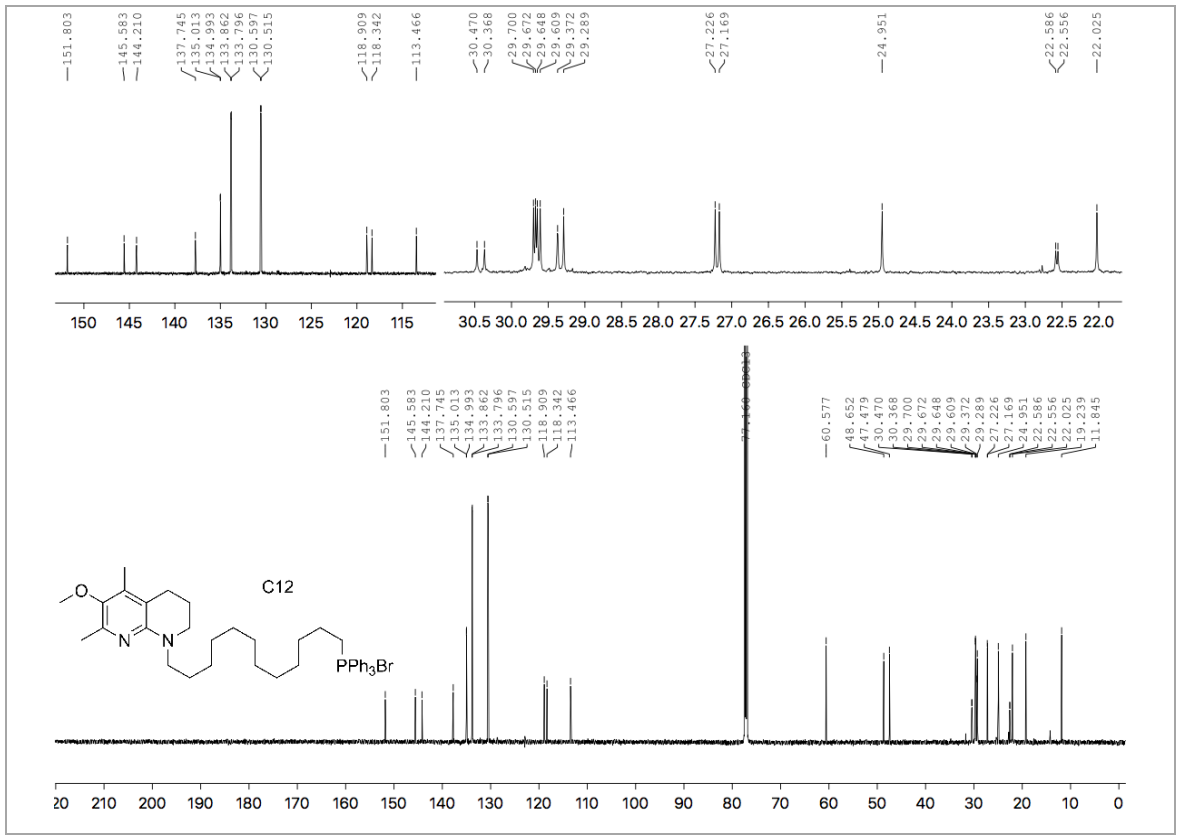
151.803
145.583
144.210
137.745
135.013
134.993
133.862
133.796
130.597
130.515
118.909
118.342
113.466
30.470
30.368
29.700
29.672
29.648
29.609
29.372
29.289
27.226
27.169
24.951
22.586
22.556
22.025
77.160
60.577
48.652
47.479
30.470
30.368
29.700
29.672
29.648
29.609
29.372
29.289
27.226
27.169
24.951
22.586
22.556
22.025
19.239
11.845
C12
PPh3Br

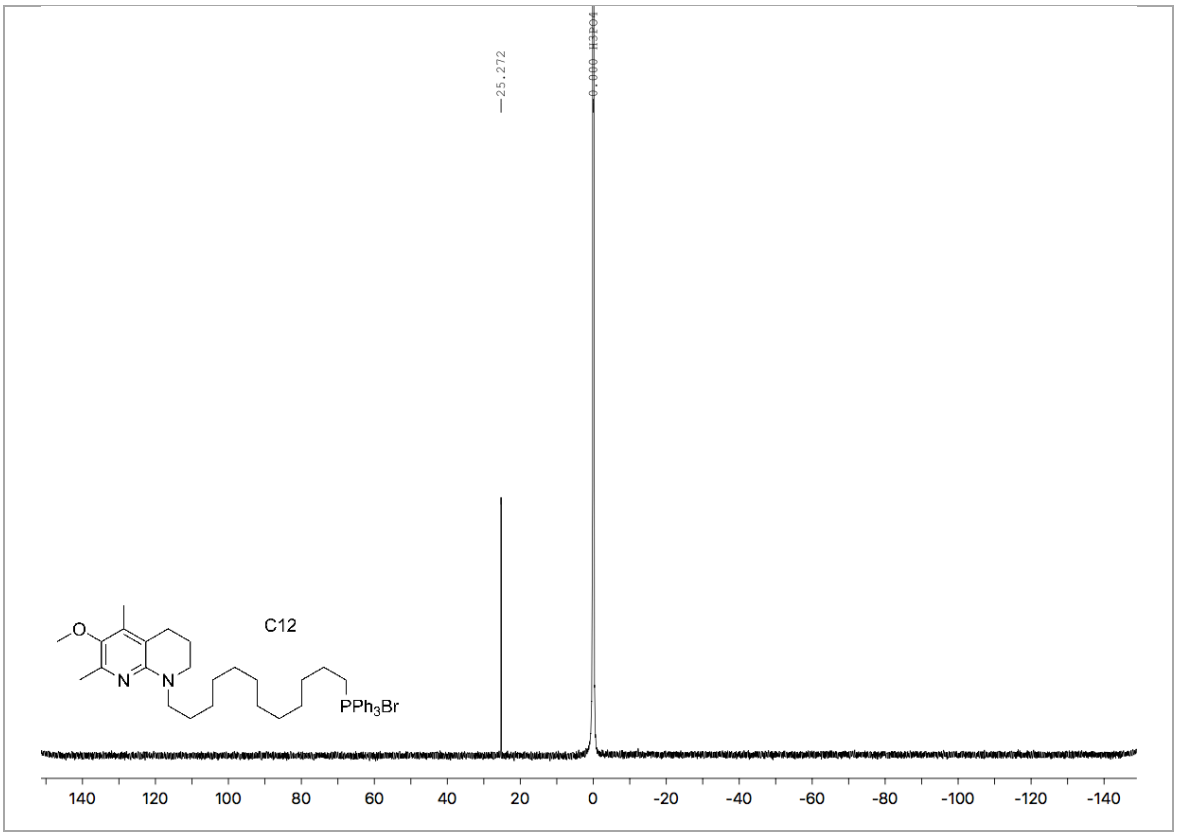
25.272
0.000 H3PO4
C12
O
N
N
PPh3Br
140
120
100
80
60
40
20
0
-20
-40
-60
-80
-100
-120
-140

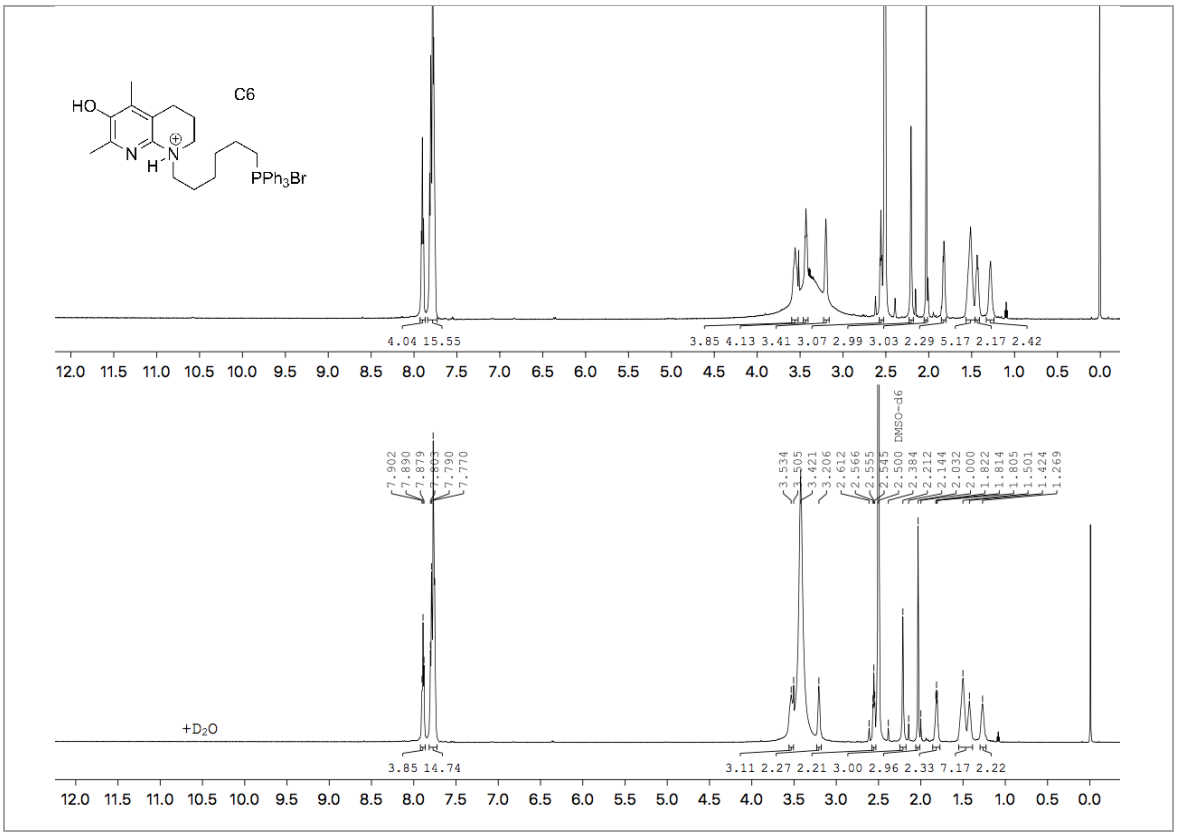
C6
HO
N
H
N
PPh3Br
4.04 15.55
3.85 4.13 3.41 3.07 2.99 3.03 2.29 5.17 2.17 2.42
12.0 11.5 11.0 10.5 10.0 9.5 9.0 8.5 8.0 7.5 7.0 6.5 6.0 5.5 5.0 4.5 4.0 3.5 3.0 2.5 2.0 1.5 1.0 0.5 0.0
7.902
7.890
7.879
7.803
7.790
7.770
3.534
3.505
3.421
3.206
2.612
2.566
2.555
2.545
DMSO-d6
2.500
2.384
2.212
2.144
2.032
2.000
1.822
1.814
1.805
1.501
1.424
1.269
+D2O
3.85 14.74
3.11 2.27 2.21 3.00 2.96 2.33 7.17 2.22
12.0 11.5 11.0 10.5 10.0 9.5 9.0 8.5 8.0 7.5 7.0 6.5 6.0 5.5 5.0 4.5 4.0 3.5 3.0 2.5 2.0 1.5 1.0 0.5 0.0

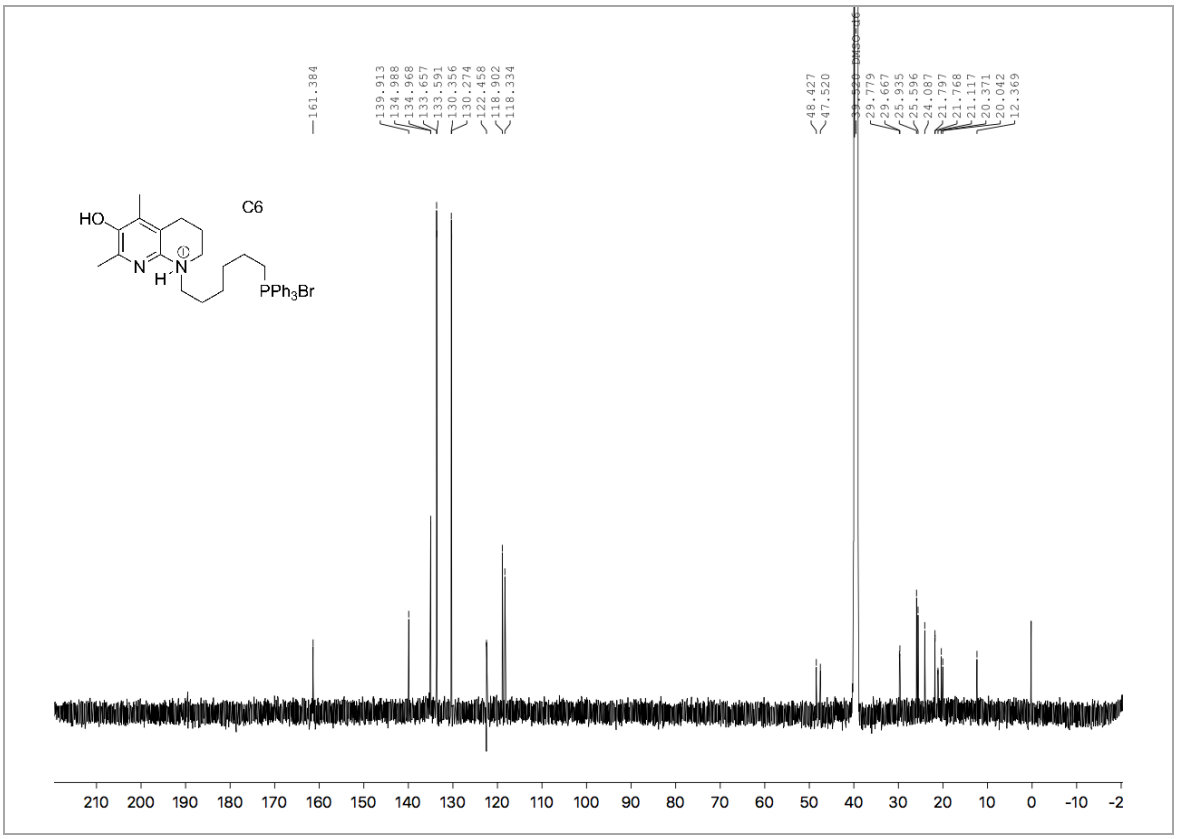
161.384
139.913
134.988
134.968
133.657
133.591
130.356
130.274
122.458
118.902
118.334
48.427
47.520
39.779
29.667
25.935
25.596
24.087
21.797
21.768
21.117
20.371
20.042
12.369
C6
HO
N
H
N
PPh3Br
210 200 190 180 170 160 150 140 130 120 110 100 90 80 70 60 50 40 30 20 10 0 -10 -2

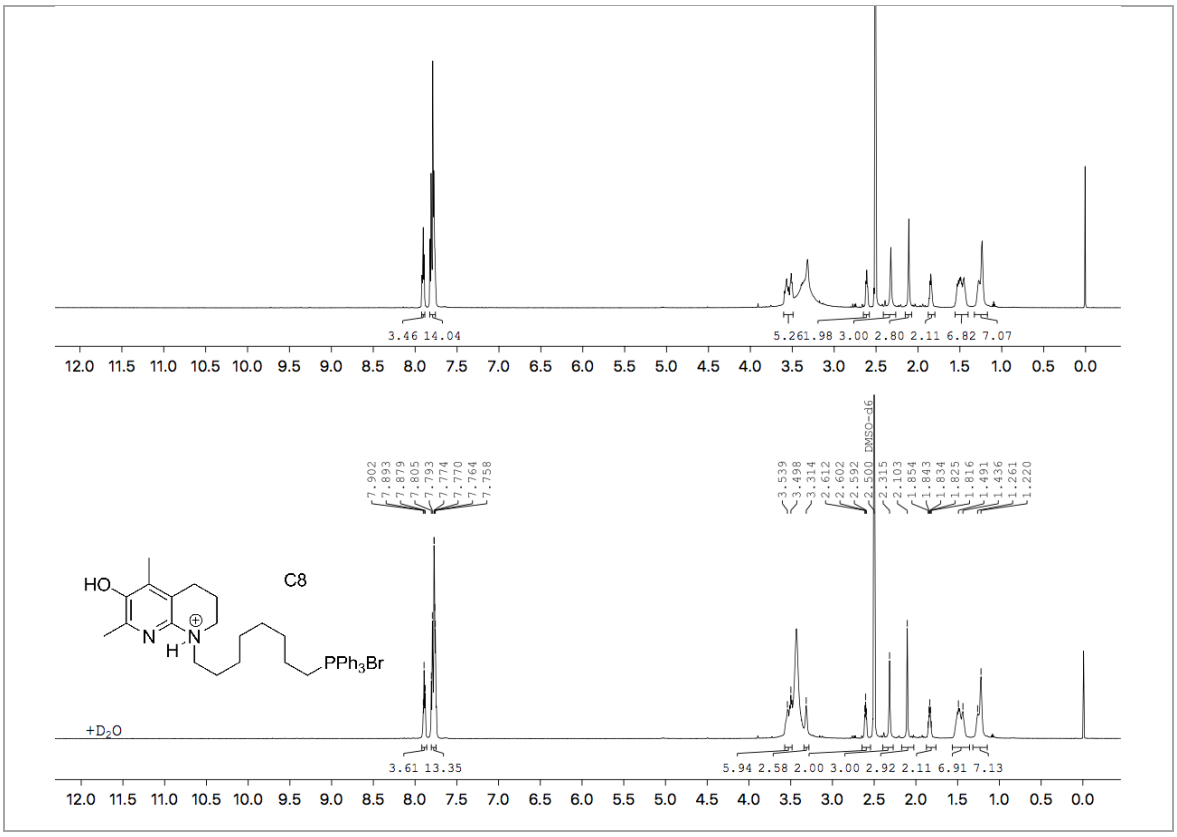
3.46 14.04
5.26 1.98 3.00 2.80 2.11 6.82 7.07
12.0 11.5 11.0 10.5 10.0 9.5 9.0 8.5 8.0 7.5 7.0 6.5 6.0 5.5 5.0 4.5 4.0 3.5 3.0 2.5 2.0 1.5 1.0 0.5 0.0
7.902
7.893
7.879
7.805
7.793
7.774
7.770
7.764
7.758
3.539
3.498
3.314
2.612
2.602
2.592
2.500 DMSO-d6
2.315
2.103
1.854
1.843
1.834
1.825
1.816
1.491
1.436
1.261
1.220
HO
C8
N
H
N
PPh3Br
+D2O
3.61 13.35
5.94 2.58 2.00 3.00 2.92 2.11 6.91 7.13
12.0 11.5 11.0 10.5 10.0 9.5 9.0 8.5 8.0 7.5 7.0 6.5 6.0 5.5 5.0 4.5 4.0 3.5 3.0 2.5 2.0 1.5 1.0 0.5 0.0

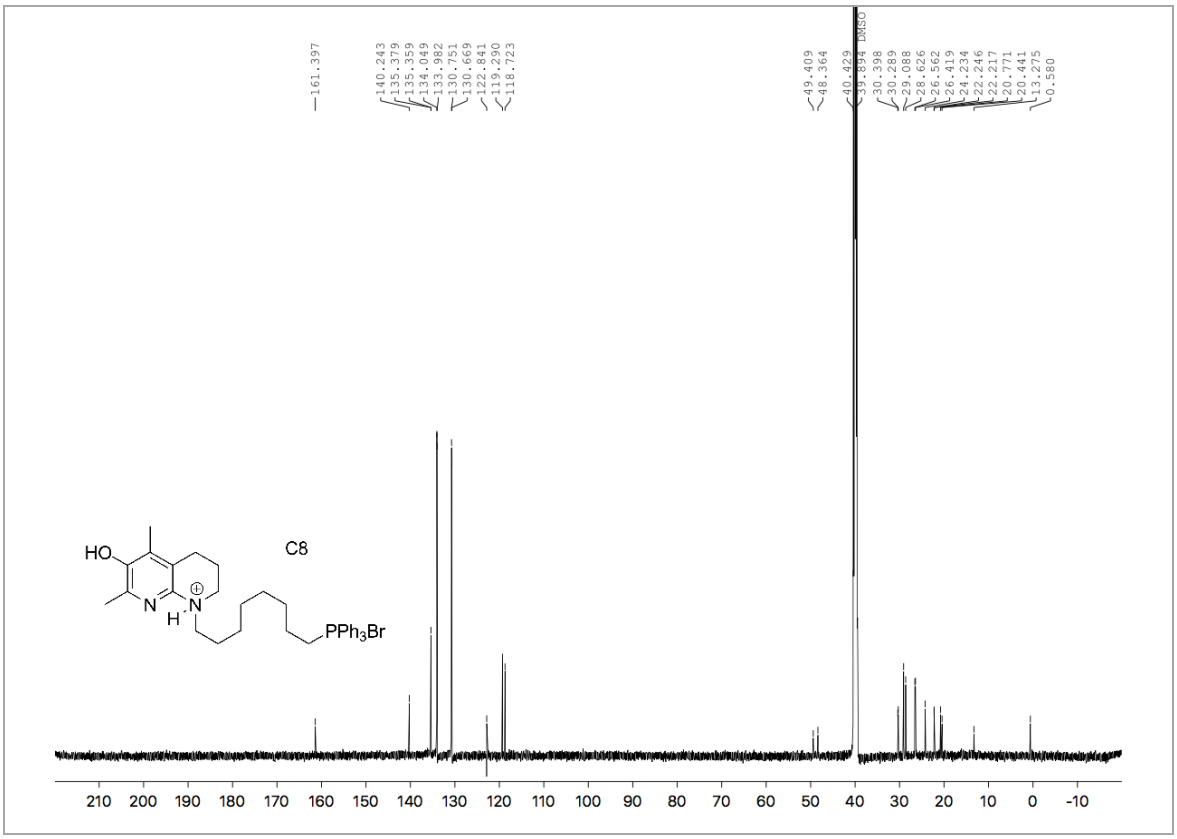
161.397
140.243
135.379
135.359
134.049
133.982
130.751
130.669
122.841
119.290
118.723
49.409
48.364
40.429
39.894 DMSO
30.398
30.289
29.088
28.626
26.562
26.419
24.234
22.246
22.217
20.771
20.441
13.275
0.580
HO
C8
N
H
N
PPh3Br
210 200 190 180 170 160 150 140 130 120 110 100 90 80 70 60 50 40 30 20 10 0 -10

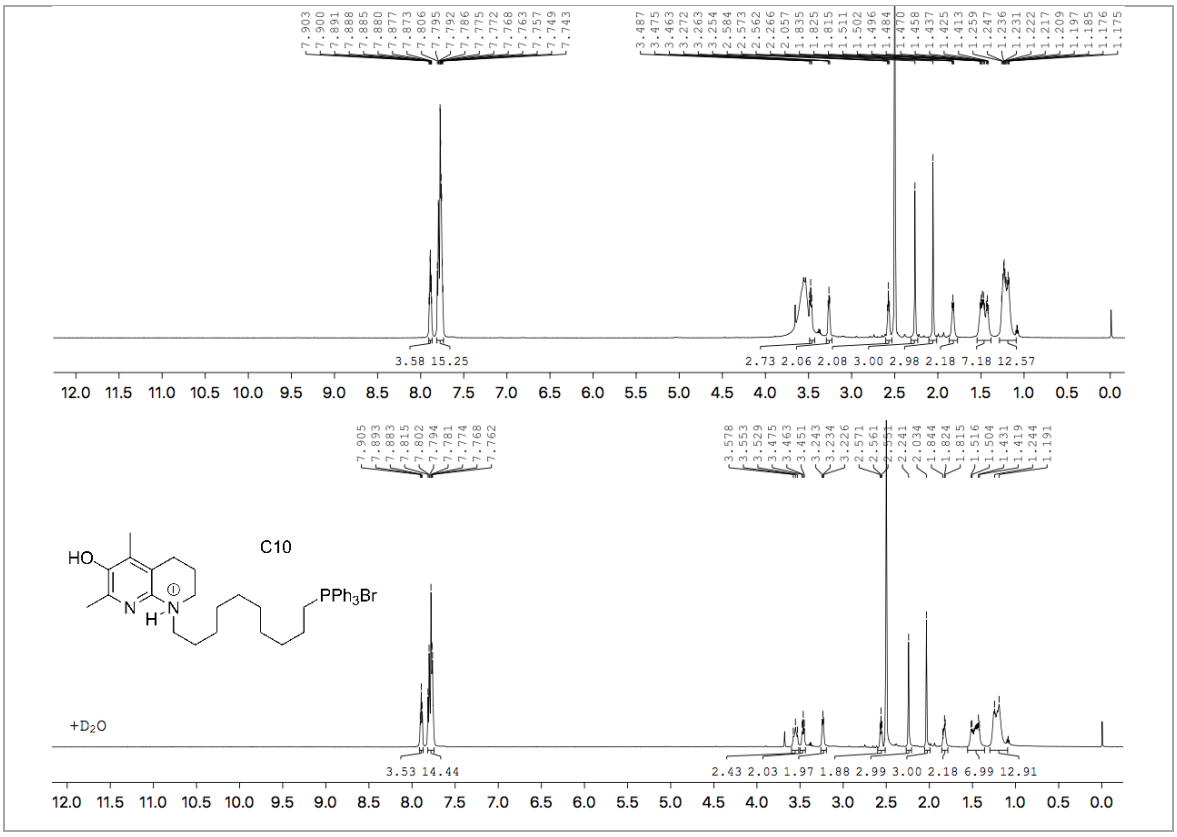
C10
HO
PPh3Br
+D2O
3.58 15.25
2.73 2.06 2.08 3.00 2.98 2.18 7.18 12.57
3.53 14.44
2.43 2.03 1.97 1.88 2.99 3.00 2.18 6.99 12.91

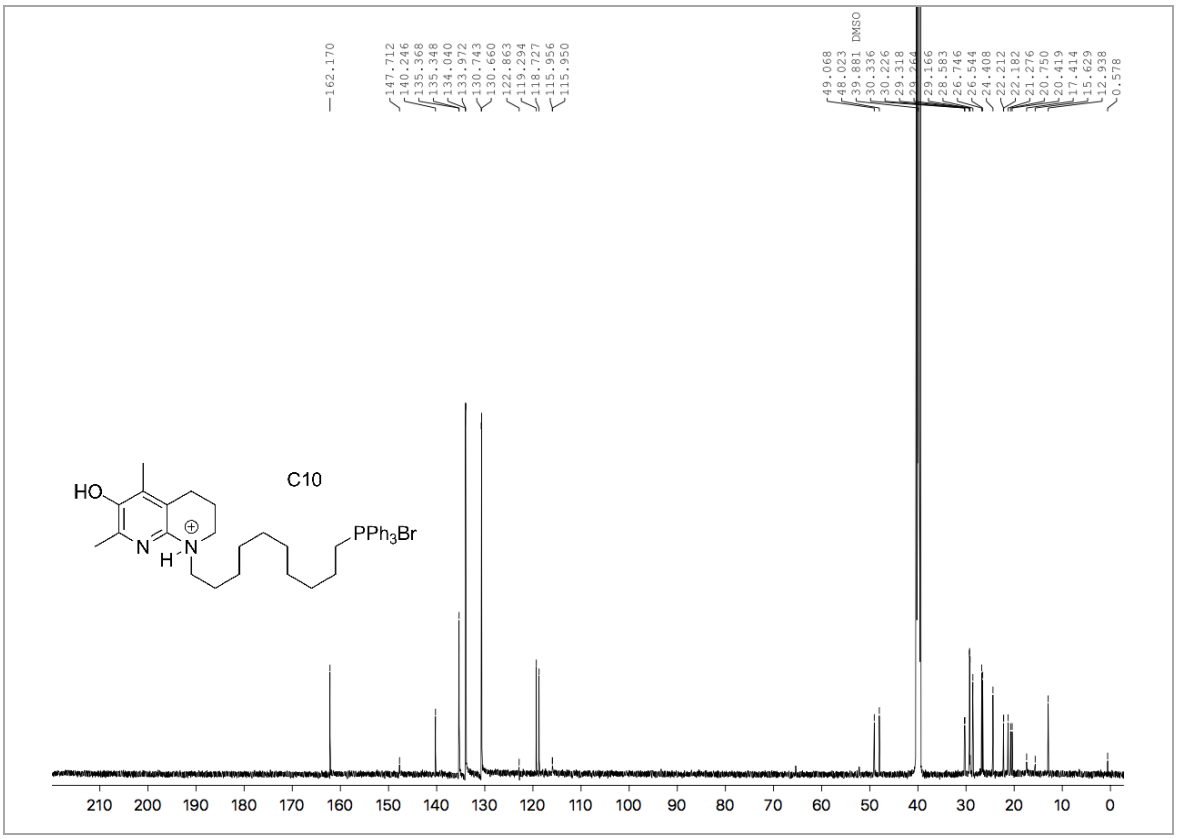
C10
HO
PPh3Br
DMSO

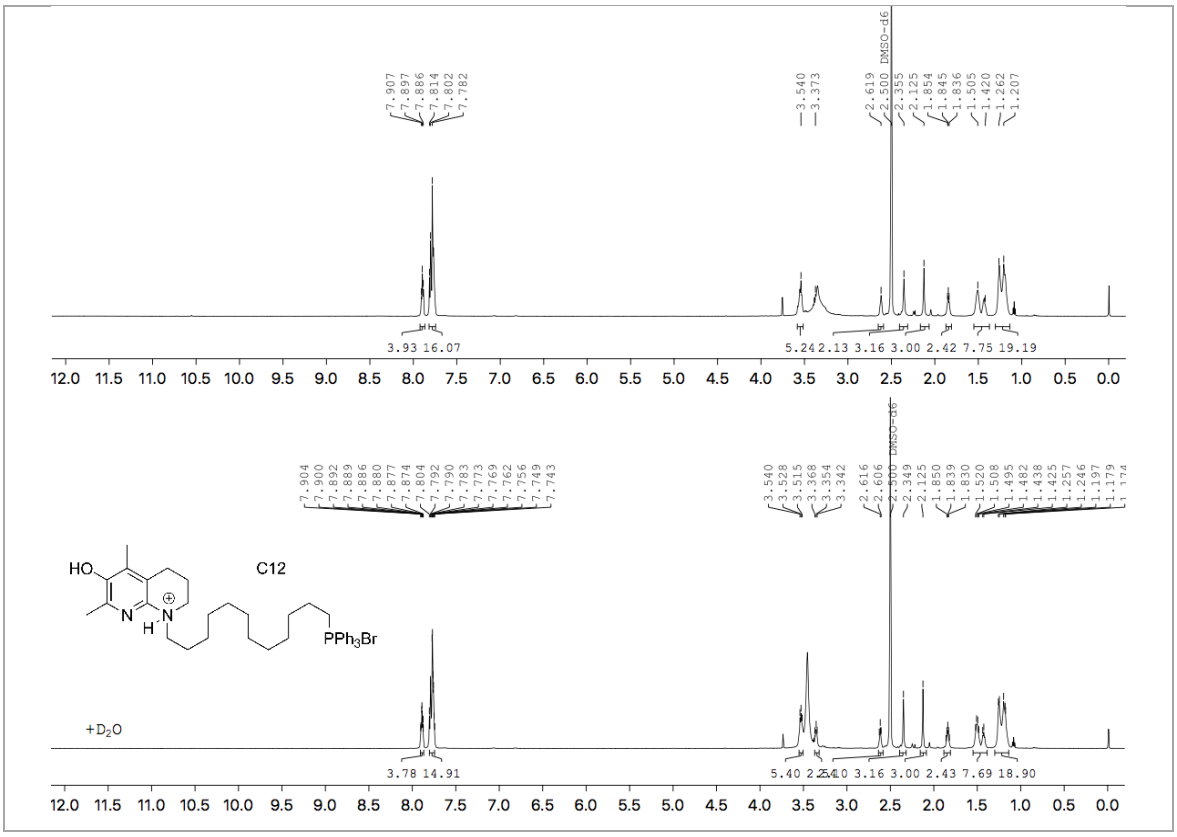
C12
+D2O

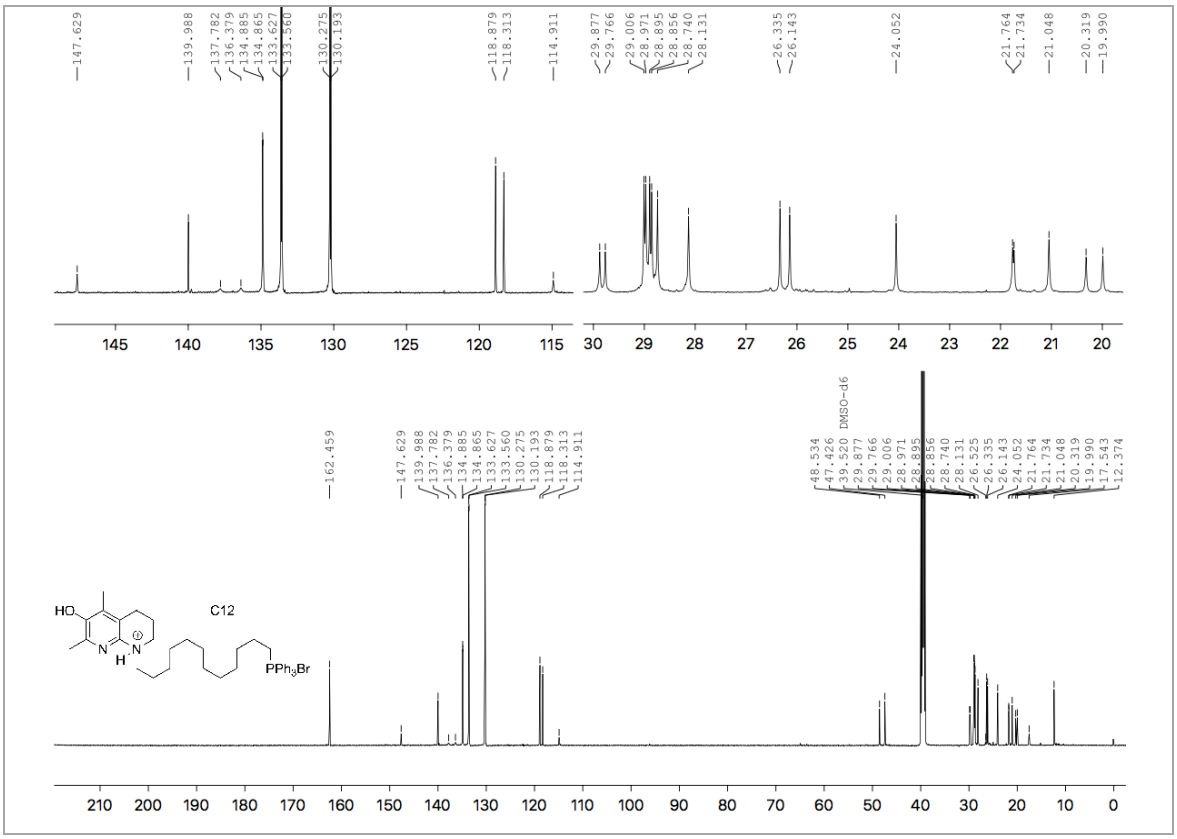
C12

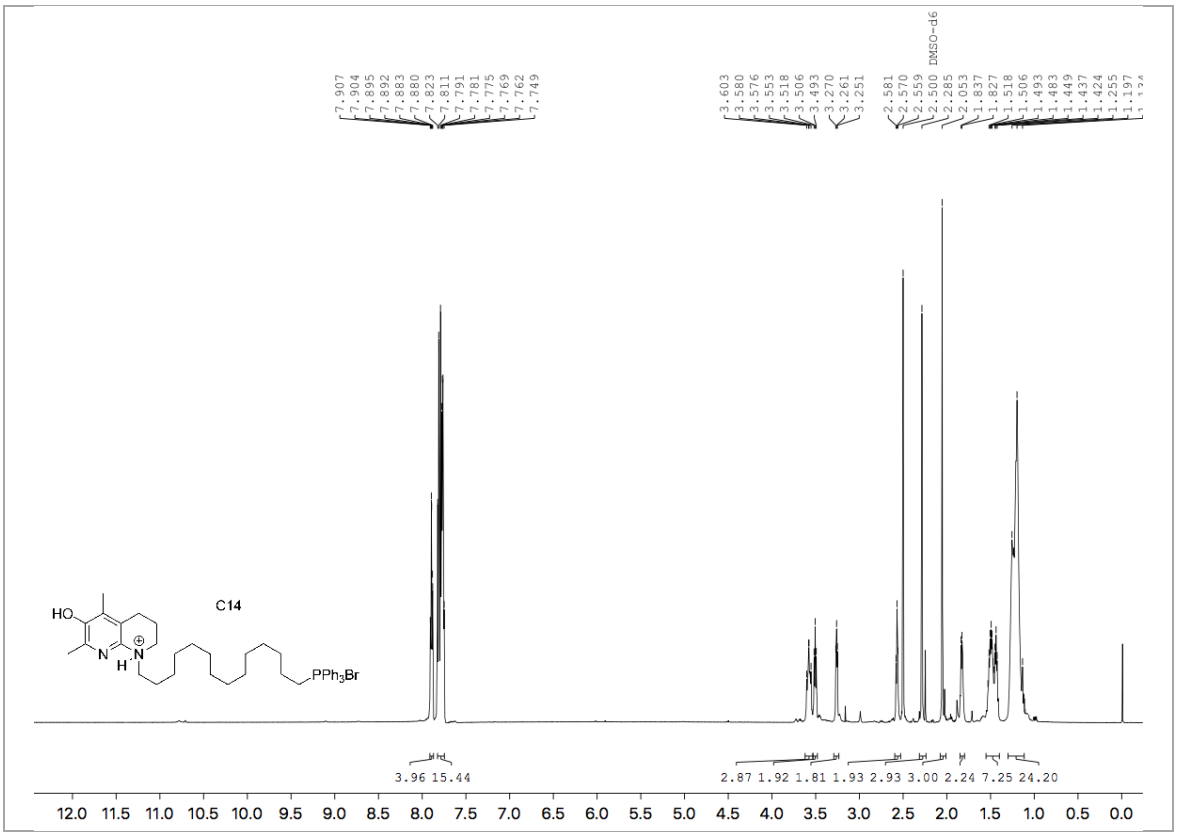
7.907
7.904
7.895
7.892
7.883
7.880
7.823
7.811
7.791
7.781
7.775
7.769
7.762
7.749
3.603
3.580
3.576
3.553
3.518
3.506
3.493
3.270
3.261
3.251
2.581
2.570
2.559
DMSO-d6
2.500
2.285
2.053
1.837
1.827
1.518
1.506
1.493
1.483
1.449
1.437
1.424
1.255
1.197
C14
HO
N
H
PPh3Br
3.96 15.44
2.87 1.92 1.81 1.93 2.93 3.00 2.24 7.25 24.20
12.0 11.5 11.0 10.5 10.0 9.5 9.0 8.5 8.0 7.5 7.0 6.5 6.0 5.5 5.0 4.5 4.0 3.5 3.0 2.5 2.0 1.5 1.0 0.5 0.0

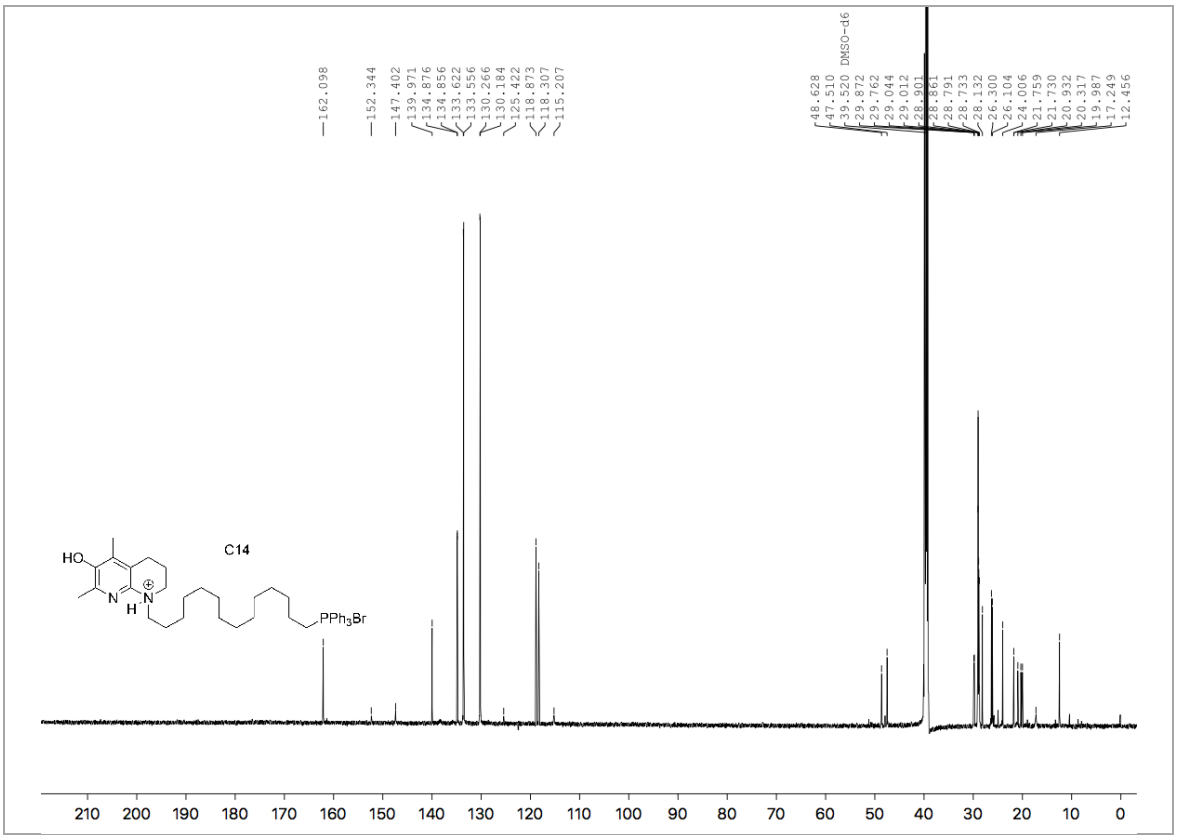
162.098
152.344
147.402
139.971
134.876
134.856
133.622
133.556
130.266
130.184
125.422
118.873
118.307
115.207
48.628
47.510
DMSO-d6
39.520
29.872
29.762
29.044
29.012
28.901
28.861
28.791
28.733
28.132
26.300
26.104
24.006
21.759
21.730
20.932
20.317
19.987
17.249
12.456
C14
HO
N
H
PPh3Br
210 200 190 180 170 160 150 140 130 120 110 100 90 80 70 60 50 40 30 20 10 0

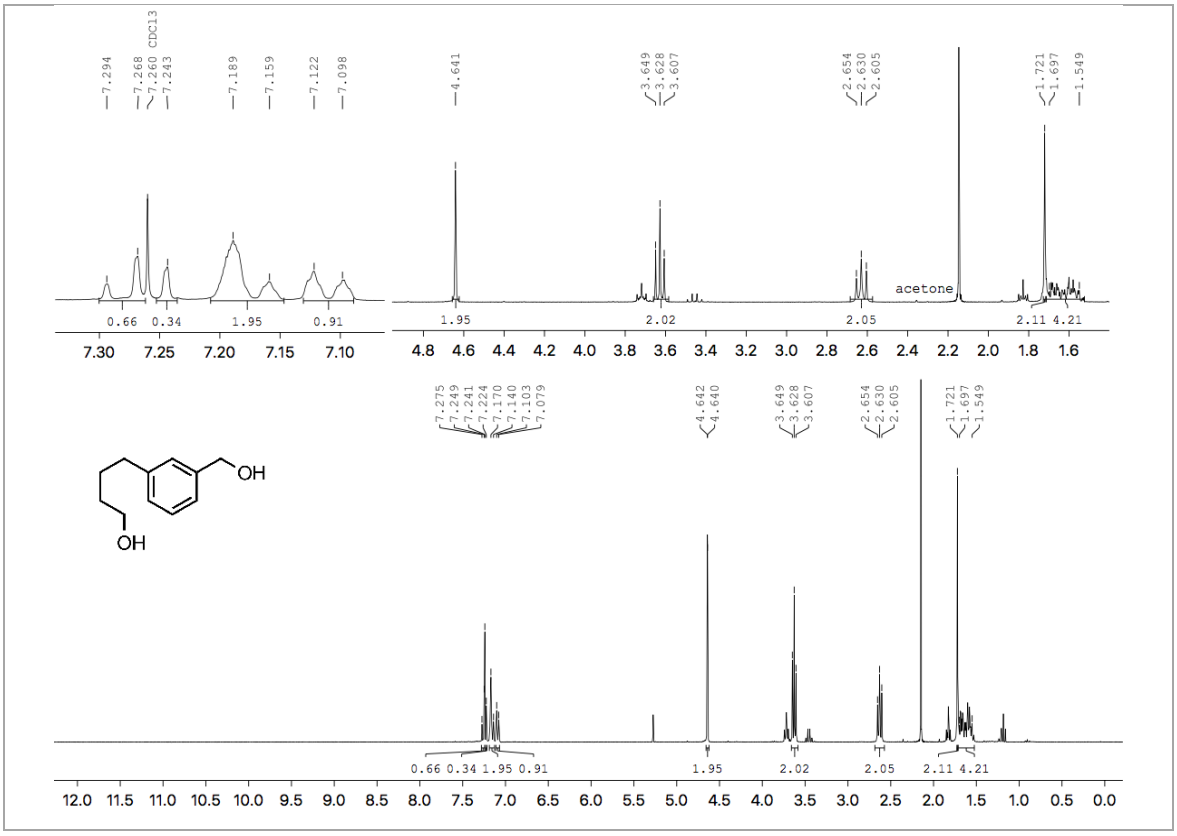
7.294
7.268
7.260 CDCl3
7.243
7.189
7.159
7.122
7.098
4.641
3.649
3.628
3.607
2.654
2.630
2.605
1.721
1.697
1.549
acetone
0.66 0.34 1.95 0.91
1.95 2.02 2.05 2.11 4.21
OH
OH

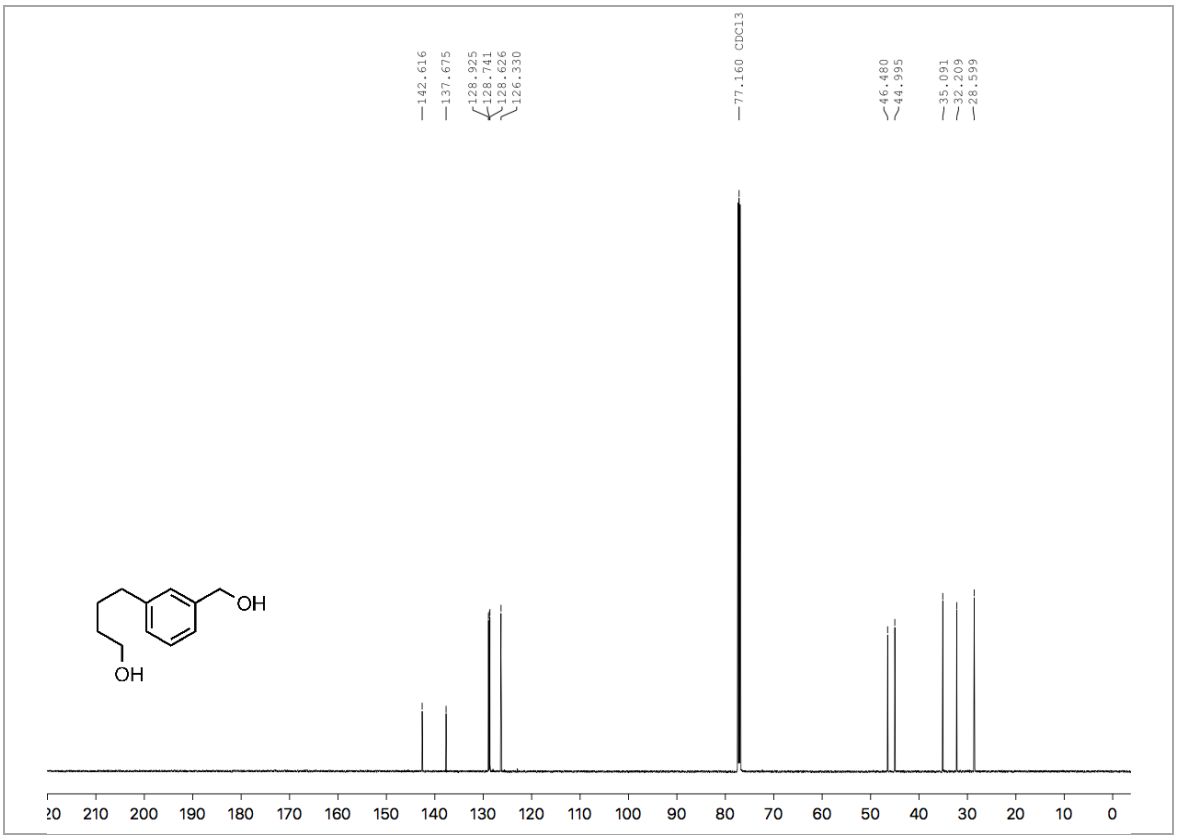
142.616
137.675
128.925
128.741
128.626
126.330
77.160 CDCl3
46.480
44.995
35.091
32.209
28.599
OH
OH

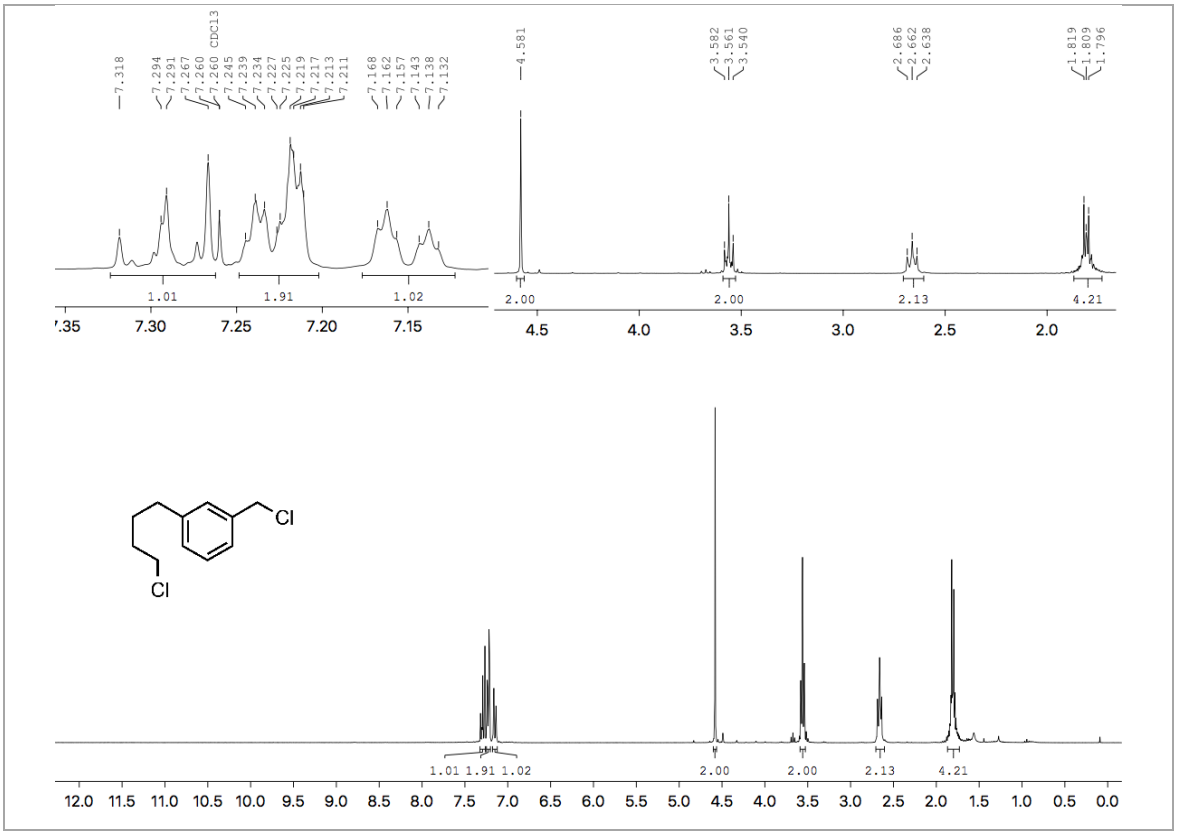
7.318
7.294
7.291
7.267
7.260
CDCl3
7.260
7.245
7.239
7.234
7.227
7.225
7.219
7.217
7.213
7.211
7.168
7.162
7.157
7.143
7.138
7.132
4.581
3.582
3.561
3.540
2.686
2.662
2.638
1.819
1.809
1.796
1.01
1.91
1.02
2.00
2.00
2.13
4.21
Cl
Cl
1.01 1.91 1.02
2.00
2.00
2.13
4.21

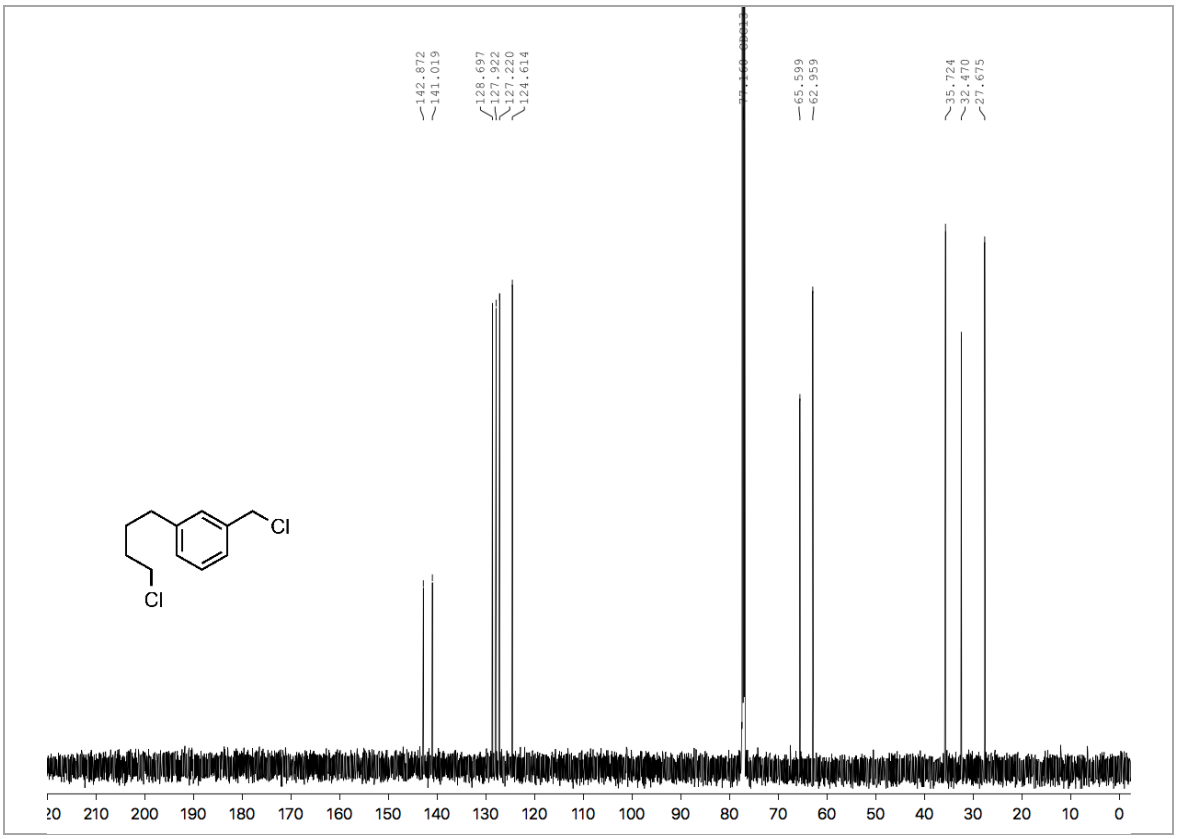
142.872
141.019
128.697
127.922
127.220
124.614
77.160
65.599
62.959
35.724
32.470
27.675
Cl
Cl

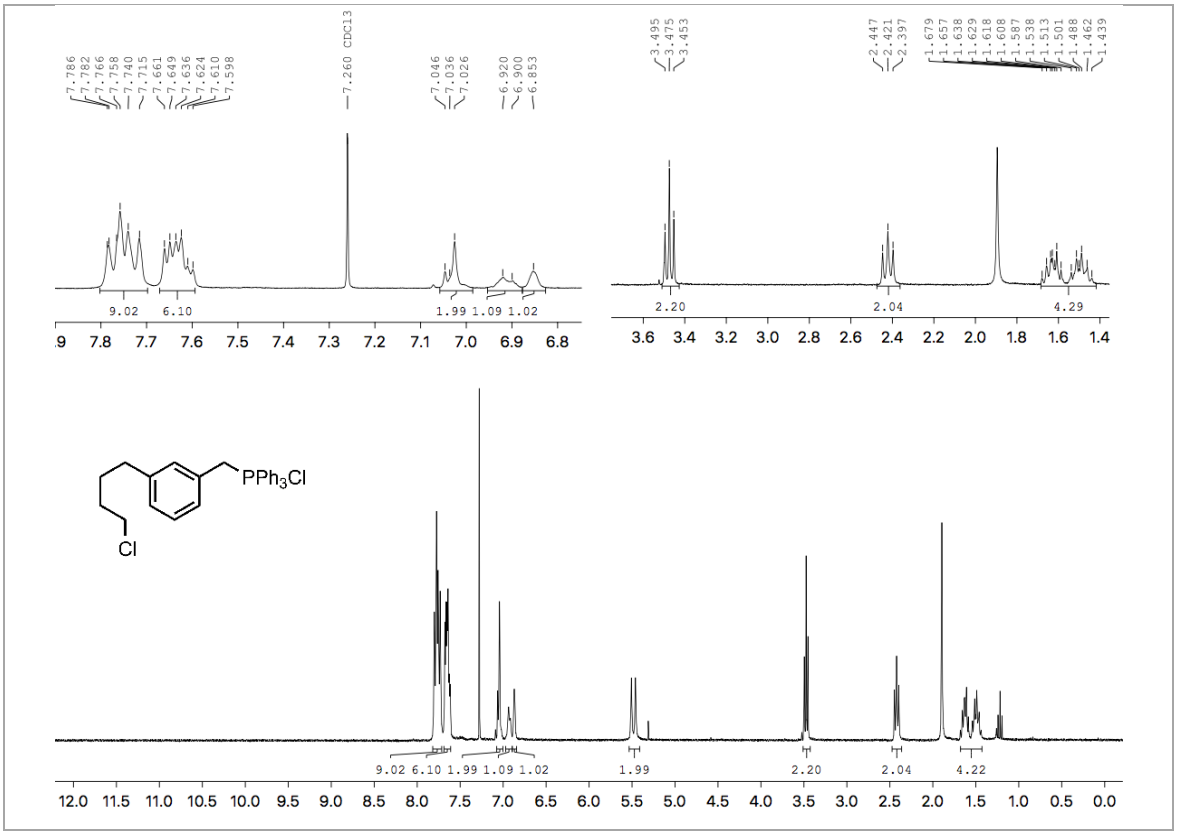
7.786
7.782
7.766
7.758
7.740
7.715
7.661
7.649
7.636
7.624
7.610
7.598
7.260 CDCl3
7.046
7.036
7.026
6.920
6.900
6.853
3.495
3.475
3.453
2.447
2.421
2.397
1.679
1.657
1.638
1.629
1.618
1.608
1.587
1.538
1.513
1.501
1.488
1.462
1.439
9.02
6.10
1.99
1.09
1.02
2.20
2.04
4.29
PPh3Cl
Cl
9.02 6.10 1.99 1.09 1.02
1.99
2.20
2.04
4.22

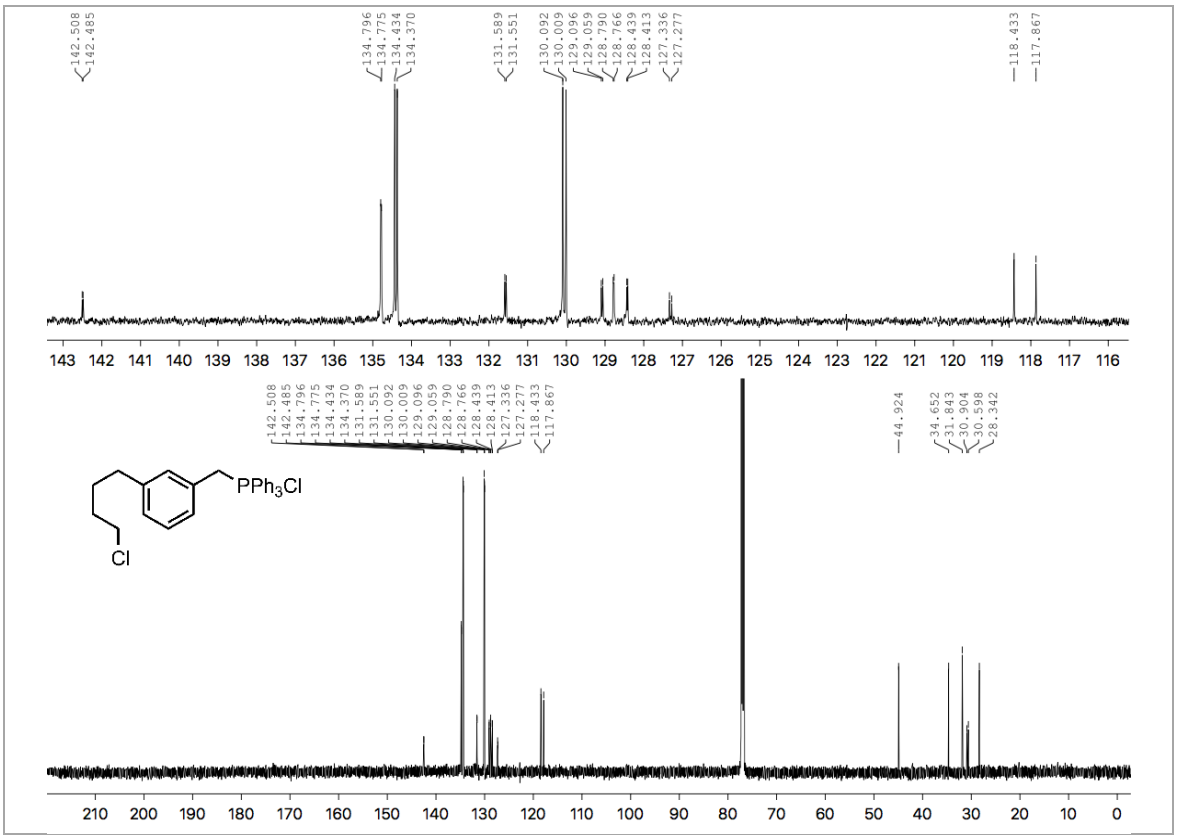
142.508
142.485
134.796
134.775
134.434
134.370
131.589
131.551
130.092
130.009
129.096
129.059
128.790
128.766
128.439
128.413
127.336
127.277
118.433
117.867
44.924
34.652
31.843
30.904
30.598
28.342
PPh3Cl
Cl

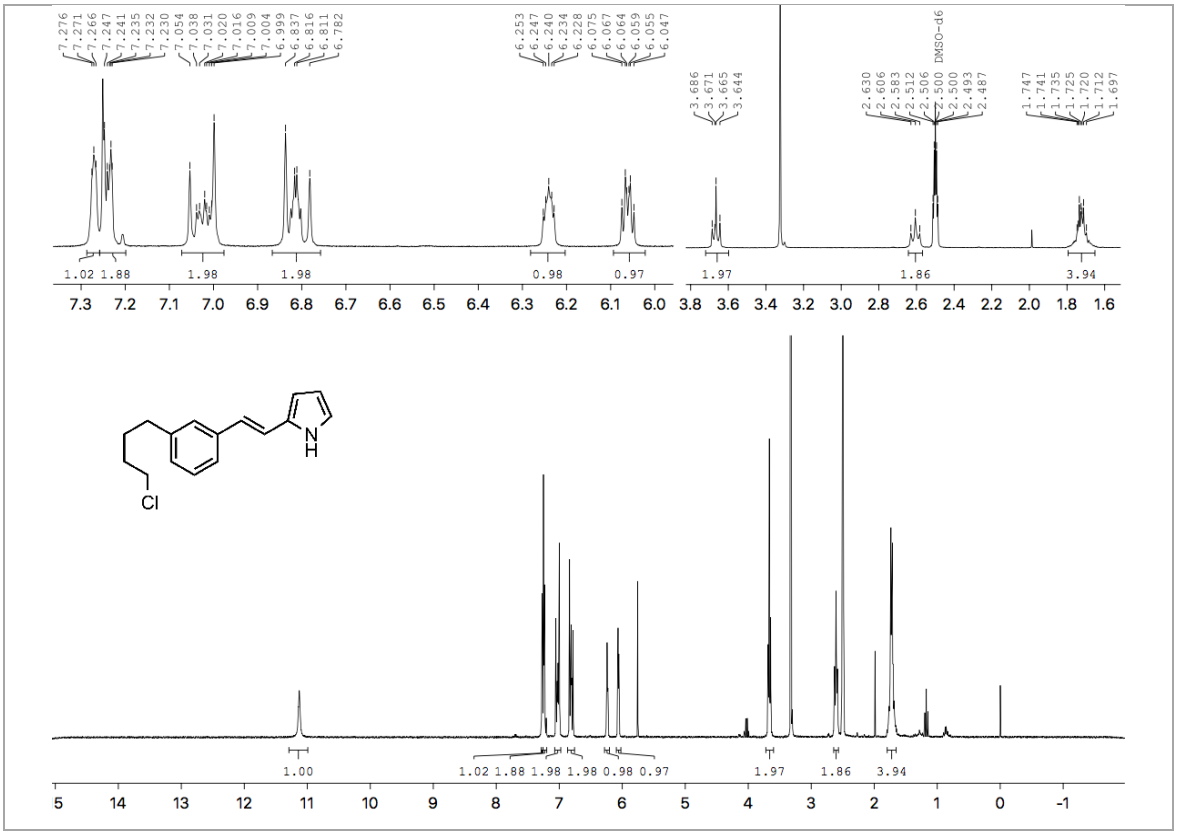
7.276
7.271
7.266
7.247
7.241
7.235
7.232
7.230
7.054
7.038
7.031
7.020
7.016
7.009
7.004
6.999
6.837
6.816
6.811
6.782
6.253
6.247
6.240
6.234
6.228
6.075
6.067
6.064
6.059
6.055
6.047
3.686
3.671
3.665
3.644
2.630
2.606
2.583
2.512
2.506
DMSO-d6
2.500
2.493
2.487
1.747
1.741
1.735
1.725
1.720
1.712
1.697
1.02 1.88
1.98
1.98
0.98
0.97
1.97
1.86
3.94
N
H
Cl
1.00
1.02 1.88 1.98 1.98 0.98 0.97
1.97
1.86
3.94

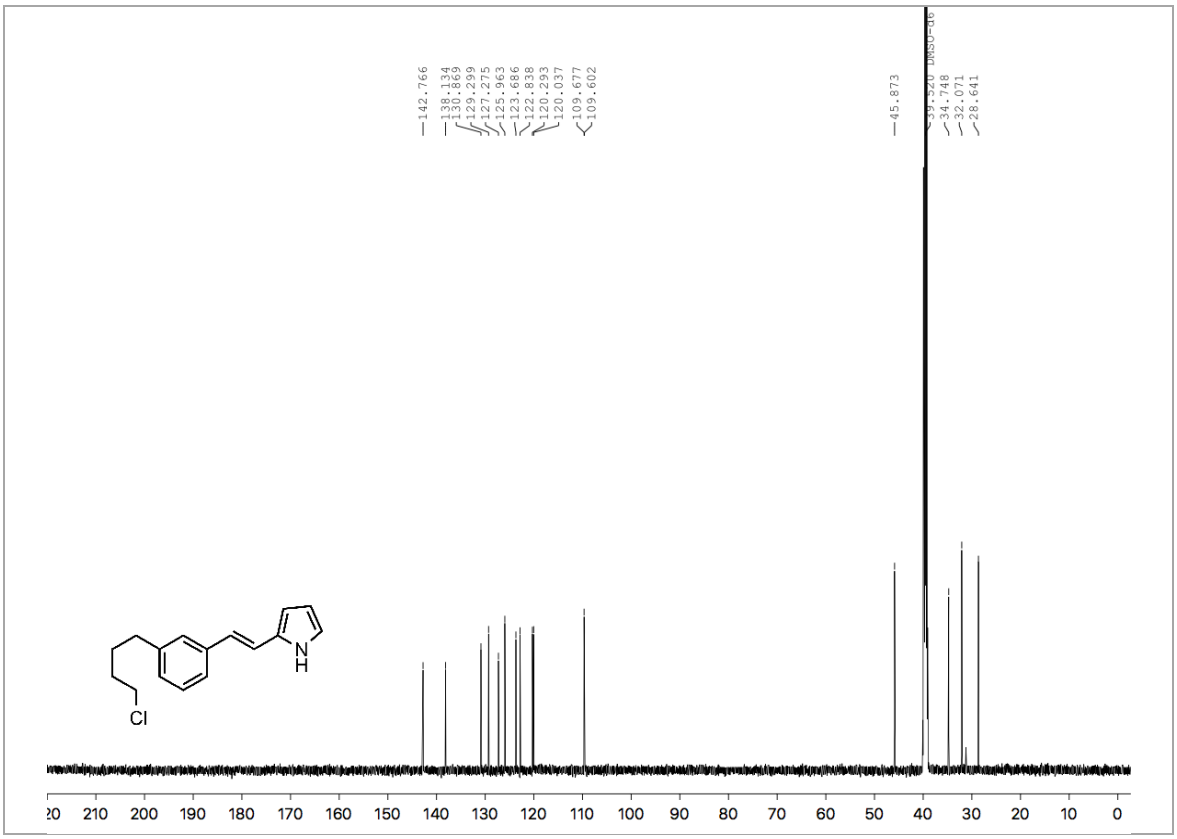
142.766
138.134
130.869
129.299
127.275
125.963
123.686
122.838
120.293
120.037
109.677
109.602
45.873
39.520
DMSO-d6
34.748
32.071
28.641
N
H
Cl

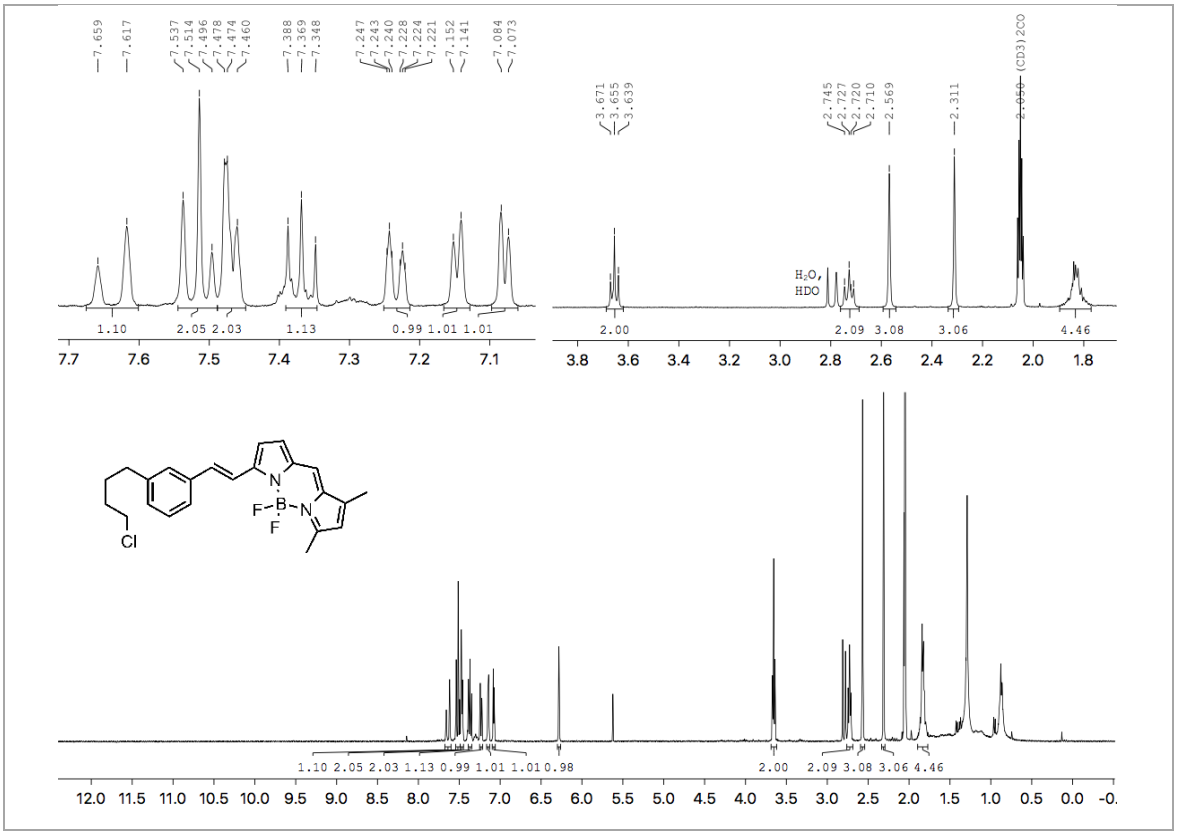
7.659
7.617
7.537
7.514
7.496
7.478
7.474
7.460
7.388
7.369
7.348
7.247
7.243
7.240
7.228
7.224
7.221
7.152
7.141
7.084
7.073
3.671
3.655
3.639
2.745
2.727
2.720
2.710
2.569
2.311
2.050
(CD3)2CO
H2O,
HDO
1.10
2.05 2.03
1.13
0.99 1.01 1.01
2.00
2.09 3.08
3.06
4.46
F
B
N
F
Cl
1.10 2.05 2.03 1.13 0.99 1.01 1.01 0.98
2.00
2.09 3.08 3.06 4.46

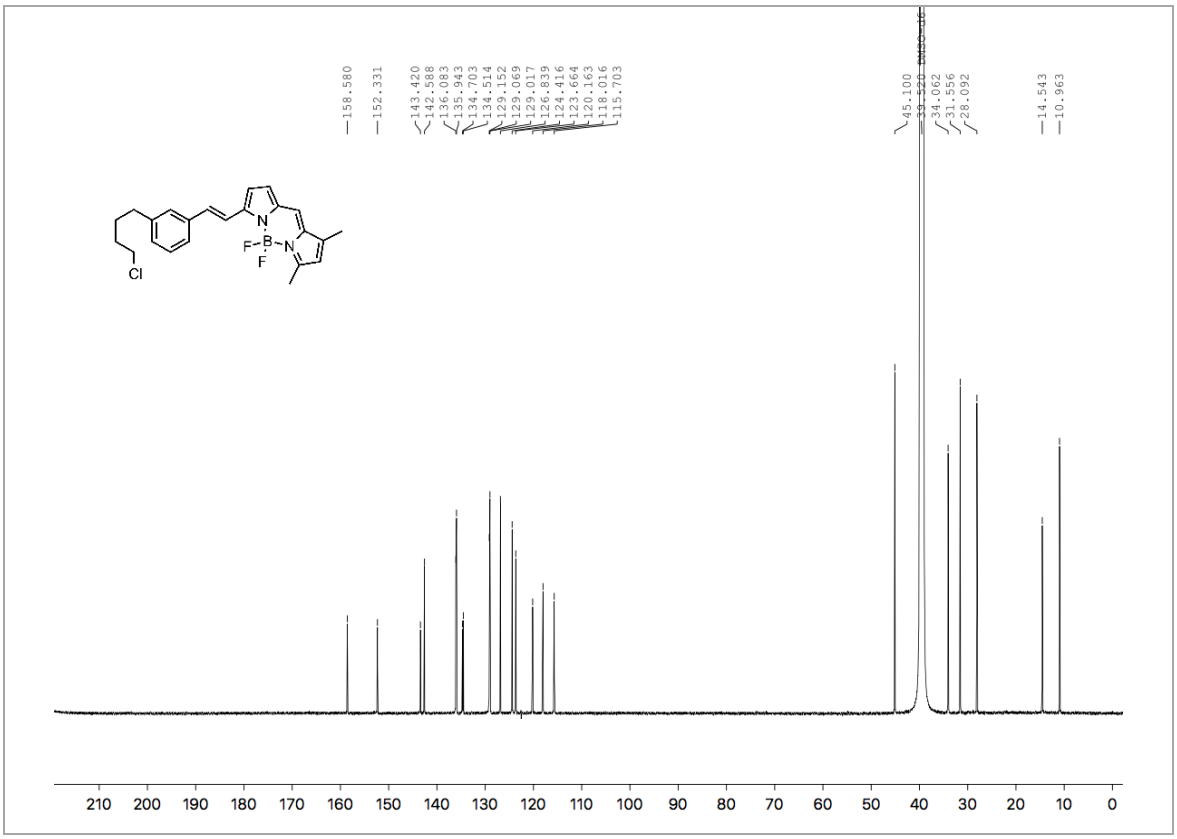
158.580
152.331
143.420
142.588
136.083
135.943
134.703
134.514
129.152
129.069
129.017
126.839
124.416
123.664
120.163
118.016
115.703
45.100
39.520
DMSO-d6
34.062
31.556
28.092
14.543
10.963
F
B
N
F
Cl

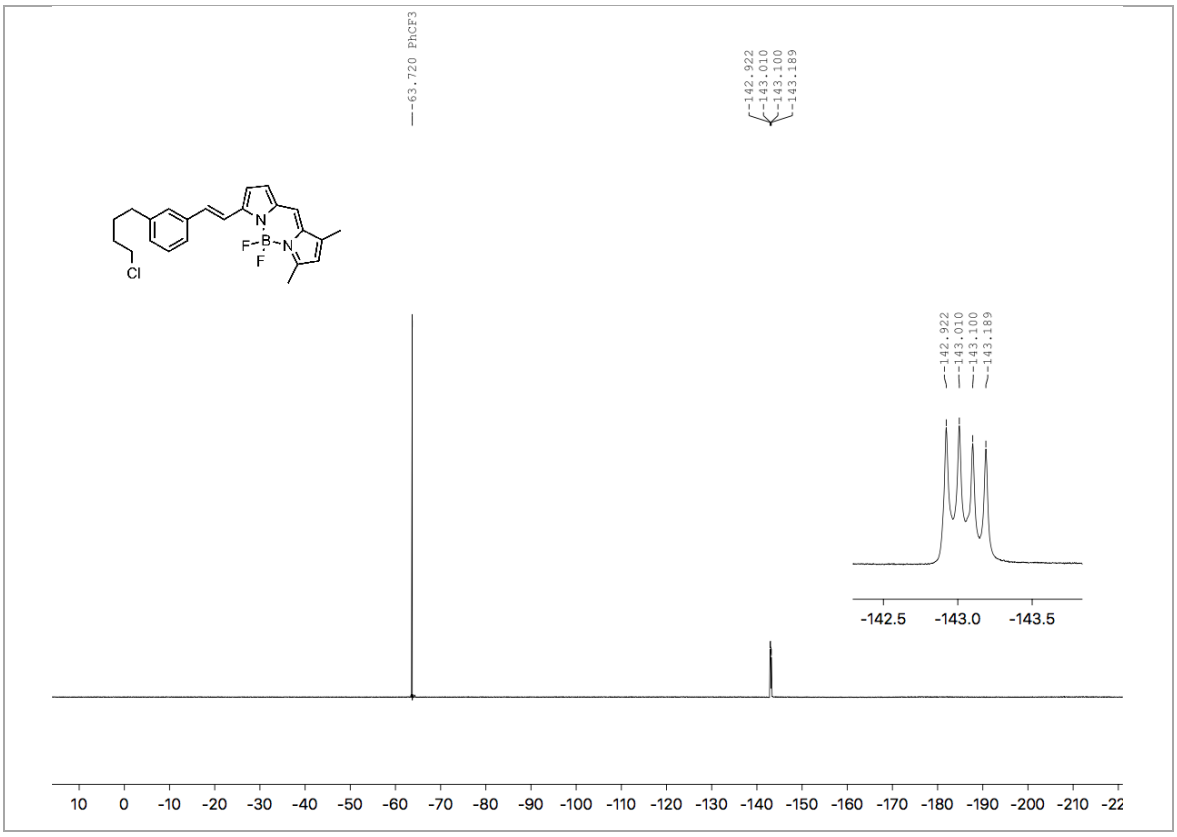
-63.720 PhCF3
-142.922
-143.010
-143.100
-143.189
Cl
F
B
N
-142.5
-143.0
-143.5
10 0 -10 -20 -30 -40 -50 -60 -70 -80 -90 -100 -110 -120 -130 -140 -150 -160 -170 -180 -190 -200 -210

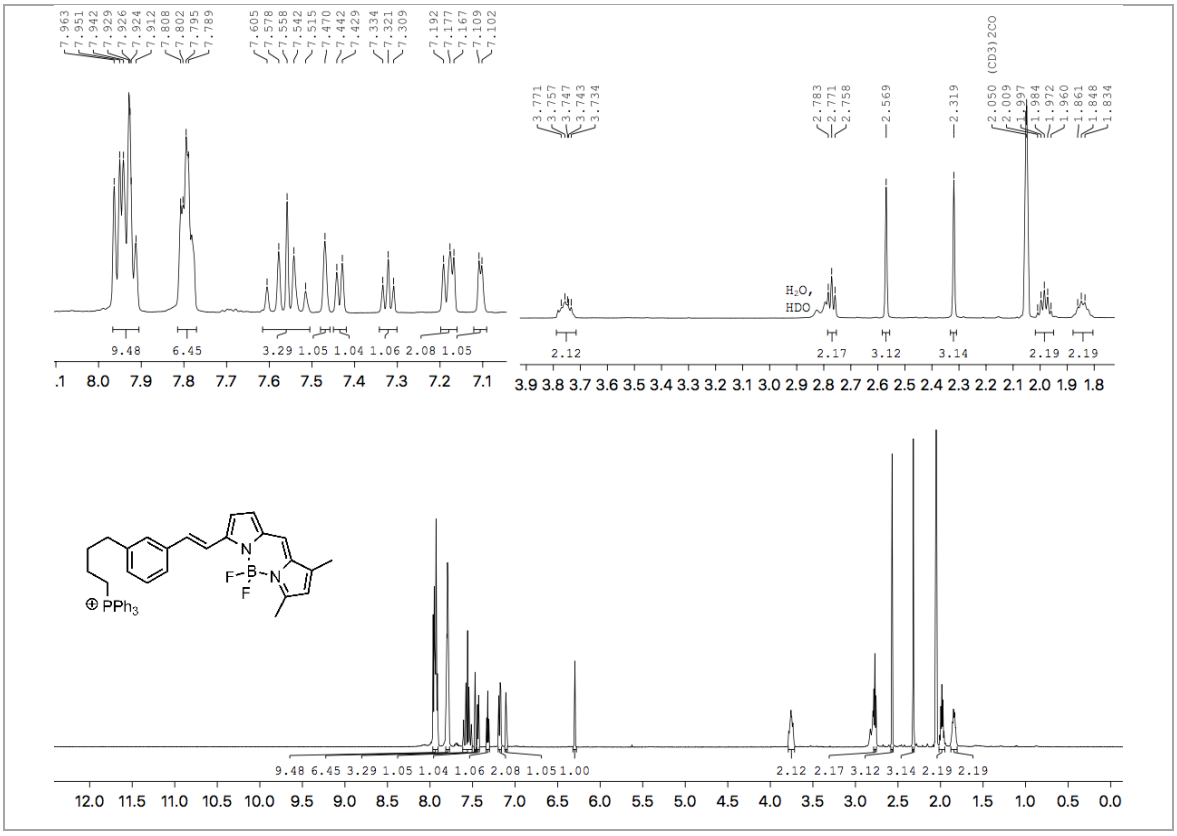
7.963 7.951 7.942 7.929 7.926 7.924 7.912 7.808 7.802 7.795 7.789
7.605 7.578 7.558 7.542 7.515 7.470 7.442 7.429 7.334 7.321 7.309
7.192 7.177 7.167 7.109 7.102
3.771 3.757 3.747 3.743 3.734
2.783 2.771 2.758 2.569 2.319 2.050 2.009 1.997 1.984 1.972 1.960 1.861 1.848 1.834
(CD3)2CO
H2O, HDO
9.48 6.45 3.29 1.05 1.04 1.06 2.08 1.05
2.12 2.17 3.12 3.14 2.19 2.19
PPh3
9.48 6.45 3.29 1.05 1.04 1.06 2.08 1.05 1.00
2.12 2.17 3.12 3.14 2.19 2.19

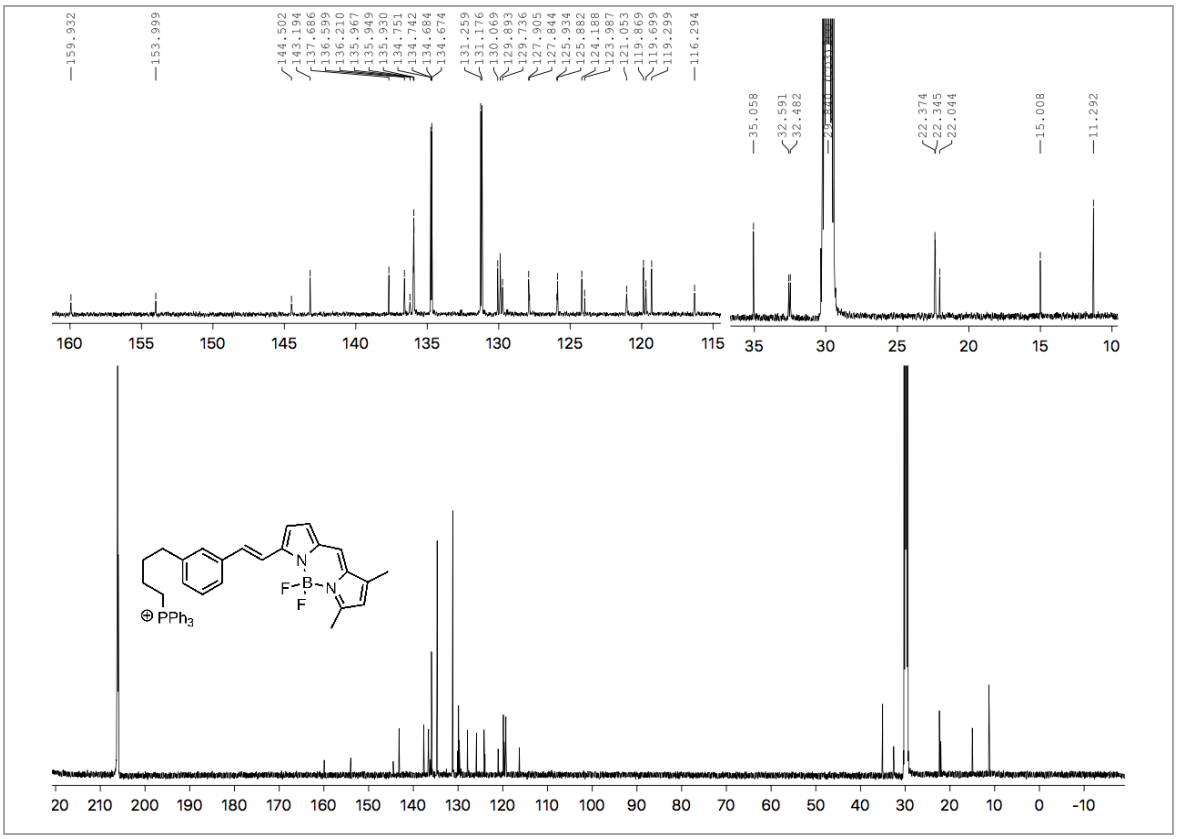
159.932 153.999
144.502 143.194 137.686 136.599 136.210 135.967 135.949 135.930 134.751 134.742 134.684 134.674
131.259 131.176 130.069 129.893 129.736 127.905 127.844 125.934 125.882 124.188 123.987 121.053 119.869 119.699 119.299 116.294
35.058 32.591 32.482 22.374 22.345 22.044 15.008 11.292
PPh3

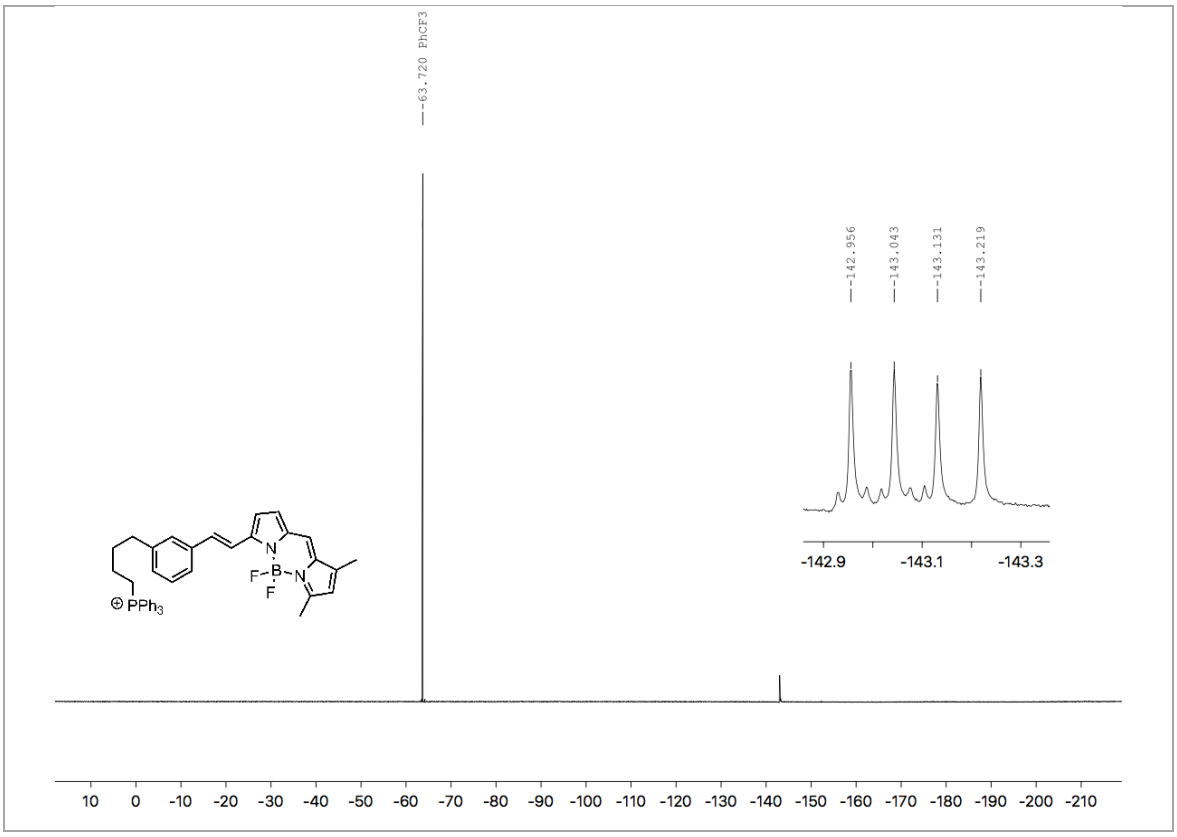
-63.720 PhCF3
-142.956
-143.043
-143.131
-143.219
-142.9
-143.1
-143.3
PPh3
10 0 -10 -20 -30 -40 -50 -60 -70 -80 -90 -100 -110 -120 -130 -140 -150 -160 -170 -180 -190 -200 -210